Development of imide- and imidazole-containing electron acceptors for use in donor-acceptor conjugated compounds and polymers

By

Duo Li

A thesis submitted to

the Faculty of Graduate Studies and Research

in partial fulfillment of the requirements for the degree of

Doctor of Philosophy

Department of Chemistry

Carleton University

Ottawa, Ontario, Canada

April 2013

© Copyright, Duo Li, Ottawa, ON, Canada, 2013

Library and Archives Canada

Published Heritage Branch

395 Wellington Street
Ottawa ON K1A 0N4
Canada

Bibliothèque et Archives Canada

Direction du Patrimoine de l'édition

395, rue Wellington
Ottawa ON K1A 0N4
Canada

Your file Votre référence
ISBN: 978-0-494-94554-4

Our file Notre référence
ISBN: 978-0-494-94554-4

NOTICE:

The author has granted a non-exclusive license allowing Library and Archives Canada to reproduce, publish, archive, preserve, conserve, communicate to the public by telecommunication or on the Internet, loan, distrbute and sell theses worldwide, for commercial or non-commercial purposes, in microform, paper, electronic and/or any other formats.

The author retains copyright ownership and moral rights in this thesis. Neither the thesis nor substantial extracts from it may be printed or otherwise reproduced without the author's permission.

AVIS:

L'auteur a accordé une licence non exclusive permettant à la Bibliothèque et Archives Canada de reproduire, publier, archiver, sauvegarder, conserver, transmettre au public par télécommunication ou par l'Internet, prêter, distribuer et vendre des thèses partout dans le monde, à des fins commerciales ou autres, sur support microforme, papier, électronique et/ou autres formats.

L'auteur conserve la propriété du droit d'auteur et des droits moraux qui protege cette thèse. Ni la thèse ni des extraits substantiels de celle-ci ne doivent être imprimés ou autrement reproduits sans son autorisation.

In compliance with the Canadian Privacy Act some supporting forms may have been removed from this thesis.

While these forms may be included in the document page count, their removal does not represent any loss of content from the thesis.

Conformément à la loi canadienne sur la protection de la vie privée, quelques formulaires secondaires ont été enlevés de cette thèse.

Bien que ces formulaires aient inclus dans la pagination, il n'y aura aucun contenu manquant.

Canada

Abstract

Conjugated organic compounds and polymers have attracted significant attention due to their potential application in electronic devices as semiconducting materials, such as organic solar cells (OSCs). In order to tune band gaps, donor-acceptor (D-A) structure is widely used, which has been proved to be one of the most effective strategies. This thesis consists of three parts: 1) design, syntheses and characterization of new weak acceptors based on imides and the systematic study of the structure-property relationship; (2) introduction of weak and strong acceptors in one polymer to achieve a broad coverage of light absorption and improve the power conversion efficiency (PCE); (3) modification of benzothiadiazole (**BT**) acceptor in order to increase the electron withdrawing ability.

Imide-based electron acceptors, 4-(5-bromothiophen-2-yl)-2-(2-ethylhexyl)-9-phenyl-1H-benzo[f]isoindole-1,3(2H)-dione (**BIDO-1**) and 4,9-bis(5-bromothiophen-2-yl)-2-(2-ethylhexyl)-benzo[f]isoindole-1,3-dione (**BIDO-2**), were designed and synthesized. In this design, naphthalene is selected as its main core to maintain a planar structure, and thienyl groups are able to facilitate the bromination reaction and lower the band gap. **BIDO-1** and **BIDO-2** were successfully coupled with different donors by both Suzuki cross-coupling and Stille cross-coupling reactions. Based on the energy levels and band gaps of the **BIDO**-containing compounds and polymers, **BIDO-1** and **BIDO-2** are proved to be weak electron acceptors. Pyromellitic diimide (**PMDI**) was also studied and found to be a stronger electron acceptor than **BIDO**.

In order to obtain broad absorption coverage, both weak acceptor (**BIDO-2**) and strong acceptor diketopyrrolopyrrole (**DPP**) were introduced in the same

polymer. The resulting polymers show two absorption bands at 400 and 600 nm and two emission peaks at 500 and 680 nm. The band gaps of the polymers are around 1.6 eV, which is ideal for OSC application. The PCE of 1.17% was achieved.

Finally, thiadiazolobenzoimidazole (**TBI**) acceptor was designed in order to increase the electron-withdrawing ability of **BT**. The key feature of **TBI** is the three electron deficient imine groups, rendering **TBI** a stronger acceptor than **BT**. Four **TBI**-containing compounds **IV-a** to **IV-d** were synthesized by reaction between diaminobenzothiadiazole and corresponding anhydride and exhibit the maximum absorption at 600 nm. The band gaps of **IV-a** to **IV-d** are smaller than that of **BT**-containing compounds, ranging from 1.60 to 1.97 eV. Moreover, all compounds are electrochromic and become absorbing at the telecommunication wavelength electrochemically.

Acknowledgements

It is my great pleasure to thank the people who made this thesis possible.

First of all, I would like to give my deep gratitude to my supervisor, Dr. Wayne Wang for his encouragement, motivation, great advices and thoughtful guidance throughout my Ph.D. study.

I would like to thank Dr. Jane Gao for her suggestions and assistance. I would also like to thank all my colleagues in the laboratory who have made my experience at Carleton University more pleasant: Wendy Hao, Saif Mia, Khama Rani Ghosh, Sukanta Kumar Saha, Yasaman Aghili and Di Zhang.

To Jim Logan, Tony O'Neil, Keith Bourque, I would like to say thank you all for support of the instrumental techniques.

I wish to thank my parents who raised me and helped me get to where I am today, my daughter, Isabella, whose smile is always a positive encouragement, and in particular my wife, Zhaohui, for her love and understanding during my study at Carleton University.

Table of Contents

List of Figures

List of Schemes

List of Tables

List of Symbols and Abbreviations

AFM	Atomic force microscopy
BBT	Benzobis(1,2,5-thidiazole)
BHJ	Bulk heterojunction
BIDO	Benzo[f]isoindole-1,3(2H)-dione
BT	Benzothidiazole
CV	Cyclic voltammograms
D-A	Donor-Acceptor
DPP	3,6-Diaryl-2,5-dihydropyrrolo[3,4-c]pyrrole-1,4-dione
DSC	Differential scanning calorimetry
EQE	External quantum efficiency
FF	Fill factor
GPC	Gel permeation chromatography
HOMO	Highest occupied molecular orbital
ICT	Intramolecular charge transfer
ITO	Indium tin oxide
LUMO	Lowest unoccupied molecular orbital
NIR	Near-Infrared
NDI	Naphthalene diimide
OFET	Organic field effect transistor
OPV	Organic photovoltaic
OSC	Organic solar cells
P3HT	Poly(3-hexylthiphenes)
[60]PCBM	[6,6]-Phenyl-C_{61}-butyric acid methyl ester
[70]PCBM	[6,6]-Phenyl-C_{71}-butyric acid methyl ester
PCE	Power conversion efficiency
PDI	Perylene diimide
PEDOT	Poly(3,4-ethylenedioxythiophene)
PITN	Polyisothianaphthene
PL	Photoluminescence

PMDI	Pyromellitic diimide
PPVs	Poly(para-phenylene vinylene)s
PSS	Poly(styrenesulfonate)
REPE	Resonance energy per π electron
TGA	Thermogravimetric analysis
UPS	Ultraviolet photoelectron spectroscopy
E_g	Band gap
E_{ox}	Onset oxidation potential
E_{red}	Onset reduction potential
τ_{exc}	Exponential life time of an exciton
J_{sc}	Short-circuit current
V_{oc}	Open-circuit voltage
λ_{max}	Maximum absorption wavelength
T_d	Decomposition Temperuature
T_g	Glass Transition Temperature

Chapter 1 Introduction to Low Band Gap Materials and Organic Solar Cells

1.1 Conjugated polymers

Conjugated polymers are carbon-based macromolecules connected by alternating double and single bonds. The interest of conjugated polymers increased considerably after the discovery of substantial increase of electrical conductivity upon electrochemical doping, which led to Nobel Prize for chemistry in 2000 to Heeger, MacDiarmid, and Shirakawa. Due to the fact that the π-orbitals are delocalized throughout the polymer backbone, single and double bonds becomes similar and the π-electrons can easily move from one bond to the other, which makes conjugated polymers to be one-dimensional semiconductors. The electronic and optical properties of conjugated polymers, coupled with their mechanical properties and intrinsic processing advantages, means that they are particularly attractive materials for the electronics industry. There are many applications including light emitting devices, nonlinear optical devices, photovoltaic devices, organic field-effect transistors, and electro-magnetic shielding.

One of the key factors that determine the usage of the conjugated polymers is the band gap. Common conjugated polymers possess a relatively large band gap, for example the band gap of poly(*p*-phenylene) is 3.0 eV. However, in some cases, lower band gap is required in particular application. Take organic solar cell for example; polymers with large band gap can only absorb UV light, wasting the visible and near-infrared light in the solar irradiation. In order to harvest more sun light, low band gap

is needed. In this chapter, the factors and principles that need to be considered to construct low band gap polymers will be discussed, followed by the introduction of the latest progress of organic solar cells.

1.2 Low band gap organic materials

1.2.1 The factors that influence the band gap

Based on the theory proposed by Roncali [1], band gaps of conjugated oligomers or polymers are determined by five contributions: 1) the energy related to the bond length alternation ($E^{\delta r}$), 2) the mean deviation from planarity (E^{θ}), 3) the aromatic resonance energy of the cycle (E^{Res}), 4) the inductive or mesomeric electronic effects of eventual substitution (E^{sub}) and 5) the intermolecular or interchain coupling in the solid state (E^{int}). Band gap (E_g) is the sum of all these contributions (Figure 1.1):

$$E^{\delta r} + E^{\theta} + E^{Res} + E^{sub} + E^{int} => E_g$$

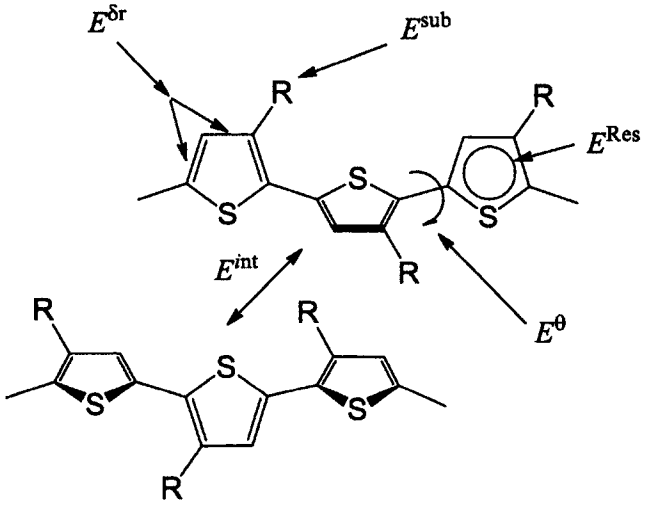

Figure 1.1. The factors that influence the band gap.

1. Bond length alternation ($E^{\delta r}$):

The degree of bond length alternation which is related to the difference between single and double bond possesses the major contribution to E_g of the conjugated materials. Conjugated polymers like poly(*p*-phenylene) have two resonance forms: aromatic and quinoid form (Figure 1.2). In the aromatic form, the benzene rings are connected by single bonds, whereas in quinoid form, they are connected by double bonds. The band gaps of these two forms are different, and in most cases, the quinoid form has a smaller band gap from calculations.[2]

Aromatic form Quinoid form

Figure 1.2. Aromatic and quinoid forms of poly(*p*-phenylene).

2. Deviation from planarity (E^{θ}):

The second factor is the planarity of conjugated system. Since conjugated polymers are normally in their aromatic form, aromatic units are connected by single bonds which allow the interannular rotation. Orbital overlap can be largely affected by the torsion angle and result in an increase of E_g.[3-4]

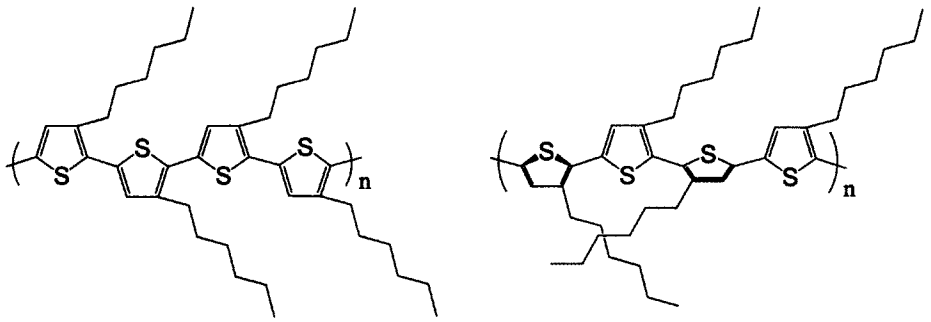

λ_{abs} = 440 nm, λ_{em} = 580 nm
Head to Tail

λ_{abs} = 413 nm, λ_{em} = 567 nm
Head to Head

Figure 1.3. The influence of torsion angle on **P3HT**.

The torsion angle between aromatic systems is determined by the steric interaction between these aromatic rings. For example, in poly(3-hexylthiphenes) (**P3HT**), head-to-head coupling leads to the polymer with blue shifted maximum absorption, emission and larger band gap compared to regioregular P3HT due to the nonplanar structure (Figure 1.3).[5, 6]

3. Aromatic resonance energy (E^{Res}):

The aromatic resonance energy is defined as the energy difference between the aromatic structure and a hypothetical reference, consisting of isolated double bonds. This aromaticity results in a competition between π-electron confinement within the rings and delocalization along the chain.[7] In 1971, Andes Hess and Schaad proposed a new approach to calculate the resonance energy based on the Hückel molecular orbital π energies.[8] This approach was also applied to the heterocycles in 1973.[9] Based on their calculation, polymer tends to have small band gap if the monomer has a small value of resonance energy per π electron (REPE). For example, the REPEs of benzene, pyrrole and thiophene are 0.065, 0.039 and 0.032, and the band gaps of corresponding polymers are 3 eV, 2.5 eV and 2 eV for poly(p-phenylene), polypyrrole and polythiophene, respectively.

4. Effects of substitution (E^{sub}):

Substituents play a very important role in changing the energetic position of the HOMO or LUMO level, respectively, via mesomeric or inductive effects. [10] Introducing electron-donating or electron-withdrawing substituents will respectively

increase the HOMO level or lower the LUMO level. These substituent effects are extensively studied and becoming a classical tool to synthesize conjugated oligomers or polymers in order to obtain desirable band gaps. This will be discussed in detail in the next section.

5. Intermolecular or interchain coupling (E^{int}).

The interactions between individual molecules that are responsible for their organization into a condensed phase can represent an important contribution to the band gap. Conjugated polymers in the solid state generally show red shifted absorption and lower band gaps as compared to the solution phase, which is attributed to an increased interaction between the chains. In some cases, polymers have bulky aliphatic side chains in order to increase solubility. However, these side chains can hinder intermolecular interactions between the backbones and increase the band gap. Moreover, regio-stereochemistry of the side groups needs to be considered, because polymers with good regioregularity tend to have good packing in their solid state. Packing of conjugated polymers will influence not only their band gaps, but the electron mobility as well and further influence the device performance.[11, 12]

1.2.2 Low band gap materials with D-A structures

The most effective and widely used strategy to construct low band gap conjugated oligomers or polymers is to employ alternating electron-donating and electron-withdrawing groups in the conjugated backbone. This idea was first proposed by Havinga and coworkers in 1992.[13] They chose squaric acid (SA) and

croconic acid (CA) as acceptors, cyanine dyes as donors and successfully obtained alternating copolymers with very low band gaps ranging from 1.2 to 0.5 eV (Figure 1.4).

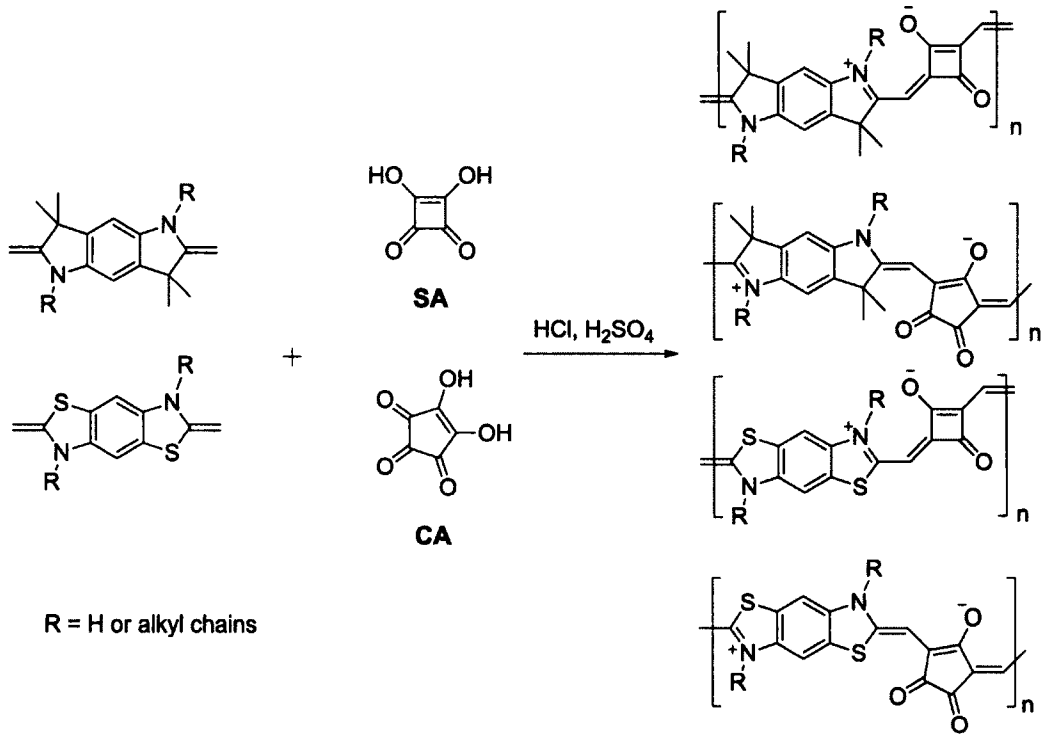

Figure 1.4. Donor-acceptor alternating copolymers proposed by Havinga.

Interaction of the donor–acceptor moieties enhances the double bond character between the repeating units, which stabilizes the low band gap quinoid forms within the polymer backbones. Hence, a conjugated polymer with an alternating sequence of appropriate donor and acceptor units in the main chain can induce a reduction in its band gap energy.

Molecular orbital calculation can also be used to explain the unusual low band gap created by the donor-acceptor system. Normally, electron-rich molecules have higher HOMO and LUMO energy levels comparing to that of electron-deficient molecules. If the HOMO level of the donor and the LUMO level of the acceptor

moiety are close in energy, hybridization of energy levels shows a low HOMO-LUMO separation, indicating a small band gap as depicted in Figure 1.5.[14] It also shows that the introduction of electron withdrawing groups reduces E_g by lowering the LUMO levels, whereas, the introduction of electron donating groups reduces E_g by raising the HOMO levels. Further reduction of band gap can be achieved by enhancing the strength of the donors and acceptors.

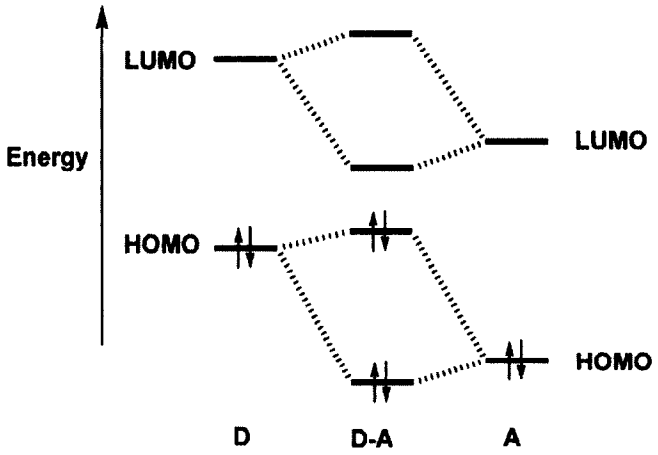

Figure 1.5. Molecular orbital hybridization in donor (D) and acceptor (A) moieties.

In order to get desirable band gaps, a variety of donors and acceptors have been synthesized and utilized to form a number of low band gap oligomers and polymers. The common donors are electron-rich heterocycles containing nitrogen or sulphur, such as pyrrole and thiophene. The widely used acceptors are compounds with electron withdrawing groups like nitro, nitrile, fluorine or heterocycles with unsaturated nitrogen atoms like quinoxalines, pyrazines and thiadiazoles.

1.2.2.1 Low band gap conjugated materials with nitro, nitrile and ketone groups

Zhang and Tour reported series of polythiophenes with alternating donor-acceptor repeat units.[15] The donor units were thiophenes containing amine or methoxy groups and the acceptors were the ones containing ketone or nitro groups (Figure 1.6).

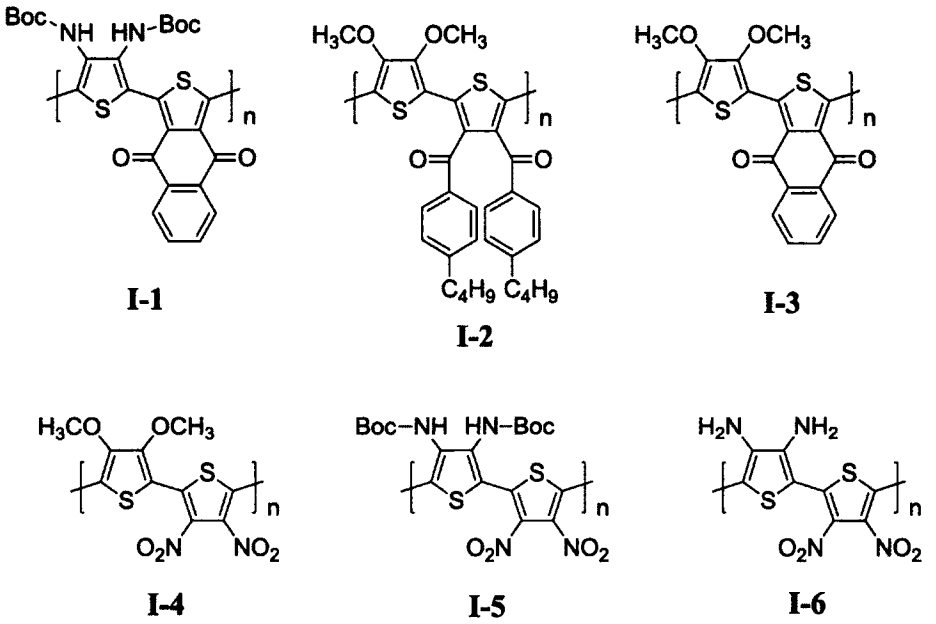

Figure 1.6. Thiophene based polymers containing nitro or ketone as acceptors.

These thiophene based polymers were all prepared by Stille cross-coupling reaction. The optical spectra of polymer **I-1** to **I-5** showed λ_{max} values ranging from 400 to 466 nm in solution and 400 to 506 nm as film, indicating relative large band gaps due to weak donor acceptor interaction and large steric hindrance. However, after removing the protection group from **I-5**, polymer **I-6** showed λ_{max} at 676 nm in solution and 768 nm as film and the corresponding optical band gaps are 1.4 eV and 1.1eV, respectively. The cause of the low band gap is due to the D-A arrangement, which induces significant intramolecular charge transfer (ICT) character along the backbone as shown in Figure 1.7.

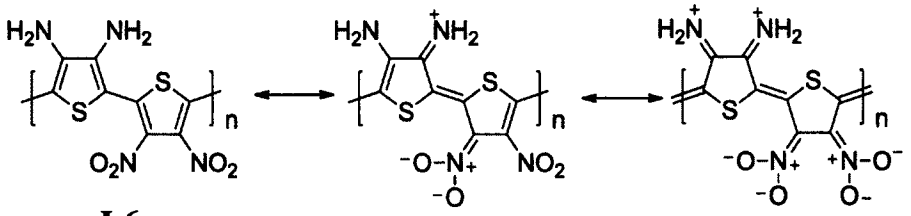

I-6

Figure 1.7. ICT character in polymer **I-6**.

Nitrile groups were introduced in polymer **I-7** as electron withdrawing unit by Zotti and coworkers and a low band gap of 1.6 eV was obtained (Figure 1.8).[16] Similar work was also reported by Lin.[17] In their work, polymer **I-8** was prepared by electropolymerization of 1,4-bis(2-cyano-2-α-thienylethenyl)benzene and showed extremely broad absorption band ranging from 300 to 700 nm with λ_{max} at 580 nm (Figure 1.8). The band gap was not provided in the paper, however, it was estimated to be lower than 1.7 eV based on the optical data.

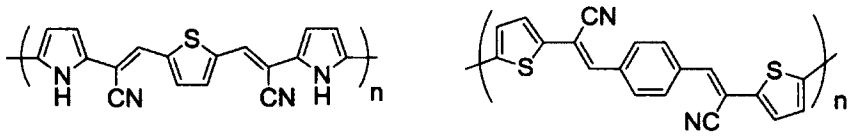

I-7 I-8

Figure 1.8. D-A polymers containing nitrile groups as acceptors.

1.2.2.2 Low band gap conjugated materials with electron deficient heterocycles

Aromatic heterocylces containing imine groups are usually electron deficient, such as pyridine and pyrazine. Normally, the more imine groups it contains in the conjugated ring system, the stronger electron withdrawing ability it has. In order to achieve maximum donor acceptor interactions, donors should be connected to carbons close to the electron deficient nitrogen. Some commonly used acceptors are listed in Figure 1.9.

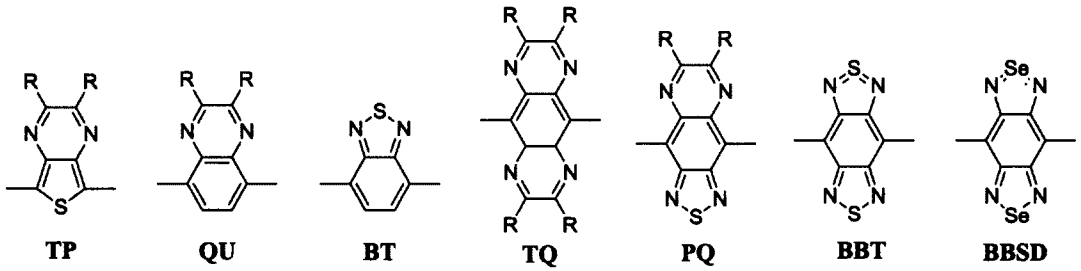

Figure 1.9. Electron withdrawing aromatic heterocycles.

In 1995, Yamshita's group reported low band gap polymer **I-9** in which thiophene was the donor and benzobis(1,2,5-thidiazole) (**BBT**) was the acceptor (Figure 1.10).[18] The band gap of **I-9** is surprisingly low, below 0.5 eV. Several advantages of the acceptor contribute to the low band gap: 1) the benzobis(1,2,5-thiadiazole) unit containing hypervalent sulfur atoms has a high electron affinity. 2) **I-9** has a strong contribution of the quinoid form since more stable classical 1,2,5-thiadiazole rings are generated in this form. 3) This system has no steric repulsion between the adjacent heterocyclic units, leading to a planar geometry.

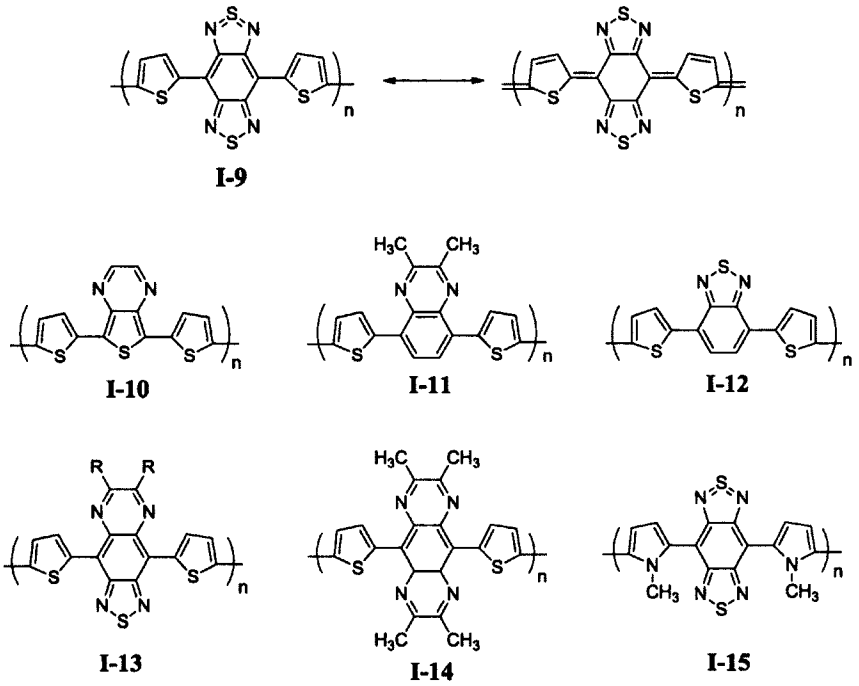

Figure 1.10. Benzobis(1,2,5-thiadiazole) containing polymers.

In 1996, they also described a series of narrow band gap polymers **I-10** to **I-16** based on different acceptors (Figure 1.10).[19] The donors were thiophene and methylpyrrole. The band gaps determined from their optical absorption spectra ranged from 0.6 to 1.4 eV. The results showed that the band gap can be widely tuned by different combinations of donors and acceptors and stronger acceptors can result in lower band gaps. Among all these acceptors studied, **BBT** was found to be the strongest.

Recently, Qian and Wang reported low band gap compounds using **BBT** as acceptor.[20] Instead of thiophene, they chose amine as donor units and prepared compound **I-16** to **1-19** through Stille cross-coupling reaction (Figure 1.11). The λ_{max} ranged from 700 to 945 nm and the emission ranged from 975 to 1255 nm. The lowest band gap of 0.73 eV came from compound **I-19**. Extended π conjugation and introduction of strong donor and strong acceptor contribute to the small band gap of **I-19**. The materials were then put into the application of near infrared OLED, and a remarkable emission at 1080 nm with external quantum efficiency (EQE) of 0.28% was obtained from **I-18**.

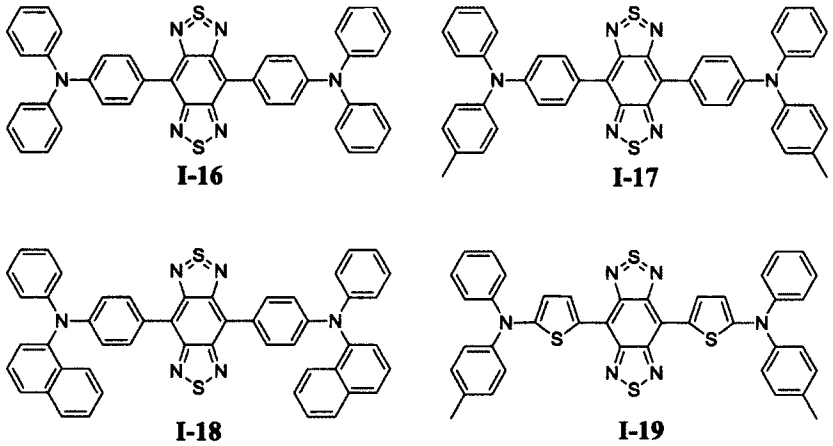

Figure 1.11. D-A compounds containing amine as donors and **BBT** as acceptor.

Qian and Wang also reported the donor acceptor compounds with benzobis(1,2,5-selenadiazole) (**BBSD**) acceptors (Figure 1.12).[21] After the sulfur atom was replaced by selenium atom, a large red shift absorption and emission was induced, followed by a much lower band gap caused by the polarizability of the selenium atom. Comparing to the other two compounds, compound **I-21** has the smallest band gap of 0.56 eV due to the more planar structure which favors the intramolecular charge transfer.

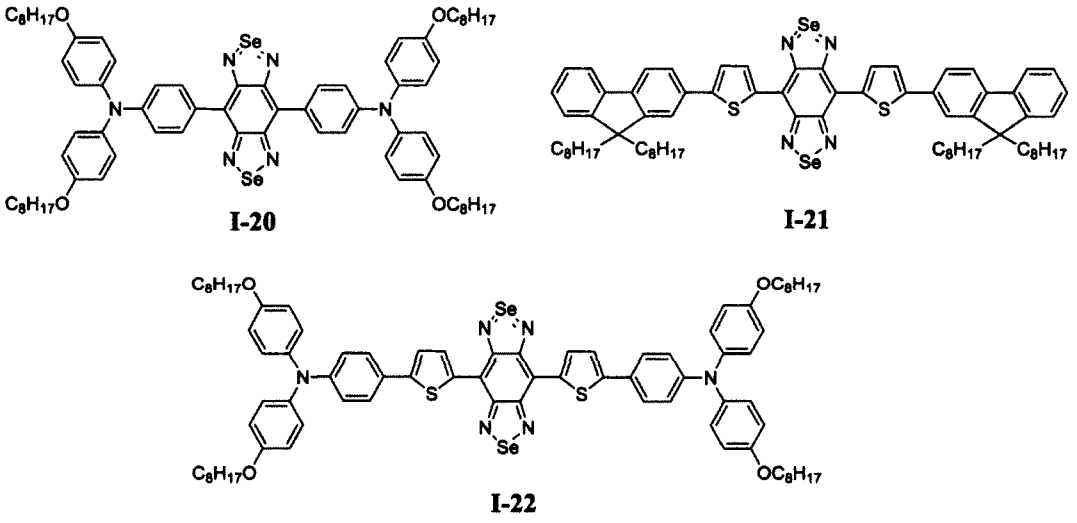

Figure 1.12. BBSD containing D-A compounds.

1.2.3 Other low band gap conjugated materials.

1.2.3.1 PITN and similar quinoid structures

Polythiophene (**PT**) received particular attention because of its wide applications in electronics. However, it has a relatively large band gap of 2.0 eV due to the limited contribution of the quinoid form. Therefore, the thiophene rings are basically connected by single bonds in the polymer and allow for large torsion angle which can increase the band gap. In order to increase the quinoid form contribution,

polyisothianaphthene (**PITN**) was synthesized.[22] The benzene ring fused to thiophene can stabilize the quinoid form and increase the double bond connection character of the polymer (Figure 1.13). Therefore, the band gap of **PITN** is only 1.1 eV.

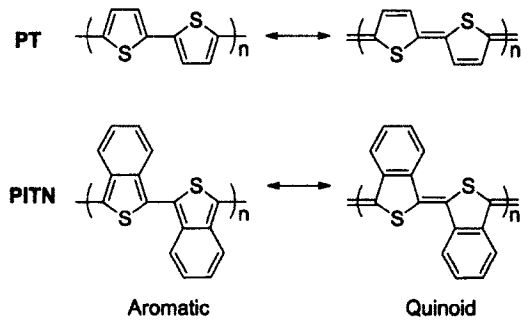

Figure 1.13. PT and **PITN**.

After **PITN** was synthesized, other related work was reported. In 1991, Ikenoue and coworkers reported a dioxymethylene substituted **PITN I-23** to improve the oxidation stability of **PITN** (Figure 1.14).[23] However, the introduction of an electron-donating substituent on the isothianaphthene ring was not able to affect the oxidation potential and the band gap much. They obtained a band gap of 1.0 eV, slightly lower than **PITN**.

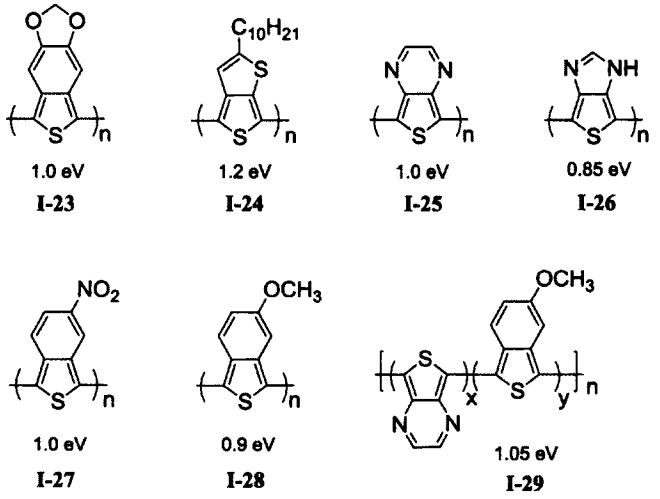

Figure 1.14. PITN derivatives.

In 1997, Pomerantz and Gu described a new low band polymer **I-24** prepared by oxidization polymerization (Figure 1.14).[24] The benzene ring was replaced by thiophene, however, the band gap is still 1.2 eV. In 2001, the Hagan group synthesized a series of **PITN** derivatives **I-25** to **I-29**.[25] Although variations were made on the substitutions and the polymer sequences, the band gap was affected very little. It was explained that other factors, such as planarity, need to be considered to further lower the band gap of **PITN**.

1.2.3.2 Ladder polymers

Another strategy of lowering the band gap is to minimize the change to the polymer structures during the single and double bond alternation. Ladder polymers have the unique structures that meet the requirements. The most famous ladder polymer is polyacene (Figure 1.15). Theoretical calculation showed that polyacene can reach a zero band gap and behave like a superconductor.[26] Due to synthetic difficulties, only hexacene which has six fused benzene rings was reported until a paper was published by Neckers's group in 2006, claiming the successful synthesis of heptacene.[27] However, heptacene is not stable in the air or solution and produces oxygen adducts.

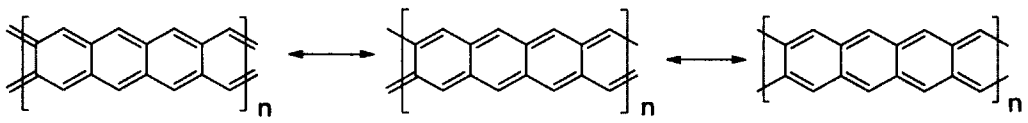

Figure 1.15. Polyacene.

1.3 Organic solar cells

Due to the growing energy needs, harvesting energy directly from sunlight using photovoltaic technology is considered to be one of the most important ways to produce clean and renewable energy. Organic solar cells (OSCs) are promising alternatives because of light weight, low cost and the potential to fabricate it onto large area of flexible substrate by solution processing. Right now, the main disadvantage associated with OSCs is the low efficiency compared to the inorganic solar cells. Efforts have been made to design and synthesize new materials and to optimize device fabrication in order to improve the efficiency.

1.3.1 Solar cell structures

1.3.1.1. Single layer OSCs

Single layer organic solar cells are the simplest organic solar cells. These cells are made by sandwiching a layer of single component organic materials between two metallic conductors, typically a layer of indium tin oxide (ITO) with high work function and a layer of low work function metal such as Al, Mg or Ca. The basic structure of such a cell is shown in Figure 1.16.

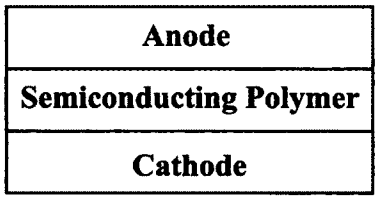

Figure 1.16. Structure of single layer OSC.

However, this type of solar cells suffers from very low power conversion efficiency (PCE) which is generally below 0.1%.[28-30] The major problem with

them is that the electric field between the two conductive electrodes is seldom sufficient to break up the photogenerated excitons. Often the electrons recombine with the holes rather than reach the electrode.

1.3.1.2. Bilayer heterojunction OSCs

A bilayer organic solar cell containing a p-type layer (electron acceptor) for hole transport and an n-type layer (electron donor) for electron transport has been implemented by Tang to improve the photocurrent of the device, as shown in Figure 1.17.[31] Excitons are generated by photoexcitation of the donor materials and diffuse to the D-A interface where exciton dissociation occurs. The separated free charge carriers transport to the respective electrodes in the opposite direction with the aid of the internal electric voltage.

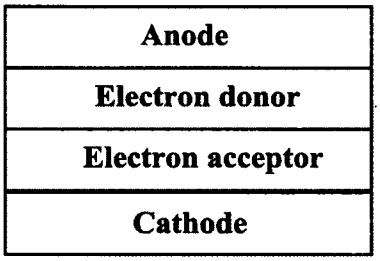

Figure 1.17. Structure of bilayer heterojunction OSC.

The diffusion length of excitons in organic electronic materials is typically in the order of 10 nm. In order for most excitons to diffuse to the interface of layers and break up into carriers, the layer thickness should also be in the same range as the diffusion length. However, at this thickness organic materials can't absorb a high percentage of sunlight due to limited extinction coefficient and will end up with a low PCE around 1%. [32,33]

1.3.1.3. Bulk heterojunction OSCs

To solve the problems mentioned for the previous organic solar cells, the concept of a bulk heterojunction (BHJ) was introduced by Yu (Figure 1.18).[34] In this type of solar cells, donors and acceptors are mixed together, forming a polymer blend. The length scale of the blend can be manipulated within the exciton diffusion length and relatively large thickness of polymer film can be maintained for light harvesting. A large D-A interfacial area may be achieved through the interpenetrating network leading to enhanced efficiency of charge separation. Two channels for the hole and electron transportation are created by the formation of bicontinuous network, and result in efficient charge collection. The PCE can be improved significantly in BHJ OSCs.

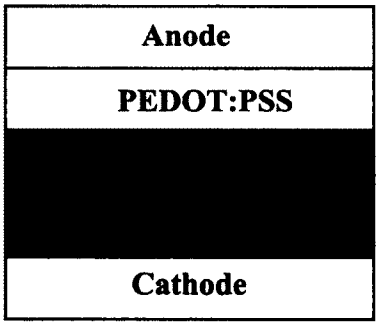

Figure 1.18. Structure of bulk heterojuction OSC.

The fabrication of BHJ OSCs is also very simple. Donor and acceptors can be mixed in the solution and then spin coated on top of conducting layer which is poly(3,4-ethylenedioxythiophene):poly(styrenesulfonate) (PEDOT:PSS) in most cases to form the active layer. PEDOT:PSS forms an Ohmic contact with the photoactive layer for effective charge collection, and also smoothes the ITO surface.

1.3.2 Working mechanism of OSCs

In general, there are four important processes for the working mechanism of OSCs (Figure 1.19): 1) absorption of light and generation of excitons, 2) diffusion of excitons to D-A interface, 3) charge separation, 4) charge transport and charge collection.

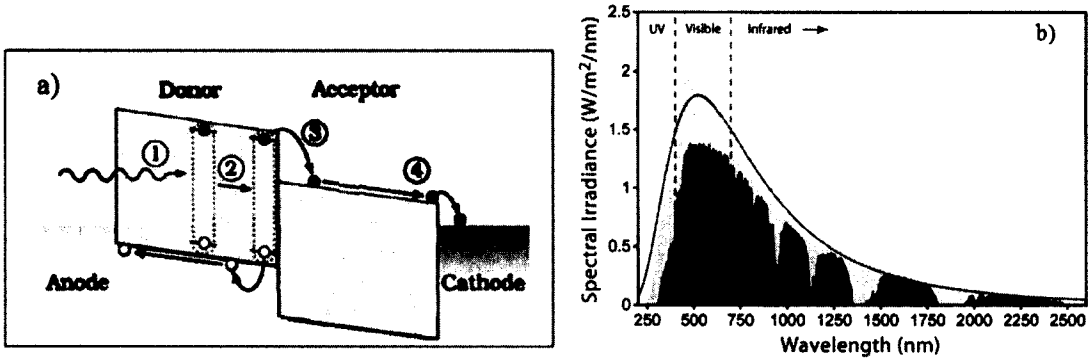

Figure 1.19. a) Working mechanism for OSC. (1) Photoexitation of the donor to generate exciton. (2) Exciton diffusion to the D-A interface. (3) Exciton dissociation. (4) Charge transportation and collection. b) Solar radiation spectrum.

1) Light absorption

The donor material can be excited from the ground state to excited state by absorbing a photon with specific frequency and becoming an exciton. For an efficient collection of photons, the absorption spectrum of the photoactive organic layer should match the solar emission spectrum and the active layer should be sufficiently thick to absorb most of the sun light. It is possible for organic materials to harvest more sunlight and increase the photocurrent by lowering the band gaps.

$$D + A + h\nu \longrightarrow D^* + A$$

2) Exciton transport

After the exciton is formed, it has to diffuse to the D-A interface to realize the charge separation. However, exciton transport is in competition with other decay processes such as luminescence or radiative recombination to the ground state. The exponential life time of an exciton (τ_{exc}) is determined by the value of the radiative and nonradiative decay rates. For an efficient solar cell all excitons have to reach the D-A interface within τ_{exc}. The distance an exciton is able to cross (L_{exc}) is given by :

$$L_{exc} = (D_{exc}\tau_{exc})^{1/2}$$

in which D_{exc} is the diffusion coefficient of the excitons. Since τ_{exc} is usually several nanoseconds for conjugated polymers, L_{exc} is limited to 10 nm. This implies that only those excitons formed within the distance of L_{exc} from the interface will contribute charge separation. To solve this problem, research has been devoted to make the interfacial area much larger, such as BHJ OSCs, so that each generated exciton is always close to the interface.

3) Charge separation

In the process of charge separation, an electron is transferred from the exciton to the acceptor material. The driving force required for the exciton dissociation is the electron affinity difference between donor and acceptor materials. At the interface the radical cation of the donor and the radical anion of the acceptor are created.

$$D^* + A \longrightarrow D^{\bullet +} + A^{\bullet -}$$

4) Charge transport and collection

In the final process, the fully separated free charge carriers will transport to the respective electrode in the opposite direction with the aid of the internal electric field and generate the photocurrent.

1.3.3 Parameters of OSCs

The important parameters of OSCs are: short-circuit current density (J_{sc}), open-circuit voltage (V_{oc}), fill factor (FF) and power conversion efficiency (PCE).

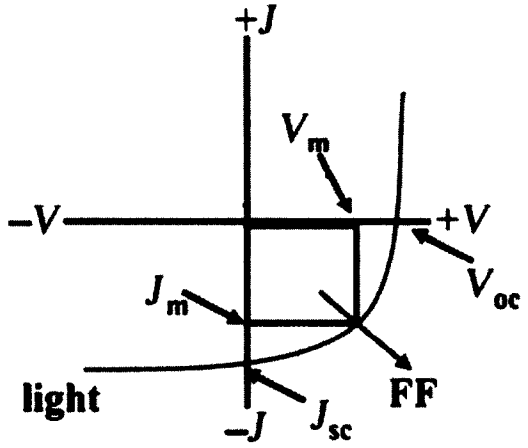

Figure 1.20. *J-V* curve and parameters of OSC.

Short-circuit current density (J_{sc}) is defined as the maximum current density generated when the organic solar cell is in short-circuit. It is determined by the amount of absorbed light and the internal conversion efficiency. Increasing the thickness of the active layer leads to the increase of light absorption, however, it can't be too thick due to the low mobility of the exciton and charge carriers. In order to get a high J_{sc}, the donor material should have desirable band gap to absorb most of the solar light [35,36] and high mobility for the transportation of the carriers.[37,38]

Open-circuit voltage (V_{oc}) is the voltage between the two the electrodes when the current is zero. It is determined by the energy levels of the donor and acceptor materials and can be estimated by the empirical equation below[39]:

$$V_{oc} = e^{-1} * (|E_{HOMO}{}^{donor}| - |E_{LUMO}{}^{acceptor}| - 0.3\ eV)$$

where e is the elementary charge and 0.3 eV is an empirical value for efficient charge separation. Since the acceptor is normally fullerene or its derivatives with a fixed LUMO level, V_{oc} value is largely dependent on HOMO level of the donor. A polymer donor with a lower HOMO level will give a higher V_{oc}. The effective way to lower the HOMO level of donor polymer is introducing less electron-rich groups such as fluorene or carbzole. [40-42]

Fill factor (FF) is calculated based the following equation:

$$FF = (J_m * V_m)/(J_{sc} * V_{oc})$$

in which J_m and V_m are the current and the voltage at the maximum power point. FF is currently the least understood parameter of all these four and is affected by many factors, such as charge carrier mobility and balance, interface recombination, series and shunt resistance in the device, film morphology and miscibility between the donor and acceptor. [43]

The power conversion efficiency (PCE) of the OSCs is defined as the ratio of maximum power output (P_{max}) to power input (P_{in}). PCE can be calculated using the following equation:

$$PCE = P_{max}/P_{in} = J_{sc} * V_{oc} * FF/P_{in}$$

The incident light power (P_{in}) is standardized at 1000 W m^{-2} for solar cell testing with a spectral intensity distribution matching that of the sun on the earth's

surface at an incident angle of 45 degree, which is called the AM 1.5 spectrum.

1.3.4 Classic n-type and p-type materials used in the OSCs

Currently, fullerene (C_{60}) and its derivatives fill an irreplaceable need for n-type materials due to various intrinsic advantages. First, the LUMO level of C_{60} is relatively low, around -3.75 eV, and is thermodynamically favorable to accept electron from an excited p-type material. Second, the LUMO level is triply degenerated. Therefore, the reduction of C_{60} can reach up to six electrons, indicating the unique stabilization of negative charges.[44] Third, photo induced electron transfer from p-type material to C_{60} is several orders of magnitude faster than the decay of luminescence or radiative recombination. [45,46] As a result, the efficiency of charge separation can be significant improved by C_{60}. However, it suffers from the poor solubility in organic solvent which limits the application in the BHJ OSCs. In 1995, the popular derivative [6,6]-phenyl-C_{61}-butyric acid methyl ester ([60]PCBM) was synthesized by Wudl and Hummelen (Figure 1.21).[47] It has a much better solubility and is commonly used to construct the OSCs with p-type materials. Another important fullerene analogue is C_{70} PCBM ([70]PCBM) (Figure 1.21). Comparing to [60]PCBM, device made of [70]PCBM gave better photovoltaic performance, due to its lower LUMO level and narrower band gap.[48,49]

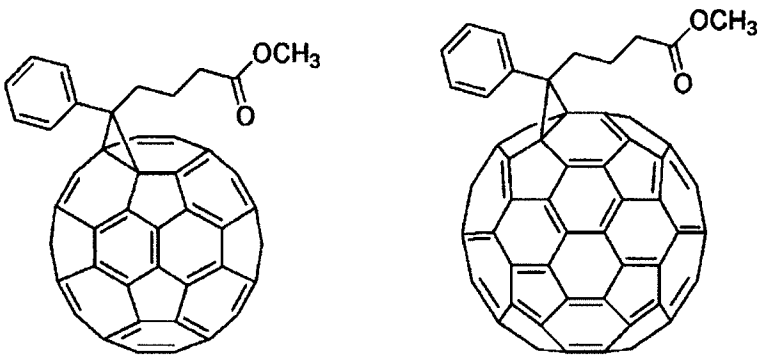

[60]PCBM [70]PCBM

Figure 1.21. Structures of [60]PCBM and [70]PCBM.

Poly(*p*-phenylene vinylene)s (**PPVs**) such as **MEH-PPV** and **MDMO-PPV** (Figure 1.22) are among the earliest conjugated polymers developed for p-type materials in the area of OSCs. The substituent on the **PPVs** allows for the tuning of the band gap. The HOMO and LUMO levels of unsubstituted **PPVs** were reported to be -5.1 and -2.7 eV, respectively, with a band gap around 2.4 eV. [50] Introducing two alkoxy groups on the phenylene ring can lower the LUMO level to -2.9 eV with the HOMO level unchanged and resulted in a lower band gap of 2.2 eV.[51] Using **PPVs** as electron donor, PCE values of 2-3% have been achieved.[51-54]

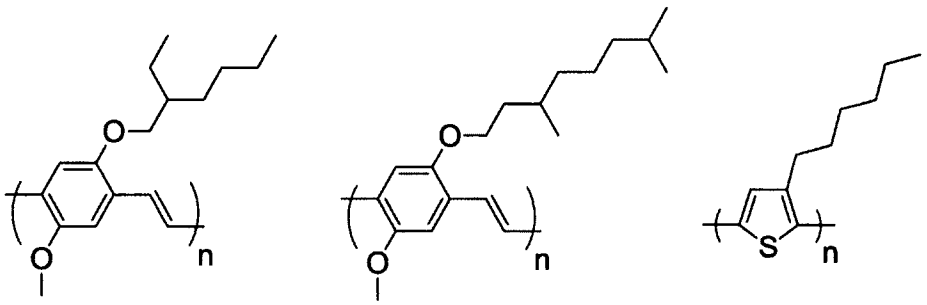

MEH-PPV MDMO-PPV P3HT

Figure 1.22. Structures of **PPVs** and **P3HT** polymers.

Poly(3-hexylthiophene) (**P3HT**) is also a widely investigated polymer donor (Figure 1.22). Because 3-hexylthiophene is an asymmetrical molecule, head to tail (HT) and head to head (HH) coupling are both possible. Mixture of both couplings can result in regioirregular **P3HT** in which planarity of the polymer was negatively affected. Some metal-catalyzed coupling methods were developed and successfully applied to the synthesis of regioregular **P3HT**.[55-58] Regioregular **P3HT** showed various outcomes including red shifted absorption in solid state and increase in mobility of the charge carriers. HOMO and LUMO levels of regioregular **P3HT** are -5.2 and -3.2 eV, repectively, with an optical band gap of 2 eV. PCE values of 3-5% have been reported. [59-66]

Continuous research was done based on classic **PPVs** and **P3HT**, however the improvements were hardly achieved. The research interest started moving to new D-A conjugated polymers due to the advantages of tunable energy levels and band gaps, large absorption coverage, higher carrier mobility. In the past decade, a variety of D-A polymers were synthesized and investigated in the OSC application and they were showing moderate to excellent performance. In the next section, a review of benzothiadiazole based and diketopyrrolopyrrole based materials will be given.

1.4 D-A conjugated oligomers or polymers used in OSCs

1.4.1 Benzothiadiazole based polymers

Benzothiadizole (**BT**) is an electron deficient heterocycle and has been used to construct n-type semiconducting polymers showing high electron mobility. Recently, **BT** was utilized as acceptor unit to synthesize low band gap conjugated materials to

fulfill the needs of p-type polymers in the area of OSCs. Materials containing **BT** unit have been extensively studied and outstanding photovoltaic performances were achieved, which will be described below.

Svensson and coworkers reported an alternating polyfluorene copolymer **I-30** containing **BT** as electron acceptor in 2003 (Figure 1.23).[67] The molecular weight M_w of **I-30** was specially controlled to 1.4 kg/mol due to the solubility problem. The polymer showed maximum absorption at 545 nm in the solid state. Devices with the configuration ITO/PEDOT:PSS/**I-30**:PCBM(1:4)/LiF/Al gave an impressive PCE value of 2.20% which is very close to the 2.50% PCE record of **MDMO-PPV** at that time (Table 1.1).

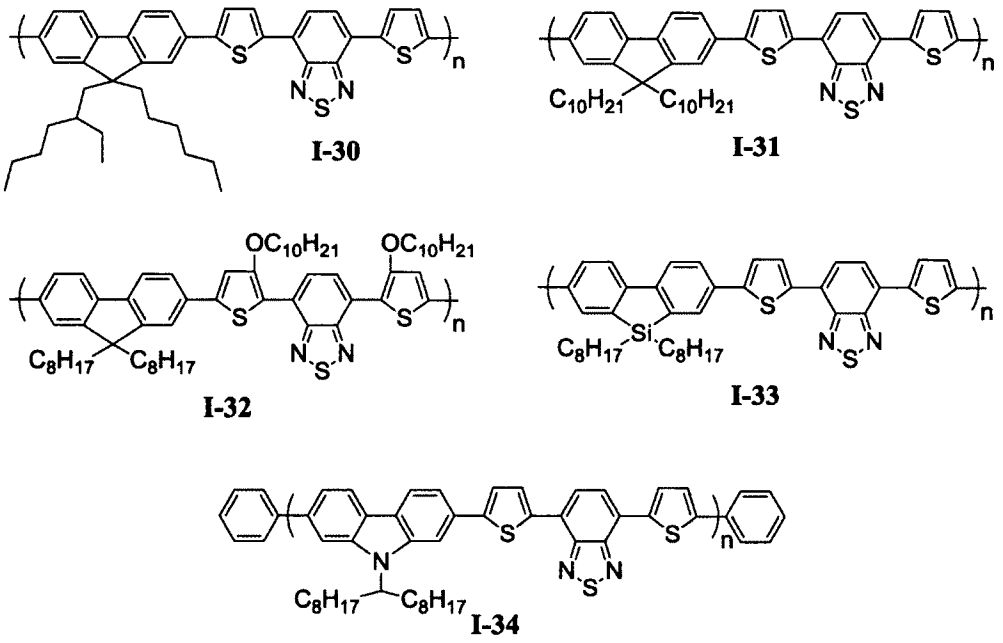

Figure 1.23. BT based polymers.

In 2007, Sloof et al. described polymer **I-31** (Figure 1.23).[68] Although the polymer back bone is the same as **I-30**, by introducing two decyl groups, the solubility of the polymer was improved and resulted in a high molecular weight of

58.4 kg/mol. Consequently, the PCE of the device increased significantly to 4.2% with a large FF of 54% (Table 1.1).

Shi et al. introduced alkoxy groups on the 3 position of thiophene in polymer **I-32** to enhance the electron donating ability of the donor unit (Figure 1.23).[69] As a result, **I-32** showed red shifted maximum absorption at 581 nm as film and a narrow band gap of 1.78 eV. The photovoltaic performance of device with the configuration ITO/PEDOT:PSS/**I-32**:PCBM(1:4)/LiF/Al was evaluated, and a J_{sc} of 4.3 mA/cm^2, a V_{oc} of 0.76 V, an FF of 48.6% and a PCE of 1.60% were reported (Table 1.1).

Polymer **I-33** containing 2,7-silafluorene as donor was reported by Wang et al. in 2008 (Figure 1.23).[70]. Replacing the carbon with silicon resulted in red shifted absorption, narrower band gap and much higher hole mobility for the polymer. The device with configuration of ITO/PEDOT:PSS/**I-33**:PCBM(1:2)/Al gave a J_{sc} of 9.50 mA/cm^2, a V_{oc} of 0.90 V, an FF of 50.7 % and a PCE of 5.40% (Table 1.1). The higher V_{oc} and FF is attributed to the lower HOMO level and good hole transport properties of the polymer, whereas the high J_{sc} is attributed to the broader absorption.

Due to the excellent behavior of carbazole in photoconductor [71,72] and OLEDs [73], it was introduced by Blouin et al. to construct donor acceptor copolymer **I-34** with **BT** in use of BHJ OSCs (Figure 1.23). [74] In order to increase the stability, the ends of the polymer were capped with benzene rings. The device configuration was ITO/PEDOT:PSS/**I-34**:PCBM(1:4)/Al. The PCE obtained from this device was 3.60% (Table 1.1).

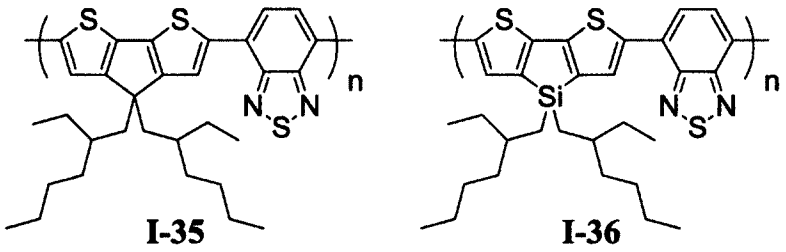

Figure 1.24. Polymers containing **BT** as acceptor and dithiophene as donor.

Mühlbacher et al. first reported a low band gap polymer **I-35** utilizing cylcopentadithiophene (**CPDT**) unit as the donor block (Figure 1.24).[75] Since **CPDT** is a strong donor, coupling with **BT** resulted in a low band gap of 1.73 eV. The solid-state absorption reached a maximum peak at 775 nm with a strong tail extending into the near-infrared region. The device made of **I-35**/[70]PCBM showed better PCE of 3.2% comparing the one made of **I-35**/[60]PCBM. However, the V_{oc} was only 0.65 eV due to the high HOMO level of the polymer (Table 1.1). With the same polymer, Peet et al. claimed significant improvement in PCE by incorporating a few volume per cent of alkanedithiols in the solution used to spin-cast active layers.[76] The dithiols influenced the morphology of the film as well as the physical interactions between the polymer chains and fullerene phases to yield higher photocurrent and FF. An impressive PCE of 5.50% was observed with J_{sc} of 16.20 mA/cm^2 and FF of 55.0% (Table 1.1).

In order to increase the mobility of polymer **I-35**, silicon was introduced on **CPDT** by Hou et al (Figure 1.24).[77] The absorption of **I-36** is similar to **I-35**, however, the hole mobility is 3 times higher than that of **I-35**. A high PCE of 5.1% was observed for the device with the configuration of ITO/PEDOT:PSS/**I-36**:PCBM(1:1)/Ca/Al. The J_{sc} and FF were 12.70 mA/cm^2 and 55.0%, respectively. V_{oc} was still low, only 0.68 V (Table 1.1).

1.4.2 Benzothiadiazole based small molecules

Despite the advantages of polymer materials such as good film-forming characteristics and film morphology, the polymers suffer from poor synthetic reproducibility and difficult purification procedures, which hinder their commercial viability. Small-molecule materials, however, offer advantages over polymeric materials in terms of ease of synthesis and purification, which greatly improves fabrication reproducibility, as well as possessing a greater tendency to self-assemble into ordered domains, which leads to high charge carrier mobilities. These properties make small molecules a promising class of donor material for BHJ solar cell applications.

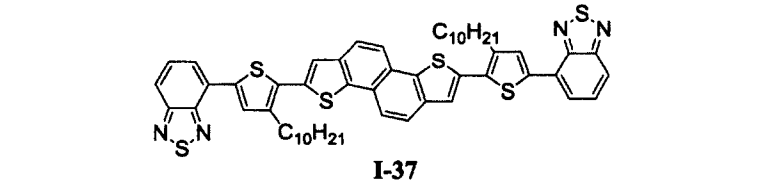

I-37

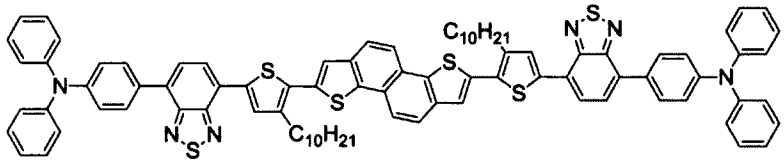

I-38

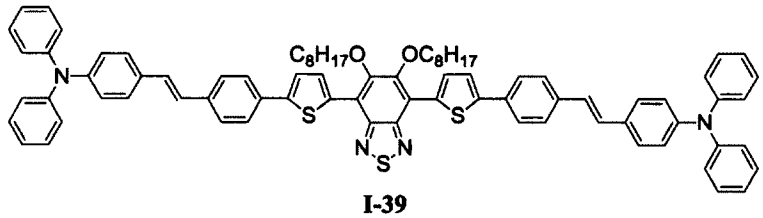

I-39

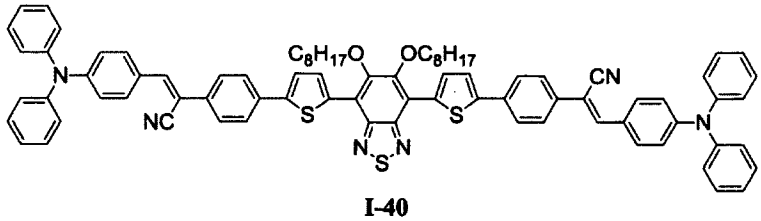

I-40

Figure 1.25. BT based small molecules **I-37** to **I-40**.

In 2011, naphthodithiophene (**NDT**) was designed by Dutta et al. and was coupled with **BT** unit to form low band gap compounds **I-37** and **I-38** (Figure 1.25). [78] Since **NDT** is a planar building block with rigid fused symmetrical structure, it was expected to reduce the band gap and enhance π-π stacking in the D-A molecules and thus improve the charge generation and charge transport. Compound **I-38** has broader and red shifted absorption at around 533 nm due to the terminal triphenylamine units. The optical band gaps of **I-37** and **I-38** were reported to be 2.16 and 1.96 eV, respectively. They had the same V_{oc} of 0.90 V in photovoltaic performance, however, due to the large difference in J_{sc}, compound **I-38** had better PCE of 2.2% (Table 1.1).

Zeng et al. reported two low band gap compounds **I-39** and **I-40** based on **BT** and triphenylamine (Figure 1.25).[79] The absorptions of both compounds cover 300 to 600 nm region. However, compound **I-40** has larger absorption intensity in the region of 500 nm, so that it can harvest more photons and contribute to a higher J_{sc} of 11.2 mA/cm^2 compared to that of compound **I-39**. Moreover, the HOMO level of compound **I-40** is lower, because of the introduction of cyano groups, resulting in a higher V_{oc} of 1.04 eV. Finally, a remarkable PCE of 3.85% was obtained from the device made of **I-40** (Table 1.1).

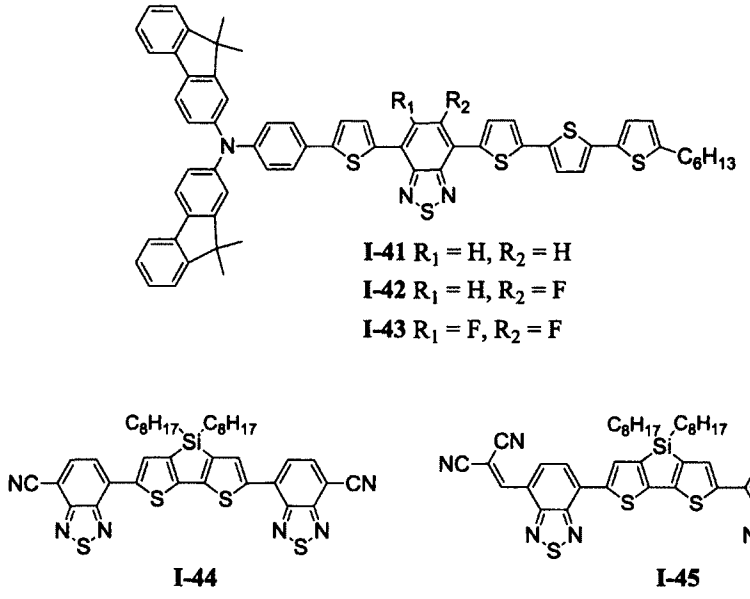

Figure 1.26. BT based small molecules **I-41** to **I-45**.

Paek and coworker developed a series of fluorine substituted p-type molecules **I-42** and **I-43** with unsymmetrical D_A-A-D_B structure (Figure 1.26).[80] Although the new structure didn't bring significant improvements in the photovoltaic performance, the introduction of fluorine led to a low lying HOMO level and a higher hole mobility for **I-43**, which contributed to V_{oc} of 0.84 V and PCE of 3.24% (Table 1.1).

Recently, Lin et al. proposed two **BT** based compounds **I-44** and **I-45** with a new structure of acceptor-acceptor-donor-acceptor-acceptor (A-A-D-A-A) (Figure 1.26).[81] Dithienosilole was selected as the donor at the center, where connected by **BT** and cyano or dicyanovinylene moieties. Because of the stronger electron-withdrawing dicyanovinylene end groups, **I-45** possesses a lower-lying LUMO level, leading to a reduced band gap of 1.70 eV. However, the thin film made of **I-45** showed a higher electron affinity than fullerene, therefore, it was hardly suitable to be paired with fullerene acceptors. In contrast, device made of **I-44** showed good performance with J_{sc} of 9.79 mA/cm^2, V_{oc} of 1.01 V and PCE of 3.70% (Table 1.1).

Table 1.1. Energy levels and device performance from **BT** based materials.

Material	HOMO (eV)	LUMO (eV)	Band gap(eV)	V_{oc} (V)	J_{sc} (mA/cm^2)	FF (%)	PCE (%)	Ref
I-30	NA	NA	NA	1.04	4.66	46.0	2.20	67
I-31	NA	NA	NA	1.00	7.70	54.0	4.20	68
I-32	-5.14	NA	1.64	0.76	4.31	48.6	1.60	69
I-33	-5.70	-3.81	1.85	0.90	9.50	50.7	5.40	70
I-34	-5.50	-3.60	1.88	0.89	6.92	63.0	3.60	74
I-35	-5.30	-3.57	1.73	0.65	11.00	47.0	3.20	75
				0.62	16.20	55.0	5.50	76
I-36	-5.05	-3.27	1.78	0.68	12.70	55.0	5.10	77
I-37	-5.16	-3.18	2.16	0.93	3.79	28.0	0.98	78
I-38	-5.34	-3.34	1.96	0.95	6.18	37.0	2.20	78
I-39	-5.25	-3.30	1.95	0.94	6.33	33.0	1.99	79
I-40	-5.32	-3.33	1.99	1.04	11.20	33.0	3.85	79
I-41	-5.09	-3.79	1.97[a]	0.80	9.29	38.0	2.70	80
I-42	-5.09	-3.76	1.98[a]	0.81	9.37	40.0	3.05	80
I-43	-5.12	-3.71	2.02[a]	0.84	9.45	41.0	3.24	80
I-44	-5.40	-3.23	2.09	1.01	9.79	38.0	3.70	81
I-45	-5.80	-3.92	1.70	NA	NA	NA	NA	81

[a] Optical band gap.

1.4.3 Diketopyrrolopyrrole based polymers

As a class of brilliant high-performance pigment, 3,6-diaryl-2,5-dihydropyrrolo[3,4-c]pyrrole-1,4-dione (**DPP**) has been applied in paints, plastic ink, electroluminescent devices, and transistors.[82-88] The **DPP** unit has a well-conjugated structure, which leads to strong π-π interaction, and the lactam part makes the **DPP** unit exhibit a high electron-withdrawing effect. Therefore, **DPP** is a very promising acceptor unit for constructing photovoltaic materials.

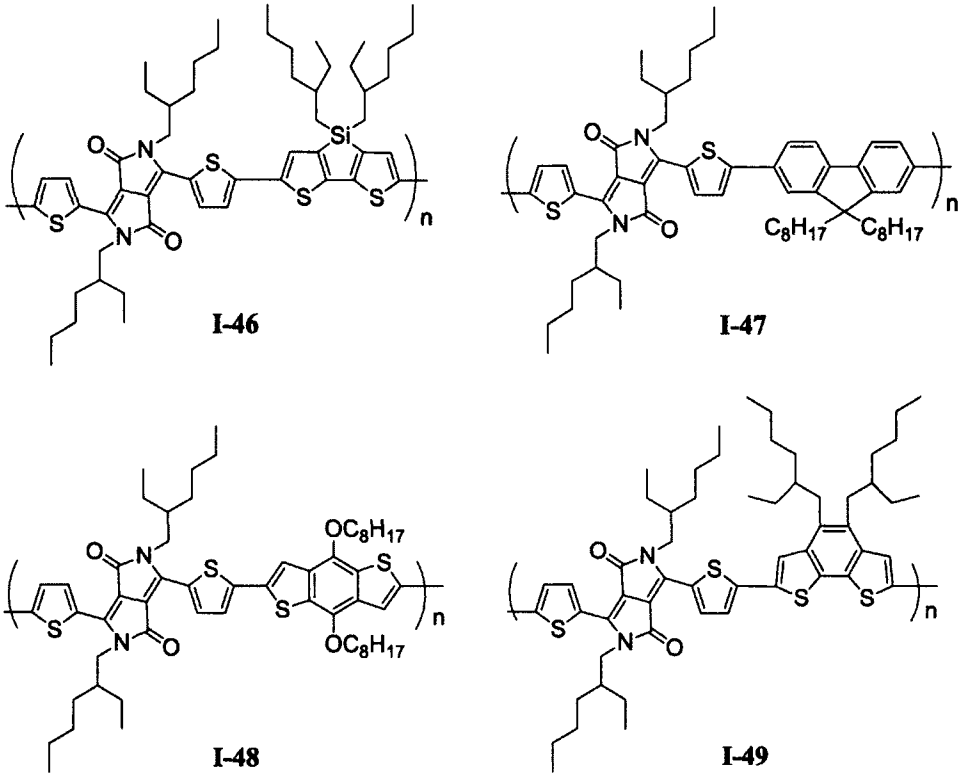

Figure 1.27. DPP based polymers **I-45** to **I-49**.

In 2009, Hou and coworkers reported a series of **DPP** based low band gap polymers **I-46** to **I-49** synthesized by introducing different donor building blocks (Figure 1.27).[89] The band gaps as well as their energy levels can be tuned by changing the electron-donating units. All polymers showed absorption peaks in the 500 to 900 nm region due to the ICT of the conjugated backbone. Since dithienosilole

was most electron rich donor among the four, polymer **I-46** showed the longest absorption of 798 nm, highest HOMO level of -5.04 eV and lowest band gap of 1.57 eV. In contrast, polymer **I-47** has the lowest HOMO level of -5.23 eV with maximum absorption at 649 nm and a band gap of 1.63 eV due to weak eletron-donating ability of fluorene. However, **I-46** with the lowest band gap was not showing the best PCE in the photovoltaic performance. Because of low V_{oc} resulting from its high HOMO level, the PCE of **I-46** was only 2.10%. Polymer **I-47** has the highest V_{oc}, but the lowest PCE due to its low J_{sc}. The best PCE of 4.31% came from polymer **I-49**, with V_{oc} of 0.68 V and J_{sc} of 10.1 mA/cm^2 (Table 1.2).

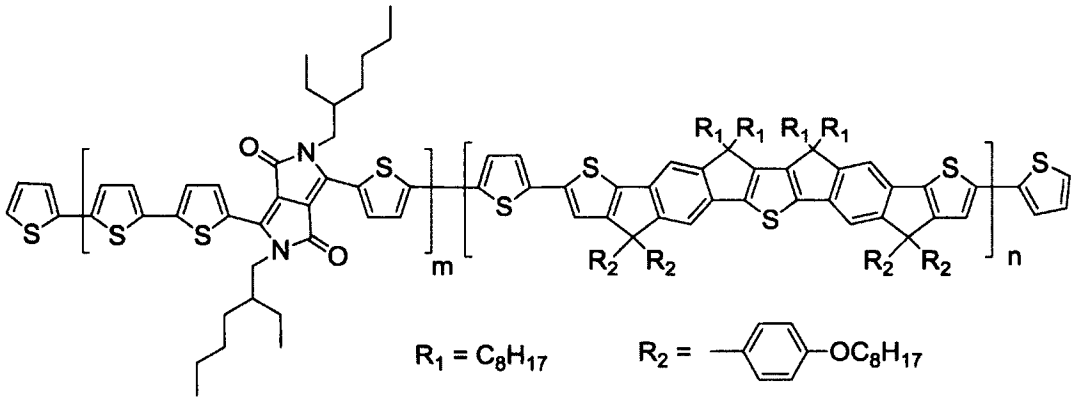

I-50 (m:n=1:1); **I-51** (m:n=2:1); **I-52** (m:n=3:1)

Figure 1.28. DPP based polymers **I-50** to **I-52**.

In 2011, Chen et al. developed a ladder-type thienyl-phenylene-thienyl-phenlylene-thienyl (**TPTPT**) unit where each thiophene ring was covalently fastened with the adjacent benzene rings by carbon bridges (Figure 1.28).[90] Then **TPTPT** was introduced in the formation of low band gap polymers with **DPP** in order to maintain a highly planar structure in the conjugated backbone. The molar feed ratio of **DPP** to **TPTPT** was adjusted to be 1:1, 2:1 and 3:1 and the corresponding polymers were **I-50**, **I-51**, **I-52**. As the content of **TPTPT** decreased, the HOMO level

decreased from -5.16 eV to -5.24 eV, whereas, the band gap increased from 1.73 eV to 1.85 eV. The best PCE of 4.3 % was obtained from polymer **I-51** which was attributed to the broader absorption window and higher hole mobility (Table 1.2).

1.4.4 Diketopyrrolopyrrole based small molecules

In 2008, Nguyen and coworkers reported a solution processable oligothiophene **I-53** with **DPP** as acceptor (Figure 1.28).[91] The optical absorption of this compound can reach up to 720 nm in the solution and 820 nm as film. The optical band gap is 2.01 eV. The solar cells fabricated by **I-53** and [60]PCBM exhibited PCE as high as 2.33% at the blend ratio of 7:3. One of the factors that contributed to the good photovoltaic performance was that **I-53** showed ordered aggregation in the solid state as evidenced by weak photoluminescence and fiber-like structures in AFM images (Table 1.2).

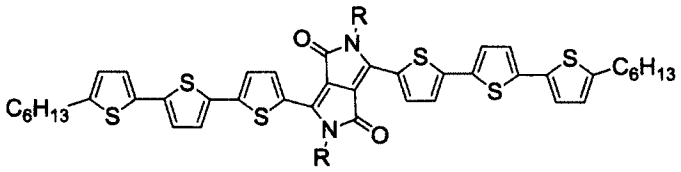

I-53 R =

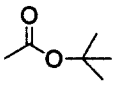

I-54 R =

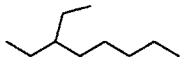

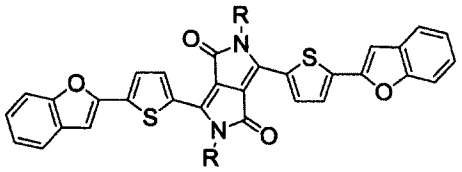

I-55 R =

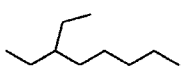

Figure 1.29. DPP based small molecules **I-53** to **I-55**.

The following year, they replaced the t-Boc groups with ethylhexyl groups and obtain compound **I-54** (Figure 1.29).[92] Additional absorption band was observed centered at 720 nm in solid state which was assigned to the strong intermolecular interaction. In comparison to the t-Boc derivative, **I-54** is more soluble and thermal stable and possesses a lower HOMO level. High degree of ordering was maintained in both pure film and blended films, resulting in good hole mobility. An improved PCE of 3.0% was obtained, with a high J_{sc} of 9.20 mA/cm^2 (Table 1.2).

In order to increase the open-circuit voltage of the BHJ solar cells, Nguyen's group designed **I-55** which contains benzofuran units (Figure 1.28).[93] It was found that the new compound has a deep HOMO level of -5.2 eV and good absorption properties with large spectral coverage. The frontier orbitals of this donor system are appropriately matched with the common fullerene acceptor [70]PCBM, which resulted in an effective charge transfer process. After thermal annealing, the BHJ solar cell based on **I-55** and [70]PCBM exhibited increased conversion of 4.40% with a high V_{oc} value of 0.92 V (Table 1.2).

Table 1.2. Energy levels and device performance from **DPP** based materials.

Material	HOMO (eV)	LUMO (eV)	Band gap(eV)	V_{oc} (V)	J_{sc} (mA/cm^2)	FF (%)	PCE (%)	Ref
I-46	-5.04	-3.47	1.57	0.55	7.50	50.8	2.10	89
I-47	-5.23	-3.60	1.63	0.78	2.00	49.9	0.78	89
I-48	-5.16	-3.51	1.65	0.68	8.40	44.3	2.53	89
I-49	-5.21	-3.63	1.58	0.68	10.10	62.7	4.31	89
I-50	-5.16	-3.43	1.73	0.70	9.64	54.0	3.60	90
I-51	-5.21	-3.41	1.80	0.68	10.78	58.0	4.30	90
I-52	-5.24	-3.39	1.85	0.68	9.27	65.0	4.10	90
I-53	-5.03	-3.00	2.03	0.67	8.42	45.0	2.33	91
I-54	-5.20[b]	NA	NA	0.75	9.20	44.0	3.00	92
I-55	-5.20[b]	3.40[c]	1.70[a]	0.92	10.0	48.0	4.40	93

[a] Optical band gap. [b] Determined by ultraviolet photoelectron spectroscopy (UPS). [c] Calculated from HOMO level and optical band gap.

1.5 Rationale and Objectives

Organic solar cells have been of great interest in recent years due to the demand of clean energy resource and their unique advantages. In order to improve the efficiency to meet the requirements of the commercialization, the effort of exploring potential materials is never ending. Among hundreds of polymers or small molecules, **DPP** and **BT** based materials show excellent performance in the area of OSCs. However, there are still problems to be solved and room for improvement.

In terms of electron withdrawing ability, **DPP** is very strong and can lead to strong absorption covering from 500 to 800 nm, after coupling with different donors. However, the absorption in region of 400 to 500 nm is rather weak. In order to

increase the short circuit current, it is necessary to put this blank region in use. As previously discussed, the band gap can be tuned by adjusting the electron withdrawing ability of the acceptors. Therefore, the first objective of this thesis research is to design and synthesize an acceptor with weak electron withdrawing ability that can provide a suitable band gap in order to absorb light in the region of 400 to 500 nm. If weak acceptors and **DPP** are both introduced in one polymer, the polymer is expected to absorb a broader range of solar irradiation and thus improve the photovoltaic performance.

BT is another important acceptor that needs some improvements. Comparing to **DPP**, the electron withdrawing ability of **BT** is weak. The absorption of the polymers containing **BT** can hardly reach to 600 nm and the band gap is also relatively large. As discussed above, fusing a number of imine groups on **BT** could enhance the electron withdrawing ability. However, addition of two imine groups make it too electron deficient, pushing the absorption beyond 700 nm. Thus, the second objective of this thesis research is to adjust the electron withdrawing ability of **BT** by adding only one imine group. Therefore, the new acceptor is expected to give suitable band gap as well as a suitable absorption centered at 600 nm.

References

(1) Roncali, J. *Chem. Rev.* **1997**, *97*, 173.

(2) Brédas, J. L. *J. Chem. Phys.* **1985**, *82*, 3808.

(3) Mulliken, R. S.; Rieke, C. A.; Brown, W. G. *J. Am. Chem. Soc.* **1941**, *63*, 41.

(4) Brédas, J. L.; Street, G. B.; Themans, B.; André, J. M. *J. Chem. Phys.* **1985**,

83, 1323.

(5) Xu, B.; S. Holdcroft, S. *Macromolecules*, **1993**, *26*, 4457.

(6) McCullough, R. D.; Lowe, R. D.; Jayraraman, M.; Anderson, D. L. *J. Org. Chem.* **1993**, *58*, 904.

(7) Hernandez, V.; Castiglioni, C.; Del Zopo, M.; Zerbi, G. *Phys. Rev. B* **1994**, *50*, 9815.

(8) Andes Hess, B. Jr.; Schaad, L. J. *J. Am. Chem. Soc.* **1971**, *93*, 305.

(9) Andes Hess, B. Jr.; Schaad, L. J. *J. Am. Chem. Soc.* **1973**, *95*, 3907.

(10) Lowe, J. P.; Kafafi, S. A. *J. Am. Chem. Soc.* **1984**, *106*, 5837.

(11) Kim, Y.; Cook, S.; Tuladhar, S. M.; Choulis, S. A.; Nelson, J.; Durrant, J. R.; Bardley, D. D. C.; Gles, M.; Mcculloch, I.; Ha, C.; Ree, M. *Nat. Mater.* **2006**, *5*, 197.

(12) Woo, C. H.; Thompson, B. C.; Kim, B. J.; Toney, M. F.; Fréchet, J. M. J. *J. Am. Chem. Soc.* **2008**, *130*, 16324.

(13) Havinga, E. E.; ten Hoeve, W.; Wynberg, H. *Polym. Bull.* **1992**, *29*, 119.

(14) Brocks, G.; Tol, A. *J. Phys. Chem.* **1996**, *100*, 1838.

(15) Zhang, Q. T.; Tour, J. M. *J. Am. Chem. Soc.* **1998**, *120*, 5355.

(16) Zotti, G.; Zecchin, S.; Schiavon, G. *Chem. Mater.* **1997**, *9*, 1876.

(17) Lin, S. C.; Chen, J. A.; Liu, M. H.; Su, Y. O.; Leung M. *J. Org. Chem.* **1998**, *63*, 5059.

(18) M. Karikomi, C. Kitamura, S. Tanaka, Y. Yamashita *J. Am. Chem. Soc.* **1995**, *117*, 6791-6792.

(19) C. Kitamura, S. Tanaka, Y. Yamashita *Chem. Mater.* **1996**, *8*, 570-578.

(20) Qian, G.; Zhong, Z.; Luo, M.; Yu, D.; Zhang, Z.; Wang, Z. Y.; Ma, D. *Adv. Mater* **2009**, *21*, 111.

(21) Qian, G.; Dai, Bo; Luo, M.; Yu, D.; Zhan, J.; Zhang, Z.; Ma, D.; Wang, Z. Y. *Chem. Mater.* **2008**, *20*, 6208.

(22) Wudl, F.; Kobayashi, M.; Heeger, A. J. *J. Org. Chem.* **1984**, *49*, 3382.

(23) Ikenoue, Y.; Wudl, F.; Heeger, A. J. *Synth. Met.* **1991**, *40*, 1.

(24) Pomerantz, M.; Gu, X. *Synth. Met.* **1997**, *84*, 243.

(25) Hagan, A. J.; Moratti, S. C.; Sage, I. C. *Synth. Met.* **2001**, *119*, 147.

(26) Mashima, A. *Synth. Met.* **1995**, *11*, 75.

(27) Mondal, R.; Shah, B. K.; Necker, D. C. *J. Am. Chem. Soc.* **2006**, *128*, 9612.

(28) Wöhrle, D.; Meissner, D. *Adv. Mater*, **1991**, *3*, 129.

(29) Kearns, D.; Calvin, M. J. *Chem. Phys.* **1958**, *29*, 950.

(30) Ghosh A.K.; Morel, D. L.; Feng, T.; Shaw, R. F.; Rowe, C. A. Jr. *J. Appl. Phys.* **1974**, *45*, 230.

(31) Tang, C. W. *Appl. Phys. Lett.* **1986**, *48*, 183.

(32) Sariciftci, N.S.; Braun, D.; Zhang, C.; Srdanov, V. I.; Heeger, A. J.; Stucky, G.; Wudl, F. *Appl. Phys. Lett.* **1993**, *62*, 585.

(33) Halls J. J. M.; Pichler, K.; Friend R. H.; Moratti, S. C.; Holmes, A. B. *Appl. Phys. Lett.* **1996**, *68*, 3120.

(34) Yu, G; Gao, J.; Hummelen, J. C.; Wudl, F.; Heeger, A. J. *Science* **1995**, *270*, 1789.

(35) Cheng, Y. J.; Yang, S. H.; Hsu, C. S. *Chem. Rev.* **2009**, *109*, 5868.

(36) Liang, Y. Y.; Yu, L. P. *Polym. Rev.* **2010**, *50*, 454.

(37) Hou, J. H.; Chen, H. Y.; Zhang, S. Q.; Li, G.; Yang, Y. *J. Am. Chem. Soc.* **2008**, *130*, 16144.

(38) Chen, H. Y.; Hou, J.; Hayden, A. E.; Yang, H.; Houk, K. N.; Yang, Y. *Adv. Mater.* **2010**, *22*, 371.

(39) Scharber, M. C.; Mühlbacher, D.; Koppe, M.; Denk, P.; Waldauf, C.; Heeger, A. J.; Brebec, C. J. *Adv. Mater.* **2006**, *18*, 789.

(40) Blouin, N.; Michaud, A.; Leclerc, M. *Adv. Mater.* **2007**, *19*, 2295.

(41) Zhou, Q.; Hou, Q.; Zheng, L.; Deng, X.; Yu, G.; Cao, Y. *Appl. Phys. Lett.* **2004**, *84*, 1653.

(42) Gadisa, A.; Mammo, W.; Anderson, M.; Admassie, S.; Zhang, F.; Adersson, M. R.; Inganäs, O. *Adv. Funct. Mater.* **2007**, *17*, 3836.

(43) Chen, D.; Liu, F.; Wang, C.; Nakahara, A.; Russell, T. P. *Nano Lett.* **2011**, *11*, 2071.

(44) Allemond, P. M.; Koch, A.; Wudl, F.; Rubin, Y.; Diederich, F.; Alvarez, M. M.; Anz, S. J.; Whetten, R. L. *J. Am. Chem. Soc.* **1991**, *113*, 1050.

(45) Sariciftci, N. S.; Smilowitz, L.; Heeger, A. J.; Wudl, F. *Science* **1992**, *258*, 1474.

(46) Morita, S.; Zakhidov, A. A.; Yoshino, K. *Solid State Commun.* **1992**, *82*, 249.

(47) Hummelen, J. C.; Knight, B. W.; LePeg, F.; Wudl, F. *J. Org. Chem.* **1995**, *60*, 532.

(48) Wienk, M. M.; Kroon, J. M.; Verhees, W. J. H.; Knol, J.; Hummelen, J. C.; van Hal, P. A.; Janssen, R. A. J. *Angew. Chem., Int. Ed.* **2003**, *42*, 3371.

(49) Yao, Y.; Shi, C.; Li, G.; Shrotriya, V.; Pei, Z.; Yang, Y. *Appl. Phys. Lett.* **2006**,

89, 153507.

(50) Alam, M. M.; Jenekhe, S. A. *Chem. Mater.* **2002**, *14*, 4775.

(51) Hoppe, H.; Sariciftci, N. S. *J. Mater. Chem.* **2006**, *16*, 45.

(52) Shaheen, S.; Brabec, C. J.; Sariciftci, N. S.; Padinger, F.; Fromherz, T.; Hummelen, J. C. *Appl. Phys. Lett.* **2001**, *78*, 841.

(53) Zheng, L.; Zhou, Q.; Deng, X.; Yuan, M.; Yu, G.; Cao, Y. *J. Phys. Chem. B* **2004**, *108*, 11921.

(54) Wang, L.; Liu, Y.; Jiang, X.; Qin, D.; Cao, Y *J. Phys. Chem. C* **2007**, *111*, 9538.

(55) Sheina, E. E.; Liu, J.; Iovu, M. C.; Laird, D. W.; McCullough, R. D. *Macromolecules* **2004**, *37*, 3526.

(56) Iovu, M. C.; Sheina, E.; Gil, R. R.; Laird, D. W.; McCullough, R. D. *Macromolecules* **2005**, *38*, 8649.

(57) Yokoyama, A.; Miyakoshi, R.; Yokozawa, T. *Macromolecules* **2004**, *37*, 1169.

(58) Miyakoshi, R.; Yokoyama, A.; Yokozawa, T. *J. Am. Chem. Soc.* **2005**, *127*, 17542.

(59) Moule, A. J.; Meerholz, K. *Adv. Mater.* **2008**, *20*, 240.

(60) Li, G.; Shrotriya, V.; Huang, J.; Yao, Y.; Moriarty, T.; Emery, K.; Yang, Y. *Nat. Mater.* **2005**, *4*, 864.

(61) Chu, C.-W.; Yang, H.; Hou, W. J.; Huang, J.; Li, G.; Yang, Y. *Appl. Phys. Lett.* **2008**, *92*, 103306.

(62) Miller, S.; Fanchini, G.; Lin, Y.-Y.; Li, C.; Chen, C.-W.; Su, W.-F.; Chhowalla, M. *J. Mater. Chem.* **2008**, *18*, 306.

(63) Ma, W.; Yong, C.; Gong, X.; Lee, K.; Heeger, A. J. *Adv. Funct. Mater.* **2005**, *15*, 1617.

(64) Ayzner, A. L.; Wanger, D. D.; Tassone, C. J.; Tolbert, S. H.; Schwartz, B. J. *J. Phys. Chem. C* **2008**, *112*, 18711.

(65) Erb, T.; Zhokhavets, U.; Gobsch, G.; Raleva, S.; Stu¨hn, B.; Schilinsky, P.; Waldauf, C.; Brabec, C. J. *Adv. Funct. Mater.* **2005**, *15*, 1193.

(66) Berson, S.; de Bettignies, R.; Bailly, S.; Guillerez, S. *Adv. Funct. Mater.* **2007**, *17*, 1377.

(67) Svensson, M.; Zhang, F.; Veenstra, S. C.; Verhees, W. J. H.; Hummelen, J. C.; Kroon, J. M.; Inganäs, O.; Andersson, M. R. *Adv. Mater.* **2003**, *15*, 988.

(68) Slooff, L. H.; Veenstra, S. C.; Kroon, J. M.; Moet, D. J. D.; Sweelssen, J.; Koetse, M. M. *Appl. Phys. Lett.* **2007**, *90*, 143506.

(69) Shi, C.; Yao, Y.; Yang, Y.; Pei, Q. *J. Am. Chem. Soc.* **2006**, *114*, 8980.

(70) Wang, E.; Wang, L.; Lan, L.; Luo, C.; Zhuang, W.; Peng, J.; Cao, Y. *Appl. Phys. Lett.* **2008**, *92*, 33307.

(71) Hoegl, H. *J. Phys. Chem.* **1965**, *69*, 755.

(72) Grazulevicius, J. V.; Strohriegl, P.; Pielichowski, J.; Pielichowski, K. *Prog. Polym. Sci.* **2003**, *28*, 1297.

(73) Morin, J. F.; Leclerc, M.; Adès, D.; Siove, A. *Macromol. Rapid Commun.* **2005**, *26*, 761.

(74) Blouin, N.; Michaud, A.; Leclerc, M. *Adv. Mater.* **2007**, *19*, 2295.

(75) Mühlbacher, D.; Scharber, M.; Morana, M.; Zhu, Z.; Waller, D.; Gaudiana, R.; Brabec, C. *Adv. Mater.* **2006**, *18*, 2884.

(76) Peet, J.; Kim, J. Y.; Coates, N. E.; Ma, W. L.; Moses, D.; Heeger, A. J.; Bazan, G. C. *Nat. Mater.* **2007**, *6*, 497.

(77) Hou, J.; Cheng, H. Y.; Zhang, S.; Li, G.; Yang, Y. *J. Am. Chem. Soc.* **2008**, *130*,16144.

(78) Dutta, P.; Yang, W.; Eom, S. H.; Lee, W. H.; Kang, I. N.; Lee, S. H. *Chem. Commun.* **2012**, *48*, 573.

(79) Zeng, S.; Yin, L.; Ji, C.; Jiang, X.; Li, K.; Li, Y.; Wang, Y. *Chem. Commun.* **2012**, *48*, 10627.

(80) Paek, S.; Cho, N.; Song, K.; Jun, M. J.; Lee, J. K.; Ko, J. *J. Phys. Chem. C* **2012**, *116*, 23205.

(81) Lin, L. Y.; Lu, C. W.; Huang, W. C.; Chen, Y. H.; Lin, H. W.; Wong, K. T. *Org. lett.* **2011**, *13*, 4962.

(82) Beyerlein, T.; Tieke, B. *Macromol. Rapid Commun.* **2000**, *21*, 182.

(83) Cao, D.; Liu, Q.; Zeng,W.; Han, S.; Peng, J.; Liu, S. *J. Polym. Sci., Part A: Polym. Chem.* **2006**, *44*, 2395.

(84) Rabindranath, A. R.; Zhu, Y.; Heim, I.; Tieke, B. *Macromolecules* **2006**, *39*, 8250.

(85) Zhu, Y.; Rabindranath,A. R.; Beyerlein, T.; Tieke, B. *Macromolecules* **2007**, *40*, 6981.

(86) Zhang, K.; Tieke, B. *Macromolecules* **2008**, *41*, 7287.

(87) Burgi, L.; Trubiez, M.; Pfeiffer, R.; Bienewald, F.; Kirner, H. J.; Winnewisser, C. *Adv. Mater.* **2008**, *20*, 2217.

(88) Tantiwiwat, M.; Tamayo, A. B.; Luu, N.; Dang, X. D.; Nguyen, T. Q. *J. Phys.*

Chem. C **2008**, *112*, 17402.

(89) Huo, L.; Hou, J.; Chen, H. Y.; Zhang, S.; Jiang, Y.; Chen, T. L.; Yang, Y. *Macromolecules* **2009**, *42*, 6564.

(90) Chen, C. H.; Cheng, Y. J.; Chang, C. Y.; Hsu, C. S. *Macromolecules* **2011**, *44*, 8415.

(91) Tamayo, A. B.; Walker, B.; Nguyen, T. Q. *J. Phys. Chem. C* **2008**, *112*, 11545.

(92) Tamayo, A. B.; Dang, X. D.; Walker, B.; Seo, J.; Kent, T.; Nguyen, T. Q. *Appl. Phys. Lett.* **2009**, *94*, 103301.

(93) Walker, B.; Tamayo, A. B.; Dang, X. D.; Zalar, P.; Seo, J.; Garcia, A.; Tantiwiwat, M.; Nguyen, T. Q. *Adv. Funct. Mater.* **2009**, *19*, 3063.

Chapter 2 Design, Synthesis and Characterization of Benzo[f]-isoindole-1,3(2H)-dione and Pyromellitic Diimide Compounds and Polymers

2. 1 Introduction

Electron-accepting imide-functionalized arylenes have been widely studied for potential use as n-type organic semiconductors.[1-4] They are also attractive building blocks for donor-acceptor (D-A) conjugated polymers for two reasons: First, the imide nitrogen allows for attachment of aliphatic chains that can impart the solubility and alter chain packing and morphology of the polymer without changing the conjugation of the polymer backbone; second, energy levels of D-A conjugated polymers can be tuned by connecting various molecules with different electron-donating ability.[5]

Naphthalene diimide (**NDI**) [6-8] and perylene diimide (**PDI**) [9-11] have been extensively studied due to their planar structure and strong electron-withdrawing property (Figure 2.1). Various D-A conjugated polymers containing these arylene imides [12-16] have been synthesized and investigated for use in organic field effect transistor (OFET) and organic solar cell (OSC). Although they are satisfactory for some device applications,[17-21] their drawbacks still exist: 1) only 2 and 6 positions of **NDI** are available for bromination. After the coupling reaction or polymerization, the torsion angle between **NDI** and the aromatic substitutes is quite large in some cases due to steric hindrance brought by the carbonyl group of the imide, and decreases the planarity of the molecules or polymers. The same is true for **PDI**. 2)

Bromination of naphthalic anhydride affords mixtures of products.[14] Because it is very difficult and time consuming to separate each isomer, the mixtures are usually used directly, which tends to lead to the inconsistent performance for the devices due to uneven packing of the molecules, low molecular weights of polymers and so on. 3) Both **NDI** and **PDI** are considered to be strong acceptors; however there is lack of work for weaker imide acceptors that are required in some electronic device applications.

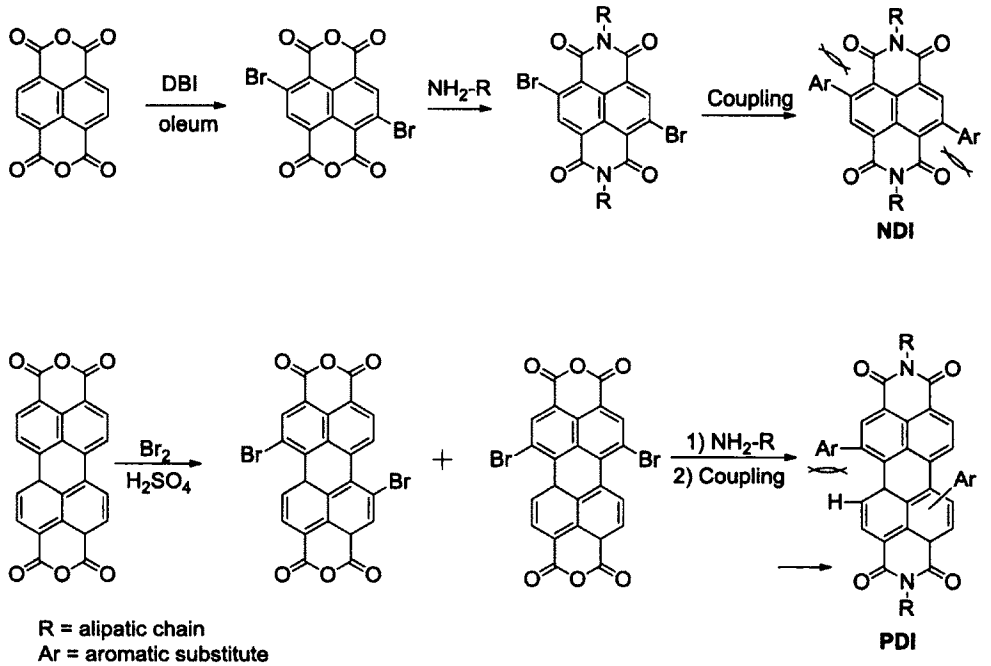

Figure 2.1. Functionalization of **NDI** and **PDI**.

Keeping the above drawbacks in mind, two new monomers, 4-(5-bromothiophen-2-yl)-2-(2-ethylhexyl)-9-phenyl-1H-benzo[f]isoindole-1,3(2H)-dione (**BIDO-1**) and 4,9-bis(5-bromothiophen-2-yl)-2-(2-ethylhexyl)-benzo[f]isoindole-1,3-dione (**BIDO-2**), were designed and synthesized (Figure 2.2). The imide building blocks still have naphthalene as a main core. However, by having the five-member ring imide at the 2 and 3 positions, steric hindrance is lowered significantly, making

the monomer more planar. The 1 and 4 positions of naphthalene are connected with aromatic groups. **BIDO-1** has one benzene and one thiophene on each side, **BIDO-2** has thiophene on both sides. The bromination is simple and straightforward, and affords one product. **BIDO-1** and **BIDO-2** were then coupled with different electron donating monomers to prepare small compounds and polymers. Their band gaps and optical properties were studied.

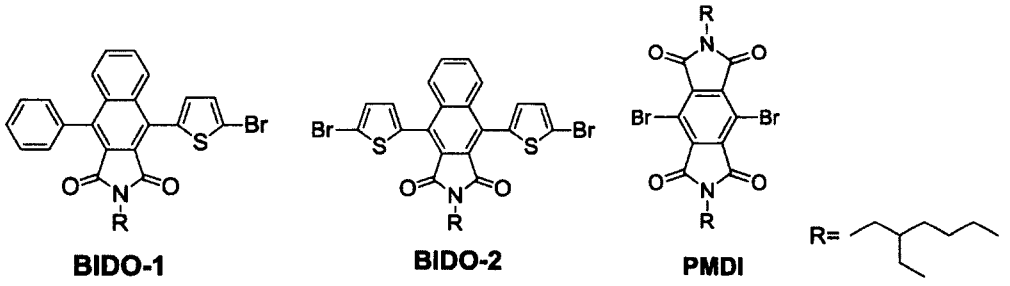

Figure 2.2. BIDO-1, BIDO-2 and **PMDI**.

Pyromellitic diimide (**PMDI**) has been overlooked as a building block for organic electronic materials. **PMDI** is widely used as monomers for aromatic polyimides for advanced applications in communications and aerospace.[21,22] There are very few examples of conjugated polymers having **PMDI** as the backbone and leaving the imide groups as side chains. Recently, Guo reported the donor–acceptor poly(phenylene ethynylene)s (**PPEs**) with **PMDI** as acceptor.[23] However, the **PPEs** have large band gap and are not successfully used in OFET and OSC.[24]

In order to lower the band gap, **PMDI**, as shown in Figure 2.2, was used as electron acceptor and polymerized with various electron donors, such as benzodithiophene. The properties of the resulting **PMDI**-based polymers were studied in this chapter and comparison was made with **BIDO** materials.

2. 2 Results and discussions

2. 2. 1 Synthesis of BIDO-1

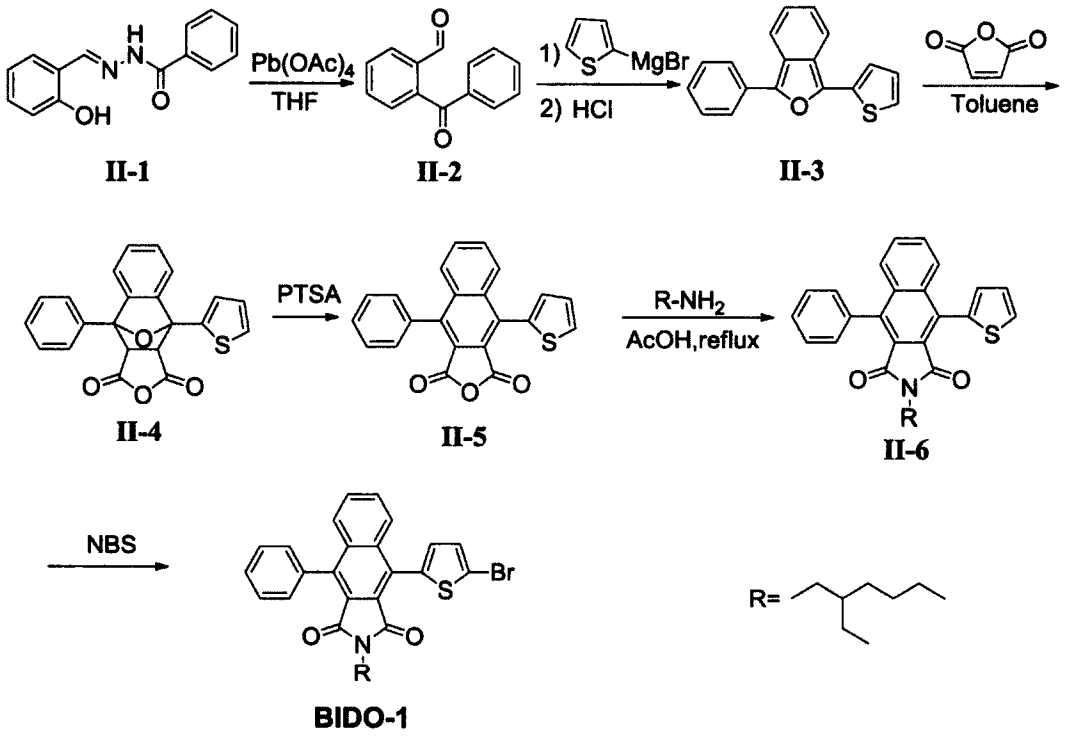

Scheme 2.1. Synthesis of **BIDO-1**.

The synthetic route toward monomer **BIDO-1** is depicted in Scheme 2.1. The synthesis started with oxidization of **II-1** by lead tetraacetate to yield **II-2**. It is a very simple method of making o-aroylbenzaldehyde. The mechanism of this carbon-carbon bond forming reaction, where the acyl group of the hydrazone formally replaces the phenolic hydroxyl group, has been elucidated by Kotali and Katritzky.[25]

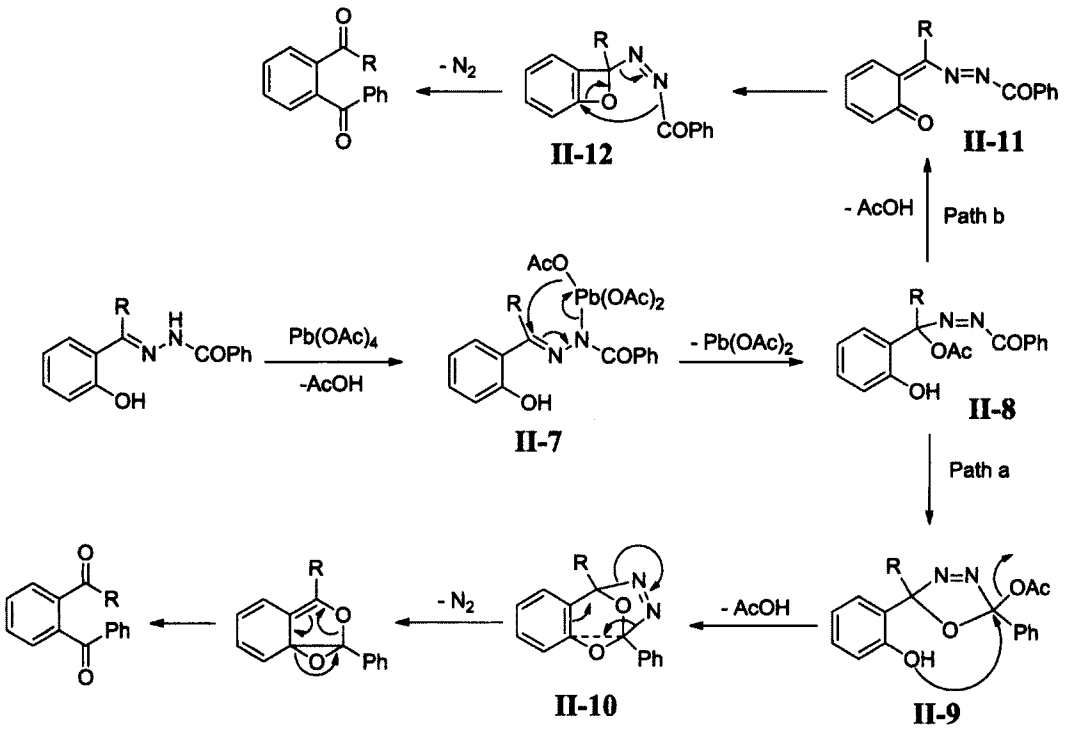

Scheme 2.2. Mechanism for synthesis of o-aroylbenzaldehyde.

The reaction initially proceeds for a substituted hydrazone with formation of the organolead intermediate **II-7,** followed by intramolecular acetoxy migration to the hydrazone carbon, giving azoacetate **II-8** (Scheme 2.2). Two possible reaction pathways for azoacetate **II-8** are initiated by either (path a) formation of 1,3,4-oxadiazoline **II-9** followed by loss of acetic acid to give the tricyclic 1,3-dioxane **II-10** or (path b) initial loss of acetic acid to give the quinone methide **II-11** and cyclization to the benzoxetane **II-12**. The two pathways differ in the origin of the two oxygens atoms of 1,2-diacylbenzene. Path a results in a migration of the original benzoyl oxygen to the hydrazone carbon, whereas in path b the benzoyl oxygen is retained. However, based on the experiment with oxygen-labeled benzoylhydrazone, path a was proved to be the right path way.

It was reported that addition of Grignard reagent to the sole aldehyde is very chemoselective at 0 °C for o-aroylbenzaldehyde. Accordingly, the reaction between **II-2** and Grignard reagent was carried out at 0 °C in dry THF.[26] After acidic hydrolysis by HCl, compound **II-3** was obtained in good yield. This compound is highly fluorescent, which is a common property of benzofuran; however, it is not stable for storage. **II-3** was immediately used in the next Diels-Alder reaction with maleic anhydride to produce compound **II-4**. The oxygen bridge was then removed by catalytic amount of *p*-toulenesulphonic acid to give compound **II-5**, followed by imidization in acetic acid with an access of 2-ethylhexylamine to form compound **II-6** in 91.5% yield. Bromination was done in acetic acid using N-bromosuccinimide to afford the final building block **BIDO-1**.

2. 2. 2 Synthesis of BIDO-2

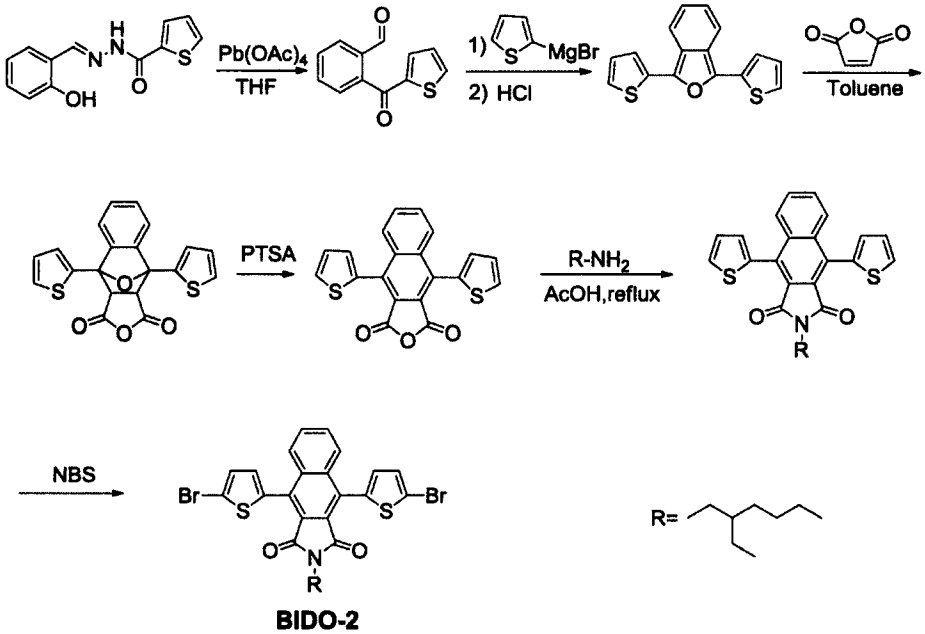

Scheme 2.3. Synthesis of **BIDO-2**.

The synthetic route toward monomer **BIDO-2** is depicted in Scheme 2.3. It follows the same procedure as for **BIDO-1** except for different starting material and bromination step. The starting material was changed into N'-benzylidenethiophene-2-carbohydrazide, which gives rise to a second thiophene group in the final product. Bromination was done in acetic acid at room temperature using N-bromosuccinimide and after about 1 hour, white precipitates came out of solution. Based on the NMR data, the white precipitate is mono-bromo compound and has poor solubility in acetic acid at room temperature. After increasing the reaction temperature to 100 °C, the monomer **BIDO-2** was obtained, along with other impurities that are probably tribromo compound or compounds with bromo on other positons other than 2 positon of the thiophene. Thus, bromination at high termperatures results in poor selectivity in this case. To overcome the solubility problem during the bromination reaction in acetic acid at room temperatue, a minimum amount of dichloromethane was added to the reaction mixture to dissolve the mono-bromo intermediate. The reaction continued overnight and desired product **BIDO-2** came out again as white precipitates. The product was filtered and washed with methanol and obtained as white solid. **BIDO-2** is soluble in most common organic solvents and pure enough for use in polymerization.

2. 2. 3 Synthesis of PMDI

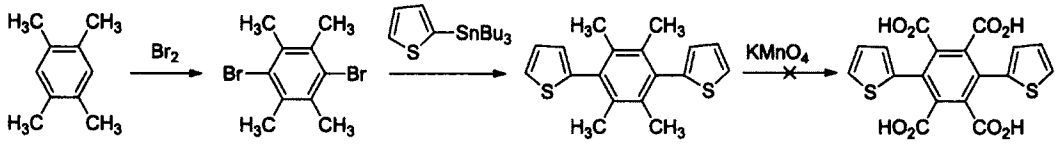

Scheme 2.4. Synthesis of thiophene substituted **PMDI**.

At the beginning, compound **II-13** in Scheme 2.4 was the target compound we were interested in, because it can form the diimide and has thienyl groups on each side, which can be brominated to become a monomer. Also, the final diimide has the similar structure with **BIDO-2** and can be coupled with the same donors or polymerized with the same monomers for the systematic study of property-structure relationship. The first two steps worked well; however, compound **II-13** can't be obtained from the oxidization reaction, because $KMnO_4$ also oxidized the thienyl groups.

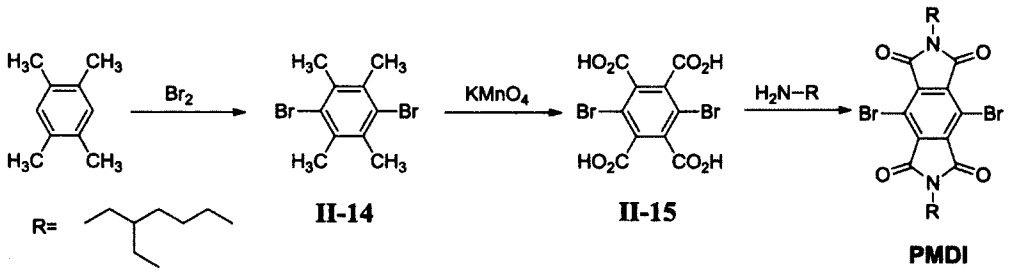

Scheme 2.5. Synthesis of **PMDI**.

In order to avoid the oxidization of thienyl groups, **PMDI** was prepared (Scheme 2.5). Synthetic route started with bromination of 1,2,4,5-tetramethylbenzene in near quantitative yield to give 1,2-dibromo-2,3,5,6-tetramethylbenzene **II-14**, which was then oxidized to the tetracarboxylic acid **II-15**. The acid then reacted with 2-ethylhexylamine in glacial acetic acid to afford **PMDI** in 71% yield.

2. 2. 4 Syntheses of the derivatives from BIDO-1, BIDO-2 and PMDI

Palladium-catalyzed cross-coupling reaction, such as Suzuki cross-coupling and Stille cross-coupling, is among the most powerful and versatile synthetic methods for carbon-carbon bond formation. The reactions have a broad scope and are highlighted by tolerance of a wide range of functionality.

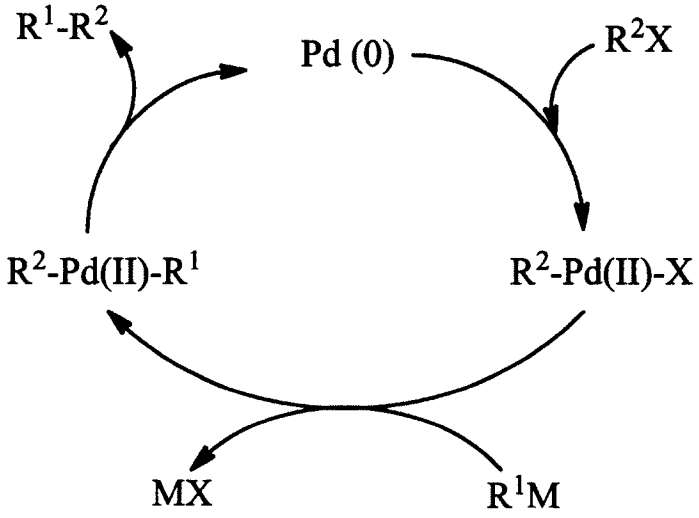

Scheme 2.6. General catalyic cycle of palladium-catalyzed cross-coupling.

As shown in Scheme 2.6, a catalytic cycle for the cross-coupling reaction of organometallics involves mainly three sequences: oxidative addition, transmetallation and reductive elimination. Oxidative addition of halide compounds to palladium (0) complex affords a stable trans-σ-palladium (II) complex and is often the rate-determining step in a catalytic cycle. It is called oxidative addition because the oxidation state of the transition metal changes from 0 to II in the process. The palladium (II) intermediate then undergoes transmetallation. The nucleophile (R^1) is transferred from the metal in the organometallic reagent to the palladium (II) complex, followed by reductive elimination to give the product (R^1-R^2) and the palladium (0) catalyst ready for another cycle.

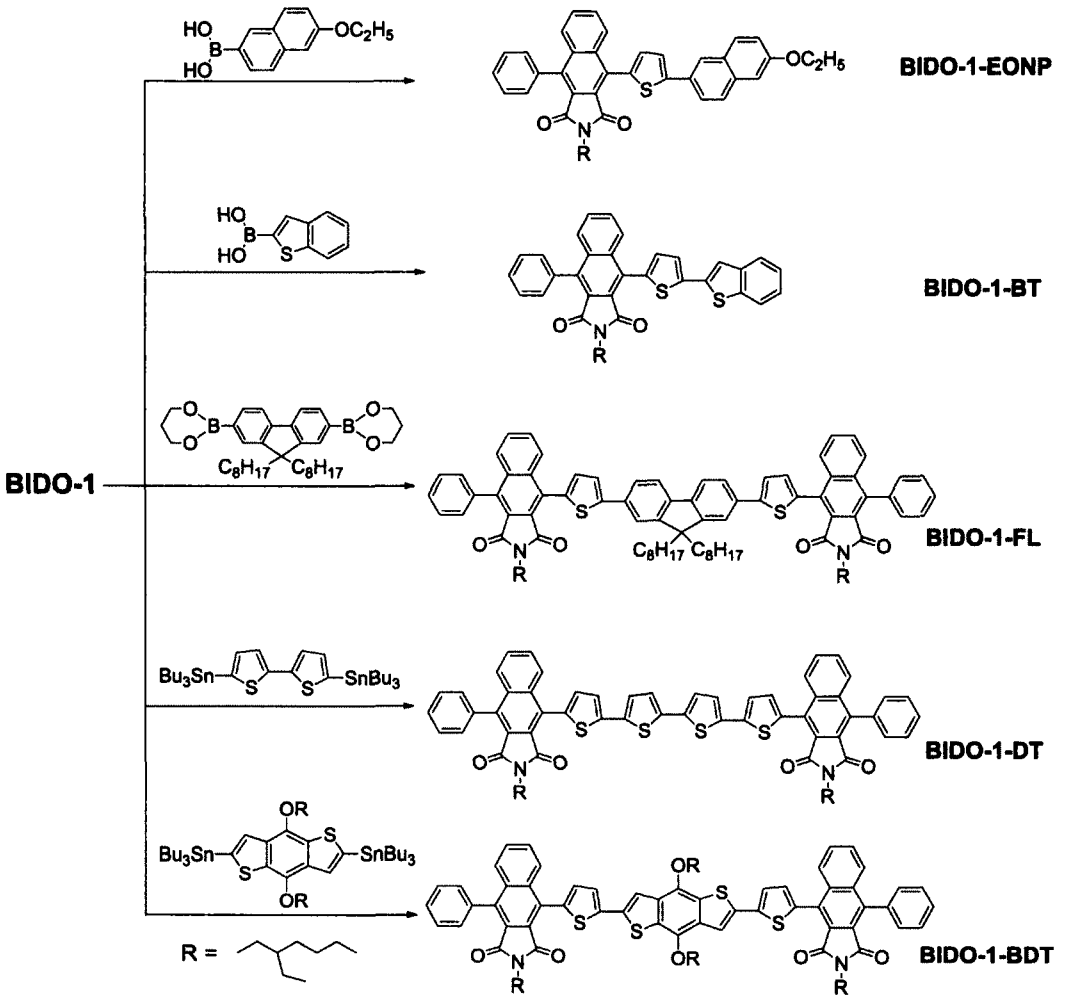

Scheme 2.7. Syntheses of **BIDO-1** derivatives.

The synthetic routes to **BIDO-1-EONP**, **BIDO-1-BT**, **BIDO-1-FL**, **BIDO-1-DT** and **BIDO-1-BDT** are outlined in Scheme 2.7. **BIDO-1-EONP**, **BIDO-1-BT** and **BIDO-1-FL** were prepared by Suzuki cross-coupling reaction and **BIDO-1-DT** and **BIDO-1-BDT** were prepared by Stille cross-coupling reaction. The boronic acids and ester were commercial available and used directly, whereas the organotin compounds were made according to the procedures in literature.[14,27] Both coupling reactions worked well for **BIDO-1** and gave good yield to each product (Table 2.1). All compounds are soluble in common organic solvents, such as THF, chloroform and toluene. However, the solubility of **BIDO-1-DT** is much lower than other

compounds. There are two reasons for the low solubility. First, the large conjugated backbone gives the molecule a highly planar structure and an ability to pack well, which prevents it from being readily dissolved in solvent. Second, the lack of aliphatic side chains causes a low solubility. Comparing to **BIDO-1-FL** and **BIDO-1-BDT**, **BIDO-1-DT** only has two ethylhexyl groups.

Table 2.1. Yields of **BIDO-1** derivatives.

Reaction	Suzuki cross-coupling			Stille cross-coupling	
Product	**BIDO-1-EONP**	**BIDO-1-BT**	**BIDO-1-FL**	**BIDO-1-DT**	**BIDO-1-BDT**
Yield	92%	82%	89%	75%	71%

As shown in Scheme 2.8, **BIDO-2-BT** and **BIDO-2-TPA** were synthesized by Suzuki cross-coupling reaction with **BIDO-2** building block in good yields (Table 2.2). **BIDO-2-TPA** is more soluble than **BIDO-2-BT** due to free rotation of the phenyl group of the triphenylamine donor.

Suzuki cross-coupling reaction doesn't work well for **PMDI**. The reason is that in the basic aqueous solution the imide can be hydrolyzed. Stille cross-coupling reaction doesn't need a base to proceed and works well for **PMDI**. Accordingly, **PMDI-TPAT** and **PMDI-FL** were prepared by Stille cross-coupling reaction in good yields. Both of them are soluble in common organic solvents.

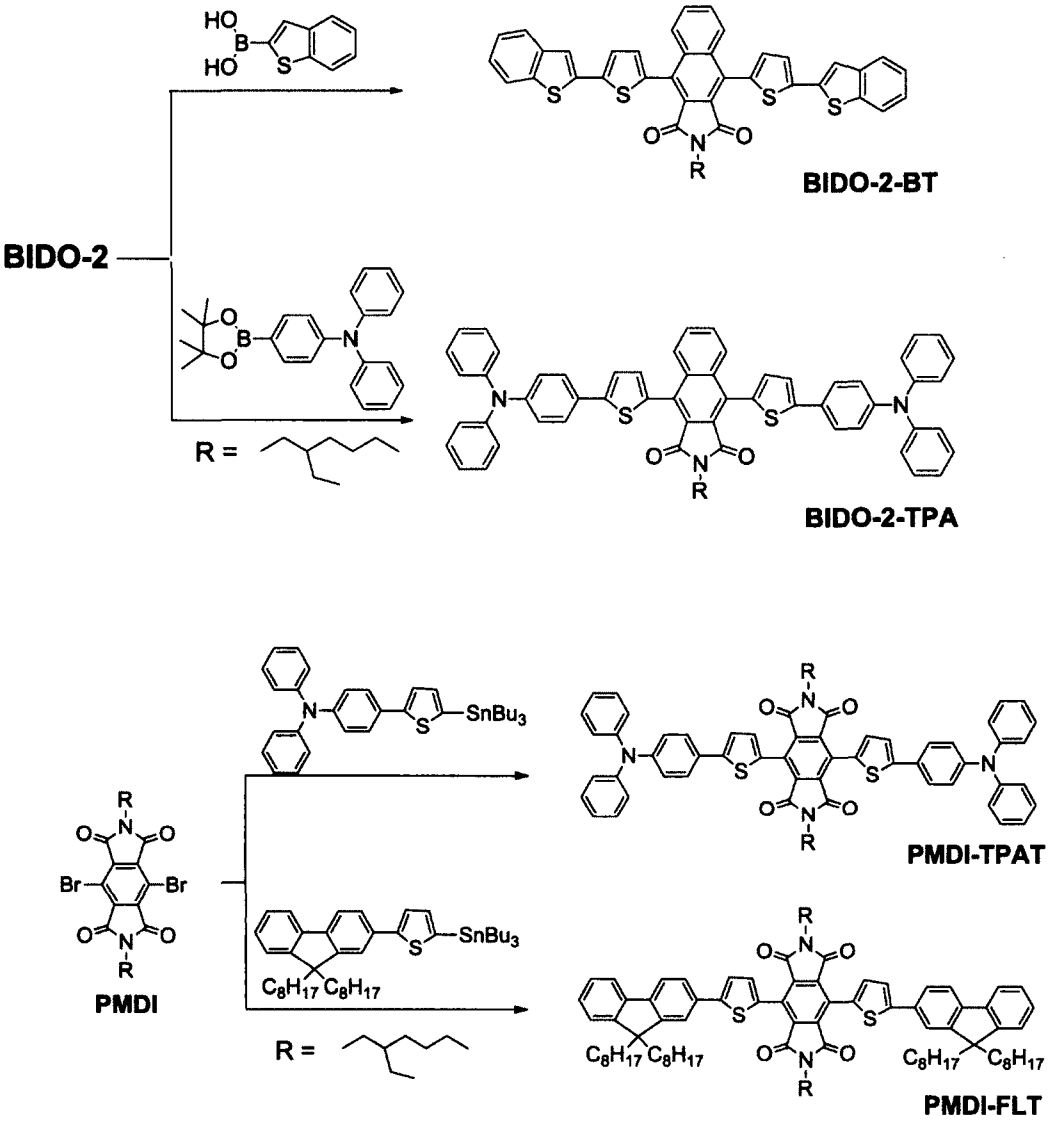

Scheme 2.8. Syntheses of small molecules from **BIDO-2** and **PMDI**.

Table 2.2. Yields of **BIDO-2** and **PMDI** derivatives.

Reaction	Suzuki cross-coupling		Stille cross-coupling	
Product	**BIDO-2-BT**	**BIDO-2-TPA**	**PMDI-TPAT**	**PMDI-FLT**
Yield	90%	88%	75%	77%

The use of thienyl groups as a connector has several advantages. First, it can increase the conjugation and lower the band gap. Second, thiophene is electron rich and can increase the electron donating ability of the donor. Third, it can adjust the planarity of the entire molecule, enhance the donor-acceptor interaction and therefore lower the band gap even further. For example, coupling **PMDI** with phenyl groups is quite difficult due to steric hindrance. The substitution by phenyl groups is expected to cause the molecule to adopt a nonplanar conformation, which reduces the conjugation length and thus increases band gap.[28] Therefore, it is essential and useful to have the thiophene as the bridging unit in the D-A system.

2. 2. 5 Syntheses of polymers based on BIDO-2 and PMDI

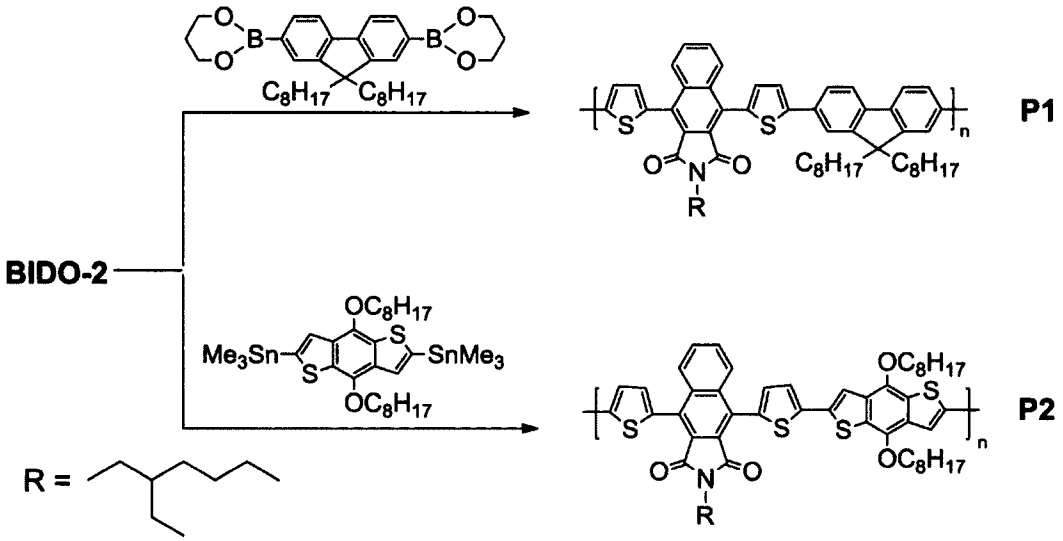

Scheme 2.9. Syntheses of **P1** and **P2.**

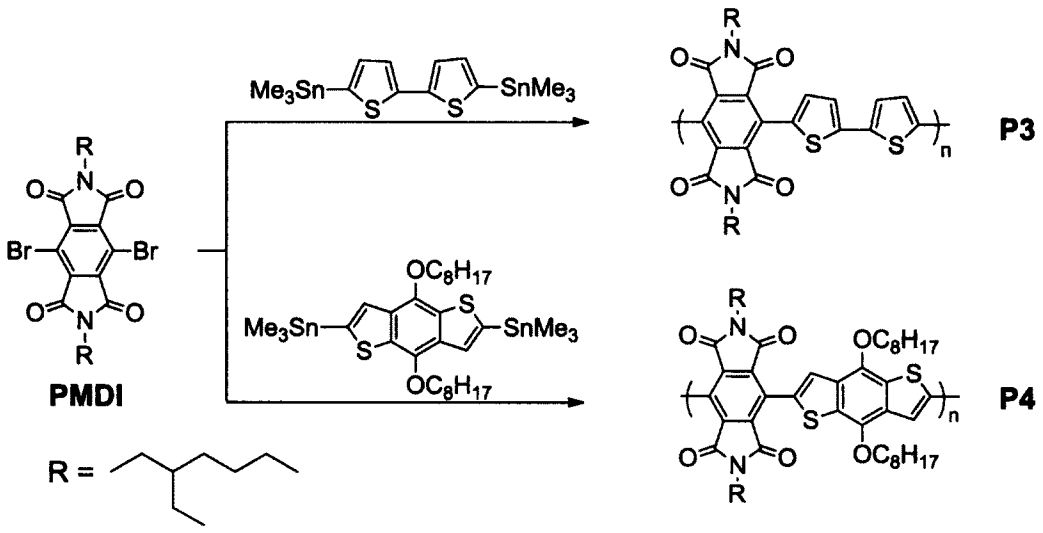

Scheme 2.10. Syntheses of **P3** and **P4.**

As shown in Scheme 2.9 and 2.10, polymer **P1** was prepared by Suzuki cross-coupling reaction between **BIDO-2** monomer and 9,9-dioctylfluorene-2,7-diboronic acid bis(1,3-propanediol) ester in THF and water using $Pd(PPh_3)_4$ as catalyst. The other three polymers **P2**, **P3** and **P4** were polymerized by Stille cross-coupling reaction. All four polymers have good solubility in common organic solvents such as chloroform, THF and chlorobenzene. Molecular weights and polydispersity indices (PDI) of these polymers were determined by gel permeation chromatography (GPC) relative to polystyrene standards (Table 2.3).

Table 2.3. Molecular weights and PDI of **P1-P4.**

Polymer	**P1**	**P2**	**P3**	**P4**
M_w (kg/mol)	111.2	154.4	45.2	229.1
PDI	2.2	4.5	2.5	5.5

2. 2. 6 Structural characterization

All the new compounds were characterized by ^{1}H NMR, ^{13}C NMR, IR and MS (see experimental Section).

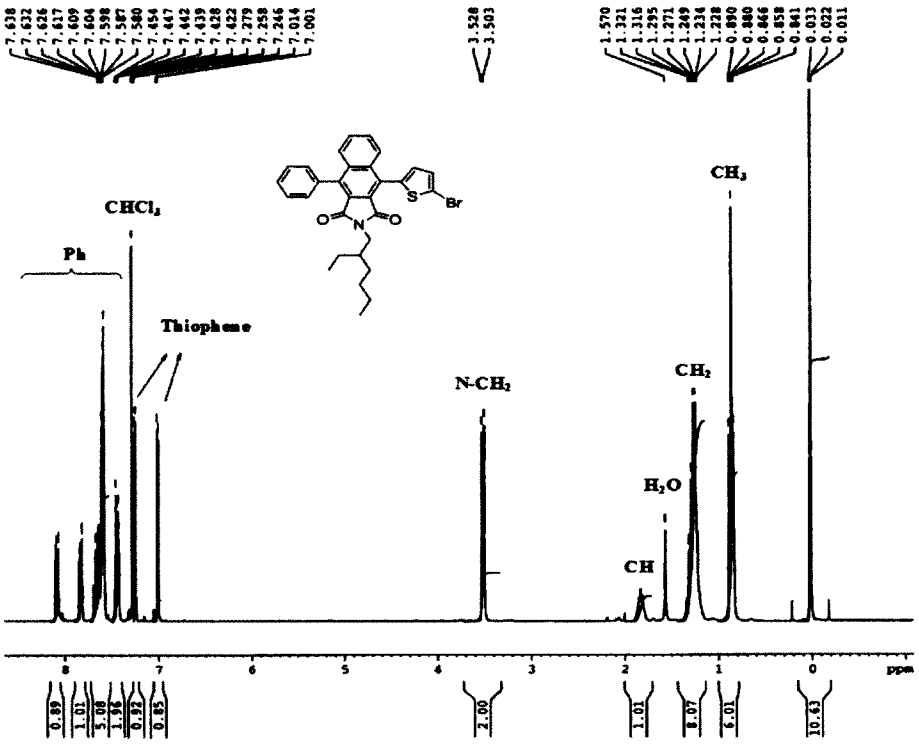

Figure 2.3. ^{1}H NMR spectrum (300 MHz, $CDCl_3$) of **BIDO-1**.

As an example, the ^{1}H NMR spectrum of **BIDO-1** displays proton resonances (ppm) at 8.10 (m, 1H), 7.84 (m, 1H), 7.70 (m, 5H), 7.45 (m, 2H), 7.26 (d, J = 3.9 Hz, 1H), 7.01 (d, J = 3.9 Hz, 1H), 3.53 (d, J = 7.5 Hz, 2H), 1.85 (m, 1H), 1.34 (m, 8H), 0.89 (m, 6H). The peak assignments are shown in Figure 2.3.

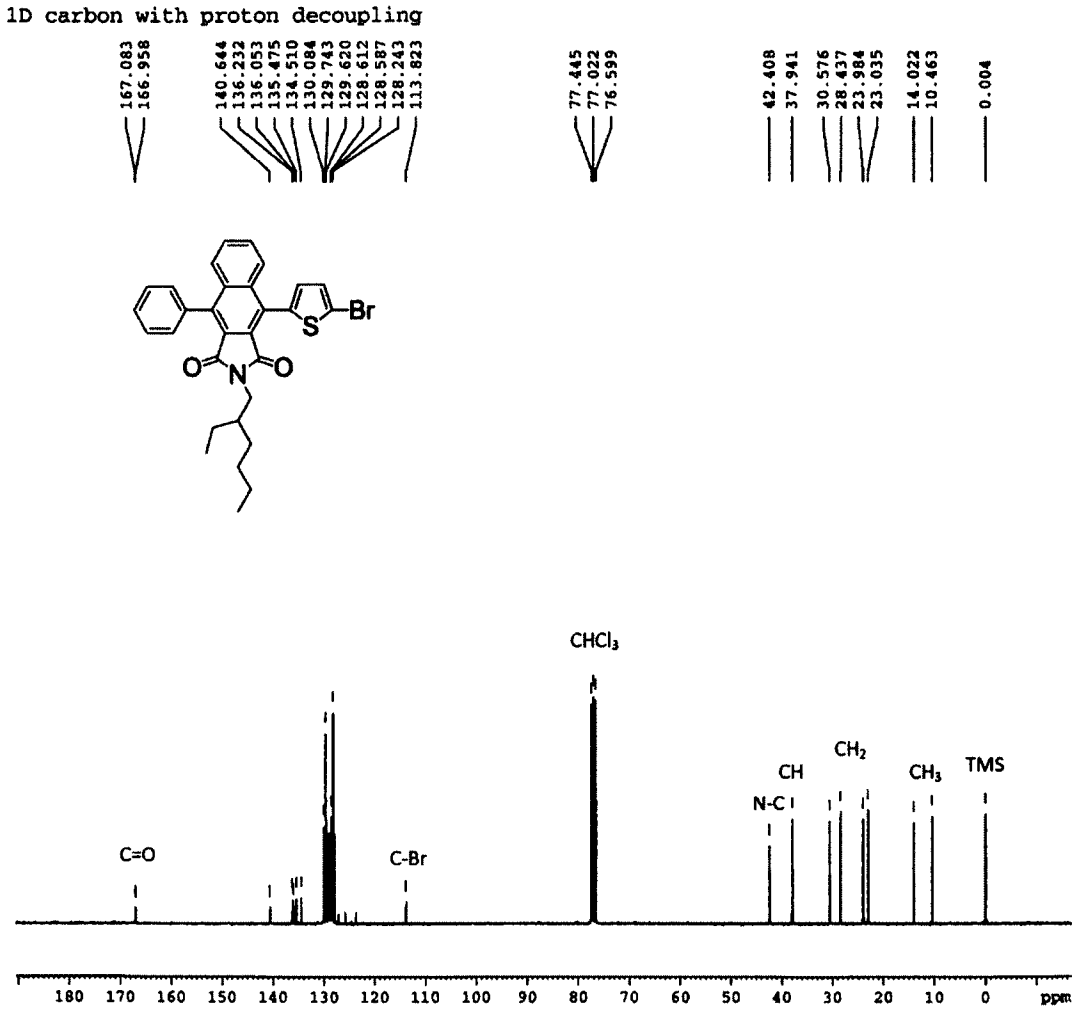

Figure 2.4. ^{13}C NMR spectrum (75 MHz, $CDCl_3$) of **BIDO-1**.

In its ^{13}C NMR spectrum (Figure 2.4), carbon resonance (ppm) at 167.1, 166.9, 140.6, 136.2, 136.0, 135.5, 134.5, 130.1, 129.7, 129.6, 128.6, 128.5, 128.2, 113.8, 42.4, 47.9, 30.6, 28.44, 24.0, 23.0, 14.0 and 10.4 were observed. Two peaks at 167.1, 166.9 were found for carbonyl carbon, due to the asymmetric structure of **BIDO-1**. Similar carbonyl peaks were also found in **BIDO-1** derivatives in their ^{13}C NMR spectra. In comparison, symmetric **BIDO-2** only has one peak at around 160.0 ppm.

The IR analysis was done with thin layer of compounds cast on the NaCl plate. In the IR spectrum of **BIDO-1** (Figure 2.5), two intense bands were observed at 1711 and 1765 cm^{-1}, which can be assigned to the imide group. Peaks at 2930 and 1608 cm^{-1} come from the C-H stretching and C=C stretching, respectively.

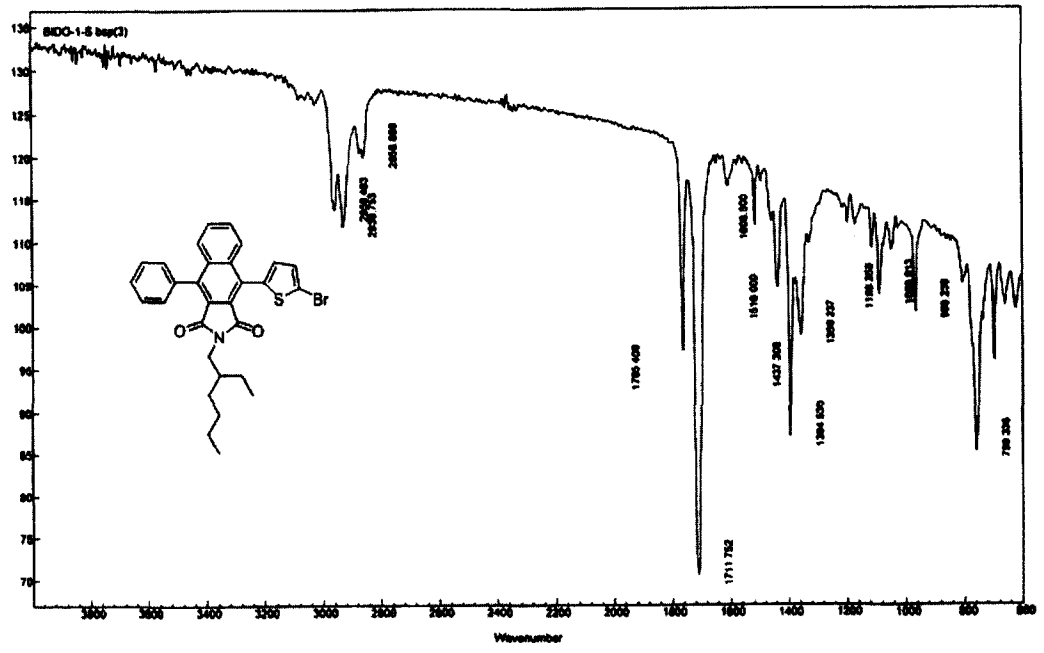

Figure 2.5. IR spectrum of **BIDO-1**.

In the MS spectrum (Figure 2.6), the molecular ion peak at M/Z 547.1 (100%) for $C_{30}H_{28}BrNO_2S$ was found. Due to isotopes of bromine atom, peak 545.1 (90%), was also observed. Peak at M/Z 435.0 may be attributed to the fragment missing the whole alkyl chain, whereas the peak at M/Z 448.0 is assigned to the one missing seven carbons of its alkyl chain with only a methyl group left on the nitrogen (See Table 2.4).

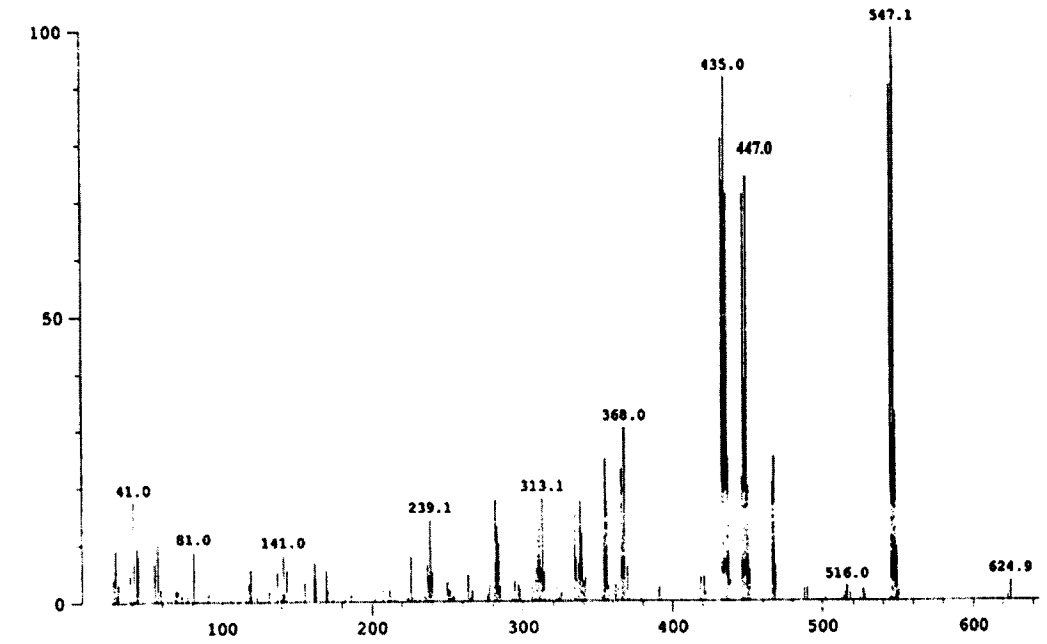

Figure 2.6. MS spectrum of **BIDO-1**.

Table 2.4. Summary of fragments in the MS spectrum of **BIDO-1**.

M/Z Peak	547.1	447.0	435.0
Molcular formula	$C_{30}H_{28}BrNO_2S$	$C_{23}H_{14}BrNO_2S$	$C_{22}H_{12}BrNO_2S$
BIDO-1 and corresponding fragments	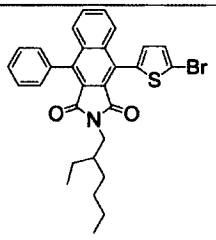	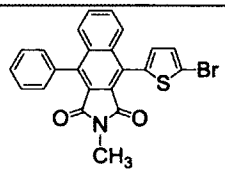	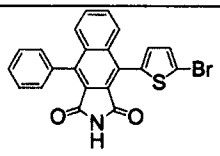

2.2.7 Thermal stability and T_g of polymers

Since thermal stability of polymers is an important factor for potential applications, it often needs to be determined by thermogravimetric analysis (TGA) and differential scanning calorimetry (DSC). TGA measures the changes in the weight (mass) of a sample as a function of temperature or time; while DSC provides a direct calorimetric measurement of the transition energy at the temperature of the transition. Therefore, the former is used to evaluate the thermal stability and the latter measures the glass transition temperature and crystallization temperature of the polymer samples.

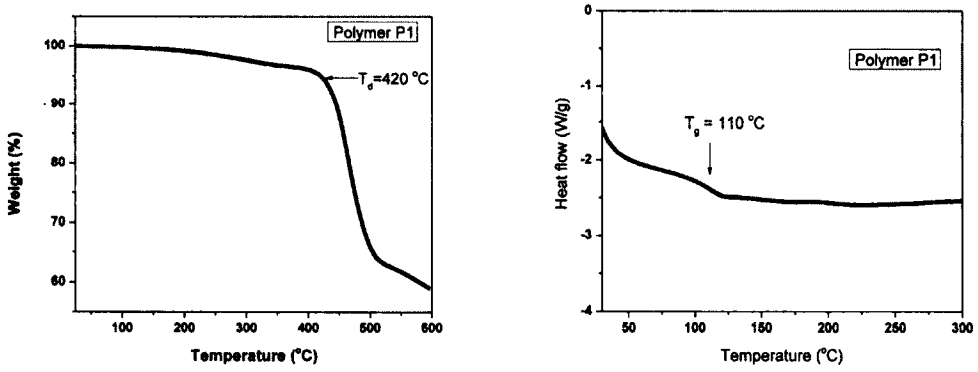

Figure 2.7. TGA (left) and DSC (right) of polymer **P1**.

Polymers **P1** to **P4** were investigated by TGA and DSC. The results are compiled in Table 2.5. The decomposition temperature (T_d), as assessed by the temperature of 5% weight loss in nitrogen, occur in the range of 358-420 °C. The T_g of these polymers range from 110 to120 °C. The T_d of polymers **P1-P4** is considered to be high, thus being suitable for film preparation and device fabrication. Among all, **P1** displayed the highest T_d due to the presence of the fluorene group which is more tolerant to high temperature.

Table 2.5. Thermal properties of polymers **P1-P4**.

Polymers	Decomposition Temperuature (T_d)	Glass Transition Temperature (T_g)
P1	420 °C	110 °C
P2	368 °C	120 °C
P3	353 °C	220 °C
P4	358 °C	-

All the polymers are amorphous based on the evidence of no crystallization peaks in DSC, which might be due to the presence of the bulky aliphatic chains that interfere the packing of the conjugated backbones. Polymers made of **PMDI** have a higher T_g due to the rigid diimide unit. The T_g was not observed for polymer **P4** below its T_d, because the rigid benzodithiophene unit further increases the T_g.

2.2.8 Optical properties of small molecules

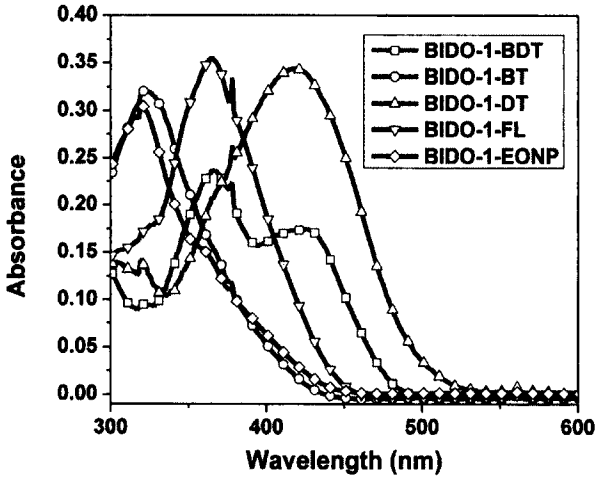

Figure 2.8. UV-vis spectra of **BIDO-1-BDT, BIDO-1-BT, BIDO-1-DT, BIDO-1-FL** and **BIDO-1-EONP** in chloroform solution.

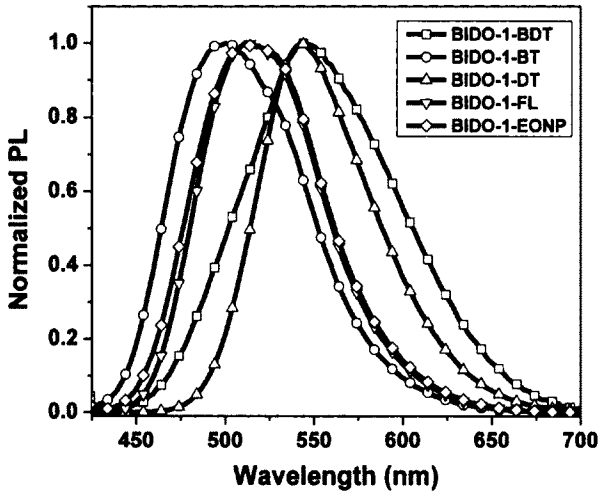

Figure 2.9. PL spectra of **BIDO-1-BDT**, **BIDO-1-BT**, **BIDO-1-DT**, **BIDO-1-FL** and **BIDO-1-EONP** in chloroform solution.

The optical properties of all the compounds were characterized. The absorptions of **BIDO-1** derivatives in chloroform are within the range of 300 to 500 nm, which are attributed to the delocalized π-π^* transition (Figure 2.8 and 2.9). Due to the weak electron withdrawing ability of **BIDO-1**, the intramolecular charge-transfer (ICT) band was not observed for all these compounds. **BIDO-1-BT** and **BIDO-1-EONP** have similar absorption peaks at around 320 nm. The UV spectrum of **BIDO-1-FL** was red shifted about 45 nm comparing to the **BIDO-1-EONP** due to the increased conjugation. Although **BIDO-1-DT** and **BIDO-1-BDT** have the same conjugation length as **BIDO-1-FL**, their absorption peaks are further red shifted about 50 nm, due to the stronger donors of dithiophene and benzodithiophene. **BIDO-1-BDT** has two absorption maxima at 366 and 422 nm. The absorption band in the visible region (422 nm) comes from the π-π^* transition benzodithiophene backbone, while the band in the UV region (366 nm) originates from the **BIDO-1** unit.

Emission maxima of **BIDO-1-EONP**, **BIDO-1-BT** and **BIDO-1-FL** were observed at around 510 nm, while the PL spectra of **BIDO-1-DT** and **BIDO-1-BDT** red shift about 45 nm (Figure 2.10). All the compounds exhibit large Stokes shifts which indicate the effective intramolecular charge transfer in the excited state between **BIDO-1** unit and the donors.[29] The quantum yields (QY), defined as the number of photons emitted in PL per absorbed photon, of all the compounds were measured, ranging from 0.66 to 2.43 %. The quenching by the imide group is believed to be the main cause of low QY.

Table 2.6. Optical properties of **BIDO-1** derivatives.

Compound	Maximum Absorption (nm)	ε_{max} ($L \cdot mol \cdot cm^{-1}$)	Excitation (nm)	Emission (nm)	Quantum Yield (%)
BIDO-1-BDT	366/422	43,080/32,310	400	546	0.66
BIDO-1-BT	322	16,467	315	500	1.63
BIDO-1-DT	419	25,349	400	543	2.43
BIDO-1-FL	365	52,282	350	515	1.61
BIDO-1-EONP	319	19,565	315	515	1.77

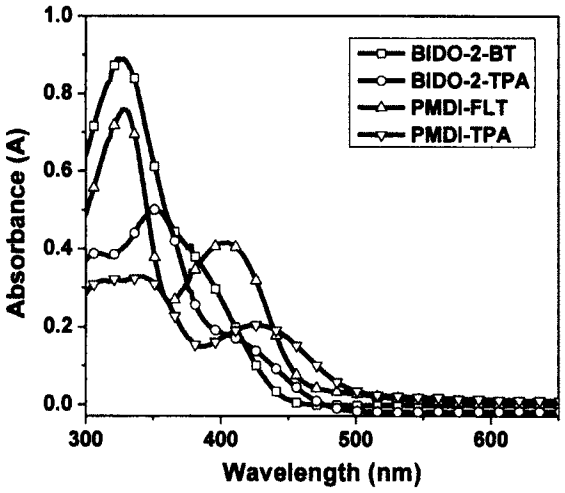

Figure 2.10. UV-vis spectra of **BIDO-2-BT, BIDO-2-TPA, PMDI-FLT and PMDI-TPA** in chloroform.

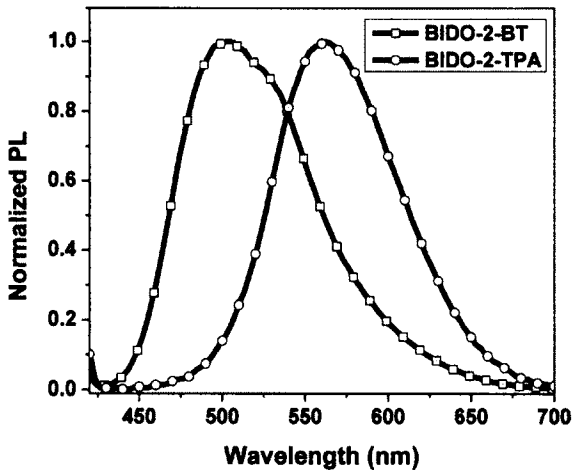

Figure 2.11. PL spectra of **BIDO-2-BT** and **BIDO-2-TPA** in chloroform.

UV-vis and PL spectra of **BIDO-2** and **PMDI** derivatives were recorded in chloroform solution (Figure 2.11 and Table 2.7). **BIDO-2-BT** displays absorption maxima at around 325 nm, while the spectrum of **BIDO-2-TPA** shifts only 27 nm to the long wavelength. Both of them have broad shoulders which can be assigned to π-π^* transition and n-π^* transition of the donors. In the spectra of **PMDI** compounds,

two peaks in UV and visible region can be attributed to the π-π* transition of **PMDI** unit and π-π* transition or n-π* transition of the donors, respectively. PL was only observed for **BIDO-2-BT** and **BIDO-2-TPA**. Because of the stronger donor-acceptor interaction in **BIDO-2-TPA**, it has more red-shifted emission at 562 nm with a larger Stokes shift of 212 nm. The absence of the PL for **PMDI** compounds is probably due to larger quenching effect from the dimide and less conjugated system resulted from the nonplanar structure of the molecules.

Table 2.7. Optical properties of **BIDO-2** and **PMDI** derivatives.

Compound	λ_{abs} (nm)	ε_{max} ($L \cdot mol \cdot cm^{-1}$)	Excitation (nm)	Emission (nm)	Quantum Yield (%)
BIDO-2-BT	325	36,462	320	505	1.42
BIDO-2-TPA	352	31,234	350	562	0.61
PMDI-TPAT	340/428	25,932/15,937	---	---	---
PMDI-FLT	330/403	28,743/15,506	---	---	---

2.2.9 Optical properties of polymers

The UV-vis spectra of polymers **P1-P4** in chloroform solution and films are shown in Figure 2.12 and 2.13, respectively. All the polymers display absorption peaks both in UV and visible region, except for polymer **P1** that has a single peak at 362 nm with a broad shoulder. The absorption profiles change little from solution to the solid state, indicating almost no π-π stacking in the solid state.[30] Thus, only a small red shift and extended absorption edge from solution to solid state were observed.

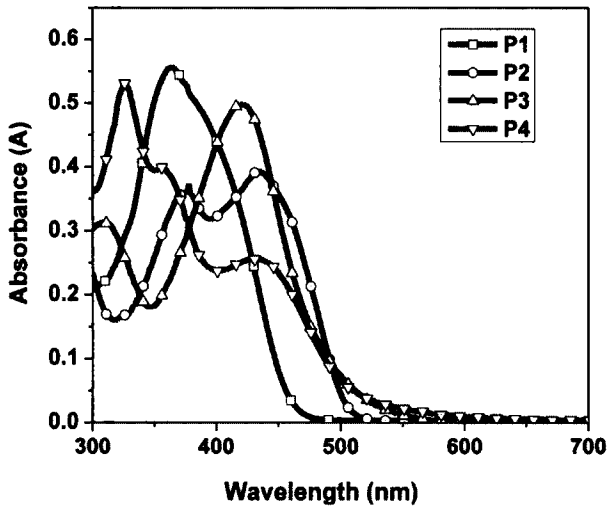

Figure 2.12. UV-vis spectra of **P1-P4** in chloroform (Concentration: **P1** = 1.9 x 10^{-2} mg/ml, **P2** = 2.2 x 10^{-2} mg/ml, **P3** = 4.4 x 10^{-2} mg/ml, **P4** = 5.3 x 10^{-2} mg/ml).

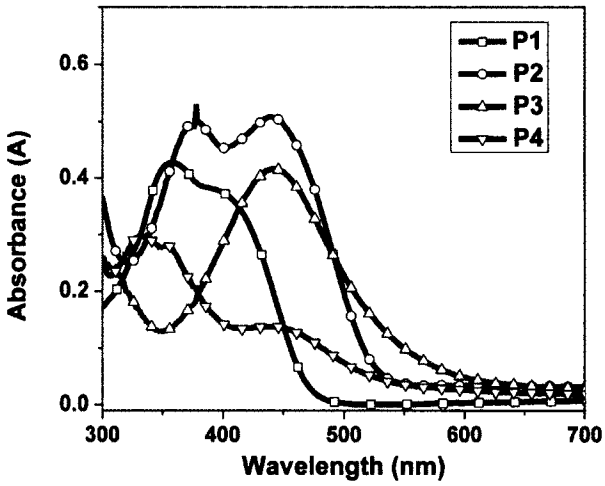

Figure 2.13. UV-vis spectra of **P1-P4** as films with the thickness of 50 nm.

The PL of the polymers in chloroform solution was also measured (Figure 2.14). Polymers **P1** and **P2** emit green light with a maximum at 515 nm and 544 nm, respectively.

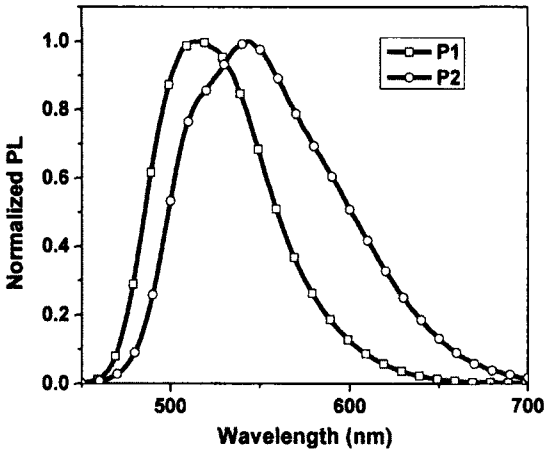

Figure 2.14. PL spectra of **P1 and P2** in chloroform.

No emission was detected for polymers **P3** and **P4**, which also happens to the reported **PMDI** polymers.[23] This can be attributed to aggregation induced and/or charge-transfer induced quenching.[31-33] Due to the large steric hindrance of the dimide groups, the nonplanar conformation of the **PMDI** polymers will decrease the conjugation and also contributes the absence of the emission.

Table 2.8. Optical properties of polymer **P1-P4**.

Polymer	λ_{abs} in chloroform (nm)	λ_{abs} from film (nm)	Excitation (nm)	Emission (nm)	Quantum Yield (%)
P1	362	363	350	515	7.3
P2	376/434	377/440	410	544	2.3
P3	309/420	442	---	---	---
P4	326/433	333/448	---	---	---

2.2.10 Electrochemical properties and band gaps of small molecules

Electrochemical cyclic voltammetry has been employed to investigate the redox properties of compounds and to estimate their HOMO and LUMO energy levels.[34] The cyclic voltammograms of compounds were measured in a 0.1 mol/L Bu_4NPF_6/dichloromethane solution using glass carbon as working electrode, platinum wire as counter electrode and silver as pseudoreference electrode. The results of the electrochemical measurements are listed in Table 2.9.

Table 2.9. Electrochemical properties of compounds.

Compound	E_{ox}[a] (V)	E_{red}[a] (V)	HOMO (eV)	LUMO (eV)	Band gap (eV)
BIDO-1-BDT	1.02	-1.13	-5.18	-3.03	2.15
BIDO-1-BT	1.48	-1.27	-5.64	-2.89	2.75
BIDO-1-DT	1.07	-1.15	-5.23	-3.01	2.22
BIDO-1-FL	1.33	-1.33	-5.49	-2.83	2.66
BIDO-1-EONP	1.47	-1.19	-5.63	-2.97	2.66
BIDO-2-BT	1.57	-1.00	-5.73	-3.16	2.57
BIDO-2-TPA	1.04	-1.25	-5.20	-2.91	2.29
PMDI-FLT	1.48	-0.49	-5.64	-3.67	1.97
PMDI-TPAT	0.94	-0.68	-5.10	-3.48	1.62

[a] The potentials were measured from the onset of the CV curves. The CV of compounds were measured in a 0.1 mol/L Bu_4NPF_6/dichloromethane solution.

The onset oxidation potentials (E_{ox}) of all the small molecules are within the range of 0.94 - 1.57 V vs NHE. Among them, **BIDO-1-BDT**, **BIDO-1-DT**, **BIDO-2-TPA** and **PMDI-TPAT** possess lower oxidation potentials, indicating stronger electron-donating ability of benzodithiphene, dithiophene and triphenylamine groups. Then onset reduction potentials (E_{red}) of all small molecules cover from -1.33 to -0.68 V vs NHE.

From the onset oxidation potentials (E_{ox}) and the onset reduction potentials (E_{red}), HOMO and LUMO energy levels as well as band gaps of the compounds were calculated according to the equations:

$$\text{HOMO} = -\, e(E_{ox} - E_{ferrocene} + 4.8)\ \text{eV}$$

$$\text{LUMO} = -\, e(E_{red} - E_{ferrocene} + 4.8)\ \text{eV}$$

$$\text{Band gap} = \text{LUMO} - \text{HOMO}\ \text{eV}$$

Where $E_{ferrocene}$ is the potential of ferrocene reference which equals 0.64 V vs NHE. The HOMO, LUMO and band gap values are included in Table 2.9. In order to see the difference clearly, the energy levels of all compounds are plotted in the Figure 2.15. The graph shows that **BIDO-1** derivatives tend to have higher HOMO levels when being connected to stronger donors. From **BIDO-1-BT** to **BIDO-1-BDT**, the HOMO levels increased 0.46 eV. However, the LUMO levels are about the same, all around -2.9 eV, because the LUMO level is mainly located on the acceptor unit, which is **BIDO-1** in this case. Therefore, the one with higher HOMO level will end up with a lower band gap. The lowest band gap among **BIDO-1** derivatives is 2.15 eV for compound **BIDO-1-BDT**, indicating that benzodithiophene has the strongest electron-donating ability among all five donors.

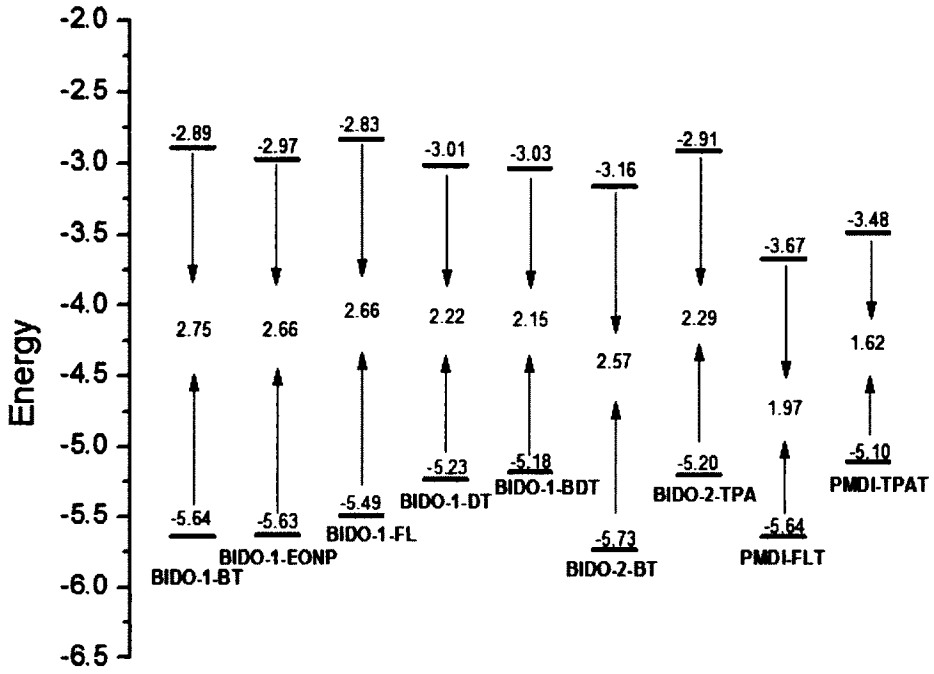

Figure 2.15. Energy levels of small molecules.

BIDO-2 derivatives have similar LUMO levels with **BIDO-1** derivatives. However, by changing the donor from benzothiophene to triphenylamine, the HOMO level increased from -5.73 eV to -5.20 eV, which means the electron donating ability of triphenylamine is a lot stronger. The band gap of **BIDO-2-TPA** is 2.29 eV. By changing the acceptor into **PMDI**, the LUMO level decreased significantly, because of the stronger electron-withdrawing property of **PMDI** unit. Combining with the strong donor diphenylaminophenylthiophenyl, the lowest band gap of 1.62 eV was found for **PMDI-TPAT**.

2.2.11 Electrochemical properties and determination of band gaps of polymers

The cyclic voltammograms of polymers were measured using the same method with small molecules in solution and the onset oxidation and reduction potentials were reported against NHE. HOMO and LUMO energy levels as well as

band gaps of polymers were calculated using the same equations above. The electrochemical data are list in Table 2.10, based on which an energy diagram is plotted (Figure 2.16).

Table 2.10. Electrochemical properties of polymer **P1-P4**.

Polymer	E_{ox}[a] (V)	E_{red}[a] (V)	HOMO (eV)	LUMO (eV)	Band gap (eV)
P1	1.13	-1.28	-5.29	-2.88	2.41
P2	0.87	-1.25	-5.03	-2.91	2.13
P3	1.72	-0.60	-5.88	-3.56	2.32
P4	1.05	-0.53	-5.21	-3.63	1.58

[a] The potentials were measured from the onset of the CV curves. The CV of compounds were measured in a 0.1 mol/L Bu_4NPF_6/dichloromethane solution.

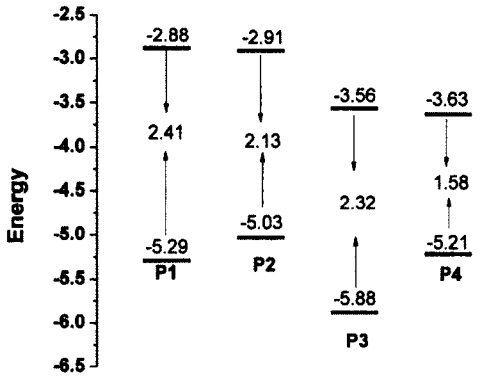

Figure 2.16. Energy levels of polymers.

As shown in Figure 2.17, **P1** has the largest band gap of 2.41 eV, indicating that **BIDO-2** is a weak acceptor. By copolymerizing **BIDO-2** with a stronger donor benzodithiophene, the HOMO level of polymer **P2** was increased to -5.03 eV, and this ends up with a smaller band gap of 2.13 eV comparing to that of **P1**. **P3** and **P4** have

lower LUMO levels around -3.60 eV, comparing to **BIDO-2** based polymers, due to stronger electron withdrawing ability of **PMDI** monomer. **P3** has a low HOMO level of -5.88 eV along with a relatively large band gap due to its low molecular weight and low electron-donating ability of dithiophene monomer. By introducing benzodithiophene, **P4** shows a high HOMO level of -5.21 eV with its LUMO level almost unchanged. This brings **P4** a surprisingly low band gap of 1.58 eV.

2.3 Conclusion

New electron withdrawing imides **BIDO-1** and **BIDO-2** have been designed and synthesized. Both Suzuki cross-coupling and Stille cross-coupling reactions were successfully used to couple them with different donors. The products show good solubility in common organic solvents. By increasing the electron-donating ability of the donors, the HOMO levels increase along with the decrease of band gaps and red shifted absorption. Moreover, based on their optical and electrochemical properties, **BIDO-1** and **BIDO-2** are judged to be weak acceptors comparing to **NDI** and **PDI** and promising building blocks for OSC applications.

PMDI monomer have been designed and synthesized, however, it can only be coupled with donors by Stille cross-coupling reaction. Due to the steric hindrance between diimde groups and the donors, the polymers of **PMDI** show higher T_g and reduced conjugation. Comparing to **BIDO** compounds and polymers, **PMDI** has a lower LUMO level, indicating its stronger electron-withdrawing ability. A relatively low band gap of 1.58 eV was obtained from polymer **P4** comparing to **PPEs**, by increasing the electron donating ability of the donor.

2.4 Experimental

2.4.1. Materials

Tetrahydrofuran (THF, Aldrich) was dried by refluxing over sodium metal and benzophenone. Other chemicals and reagents purchased from Aldrich and TCI were used directly without further purification. Macherey-Nagel precoated TLC plates (silica gel 60G/UV254, 0.25mm) were used for thin-layer chromatography (TLC) analysis. Silica gel (Silicycle Chemical Division, 0.04-0.006 mm, 230-400 mesh) was used as the stationary phase for column chromatography.

2.4.2. Instruments

^{1}H NMR spectra and ^{13}C NMR spectra were measured on Bruker Advance 300 instrument at 300 MHz and 75 MHz respectively. IR spectra were recorded on Varian 1000 FT-IR Scimitar Series. UV-vis spectra were measured on Perkin ELMER Lambda 900. PL spectra were measured on ManDEL Scientific RF-1501 spectrofluorophotometer. Differential scanning calorimetry and thermogravimetric analyzers were conducted on a TA Q100 and Hi-Res TGA 2950 under N_2 gas, at a heating rate of 10 °C. High Resolution ESI spectra were recorded on the 7.0T Actively Shielded Fourier Transform Ion Cyclotron Resonance Mass Spectrometers. Cyclic voltammograms (CV) and other electrochemical experiments were performed on a BAS 100 electrochemical workstation. Glass carbon working electrode, platinum counter electrode and silver pseudoreference electrode were used together, all the potentials were corrected using ferrocenium/ferrocene (Fc^{+}/Fc^{0}) and reported relative to NHE.

2.4.3. Determination of PL quantum Yield

The general procedure is as follows:

(1) Record the UV-vis absorbance spectrum of standard sample (perylene) in toluene solution. Record the absorbance at the excitation wavelength (404 nm) to be used.

(2) Record the fluorescence spectrum of the same solution in the 10 mm fluorescence cuvette. Calculate the integrated fluorescence intensity which is the area of the fluorescence spectrum.

(3) Repeat steps (1) and (2) for another two solutions with increasing concentrations of perylene.

(4) Plot the linear fit of integrated fluorescence intensity vs absorbance and record the gradient (Grad) of the line.

(5) Repeat steps (1) to (4) for synthesized samples in chloroform.

Absolute quantum yield of the samples are calculated using the standard which has known fluorescence quantum yield value (71% for perylene), according to the folloing equation :

$$\Phi_X = \Phi_{ST}(Grad_X/Grad_{ST})(n_X/ n_{ST})^2$$

Where the subscripts ST and X denote standard and synthesized samples respectively, Φ is the quantum yield, Grad is the gradient from plot, n is the refractive index of solvent.

2.4.4. Synthesis

2-benzoylbenzaldehyde (II-2)

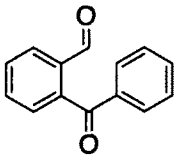

N'-(2-hydroxybenzylidene)benzohydrazide (23.00 g, 100.00 mmol) was dissolved in THF (40 mL) at room temperature and then cooled to 0°C. lead tetraacetate (46.70 g, 100.00 mmol) was gradually added to the solution. The resulting mixture was stirred for 4 h at 0 °C. Progress of the reaction was monitored by the evolution of nitrogen. The solvent was removed under reduce pressure. Ethyl acetate (60 mL) was added to the residue and the suspension was filtered over celite. The organic layer was washed with a saturated solution of $NaHCO_3$, brine and dried over sodium sulfate anhydrous. The solvent was removed under reduced pressure and the oily residue was purified by flash column chromatography (silica gel) using dichloromethane and hexane to give yellow solid (18.70 g, 89 % yield). ^1H NMR ($CDCl_3$, 300 MHz) δ (ppm): 7.26-7.51 (m, 3H), 7.60 (t, 1H, J = 7.4 Hz), 7.67 (m, 2H), 7.79 (m, 2H), 8.02 (m, 1H), 10.02 (s, 1H). ^{13}C NMR ($CDCl_3$, 75 MHz) δ (ppm): 128.7, 128.9, 130.0, 130.1, 130.7, 133.4, 133.7, 135.5, 137.0, 141.5, 190.6, 196.6. EI-MS (m/z): 210.1 (100%), calculated: 210.1.

1-phenyl-3-(thiophen-2-yl)isobenzofuran (II-3)

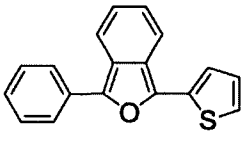

Mg (0.53 g, 22.00 mmol) was combined with 2-bromothiophene (3.26 g,

20.00 mmol) in 70 ml newly-distilled THF. The reaction was initiated by slight heating and controlled over ice bath. After most of the Mg was gone, the system was refluxing for half an hour. Then it was cooled in ice bath. The Grignard reagent was added into the THF solution of 2-benzoylbenzaldehyde (4.60 g, 20.00 mmol) at 0 °C. Then the system was stirred for an hour at 0 °C and another half an hour at room temperature. After that, HCl (10 M, 6 ml) was diluted into 40 ml and added into the solution, and the system was stirring for one and half hour. Then the mixture was extracted with ether three times. The ether phase was collected and washed with water, saturated solution of $NaHCO_3$, brine and dried over sodium sulfate anhydrous. The solvent was removed under reduced pressure and the product was purified by column chromatography (silica gel) using dichloromethane and hexane to give yellow solid (3.70 g, 68% yield). Due to its poor stability, it was used to make next product right away. ^1H NMR ($CDCl_3$, 300 MHz) δ (ppm): 7.97-7.94 (m, 2H), 7.85-7.75 (m, 2H), 7.55-7.48 (m, 3H), 7.35-7.16 (m, 3H), 7.07-7.03 (m, 2H). ^{13}C NMR ($CDCl_3$, 75 MHz) δ (ppm): 128.9, 127.8, 126.9, 125.5, 125.1, 124.7, 124.0, 122.2, 120.0. EI-MS (m/z): 276.1 (100%), calculated: 276.1.

4-phenyl-9-(thiophen-2-yl)naphtho[2,3-c]furan-1,3-dione (II-5)

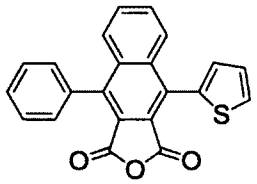

1-phenyl-3-(thiophen-2-yl)isobenzofuran (1.38 g, 5.00 mmol) was combined with maleic anhydride (0.68 g, 7.00 mmol) in 40 ml toluene. After refluxing for 12 hours, *p*-toluenesulfonic acid (PTSA) (0.05 g, 0.29 mmol) was added during the

reflux, after another 2 hours, the reaction was stopped and filtered when it was hot. The filtrate was slowly cooled to room temperature and then cooled in the fridge overnight. Then, the green crystals were filtered and dried in the vacuum (1.50 g, 84% yield). ^{1}H NMR (300 MHz, $CDCl_3$) δ (ppm): 8.19-8.16 (m, 1H), 7.96-7.93 (m, 1H), 7.78-7.68 (m, 3H), 7.64-7.59 (m, 3H), 7.48-7.44 (m, 2H), 7.34-7.37 (m, 2H). ^{13}C NMR (75 MHz, $CDCl_3$) δ (ppm): 161.6, 161.5, 143.4, 137.1, 136.0, 135.1, 133.4, 132.7, 132.3, 130.3, 130.1, 129.9, 129.7, 129.6, 129.5, 129.4, 129.1, 128.9, 128.6, 128.5, 128.1, 127.6, 127.4, 126.7, 123.8, 122.2. EI-MS (m/z): 356.1 (100%), calculated: 356.1.

2-(2-ethylhexyl)-4-phenyl-9-(thiophen-2-yl)-1H-benzo[f]isoindole-1,3(2H)-dione (II-6)

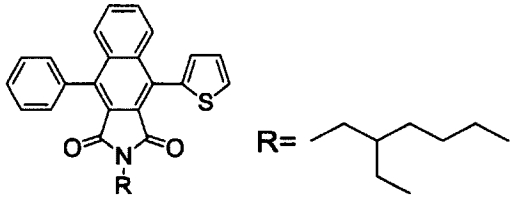

To a solution of 4-phenyl-9-(thiophen-2-yl)naphtho[2,3-c]furan-1,3-dione (0.43 g, 1.20 mmol) in acetic acid (10 ml), was added 2-ethylhexylamine (0.82 ml, 5.00 mmol) dropwise at room temperature. The mixture was then heated to reflux and stirred overnight. Then the solution was cooled to room temperature, and poured into 150 ml water. The precipitate was collected by filtration and recrystallized in ethanol to give 0.55 g yellow crystal (98% yield). ^{1}H NMR (300 MHz, $CDCl_3$) δ (ppm): 8.05-8.03 (m, 1H), 7.85-7.81 (m, 1H), 7.66-7.58 (m, 6H), 7.47-7.43 (m, 2H), 7.32-7.30 (m, 1H), 7.26-7.24 (m, 1H), 3.52-3.50 (d, J = 7.5 Hz, 2H), 1.87-1.82 (m, 1H), 1.35-1.24

(m, 8H), 0.90-0.84 (m, 6H). ^{13}C NMR (75 MHz, $CDCl_3$) δ (ppm): 167.2, 167.1, 140.1, 136.5, 135.4, 134.7, 134.4, 131.6, 129.8, 129.7, 129.1, 128.9, 128.8, 128.4, 128.2, 127.2, 127.1, 125.6, 124.8, 42.3, 37.9, 30.5, 28.4, 24.0, 23.0, 14.0, 10.5. EI-MS (m/z): 467.0 (100%), calculated: 467.2.

BIDO-1

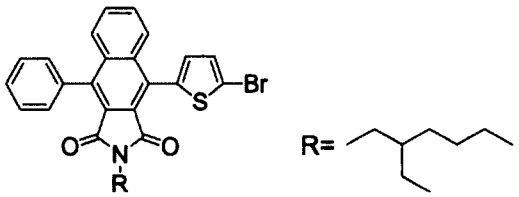

2-(2-ethylhexyl)-4-phenyl-9-(thiophen-2-yl)-1H-benzo[f]isoindole-1,3(2H)-dione (4.67 g, 10 mmol) was combined with N-Bromosuccinimide (NBS) (1.80 g, 10.00 mmol) in acetic acid (70 ml). The mixture was refluxed for overnight, and then cooled to room temperature and poured into cold water (200 ml). The solid was filtered, washed with water, dried in vacuum and purified by column chromatography (silica gel) using dichloromethane and hexane to give white solid (4.80 g, 88 % yield). ^{1}H NMR (300 MHz, $CDCl_3$) δ (ppm): 8.10 (m, 1H), 7.84 (m, 1H), 7.70 (m, 5H), 7.45 (m, 2H), 7.26 (d, J = 3.9 Hz, 1H), 7.01 (d, J = 3.9 Hz, 1H), 3.53 (d, J = 7.5 Hz, 2H), 1.85 (m, 1H), 1.34 (m, 8H), 0.89 (m, 6H). ^{13}C NMR (75 MHz, $CDCl_3$) δ (ppm): 167.1, 166.9, 140.6, 136.2, 136.0, 135.5, 134.5, 130.1, 129.6, 129.2, 129.1, 129.0, 128.8,128.7, 128.5, 128.0, 127.2, 125.8, 124.5, 123.7, 113.8, 42.4, 47.9, 30.6, 28.44, 24.0, 23.0, 14.0,10.4. EI-MS (m/z): 547.1 (100%), calculated: 547.1.

2-(thiophene-2-carbonyl)benzaldehyde

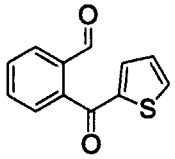

Similar procedures of making 2-benzoylbenzaldehyde were followed to prepare 2-(thiophene-2-carbonyl)benzaldehyde. Instead of using N'-(2-hydroxybenzylidene)benzohydrazide, N'-(2-hydroxybenzylidene)thiophene-2-carbohydrazide (2.00 g, 8.12 mmol) was added into reaction. The product was obtained as yellow solid (1.60 g, 91% yield) by column chromatography (silica gel). ^{1}H NMR (300 MHz, $CDCl_3$) δ (ppm): 10.05 (s, 1H), 8.01-7.98 (m, 1H), 7.76-7.74 (m, 1H), 7.68-7.64 (m, 3H), 7.39-7.38 (m, 1H), 7.11-7.08 (m, 1H). ^{13}C NMR (75 MHz, $CDCl_3$) δ (ppm): 190.4, 188.1, 144.1, 141.0, 135.8, 135.7, 135.0, 133.4, 130.9, 129.7, 128.6, 128.5. EI-MS (m/z): 216.0 (100%), calculated: 216.0.

1,3-di(thiophen-2-yl)isobenzofuran

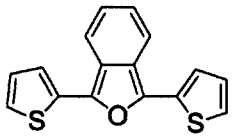

Similar procedures of making 1-phenyl-3-(thiophen-2-yl)isobenzofuran were followed to prepare 1,3-di(thiophen-2-yl)isobenzofuran. Instead of using 2-benzoylbenzaldehyde, 2-(thiophene-2-carbonyl)benzaldehyde (4.33 g, 20.00 mmol) was used in this reaction. The product was obtained as red solid (4.04 g, 72% yield) by column chromatography (silica gel). Due to its poor stability, it was used to make next product right away. ^{1}H NMR (300 MHz, $CDCl_3$) δ (ppm): 7.75-7.70 (m, 2H), 7.52-7.50 (m, 2H), 7.34-7.32 (m, 2H), 7.17-7.14 (m, 2H), 7.07-7.02 (m, 2H). ^{13}C

NMR (75 MHz, $CDCl_3$) δ (ppm): 139.7, 133.4, 127.8, 125.4, 124.0, 122.3, 121.3, 119.8. EI-MS (m/z): 282.0 (100%), calculated: 282.0.

4,9-di(thiophen-2-yl)naphtho[2,3-c]furan-1,3-dione

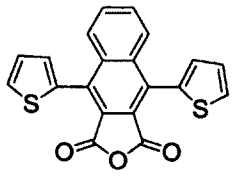

Similar procedures of making 4-phenyl-9-(thiophen-2-yl)naphtho[2,3-c]furan-1,3-dione were followed to prepare 4,9-di(thiophen-2-yl)naphtho[2,3-c]furan-1,3-dione. Instead of using 1-phenyl-3-(thiophen-2-yl)isobenzofuran, 1,3-di(thiophen-2-yl)isobenzofuran (1.40 g, 5.00 mmol) was used in this reaction. The product was obtained as green crystals (1.20 g, 66% yield). ^1H NMR (300 MHz, $CDCl_3$) δ (ppm): 8.18-8.14 (m, 2H), 7.79-7.74 (m, 2H), 7.70-7.68 (m, 2H), 7.34-7.28 (m, 4H). ^{13}C NMR (75 MHz, $CDCl_3$) δ (ppm): 161.2, 137.0, 135.9, 132.5, 130.4, 129.9, 128.6, 128.2, 127.4. EI-MS (m/z): 362.0 (100%), calculated: 362.0.

2-(2-ethylhexyl)-4,9-di(thiophen-2-yl)-1H-benzo[f]isoindole-1,3(2H)-dione

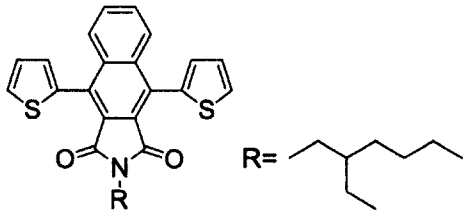

To a solution of 4,9-di(thiophen-2-yl)naphtho[2,3-c]furan-1,3-dione (0.44 g, 1.20 mmol) in acetic acid (10 ml), was added 2-ethylhexylamine (0.82 ml, 5.00 mmol) dropwise at room temperature. The mixture was then heated to reflux and stirred

overnight. Then the solution was cooled to room temperature, and poured into 150 ml water. The precipitate was collected by filtration and recrystallized in ethanol to give yellow crystal (0.52 g, 91% yield). ^{1}H NMR (300 MHz, $CDCl_3$) δ (ppm): 8.05-8.01 (m, 2H), 7.66-7.63 (m, 4H), 7.32-7.27 (m, 2H), 7.24-7.23 (d, J = 3.0 Hz, 2H), 3.53-3.51 (d, J = 7.2 Hz, 2H), 1.86-1.82 (m, 1H), 1.30-1.23 (m, 8H), 0.91-0.84 (m, 6H). ^{13}C NMR (75 MHz, $CDCl_3$) δ (ppm): 166.8, 136.3, 134.1, 132.5, 129.2, 129.1, 128.2, 127.3, 127.1, 125.6, 42.4, 37.9, 30.5, 28.4, 23.9, 23.0, 14.0, 10.4. EI-MS (m/z): 473.2 (100%), calculated: 473.1.

BIDO-2

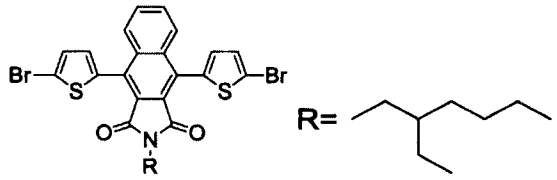

2-(2-Ethylhexyl)-4,9-di(thiophen-2-yl)-1H-benzo[f]isoindole-1,3(2H)-dione (0.50 g, 1.06 mmol) was dissolved in 25 ml acetic acid and N-Bromosuccinimide (NBS) (0.27 g, 1.50 mmol) was added at room temperature. After the solution was stirred for 1 hour, CH_2Cl_2 was added to dissolve the precipitate. Then another portion of NBS (0.18 g, 1.00 mmol) was added and the reaction continued for 12 hours at room temperature. The precipitate was isolated by filtration and recrystallized in acetone three times to give white solid (0.59 g, 88 % yield). ^{1}H NMR (300 MHz, $CDCl_3$) δ (ppm): 8.09-8.05 (m, 2H), 7.72-7.67 (m, 2H), 7.25-7.24 (d, J = 3.6 Hz, 2H), 6.99-6.98 (d, J = 3.6 Hz, 2H), 3.55-3.53 (d, J = 7.5 Hz, 2H), 1.87-1.82 (m, 1H), 1.35-1.24 (m, 8H), 0.90-0.84 (m, 6H). ^{13}C NMR (75 MHz, $CDCl_3$) δ (ppm): 166.5, 136.1, 135.5, 131.5, 130.1, 129.7, 129.5, 128.0, 125.6, 114.1, 42.5, 38.0, 30.6, 28.4, 24.0,

23.0, 14.0, 10.5. EI-MS (m/z): 628.9 (100%), calculated: 629.0.

BIDO-1-EONP

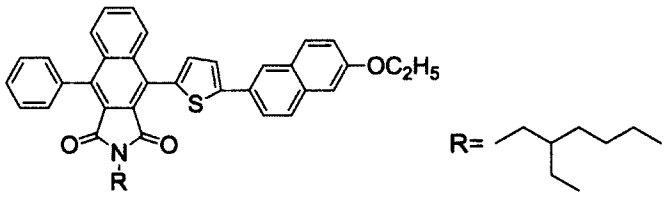

BIDO-1 (0.55 g, 1 mmol) and (6-ethoxynaphthalen-2-yl)boronic acid (0.22 g, 1.00 mmol) were combined in 25 ml THF. Then 20 ml K_2CO_3/water solution (0.1g/ml) was added. The system was degassed, followed by the addition of $Pd(PPh_3)_4$ (20mg). Then the system was degassed again and heated to reflux under argon protection for 24 h. The resulting solution was cooled to room temperature and extracted with 100ml $CHCl_3$. Then organic phase was washed with water, brine and dried over sodium sulfate anhydrous. The solvent was removed by rotary evaporation and the residue was purified by column chromatography (silica gel) to get yellow solid (0.59 g, 92% yield), ^{1}H NMR (300 MHz, $CDCl_3$) δ (ppm): 8.25-8.22 (m, 1H), 8.08 (s, 1H), 7.86-7.76 (m, 4H), 7.70-7.58 (m, 6H), 7.49-7.46 (m, 2H), 7.48-7.46 (m, 2H), 7.26-7.25(d, J = 3.6 Hz, 1H), 7.19-7.16 (m, 2H), 4.21-4.19 (m, 2H), 3.55-3.52 (d, J = 7.5 Hz, 2H), 1.90-1.80 (m, 1H), 1.56-1.50 (t, 3H), 1.33-1.25 (m, 8H), 0.89-0.84 (m, 6H). ^{13}C NMR (75 MHz, $CDCl_3$) δ (ppm): 167.3, 167.1, 157.3, 146.7, 140.2, 136.5, 135.5, 134.7, 134.1, 133.3, 131.5, 130.5, 129.8, 129.6, 129.4, 129.0, 128.9, 128.5, 128.4, 128.2, 127.3, 125.6, 124.8, 124.3, 123.8, 122.9, 119.7, 106.6, 63.5, 42.3, 37.9, 30.6, 28.4, 24.0, 23.0, 14.8, 14.0, 10.5. EI-MS (m/z): 547.1 (100%), calculated: 547.1. EI-MS (m/z): 637.2 (100%), calculated: 637.3.

BIDO-1-BT

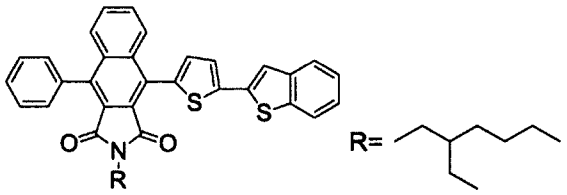

Similar procedures of making **BIDO-1-EONP** were followed, using benzo[b]thiophen-2-ylboronic acid (0.18 g, 1.00 mmol) instead of (6-ethoxynaphthalen-2-yl)boronic acid. The product is yellow solid (0.49 g, 82% yield). ^{1}H NMR (300 MHz, $CDCl_3$) δ (ppm): 8.20-8.17 (d, J = 7.8, 1H), 7.86-7.82 (m, 2H), 7.79-7.76 (m, 1H), 7.71-7.60 (m, 6H), 7.50-7.45 (m, 4H), 7.41-7.30 (m, 2H), 7.22-7.20(d, J = 4.2 Hz, 1H) 3.54-3.52 (d, J = 7.2 Hz, 2H), 1.86-1.80 (m, 1H), 1.33-1.26 (m, 8H), 0.91-0.85 (m, 6H). ^{13}C NMR (75 MHz, $CDCl_3$) δ (ppm): 167.1, 166.9, 140.5, 140.4, 139.4 139.3, 136.9, 136.3, 135.5, 134.6, 134.4, 131.6,130.8, 129.8, 129.2, 129.0, 128.8, 128.6, 128.5, 128.2, 127.9,127.2, 127.2, 125.7, 125.1, 124.7, 124.6, 123.8, 123.5, 122.2, 120.1, 42.4, 38.0, 30.6, 28.5, 24.0, 23.0,14.1, 14.0. EI-MS (m/z): 599.2 (100%), calculated: 599.2.

BIDO-1-FL

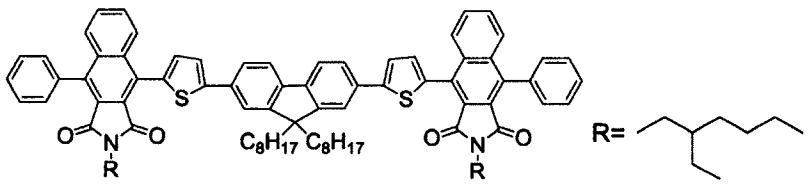

Similar procedures of making **BIDO-1-EONP** were followed, using 9,9-dioctylfluorene-2,7-diboronic acid bis(1,3-propanediol) ester (0.28 g, 0.50 mmol) instead of (6-ethoxynaphthalen-2-yl)boronic acid. Yellow solid (1.18 g, 89% yield) ^{1}H NMR (300 MHz, $CDCl_3$) δ (ppm): 8.25-8.22 (m, 2H), 7.84-7.80 (m, 2H), 7.74-7.58

(m, 18H), 7.49-7.46 (m, 4H), 7.27-7.26 (d, J = 3.6 Hz, 2H), 3.55-3.53 (d, J = 7.5 Hz, 4H), 2.20-2.00 (m, 4H), 1.95-1.78 (m, 2H), 1.39-1.05 (m, 36H), 0.95-0.65 (m, 22H). ^{13}C NMR (75 MHz, $CDCl_3$) δ (ppm): 167.3, 167.2, 151.8, 147.1, 140.5, 140.3, 136.5, 135.5, 134.7, 133.30, 133.0, 131.5, 130.4, 129.8, 129.1, 129.0, 128.9, 128.8, 128.6, 128.5, 128.3, 128.2, 127.2, 127.1, 125.6, 125.0, 123.8, 123.0, 120.2, 120.0, 55.4, 42.4, 40.7, 37.9, 31.8, 30.6, 30.1, 29.3, 28.4, 24.0, 23.9, 23.1, 22.6, 14.1, 14.0, 10.5. EI-MS (m/z): 1320.7 (100%), calculated: 1320.7.

BIDO-1-DT

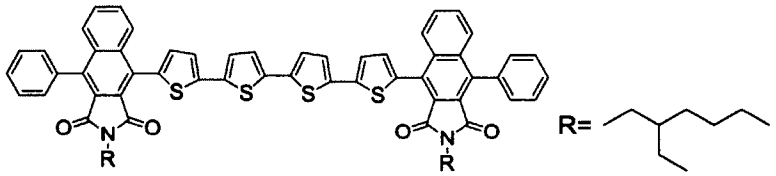

BIDO-1 (0.55 g, 1 mmol) was combined with 5,5'-bis(tributylstannyl)-2,2'-bithiophene (0.37 g, 0.50 mmol) in toluene (50 ml) . Argon was flowed into the mixture for 20 minutes to remove the oxygen. Then $Pd(PPh_3)_4$ (0.02 g) was added and argon was flowed for another 10 minutes. The mixture was heated to 100 °C and maintained for 24 hours under Argon. After cooling, the mixture was diluted with dichloromethane and washed with saturated aqueous potassium fluoride and brine. The separated organic layer was dried over $MgSO_4$ and the product was obtained as red solid (0.82 g, 75% yield) by column chromatography (silica gel). ^{1}H NMR (300 MHz, $CDCl_3$) δ (ppm): 8.20-8.18 (d, J = 8.1 Hz, 2H), 7.85-7.82(d, J = 8.1 Hz, 2H), 7.11-7.56 (m, 10H), 7.47-7.45 (m, 4H), 7.39-7.38(d, J = 6.6 Hz, 2H), 7.21-7.16 (m, 6H), 3.54-3.52 (d, J = 7.5 Hz, 4H), 1.95-1.78 (m, 2H), 1.33-1.05 (m, 16H), 0.89-0.84 (m, 12H). ^{13}C NMR (75 MHz, $CDCl_3$) δ (ppm): 167.3, 167.2, 140.4, 139.1, 136.4,

136.2, 136.0, 135.5, 134.6, 133.4, 130.8, 129.8, 129.1, 128.9, 128.5, 128.2, 124.8, 124.4, 123.8, 42.4, 37.9, 30.6, 28.5, 24.0, 23.0, 14.0, 10.5. EI-MS (m/z): 1096.3 (100%), calculated: 1096.3.

BIDO-1-BDT

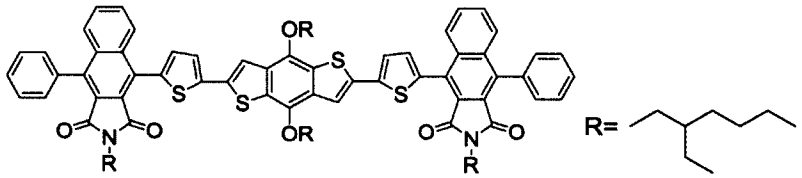

Similar procedures of making **BIDO-1-BT** were followed, using 2,6-(4,8-bis((2-ethylhexyl)oxy)benzo[1,2-b:4,5-b']dithiophene-2,6-diyl)bis(tributylstannane) (0.51 g, 0.50 mmol) instead of 5,5'-bis(tributylstannyl)-2,2'-bithiophene. Yellow solid (0.98 g, 71% yield). ^{1}H NMR (300 MHz, $CDCl_3$) δ (ppm): 8.21-8.18 (d, J = 7.8 Hz, 2H), 7.87-7.84 (d, J = 7.8 Hz, 2H), 7.70-7.60 (m, 12H), 7.53-7.45 (m, 6H), 7.24-7.22 (d, J = 3.9 Hz, 2H), 4.30-4.20 (m, 4H), 3.55-3.52 (d, J = 7.2 Hz, 4H), 1.90-1.80 (m, 4H), 1.78-1.53 (m, 12H), 1.42-1.51 (m, 4H), 1.40-1.21 (m, 16H), 1.10-0.80 (m, 24H). ^{13}C NMR (75 MHz, $CDCl_3$) δ (ppm): 167.2, 167.1, 144.2, 140.5, 139.5, 136.3, 135.5, 134.6, 132.4, 130.7, 130.4, 129.8, 129.4, 129.2, 129.0, 128.6, 128.2, 125.7, 125.4, 123.8, 116.5, 42.4, 40.7, 38.0, 30.6, 30.4, 29.2, 28.4, 28.3, 26.7, 24.0, 23.8, 23.1, 23.0, 17.2, 14.2, 14.0, 13.6, 11.3, 10.5. EI-MS (m/z): 1376.6 (100%), calculated: 1376.6.

BIDO-2-BT

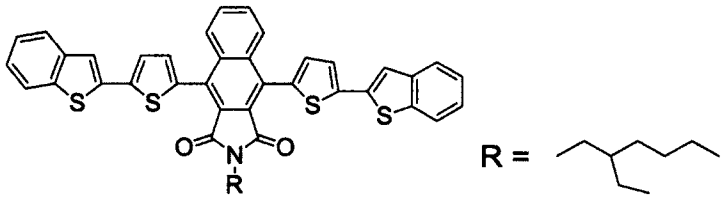

BIDO-2 (0.63 g, 1.0 mmol) and benzo[b]thiophen-2-ylboronic acid (0.36 g, 2.00 mmol) were combined in 25 ml THF. Then 20 ml K_2CO_3/water solution (0.1 g/ml) was added. The system was degassed, followed by the addition of $Pd(PPh_3)_4$ (0.02 mg). Then the system was degassed again and heated to reflux under argon protection for 24 h. The resulting solution was cooled to room temperature and extracted with 100 ml $CHCl_3$. Then organic phase was washed with water, brine and dried over sodium sulfate anhydrous. The solvent was removed by rotary evaporation and the residue was purified by column chromatography (silica gel) to get yellow solid (0.66 g, 90% yield). ^{1}H NMR (300 MHz, $CDCl_3$) δ (ppm): 8.21-8.16 (m, 1H), 8.09-8.06 (m, 1H), 7.85-7.66 (m, 6H), 7.53-7.32 (m, 7H), 7.26-7.24 (m, 1H), 7.21-7.18 (m, 1H), 7.01-6.98(m, 1H), 3.58-3.54 (m, 2H), 1.95-1.78 (m, 2H), 1.32-1.24 (m, 8H), 0.91-0.87 (m, 6H). ^{13}C NMR (75 MHz, $CDCl_3$) δ (ppm): 167.2, 140.3, 139.6, 139.2, 136.2, 134.0, 132.1, 132.0, 131.9, 130.4, 130.1, 129.7, 129.5, 129.4, 128.5, 128.4, 128.2, 128.0, 125.1, 124.7, 124.6, 123.5, 122.1, 114.0, 42.5, 38.0, 30.6, 28.4, 24.0, 23.0, 14.0, 10.4. EI-MS (m/z): 737.2 (100%), calculated: 737.2.

BIDO-2-TPA

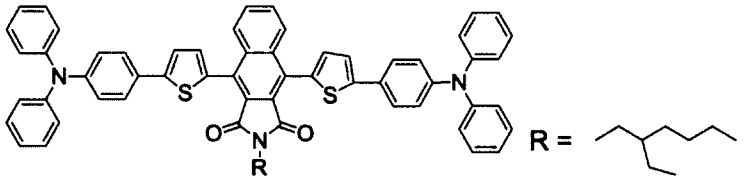

Similar procedures of making **BIDO-2-BT** were followed, using 4-(diphenylamino)phenylboronic acid pinacol ester (0.74 g, 2.00 mmol) instead of benzo[b]thiophen-2-ylboronic acid. The product is yellow solid (0.85 g, 88% yield). ^{1}H NMR (300 MHz, $CDCl_3$) δ (ppm): 8.20-8.17 (m, 2H), 7.69-7.66 (m, 2H), 7.59-7.56 (d, J = 8.7 Hz, 4H), 7.42-7.41 (d, J = 3.6 Hz, 2H), 7.33-7.28 (m, 8H), 7.19-7.04 (m, 18H), 3.57-3.54 (d, J = 7.2 Hz, 2H), 1.95-1.78 (m, 2H), 1.34-1.29 (m, 8H), 0.90-0.86 (m, 6H). ^{13}C NMR (75 MHz, $CDCl_3$) δ (ppm): 166.8, 147.4, 146.4, 136.4, 132.5, 123.4, 130.4, 129.3, 129.2, 128.3, 128.1, 126.7, 125.5, 124.5, 123.6, 123.1, 122.2, 42.4, 37.9, 30.6, 28.4, 24.0, 23.0, 14.0, 10.4. EI-MS (m/z): 959.4 (100%), calculated: 959.4.

3,6-Dibromotetramethylbenzene

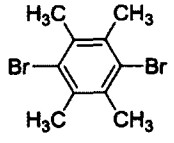

To a stirred solution of 1,2,4,5-tetramethylbenzene (2.50 g, 18.66 mmol) and iodine (0.10 g, 0.78 mmol) in dichloromethane (30 ml), a solution of bromine (2.4 ml, 7.46 g, 46.7 mmol) in dichloromethane (10 ml) was added dropwise at room temperature under exclusion of light. The reaction mixture was refluxed for 1h. Aqueous NaOH (5 M, 50 ml) was added subsequently to destroy the excess bromine.

The aqueous layer was separated; the organic layer was washed with water and dried with anhydrous $MgSO_4$. The product was recrystallized using ethyl acetate to get needle like crystals. The yield is 5.10 g (95%). ^1H NMR (300 MHz, $CDCl_3$): δ 2.46 (s, 12H). ^{13}C NMR (75 MHz, $CDCl_3$): δ 22.6, 128.1, 135.0. EI-MS (m/z): 291.9 (100%), calculated: 291.9.

3,6-dibromobenzene-1,2,4,5-tetracarboxylic acid

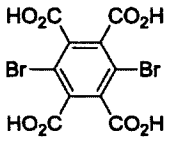

3,6-Dibromotetramethylbenzene (7.10 g, 24.40 mmol), pyridine (300 ml) and water (40 ml) were heated (100 °C) with stirring. Solid $KMnO_4$ (19.40 g, 122.00 mmol) was added in small portions and the mixture refluxed for overnight. The warm solution was separated from the MnO_2 by filtration and the solvent was distilled under reduced pressure. Water (400 ml) and NaOH (16.00 g) were added to the residue. The mixture was heated (100 °C) and $KMnO_4$ (19.40 g, 122.00 mmol) was added. After refluxing for 3 hours, the excess KMnO4 was destroyed by cautious addition of ethanol (20 ml). The hot solution was separated from the solid MnO_2 by filtration and acidified with aqueous HCl (5 M). The precipitate was collected by filtration, washed with water and dried in vacuum (white solid 5.20 g, 58% yield). The product was used in next step without further purification.

Pyromellitic diimide (PMDI)

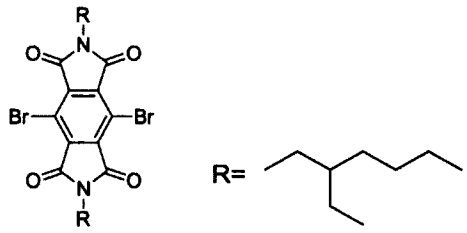

3,6-dibromobenzene-1,2,4,5-tetracarboxylic acid (4.12 g, 10.00 mmol) was combined with 2-ethylhexan-1-amine (3.88 g, 30.00 mmol) in acetic acid (50 ml). The mixture was refluxed for overnight and then cooled to room temperature. The precipitate was filtered from the solution, washed with methanol and dried in vacuum (white solid 4.50 g, 75 % yield). ^{1}H NMR (300 MHz, $CDCl_3$) δ (ppm): 3.63-3.65 (d, 4H) 1.81-1.89 (m, 2H), 1.24-1.39 (m, 16H), 0.88-0.96 (m, 12H). ^{13}C NMR (75 MHz, $CDCl_3$) δ (ppm): 163.8, 136.1, 114.1, 42.9, 38.2, 30.5, 28.5, 23.9, 22.9, 14.0, 10.36. EI-MS (m/z): 598.1 (100%), calculated: 598.1.

PMDI-TPAT

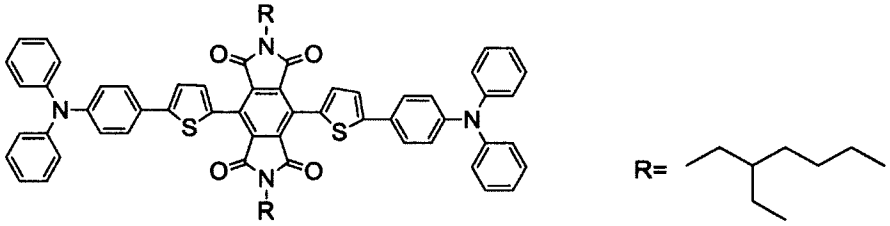

Tributyl[5-(4-(N,N-diphenylamino)phenyl)thiophen-2-yl]stannne (1.23 g, 2.00 mmol) was combined with **PMDI** (0.58 g, 1.00 mmol) in toluene (70 ml) . Argon was flowed into the mixture for 20 minutes to remove the oxygen. Then $Pd(PPh_3)_4$ (0.02 g) was added and argon was flowed for another 10 minutes. The mixture was heated to 100 °C and maintained for 24 hours under Argon. After

cooling, the mixture was diluted with dichloromethane and washed with saturated aqueous potassium fluoride and brine. The separated organic layer was dried over $MgSO_4$ and the product was obtained as dark red solid (0.82 g, 75% yield) by column chromatography (silica gel). ^{1}H NMR (300 MHz, $CDCl_3$) δ (ppm): 7.56-7.53 (m, 4H), 7.35-7.24 (m, 12H), 7.16-7.04 (m, 16H), 3.54-3.52 (d, J = 7.5 Hz, 4H), 1.83-1.79 (m, 2H), 1.34-1.27 (m, 16H), 0.90-0.85 (m, 12H). ^{13}C NMR (75 MHz, $CDCl_3$) δ (ppm): 165.1, 147.6, 147.4, 135.1, 131.5, 130.4, 129.3, 127.9, 126.9, 124.5, 123.4, 123.1, 121.9, 42.6, 38.0, 30.5, 28.4, 23.9, 23.0, 14.0, 10.4. EI-MS (m/z): 1090.5 (100%), calculated: 1090.5.

PMDI-FT

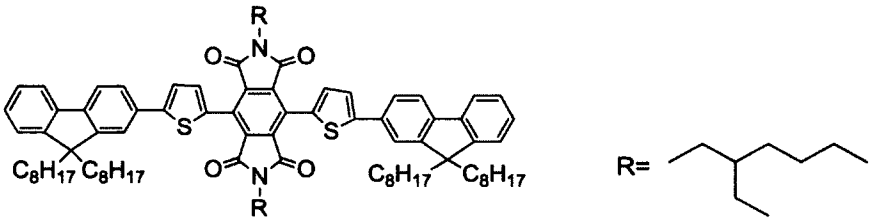

Similar procedures of making **PMDI-TPAT** were followed to prepare **PMDI-FT**. Instead of using Tributyl[5-(4-(N,N-diphenylamino)phenyl)thiophen-2-yl]stannne, tributyl[5-(4-(N,N-diphenylamino)phenyl)thiophen-2-yl]stannne (1.52 g, 2.00 mmol) was added into reaction. The product was obtained as red solid (1.06 g, 77% yield) by column chromatography (silica gel). ^{1}H NMR (300 MHz, $CDCl_3$) δ (ppm): 7.73-7.65 (m, 8H), 7.53-7.51 (d, J = 3.6 Hz, 2H), 7.36-7.34 (m, 6H), 7.31-7.30 (d, J = 3.6 Hz, 2H), 3.57-3.55 (d, J = 7.2 Hz, 4H), 2.04-1.99 (t, 8H), 1.85-1.75 (m, 2H), 1.45-1.02 (m, 56H), 0.90-0.81 (m, 24H), 0.73-0.60 (m, 8H). ^{13}C NMR (75 MHz, $CDCl_3$) δ (ppm): 165.3, 151.4,151.0, 148.6, 141.2, 140.6, 135.3, 132.7, 131.6, 130.6,

128.4, 127.3, 126.9, 125.2, 122.8, 127.3, 126.9, 125.2, 122.8, 122.7, 120.2, 120.0, 119.8, 55.2, 42.7, 40.6, 38.1, 31.8, 30.6, 30.2, 29.3, 28.4, 24.0, 23.8, 23.0, 22.6, 14.1, 10.5. EI-MS (m/z): 1380.9 (100%), calculated: 1380.9.

Synthesis of polymer P1

BIDO-2 (0.32 g, 0.50 mmol) and 9,9-dioctylfluorene-2,7-diboronic acid bis(1,3-propanediol) ester (0.28 g, 0.50 mmol) were combined in 8 ml THF. Then 10 ml K_2CO_3/water solution (0.1 g/ml) was added. The system was degassed, followed by the addition of $Pd(PPh_3)_4$ (0.01 g). Then the system was degassed again and heated to reflux under argon protection for 48 h. The resulting solution was cooled to room temperature and diluted with 100 ml $CHCl_3$, then washed with water, brine and dried over sodium sulfate anhydrous. After that, the solution was concentrated into 10-15ml and the polymer was precipitated by adding the solution in 200 ml methanol. The polymer was then subjected to Soxhlet extraction with acetone and chloroform and recovered by precipitating in methanol to give 0.35 g yellow spheres (yield, 81%). ^{1}H NMR (300 MHz, $CDCl_3$) δ (ppm): 8.28-8.24 (m, 2H), 7.78-7.61 (m, 12H), 3.57 (s, 2H), 2.09-1.90 (m, 5H), 1.34-1.14 (m, 28H), 0.92-0.73 (m, 16H). ^{13}C NMR (75 MHz, $CDCl_3$) δ (ppm): 166.9, 151.7, 147.2, 140.5, 136.4, 133.0, 132.5, 132.1, 132.0, 130.5, 129.3, 128.6, 128.4, 125.6, 125.0, 122.9, 120.2, 120.0, 55.4, 40.7, 38.0, 31.8, 30.6, 30.1, 29.3, 28.4, 24.8, 24.0, 23.8, 23.0, 22.6, 14.1, 14.0, 10.5.

Synthesis of polymer P2

BIDO-2 (0.32 mg, 0.50 mmol) was combined with 2,6-Bis(trimethyltin)-4,8-

bis(octyloxy)benzo[1,2-b:4,5-b']dithiophene (0.39 g, 0.50 mmol) in toluene (50 ml). Argon was flowed into the mixture for 20 minutes to remove the oxygen. Then $Pd(PPh_3)_4$ (0.01 g) was added and argon was flowed for another 10 minutes. The mixture was heated to 100 °C and stirred for 3 days under Argon. After cooling to room temperature, the polymer was precipitated in methanol (200 ml). Then, the solid was filtered, dissolved in little amount CH_2Cl_2 and precipitated again in methanol (200 ml). The polymer was obtained as yellow fiber (0.40 g, 87% yield). ^{1}H NMR (300 MHz, $CDCl_3$) δ (ppm): 8.22 (s, 2H), 7.70-7.54 (m, 6H), 7.27 (s, 2H), 4.35 (s, 4H), 3.58 (s, 2H), 1.96 (s, 5H), 1.64 (s, 4H), 1.33 (s, 24H), 0.89 (s, 12H). ^{13}C NMR (75 MHz, $CDCl_3$) δ (ppm): 166.7, 144.3, 144.1, 139.6, 136.6, 136.2, 134.2, 133.2, 132.4, 132.1, 131.9, 130.5, 129.8, 129.5, 128.9, 128.2, 125.9, 125.4, 124.1, 118.2, 116.6, 38.0, 31.8, 30.5, 29.4, 29.3, 28.4, 26.1, 24.0, 23.0, 22.7, 14.2, 14.1, 14.0, 10.5.

Synthesis of polymer P3

PMDI (0.29 g, 0.50 mmol) was combined with 5,5'-bis(trimethylstannyl)-2,2'-bithiophene (0.25 g, 0.50 mmol) in toluene (70 ml). Argon was flowed into the mixture for 20 minutes to remove the oxygen. Then $Pd(PPh_3)_4$ (0.01 mg) was added and argon was flowed for another 10 minutes. The mixture was heated to 100 °C and stirred for 3 days under Argon. After cooling to room temperature, the polymer was precipitated in methanol (200 ml). Then, the solid was filtered, dissolved in little amount CH_2Cl_2 and precipitated again in methanol (200 ml). The polymer was obtained as brown fiber (0.21 g, 72 % yield). ^{1}H NMR (300 MHz, $CDCl_3$) δ (ppm): 7.41-7.39 (d, J = 3.3 Hz, 2H), 7.25-7.23 (d, J = 3.3Hz, 2H), 3.56 (s, 4H), 1.90-1.80

(m, 2H), 1.32-1.30 (m, 16H), 0.93-0.90 (m, 12H). ^{13}C NMR (75 MHz, $CDCl_3$) δ (ppm): 165.0, 139.9, 135.2, 131.2, 130.0, 129.0, 124.1, 42.6, 38.0, 30.5, 28.4, 23.9, 23.0, 14.0, 10.4.

Synthesis of polymer P4

Similar procedures of making polymer **P4** were followed to **P3**. Instead of using 5,5'-bis(trimethylstannyl)-2,2'-bithiophene, 2,6-Bis(trimethyltin)-4,8-bis(octyloxy) benzo[1,2-b:4,5-b']dithiophene (0.39 g, 0.50 mmol) was added into reaction. The polymer was obtained as yellow fiber (0.38 g, 87% yield). ^{1}H NMR (300 MHz, $CDCl_3$) δ (ppm): 7.66 (s, 2H), 4.41 (s, 4H), 3.56 (s, 4H), 1.92-1.82 (m, 6H), 1.58-1.30 (m, 32H), 0.89 (s, 18H). ^{13}C NMR (75 MHz, $CDCl_3$) δ (ppm): 164.6, 144.6, 135.4, 134.9, 131.8, 131.3, 130.7, 130.3, 127.8, 123.5, 42.5, 38.1, 31.8, 30.6, 30.5, 29.4, 29.3, 28.5, 28.3, 26.1, 23.9, 22.9, 22.7, 14.1, 14.0, 10.4.

References

(1) Jung, B. J.; Tremblay, N. J.; Yeh, M. L.; Katz, H. E. *Chem. Mater.* **2011**, *23*, 568.

(2) Anthony, J. E.; Facchetti, A.; Heeney, M.; Marder, S. R.; Zhan, X. *Adv. Mater.* **2011**, *22*, 3876.

(3) Zhan, X.; Facchetti, A.; Barlow, S.; Marks, T. J.; Ratner, M. A.; Wasielewski, M. R.; Marder, S. R. *Adv. Mater.* **2011**, *23*, 268.

(4) Huang, C.; Barlow, S.; Marder, S. R. *J. Org. Chem.* **2011**, *76*, 2386.

(5) Guo, X.; Watson, M. D. *Org. Lett.* **2008**, *10*, 5333.

(6) Katz, H. E.; Lovinger, A. J.; Johnson, J.; Kloc, C.; Siegrist, T.; Li, W.; Lin, Y.; Dodabalapur, A. *Nature* **2000**, *404*, 478.

(7) Jones, B. A.; Facchetti, A.; Marks, T. J.; Wasielewski, M. R. *Chem. Mater.* **2007**, *19*, 2703.

(8) Gao, X.; Di, C.; Hu, Y.; Yang, X.; Fan, H.; Zhang, F.; Liu, Y.; Li, H.; Zhu, D. *J. Am. Chem. Soc.* **2010**, *132*, 3697.

(9) Schmidt, R.; Oh, J. H.; Sun, Y.-S.; Deppisch, M.; Krause, A.-M.; Radacki, K.; Braunschweig, H.; Kunemann, M.; Erk, P.; Bao, Z.; Wurthner, F. *J. Am. Chem. Soc.* **2009**, *131*, 6215.

(10) Piliego, C.; Jarzab, D.; Gigli, G.; Chen, Z.; Facchetti, A.; Loi, M. A. *Adv. Mater.* **2009**, *21*, 1573.

(11) Ortiz, R. P.; Herrera, H.; Blanco, R.; Huang, H.; Facchetti, A.; Marks, T. J.; Zheng, Y.; Segura, J. L. *J. Am. Chem. Soc.* **2010**, *132*, 8440.

(12) Zhan, X.; Tan, Z.; Domercq, B.; An, Z.; Zhang, X.; Barlow, S.; Li, Y.; Zhu, D.; Kippelen, B.; Marder, S. R. *J. Am. Chem. Soc.* **2007**, *129*, 7246.

(13) Guo, X.; Watson, M. D. *Org. Lett.* **2008**, *10*, 5333.

(14) Chen, Z.; Zheng, Y.; Yan, H.; Facchetti, A. *J. Am. Chem. Soc.* **2009**, *131*, 8.

(15) Durban, M. M.; Kazarinoff, P. D.; Luscombe, C. K. *Macromolecules* **2010**, *43*, 6348.

(16) Kudla, C. J.; Dolfen, D.; Schottler, K. J.; Koenen, J.-M.; Breusov, D.; Allard, S.; Scherf, U. *Macromolecules* **2010**, *43*, 7864.

(17) Zhan, X.; Tan, Z.; Zhou, E.; Li, Y.; Misra, R.; Grant, A.; Domercq, B.; Zhang,

X.; An, Z.; Zhang, X.; Barlow, S.; Kippelen, B.; Marder, S. R. *J. Mater. Chem.* **2009**, *19*, 5794.

(18) Durban, M. M.; Kazarinoff, P. D.; Luscombe, C. K. *Macromolecules* **2010**, *43*, 6348.

(19) Yan, H.; Chen, Z.; Zheng, Y.; Newman, C.; Quinn, J. R.; Dotz, F.; Kastler, M.; Facchetti, A. *Nature* **2009**, *457*, 679.

(20) Rivnay, J.; Toney, M. F.; Zheng, Y.; Kauvar, I. V.; Chen, Z.; Wagner, V.; Facchetti, A.; Salleo, A. *Adv. Mater.* **2010**, *22*, 4359.

(21) Hergenrother, P. M. *High Perform. Polym.* **2003**, *15*, 3.

(22) Ghosh, M. K.; Mittal, K. L. *Eds. Polyimides: Fundamentals and Applications; Marcel Dekker: New York*, **1996**.

(23) Guo, X.; Watson, M. D. *Macromolecules* **2011**, *44*, 6711.

(24) Voskerician, G.; Weder, C. *Adv. Polym. Sci.* **2005**, *177*, 209.

(25) Katritzky, A. R.; Harris, P. A.; Kotali, A. J. *J. Org. Chem.* **1991**,*56*,5049.

(26) Jacq, J.; Einhorn, C.; Einhorn, J. *Org. let.* **2008**, *17*, 3757.

(27) Hou, J.; Chen, H.Y.; Zhang, S.; Chen, R. I; Yang, Y.; Wu, Y.; Li, G. *J. Am. Chem. Soc.* **2009**, *131*, 15586.

(28) Rhee, T. H.; Choi, T.; Chung, E. Y.; Suh, D. H. *Macromol.Chem. Phys.* **2001**, *202*, 906.

(29) Balaji, G.; Shim, W. L.; Parameswaran, M.; Valiyaveettil, S. *Org. Lett.* **2009**, *19*, 4450.

(30) Sista, P.; Nguyen, H.; Murphy, J. W.; Hao, J.; Dei, D. K.; Palaniappan, K.; Servello, J.; Kuaratne, R. S.; Gnade, B. E.; Xue, B.; Dastoor, P.; Biewer, M.

C.; Stefan, M. C. *Macromolecules* **2010**, *43*, 8063.

(31) Jenekhe, S. A.; Osaheni, J. A. *Science* **1994**, *265*, 765.

(32) Li, J.; Kendig, C. E.; Nesterov, E. E. *J. Am. Chem. Soc.* **2007**, *129*, 15911.

(33) Zhao, X.; Pinto, M. R.; Hardison, L. M.; Mwaura, J.; Muller, J.; Jiang, H.; Witker, D.; Kleiman, V. D.; Reynolds, J. R.; Schanze, K. S. *Macromolecules* **2006**, *39*, 6355.

(34) Li, Y. F.; Cao, Y.; Gao, J.; Wang, D. L.; Yu, G.; Heeger, A. J. *Synth. Met.* **1999**, *99*, 243.

Chapter 3 Synthesis and Characterization of Benzo[f]isoindole-1,3-dione and Diketopyrrolopyrrole Based Polymers and Their Photovoltaic Performance

3. 1 Introduction

Conjugated polymers have been an area of great interest due to their applications in the fields of electronic and optoelectronic devices. For example, conjugated polymers are currently used as semiconducting materials in organic field-effect transistors (OFET),[1, 2] organic light-emitting diodes (OLED),[3] organic solar cells (OSCs) [4-8] and sensors, etc. The advantages of conjugated polymers are not only the low cost, and solution processable, but also the tunable properties by changing the structure of the polymers. In recent years, conjugated polymers have attracted considerable attention in the area of bulk heterojunction (BHJ) OSCs,[5-9] however, the efficiency of OSC is relatively low compared to the inorganic solar cells. One of the main reasons is the mismatch between the absorption spectra of polymers and the solar irradiance spectrum. To overcome this problem, low band gap polymers have been designed and prepared.[10-21] The key strategy is copolymerization of strong electron-donating and electron-accepting monomers.

Low band gap polymers have absorption in the long wavelength region. However, a lot of low band gap polymers do not have or have very small absorbance in the short wavelength region (300 - 500 nm).[22, 23] Taking diketopyrrolopyrrole (**DPP**) based polymers for example (Figure 3.1), after copolymerization with fluorene, polymer **PDPP-F** shows absorption at around 600 nm. The absorbance at

400 nm is so weak that it can be ignored. To our knowledge, the best PCE of the device made from polymer **PDPP-F** is only 0.78%.[23] One of the reasons may be lack of absorbance at 400 nm region. As we know, **DPP** is a strong acceptor and it moves the absorbance to 650 nm or even further.[24-26] If a weak acceptor is introduced in this polymer, additional absorption at 400 nm can be realized which will cover the blank region of the spectrum.

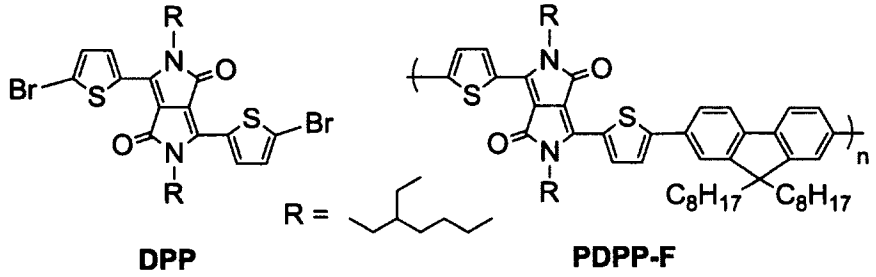

Figure 3.1. DPP monomer and **DPP**-fluorene polymer.

In chapter 2, we designed and prepared 4,9-bis(5-bromothiophen-2-yl)-2-(2-ethylhexyl)-benzo[f]isoindole-1,3-dione (**BIDO-2**) monomer as a weak acceptor. In this chapter **BIDO-2** was copolymerized with **DPP** in order to add short wavelength absorbance to the polymer. As we know, the packing of the polymers in the active layer of OSC is crucial to achieve better photovoltaic performance. A good packing of the polymer enables efficient and rapid charge transport, which directly improves PCE of the device.[27, 28] The naphthalene part of **BIDO-2** was designed to give the molecule a good packing ability because of its planar structure. Thienyl group is commonly used in the solar cell materials, because it has a high mobility of electrons.[27] That's one of the reasons why thienyl groups appear in **BIDO-2** molecules. The other reason is that with thienyl groups **BIDO-2** is supposed to have the similar reactivity with **DPP**. Thus, by changing the monomer feed ratio, the ratio

between **BIDO** and **DPP** in the copolymers can be controlled.

P1 was selected as model polymer, which shows absorbance at 400 nm and proved **BIDO-2** is a weak acceptor. Then **BIDO-2**, **DPP** and 9,9-dioctylfluorene were copolymerized, to yield **Pa**, **Pb** and **Pc**. The effect of different amount of **BIDO-2** on the optical and electrochemical properties was investigated. The photovoltaic performance of **Pa**, **Pb** and **Pc** was tested, and improved PCE was obtained.

3.2 Results and discussions

3.2.1 Syntheses of polymers

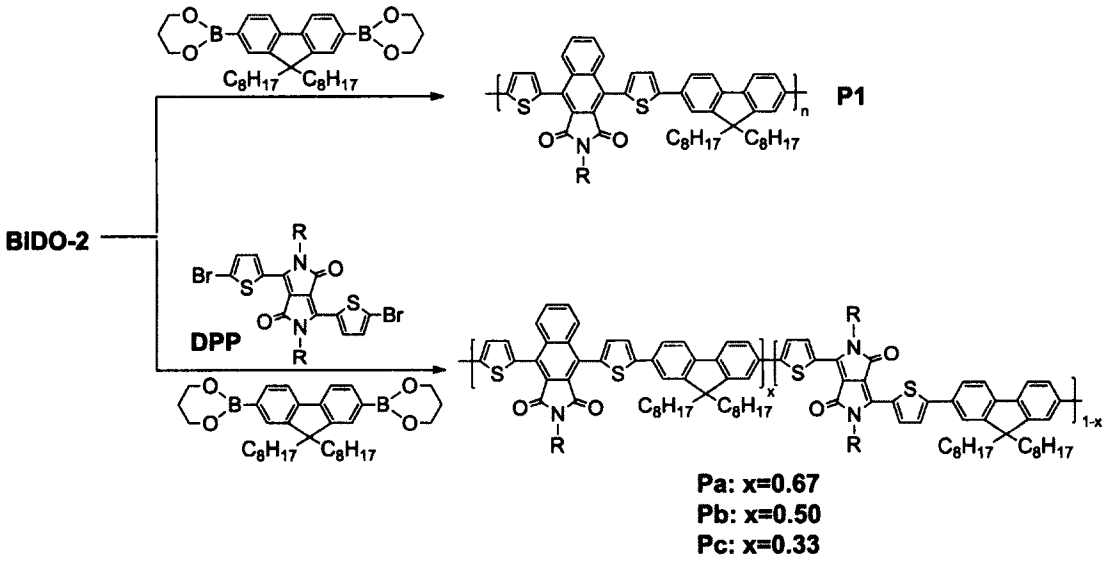

Scheme 3.1. Syntheses of polymers **Pa**, **Pb** and **Pc**.

As shown in Scheme 3.1, polymerizations were done by Suzuki cross-coupling reaction with $Pd(PPh_3)_4$ as catalyst. **P1** was prepared by polymerizing **BIDO-2** monomer with 9,9-dioctylfluorene-2,7-diboronic acid bis(1,3-propanediol) ester. By changing the ratio between **BIDO-2** and **DPP** to 2:1, 1:1 and 1:2, copolymers **Pa**, **Pb** and **Pc** were obtained, respectively. All the polymers have good solubility in common organic solvents such as chloroform, THF and chlorobenzene. Molecular weights and polydispersity indices (PDI) of the polymers were determined by gel permeation chromatography (GPC) relative to polystyrene standards (Table 3.1). **P1** has a higher molecular weight of 111.2 kg/mol with a PDI of 2.2. **Pa** and **Pb** have molecular weight of 76.3 kg/mol and 74.6 kg/mol, respectively. Comparing to these three polymers, **Pc** has the lowest molecular weight of 33.3 kg/mol.

Table 3.1. Molecular weights and PDI of polymers.

Polymer	M_w (kg/mol)	PDI
P1	111.2	2.2
Pa	76.3	2.6
Pb	94.6	2.6
Pc	33.3	2.1

3.2.2 IR characterization

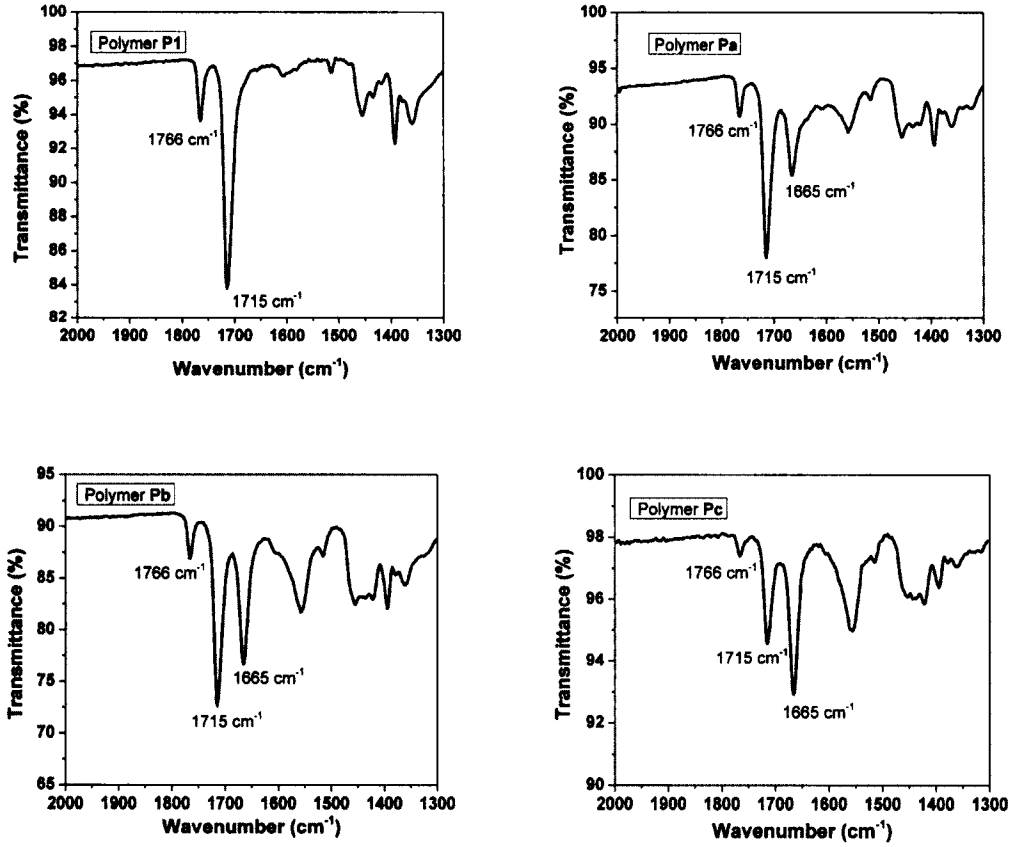

Figure 3.2. IR spectra of polymer **P1**, **Pa**, **Pb** and **Pc**.

IR analysis was done with thin films of polymers cast on the NaCl salt plates. As shown in Figure 3.2, polymer **P1** containing imide groups shows intense C=O peaks at 1715 and 1766 cm^{-1}. After adding **DPP** monomer to the polymers, a new C=O peak shows up at 1665 cm^{-1} which can be assigned to the amide group of the

DPP unit. As the content of **DPP** increases from polymer **Pa** to **Pc**, the intensity of band at 1665 cm^{-1} increases as well. The observation proves that **DDP** was successfully copolymerized into the polymer with **BIDO-2** and ratio of the two in the polymer is related to feed ratio of the monomers.

3.2.3 NMR characterization

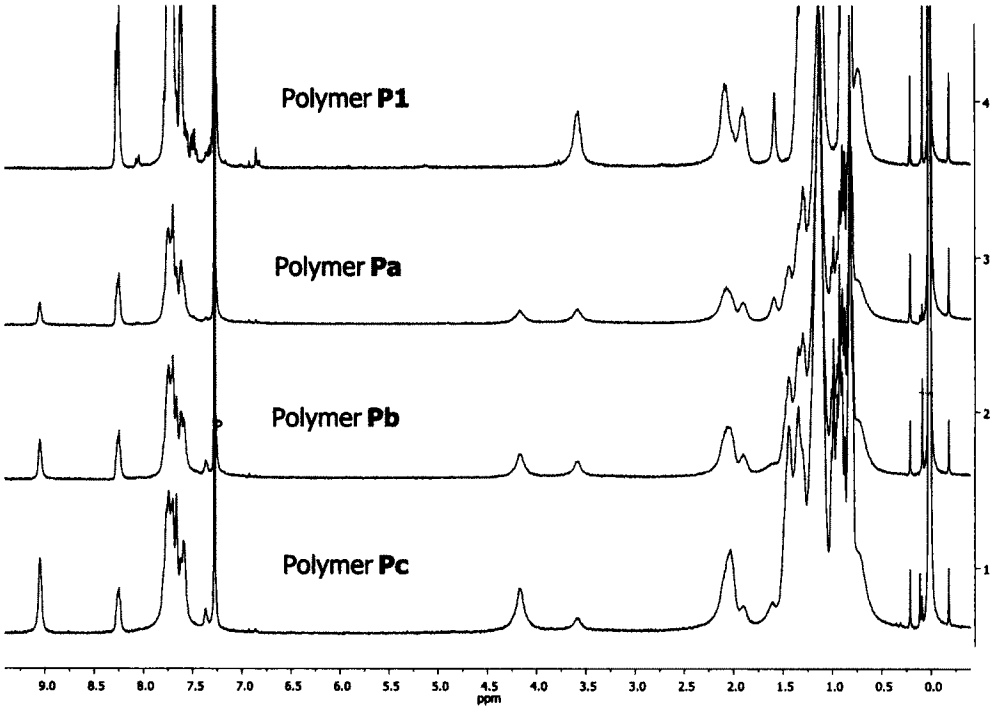

Figure 3.3. ^{1}H NMR spectra of polymer **P1**, **Pa**, **Pb** and **Pc** in $CDCl_3$.

All polymers were characterized by ^{1}H NMR and ^{13}C NMR spectroscopy. In the ^{1}H NMR spectra, polymers display proton resonances both in the aliphatic region (0-3.0 ppm) due to alkyl chains and the aromatic region (6.50-9.5 ppm) due to the conjugated backbone of the polymers. Because of the high degree of overlapping of peaks, peak assignments of polymers are impossible in these two regions. However, valuable information can be obtained from the region of 3.0-5.0 ppm, where protons

from N-CH_2 groups exhibit resonance peaks with no overlapping. The peak at 3.57 ppm is assigned to N-CH_2 of the imide group from **BIDO-2**, whereas the one at 4.18 ppm is assigned to N-CH_2 of **DPP** (Figure 3.3).

Quantitative study of the polymer structure can be achieved by comparing the integration of the two peaks. The data are summarized in Table 3.2. After calculation, the actual percentage of **DPP** in the polymer was obtained and by comparing with the calculated value, the amount of **DPP** in the polymer was found to be slightly lower. The reason is probably due to the lower reactivity of **DPP** monomers. Another evidence is the low molecular weight of **Pc**. Because lower reactivity of monomer can result in lower molecular weight of polymer, **Pc** has the largest amount of **DPP** but the lowest molecular weight.

Table 3.2. The ratio of **BIDO-2** and **DPP** in polymer **Pa**, **Pb** and **Pc**.

Polymers	**BIDO-2:DPP** in feed	**DPP** (%) Calculated	H_{BIDO-2}:H_{DPP} by ^{1}H NMR	**BIDO-2:DPP** in polymer	**DPP** (%) in polymer
Pa	2 : 1	33	2 : 1.77	2 : 0.89	31
Pb	1 : 1	50	2 : 2.78	1 : 0.70	41
Pc	1 : 2	67	2 : 5.58	1 : 1.40	58

3.2.4 Thermal stability and T_g of polymers

Since the polymers are to be used in OSCs, the thermal property is one of the major factors that need to be determined. Polymers were characterized by thermogravimetric analysis (TGA) and differential scanning calorimetry (DSC) (Figure 3.4). The data are summarized in Table 3.3.

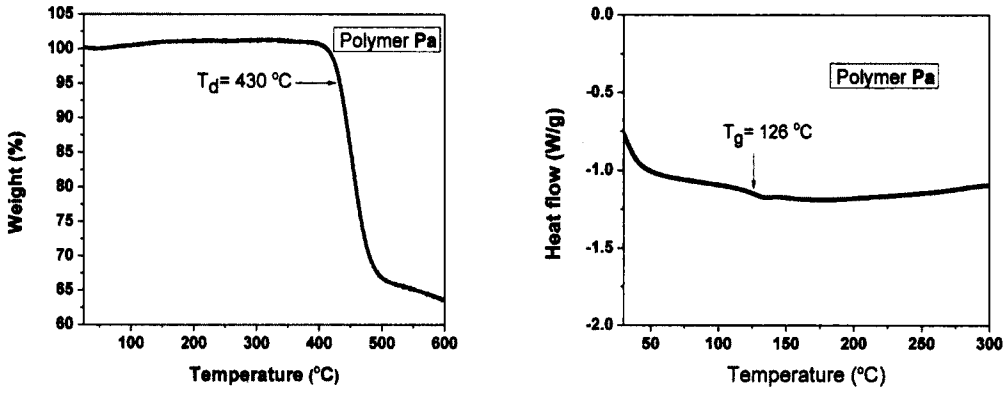

Figure 3.4 TGA (left) and DSC (right) of polymer **Pa.**

All polymers have very high decomposition temperature (T_d) above 400 °C, thus being suitable for the device fabrication. During the fabrication of the device, the polymer films need to be annealed at certain temperature. Usually people choose the temperature above T_g, because chain fragments of polymers can move or rotate to have more stable conformation above T_g and, at the same time, morphology of the active layer can be optimized during this process and solar cell performance can be improved. T_g of our polymers are round 120 °C and the annealing temperature was selected to be 150 °C. All polymers are amorphous based on the evidence of no crystallization peaks in DSC, which is due to the presence of the bulky aliphatic chains that interfere the packing of the conjugated backbones.

Table 3.3. Thermal properties of polymers.

Polymers	Decomposition Temperature (T_d)	Glass Transition Temperature (T_g)
P1	420 °C	110 °C
Pa	430 °C	126 °C
Pb	408 °C	121 °C
Pc	425 °C	122 °C

3.2.5 Optical properties

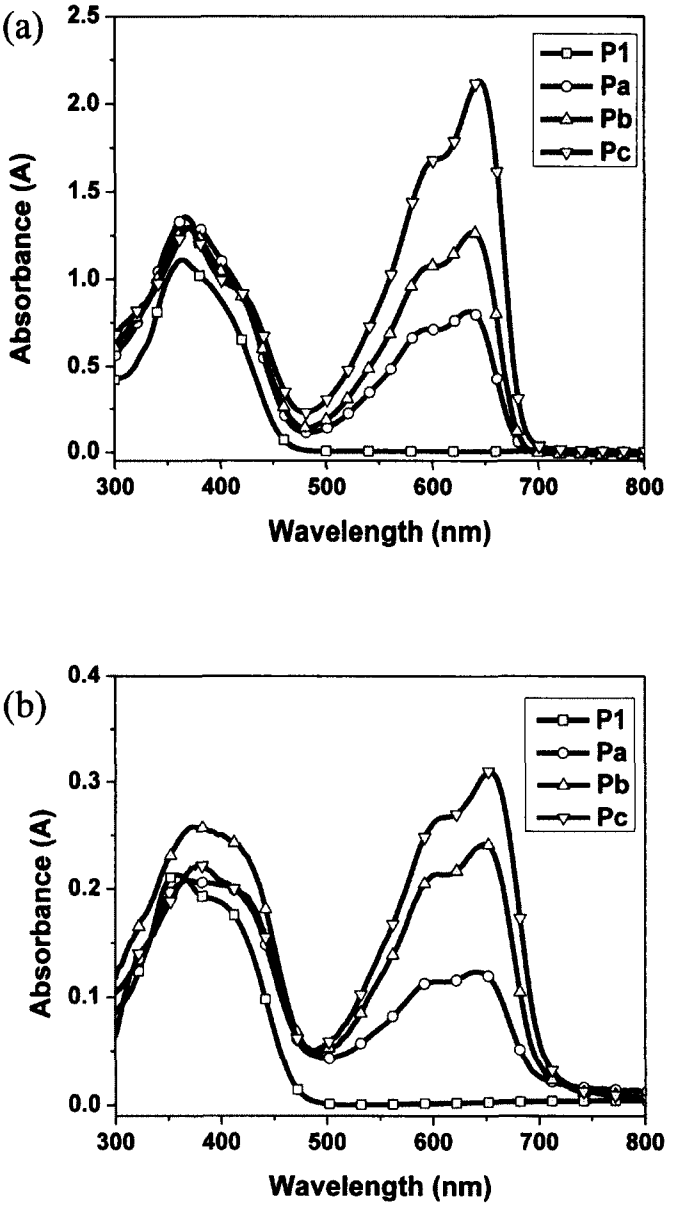

Figure 3.5. Absorption spectra of polymer **P1**, **Pa-Pc** in chloroform (a) (concentration: **P1** = 3.8 x 10^{-2} mg/mL, **Pa** = 5.2 x 10^{-2} mg/mL, **Pb** = 8.5 x 10^{-2} mg/mL, **Pc** = 2.12 x 10^{-2} mg/mL) and as thin films (b) with the thickness of 30 nm.

Table 3.4. UV-vis absorptions of polymers.

Polymer	λ_{abs} (nm) in solution	λ_{abs} (nm) Film
P1	362	363
Pa	368/635	370/642
Pb	369/638	377/648
Pc	370/645	380/653

The absorption spectra of the polymers in chloroform and as film are shown in Figure 3.5. **P1** has only one λ_{max} at 362 nm, which can be assigned to the π-π^* transition of the conjugated polymer backbone. By copolymerizing with **DPP** monomer, **Pa**, **Pb** and **Pc** are showing additional λ_{max} at around 650 nm with different intensity, which is attributed to the intramolecular charge transfer (ICT) between **DPP** and fluorene segments.[29] It is very clear that the intensity of peak at longer wavelength is increasing as the proportion of **BIDO-2** decreases. And it is interesting that the absorbance intensities of π-π^* transition band and ICT band have almost the same ratio of **BIDO-2** and **DPP**. With 67% of **BIDO-2**, the absorbance of π-π transition band is as twice intense as ICT band for **Pa**. Whereas, **Pb** (50% **BIDO-2**) has equal intensity for the two bands and **Pc** (33% **BIDO-2**) has more intense ICT band. The absorption spectra of the polymers in thin films showed red shifted absorption compared to the ones in solution and all the thin films spectra are a little broader, indicating intermolecular interaction in the solid state. However, the relatively small shift from the solution to the film is probably due to rigid conformation of polymers both in the solution and in the solid state.

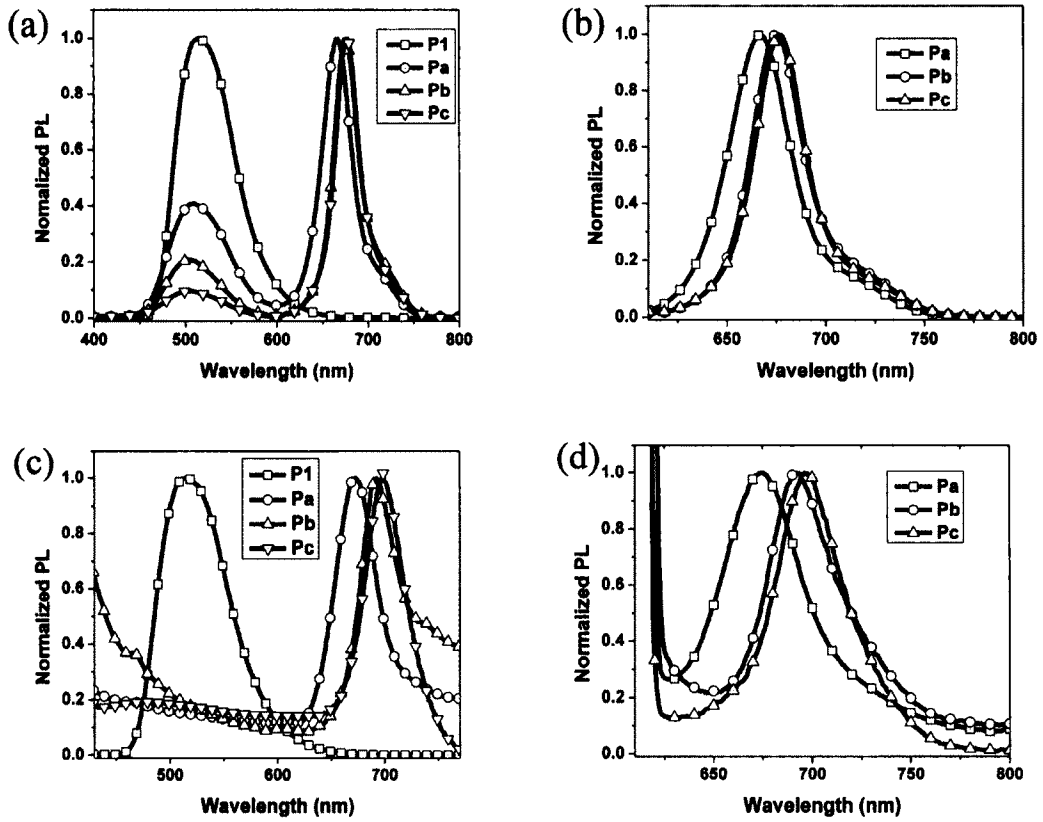

Figture 3.6. Normalized PL spectra of polymers in chloroform, excited at 350 nm (a) and 600 nm (b), and as films, excited at 400 nm (c) and 600 nm (d).

Table 3.5. PL and quantum yield of polymers.

Polymer	$\lambda_{ex}/\lambda_{em}$ in solution (nm)	$\lambda_{ex}/\lambda_{em}$ in solution (nm)	$\lambda_{ex}/\lambda_{em}$ Film (nm)	$\lambda_{ex}/\lambda_{em}$ Film (nm)	Quantum Yield [a]
P1	350/515	---	400/514	---	7.3
Pa	350/509, 666	600/666	400/673	600/673	3.5
Pb	350/504, 675	600/675	400/692	600/693	2.5
Pc	350/504, 677	600/677	400/700	600/697	1.8

[a] Fluorescence quantum yield of films were determined using an integrating sphere (with the excitation wavelength at 409 nm).

The fluorescence spectra of the polymers have been recorded, shown in Figure 3.6. In chloroform solution, polymer **P1** displays emission at 515 nm under the excitation at 350 nm, while the other three polymers show two emission peaks at around 505 and 670 nm. From **Pa** to **Pc**, as the **BIDO-2** portion decreases, the emission intensities at 505 nm decreases as well. The polymer solutions of **Pa**, **Pb** and **Pc** were also excited at 600 nm, the emission at 670 nm showed up at the exact same place. Therefore, it is very obvious that the 505 nm emission comes from the **BIDO-2** segments and the emission at 670 nm comes from the **DPP** segments. Since the emission at 505 nm partially covers the ICT band of the polymer, fluorescence resonance energy transfer (FRET) can be realized in polymer **Pa**, **Pb** and **Pc**, which contributes the two emission peaks at different wavelength. The fluorescence spectra of the thin films were also collected. Exited at 400 nm, **P1** showed emission at 514 nm. However, the emissions at this region can't be observed for **Pa**, **Pb** and **Pc**. They only showed emission peaks at around 700 nm. In the solid state, polymers are closely packed, where FRET will be enhanced, therefore more energy goes to the lower band gap leaving no emission in the short wavelength region. If excited at 600 nm, the emission at 700 nm also showed up for the last three polymers. The fluorescence quantum yields of the polymers were measured and listed in Table 3.5. The quantum yields of **Pa** to **Pc** are lower than that of **P1** due to the energy lose as nonradiative decay during the FRET process.

3.2.6 Electrochemical properties and band gaps

Electrochemical cyclic voltammetry (CV) was performed to determine the

HOMO and LUMO energy levels of the polymers. From the value of onset oxidation potential E_{ox} and onset reduction potential E_{red}, the HOMO and LUMO levels as well as the band gap E_g were calculated and listed in Table 3.6 and a diagram of energy levels is plotted based on these values (Figure 3.7). The data show that **P1** has the highest LUMO level of -2.88 eV, and largest band gap of 2.41 eV among four polymers. This is because LUMO level of the D-A polymer is determined by the electron withdrawing ability of the acceptor. As a weak acceptor, **BIDO-2** can't lower the LUMO level much. However, introduction of strong acceptor **DPP** has big impact on lowering the LUMO level. Therefore, for polymer **Pa**, **Pb** and **Pc**, the LUMO levels were decreased to -3.6 eV. Because the donors of these three polymers are the same with **P1**, the HOMO levels of all polymers are similar, around -5.30 eV. This results in a significant decrease of the band gap for **Pa**, **Pb** and **Pc**. However, changing **DPP** portion does not change the band gap much. Therefore, **Pa**, **Pb** and **Pc** have similar energy levels and band gaps. In comparison, the energy levels and band gaps of our **DPP** containing polymers are similar with the ones of **PDPP-F**.

Table 3.6. Electrochemical properties and band gaps of polymers.

Polymer	E_{ox}[a] (V)	E_{red}[a] (V)	HOMO (eV)	LUMO (eV)	Band gap (eV)
P1	1.13	-1.28	-5.29	-2.88	2.41
Pa	1.14	-0.40	-5.30	-3.76	1.54
Pb	1.19	-0.48	-5.35	-3.68	1.67
Pc	1.21	-0.45	-5.37	-3.71	1.66

[a] The potentials were measured from the onset of the CV curves. The CV of compounds were measured in a 0.1 mol/L Bu_4NPF_6/dichloromethane solution.

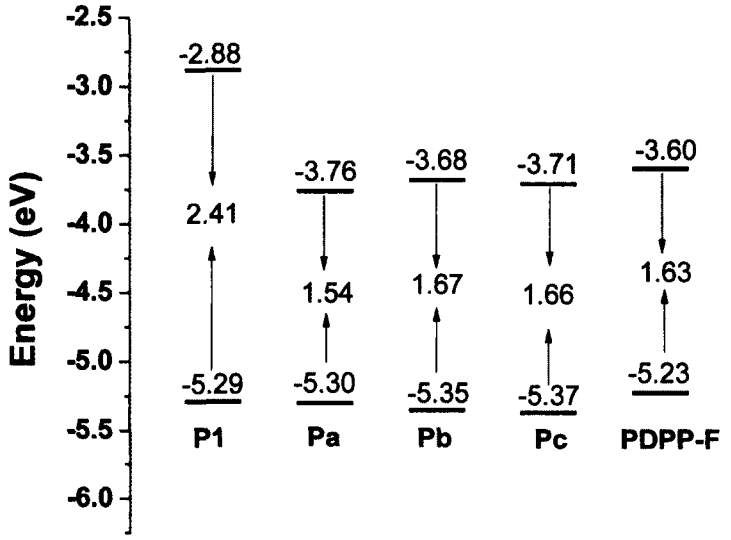

Figure 3.7. Energy levels of polymers and [70]PCBM.

3.2.7 Solar cell performance

The photovoltaic properties of **Pa**, **Pb** and **Pc** were investigated by fabricating BHJ solar cells with the configuration of ITO/PEDOT:PSS/polymer:[70]PCBM/ LiF/Al. As summarized in Table 3.7, the active layers were made with polymer/[70]PCBM blend with the ratio of 1:1 and 1:2 with the thickness of 80 nm, and the current density-voltage (*J-V*) characteristics of devices under white light illumination are shown in Figure 3.8. High open circuit voltages V_{oc} ranging from 0.82 to 0.91V were observed for these polymers, which is because of the low HOMO levels. Due to the small differences between their HOMO levels, the V_{oc} of polymers are very close to each other. It is also observed that devices made of **Pb** and **Pc** are showing bigger short circuit current J_{sc} than the device of **Pa**. The reason is that, although the spectrum of solar irradiation covers from 350 to 3000 nm, its maximum

intensity is at about 680 nm, **Pa** has a smaller proportion of long wavelength absorption, which makes it harvest less sun light in this region and resulted in a smaller J_{sc}. By increasing the **DPP** portion to 50% in **Pb**, highest J_{sc} of 4.50 mA/cm^2 was observed with a PCE of 1.11%. The highest PCE of 1.17% comes from **Pc** due to its higher FF.

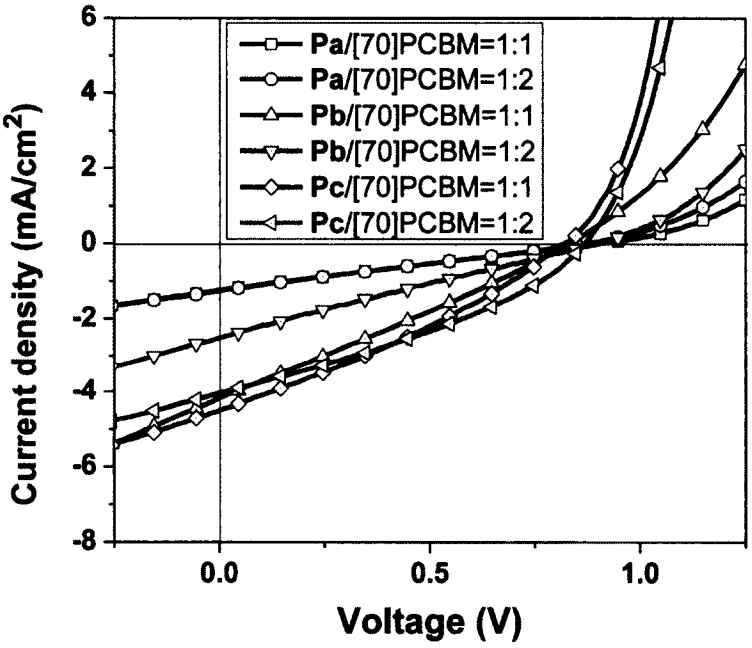

Figure 3.8. Current density-voltage curves of devices made from **Pa**, **Pb** and **Pc**.

Comparing the PCE at different polymer/[70]PCBM ratios, it was observed that at the ratio of 1:2, the devices gave better photovoltaic performance. It is probably due to optimized phase separation at this ratio. Atomic force microscopy (AFM) was utilized to further investigate the reasons.

In comparison to the solar cell performance of polymer **PDPP-F**, the J_{sc} of **Pb** is over two times higher than the one of **PDPP-F** and it is believed that additional absorption in the 400 nm region from **BIDO-2** unit plays a very important role in this

improvement. The highest PCE obtained is increased about 50% comparing to the PCE of **PDPP-F**, which was reported to be only 0.78%. However, the FF of **Pa**, **Pb** and **Pc** are relatively small. As we know, FF is related to a lot of factors, such as charge carrier mobility and balance, interface recombination, film morphology and miscibiliy of p-type and n-type material. Since **BIDO-2** and **DPP** momoners are appearing in the polymer backbone in a random way, the poor regioregularity of the polymers may have some negative effectives on polymer packing in the solid state. And this can affect the mobility of carriers and result in small FF values.

Table 3.7. Photovoltaic properties of polymer **Pa**, **Pb** and **Pc.**

Polymer/[70]PCBM weight ratio	V_{oc} (V)	J_{sc} (mA/cm^2)	FF	PCE (%)
Pa/[70]PCBM=1:1	0.90	1.21	0.23	0.26
Pa/[70]PCBM=1:2	0.91	2.49	0.24	0.54
Pb/[70]PCBM=1:1	0.87	1.26	0.25	0.27
Pb/[70]PCBM=1:2	0.82	4.50	0.30	1.11
Pc/[70]PCBM=1:1	0.83	4.18	0.26	0.92
Pc/[70]PCBM=1:2	0.86	4.04	0.34	1.17

2.2.8 Morphology of polymer blends

Controlling the morphology of the active layer is a key requirement to achieve high PCE. As the exciton diffusion length is limited to 10 nm, an intimate mixing of the donor and the acceptor materials is needed for efficient charge separation and transport in OSCs.[30] Therefore, the morphology of the active layer was measured by AFM. As shown in Figure 3.9, there are large domains appearing in the active

layers which were made from 1:1 ratio of polymer/[70]PCBM mixture. However, at 1:2 ratio, the domains become smaller and evenly separated, which is ideal for charge separation and transportation, and this is in good agreement with the better PCE obtained from these devices.

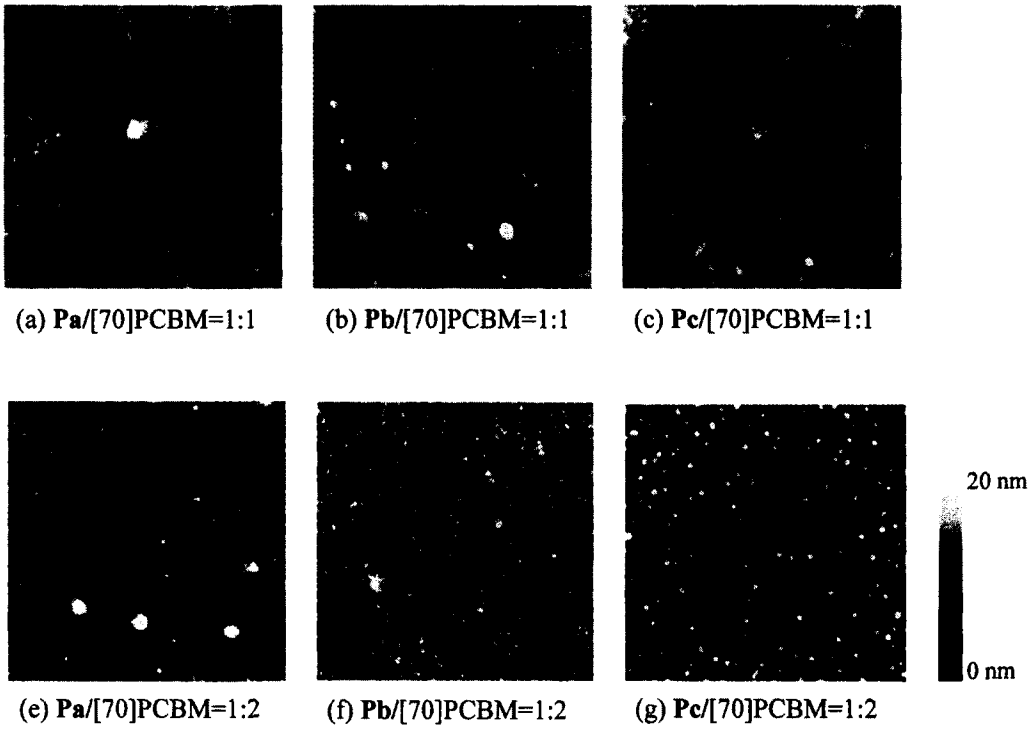

Figure 3.9. AFM height images of polymer:[70]PCBM blends. The size of the images is 5 μm×5 μm.

3.3 Conclusion

BIDO-2 monomer was successfully copolymerized with fluorene and **DPP** to make **Pa**, **Pb** and **Pc** by Suzuki cross-coupling reaction. All polymers have high molecular weights which were determined by GPC. The optical and electrochemical properties of the polymers were investigated. Model polymer **P1** shows absorption at

400 nm and has largest band gap of 2.41 eV, which proves that **BIDO-2** is acting as a weak acceptor in the polymer backbone. By copolymerizing with **DPP** monomer, polymers show absorption at both 400 and 650 nm regions, and have smaller band gaps. The absorption intensity of ICT band increases, as the proportion of **BIDO-2** decreases. Fluorescence spectra of **Pa, Pb** and **Pc** show emissions at 505 and 670 nm, which reveals that FRET happens in the polymers. The solar cell performance of **Pa, Pb** and **Pc** were studied. They have similar V_{oc}, however different J_{sc}. Larger J_{sc} were obtained from **Pb** and **Pc,** because they have enough absorption at long wavelength region. The morphology of the active layer was investigated by AFM. It shows smaller domains and better phase separation at the polymer/[70]PCBM ratio of 1:2. The highest PCE of 1.17% came from **Pc** at this ratio. Comparing it with the PCE of **PDPP-F** polymer, it increases about 50%. For this increase, the absorption from **BIDO-2** segments plays an important role. Since **BIDO-2** and **DPP** are appearing in the polymer backbone in a random way, poor regioregularity of the polymer affects the stacking of the polymer in solid states and results in limited improvement of PCE.

3.4 Experimental

3.4.1 Materials

Tetrahydrofuran (THF, Aldrich) was dried by refluxing over sodium solid and benzophenone. Other chemicals and reagents purchased from Aldrich and TCI were used directly without further purification.

3.4.2 Instruments

^{1}H NMR spectra and ^{13}C NMR spectra were measured on Bruker Advance

300 instrument at 300 MHz and 75 MHz respectively. IR spectra were recorded on Varian 1000 FT-IR Scimitar Series. UV-vis spectra were measured on Perkin ELMER Lambda 900. PL spectra were measured on ManDEL Scientific RF-1501 spectrofluorophotometer. Differential scanning calorimetry and thermogravimetric analyzers were conducted on a TA Q100 and Hi-Res TGA 2950 under N_2 gas, at a heating rate of 10 °C. High Resolution ESI spectra were recorded on the 7.0T Actively Shielded Fourier Transform Ion Cyclotron Resonance Mass Spectrometers. Cyclic voltammograms (CV) and other electrochemical experiments were performed on a BAS 100 electrochemical workstation. Glass carbon working electrode, platinum counter electrode and silver pseudoreference electrode were used together, all the potentials were corrected using ferrocenium/ferrocene (Fc^+/Fc^0) and reported relative to NHE.

3.4.3 Solar cell preparation and characterization

ITO coated glass substrates were cleaned with deionized water, acetone, and isopropanol successively by sonication for 5 min each and then dried in vacuum. After that, the ITO substrates were treated with UV-ozone and transferred into a glove box. After spin-coating 35 nm layer of poly(3,4-ethylenedioxythiophene):poly (styrenesulfonate) (PEDOT:PSS), they were baked at 130 °C for 30 min. The respective polymer and [70]PCBM were dissolved in *o*-dichlorobenzene and mixed in a weight ratio of 1:1 and 1:2. By spin-casting the polymer blend onto the PEDOT-PSS/substrate at a speed of 1500 rpm for 60 s, an active layer with 80 nm thickness was formed. Then they were baked at 150 °C for 5 min, then LiF (1 nm) and Al (100

nm) were thermally evaporated under vacuum lower than 3×10^{-6} Torr on the top of the active layer. For thermal annealing, the completed devices were placed directly onto a digitally controlled hot plate and heated to 150 °C for the desired time. All current-voltage (I-V) characteristics of the devices were measured under simulated AM1.5G irradiation (100 mW cm^{-2}) using a Xe lamp-based Newport 91160 300-W Solar Simulator. The light intensity was adjusted with an NREL-calibrated Si solar cell with a KG-5 filter.

3.4.4 Synthesis

Polymer Pa

BIDO-2 (0.32 g, 0.50 mmol), **DPP** (0.17 g, 0.25 mmol) and 9,9-dioctylfluorene-2,7-diboronic acid bis(1,3-propanediol) ester (0.42 g, 0.75 mmol) were combined in 10 ml THF. Then 10 ml K_2CO_3/water solution (0.1g/ml) was added. The system was degassed, followed by the addition of $Pd(PPh_3)_4$ (10mg). Then the system was degassed again and heated to reflux under argon protection for 48 h. The resulting solution was cooled to room temperature and diluted with 100 ml $CHCl_3$, then washed with water, brine and dried over sodium sulfate anhydrous. After that, the solution was concentrated into 10-15ml and the polymer was precipitated by adding the solution in 200 ml methanol. The polymer was then subjected to Soxhlet extraction with acetone and chloroform and recovered by precipitating in methanol to give dark blue polymer (0.58 g, 87% yield). ^{1}H NMR (300 MHz, $CDCl_3$) δ (ppm): 9.05 (s, 1H), 8.27-8.24 (m, 2.4H), 7.74-7.59 (m, 18.8H), 4.27 (s, 1.8H), 3.59-3.57 (d, J = 6 Hz, 2H), 2.09-1.90 (m, 8.3H), 1.59-1.13 (m, 66H), 1.01-0.74 (m, 40H). ^{13}C

NMR (75 MHz, $CDCl_3$) δ (ppm): 166.9, 151.9, 151.7, 147.2, 140.5, 140.1, 139.7, 136.4, 133.4, 133.0, 132.5, 130.5, 129.3, 128.5, 125.6, 125.0, 122.9, 120.2, 120.0, 108.2, 55.4, 40.5, 39.3, 38.0, 31.8, 30.6, 30.4, 30.1, 30.0, 29.3, 29.2, 28.6, 28.4, 24.0, 23.8, 23.1, 23.0, 22.6, 14.1, 14.0, 10.6.

Polymer Pb

Polymer **Pb** was prepared by the same method with **Pa**, but using **BIDO-2** (0.24 g, 0.38 mmol), **DPP** (0.26 g, 0.38 mmol) and 9,9-dioctylfluorene-2,7-diboronic acid bis(1,3-propanediol) ester (0.42 g, 0.76 mmol). Dark blue polymer was obtained (0.54 g, 81%). ^{1}H NMR (300 MHz, $CDCl_3$) δ (ppm): 9.05 (s, 1.5H), 8.26-8.23 (m, 2H), 4.17 (s, 2.8H), 3.59 (s, 2H), 2.09-1.90 (m, 10H), 1.14-0.79 (m, 115.6H). ^{13}C NMR (75 MHz, $CDCl_3$) δ (ppm): 166.9, 161.8, 152.2, 152.0, 151.9, 151.7, 147.2, 147.0, 141.7, 140.5, 140.1, 139.7, 136.9, 136.4, 133.4, 133.0, 132.4, 132.0, 130.5, 129.3, 128.5, 125.6, 125.0, 124.3, 122.9, 120.4, 120.2, 119.7, 55.4, 46.0, 40.5, 39.3, 38.0, 31.8, 31.7, 30.6, 30.4, 30.0, 29.3, 29.2, 28.6, 28.4, 24.0, 23.7, 23.1, 23.0, 22.6, 14.1, 14.0, 10.6.

Polymer Pc

Polymer **Pc** was prepared by the same method with **Pa**, but using **BIDO-2** (0.16 mg, 0.25 mmol), **DPP** (0.34 mg, 0.50 mmol) and 9,9-dioctylfluorene-2,7-diboronic acid bis(1,3-propanediol) ester (0.42 g, 0.75 mmol). Dark blue polymer was obtained (0.50 g, 75%). ^{1}H NMR (300 MHz, $CDCl_3$) δ (ppm): 9.05 (s, 3.4H), 8.26-8.23 (m, 2.4H), 7.76-7.59 (m, 25.3H), 4.17 (s, 5.6H), 3.59-3.57 (d, J = 7.5 Hz, 2H),

2.09-1.90 (m, 14.4H), 1.61-0.79 (m, 171.9H). ^{13}C NMR (75 MHz, $CDCl_3$) δ (ppm): 166.9, 161.8, 152.2, 152.0, 151.9, 151.7, 150.3, 141.2, 139.7, 136.9, 136.4, 133.0, 132.4, 130.6, 129.3, 128.6, 125.6, 125.4, 124.4, 120.6, 120.4, 120.2, 108.3, 55.5, 55.4, 46.0, 40.5, 39.3, 31.7, 30.6, 30.4, 30.0, 29.9, 29.2, 28.6, 28.4, 24.0, 23.7, 23.1, 23.0, 22.6, 14.1, 14.0, 10.6.

References

(1) Sirringhaus, H.; Tessler, N.; Friend, R. H. *Science* **1998**, *280*, 1741.

(2) Svensson, M.; Zhang, F. L.; Veenstra, S. C.; Verhees, W. J. H.; Hummelen, J. C.; Kroon J.M.; Inganäs, O.; Andersson, M. R. *Adv. Mater.* **2003**, *15*, 988.

(3) Müller, D. C.; Falcou, A.; Reckefuss, N.; Rojahn, M.; Wlederhirm, V.; Rudati, P.; Frohne, H.; Nuyken, O.; Becker, H.; Meerhotz, K. *Nature* **2003**, *421*, 829.

(4) Günes, S.; Neugebauer, H.; Sariciftci, N. S. *Chem. Rev.* **2007**, *107*, 1324.

(5) Son, H. J.; Wang, W.; Xu, T.; Liang, Y.; Wu, Y.; Li, G.; Yu, L. *J. Am. Chem. Soc.* **2011**, *133*, 1885.

(6) He, F.; Wang, W.; Chen, W.; Xu, T.; Darling, S. B.; Strzalka, J.; Liu, Y.; Yu, L. *J. Am. Chem. Soc.* **2011**, *133*, 3284.

(7) Hou, J.; Chen, H.Y.; Zhang, S.; Li, G.; Yang, Y. *J. Am. Chem. Soc.* **2008**, *130*, 16144.

(8) Hou, J.; Chen, H. Y.; Zhang, S.; Chen, R. I.; Yang, Y.; Wu, Y.; Li, G. *J. Am. Chem. Soc.* **2009**, *131*, 15586.

(9) Chen, J.; Cao, Y. *Acc. Chem. Res.* **2009**, *42*, 1709.

(10) Zoobelt, A. P.; Fonrodona, M.; Wienk, M. M.; Sieval, A. B.; Hummelen, J. C.; Janssen, R. A. *J. Org. Lett.* **2009**, *11*, 903.

(11) Hou, J.; Park, M. H.; Zhang, S.; Yao, Y.; Chen, L. M.; Li, J. H.; Yang, Y. *Macromolecules* **2008**, *41*, 6012.

(12) Zhou, Q.; Hou, Q.; Zhang, L.; Deng, X.; Yu, G.; Cao, Y. *Appl. Phys. Lett.* **2004**, *84*, 1653.

(13) Slooff, L. H.; Veenstra, S. C.; Kroon, J. M.; Moet, D. J. D.; Sweelssen, J.; Koetse, M. M. *Appl. Phys. Lett.* **2007**, *90*, 143506.

(14) Blouin, N.; Michaud, A.; Leclerc, M. A. *Adv. Mater.* **2007**, *19*, 2295.

(15) Shi, C.; Yao. Y.; Yang, Y.; Pei, Q. *J. Am. Chem. Soc.* **2006**, *128*, 8980.

(16) Zhou, E.; Nakamura, M.; Nishizawa, T.; Zhang, Y.; Wei, Q.; Taijima, K.; Yang, C.; Hashimoto, K. *Macromoleculs* **2008**, *41*, 8302.

(17) Lu, J.; Liang, F.; Drolet, N.; Ding, J.; Tao, Y. *Chem. Comm.* **2008**, 5315.

(18) Chen, C. P.; Chan, S. H.; Chao, T. C.; Ting, C.; Ko, B. T. *J. Am. Chem. Soc.* **2008**, *130*, 12828.

(19) Muhlbacher, D.; Scharber, M.; Morana, M.; Zhu, Z.; Waller, D.; Guadiana, R.; Brabec, C. *Adv. Mater.* **2006**, *18*, 2884.

(20) Peet, J.; Kim, J. Y.; Coats, N. E.; Ma, W. L.; Moses, D.; Heeger, A. J.; Bazan, G. C. *Nat. Mater.* **2007**, *6*, 497.

(21) Lee, J. K.; Ma, W. L.; Barbec, C. J.; Yuen, J.; Moon, J. S.; Kim, J. Y.; Lee, K.; Bazan, G. C.; Heeger, A. J. *J. Am. Chem. Soc.* **2008**, *130*, 3619.

(22) Zhou, E.; Yamakawa, S.; Tajima, K.; Yang, C.; Hashimoto, K. *Chem. Mater.* **2009**, *21*, 4055.

(23) Zoombelt, A. P.; Mathijssen, S. G. J.; Turbiez, M. G. R.; Wienk, M. M.; Janssen, R. A. J. *J. Mater. Chem.* **2010**, *20*, 2240.

(24) Wienk, M. M.; Turbiez, M.; Gilot, J.; Janssen, R. A. J. *Adv. Mater.* **2008**, *20*, 2556.

(25) Tamayo, A. B.; Dang, X. D.; Walker, B.; Seo, J.; Kent, T.; Nguyen, T. Q. *Appl. Phys. Lett.* **2009**, *94*, 103301.

(26) Mei, J.; Graham, K. R.; Stalder, R.; Reynolds, J. R. *Org. Lett.* **2010**, *12*, 660.

(27) Sirringhaus, H.; Brown, P. J.; Friend, R. H.; Nielsen, M. M.; Bechgaard, K.; Langeveld-Voss, B. M. W.; Spiering, A. J. H.; Janssen, R. A. J.; Meijer, E. W.; Herwig, P.; de Leeuw, D. M. *Nature* **1999**, *401*, 685.

(28) Yang, X.; Loos, J,; Veenstra, S. C.; Verhees, W. J. H.; Wienk, M. M.; Kroon, J. M.; Michels, M. A. J.; Janssen, R. A. J. *Nano Lett.* **2005**, *5*, 579.

(29) Tamayo, A. B.; Walker, B.; Nguyen, T. Q. *J. Phys. Chem. C.* **2008**, *112*, 11545.

(30) van Bavel, S.; Veenstra, S.; Loos, J. *Macromol. Rapid. Commun.* **2010**, *6*, 1835.

Chapter 4 Synthesis and Characterization of Thiadiazolobenzo-imidazole Based Low Band Gap Chromophores

4.1 Introduction

Organic compounds with π-conjugated structures have attracted significant attention due to their potential as semiconducting materials in optoelectronic devices, such as organic field-effect transistors (OFETs),[1-4] organic solar cells (OSCs) [5-7] and organic light-emitting diodes (OLED).[8] However, compared to their inorganic semiconductors, the band gaps of organic materials are relatively large and this limits the performance of the devices in some applications, such as OSCs. One of the most widely used strategies to narrow the band gap is coupling an electron-rich (donor) with an electron-deficient (acceptor) unit in the conjugated backbone.[9-10]

2,1,3-Benzothiadiazole (**BT**) is one of the most commonly used acceptor to construct semiconducting materials due to its electron-withdrawing ability and high electron mobility (Figure 4.1).[11-16] However, its electron-withdrawing ability is a little weak to construct donor-acceptor (D-A) compound with desirable low band gap. For example, the suitable band gap in application of OSCs is around 1.6 eV. While, simply coupling **BT** with a common electron donor such as fluorenylthienyl (**FT**) can only achieve the band gap of 2.0 eV for **BT-FT** (Figure 4.2).[17] In order to reach that goal, stronger donors and longer conjugation length are required, however, these special requirements limit the selection of donors and lots of tedious synthetic work can't be avoided.

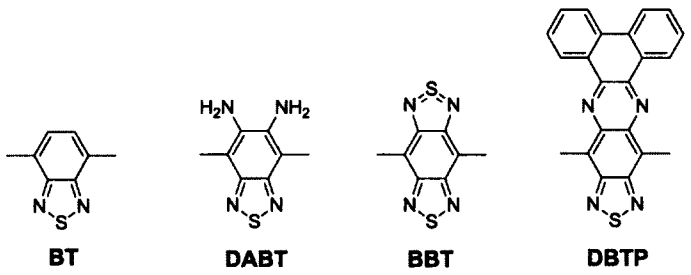

Figure 4.1. Structures of **BT**, **DABT**, **BBT** and **DBTP**.

Structural modifications of **BT** unit have been done mainly by introducing additional groups onto the benzene ring. A common strategy would be converting diaminobenzothiadiazole (**DABT**) to a number of heterocyclic compounds by ring closing reaction. Compounds **BBT** and **DBTP** have been extensively studied for OLED and are very strong acceptors.[18-20] By coupling with donors, the band gaps of D-A compounds can be brought down to 1.3 eV and below (Figure 4.2). The maximum absorptions of these compounds range from 700 to 950 nm. Their emissions are even more red-shifted into the NIR region. However, lack of high absorbance in the visible region and extremely low band gap make them not suitable in other applications such as OSCs.

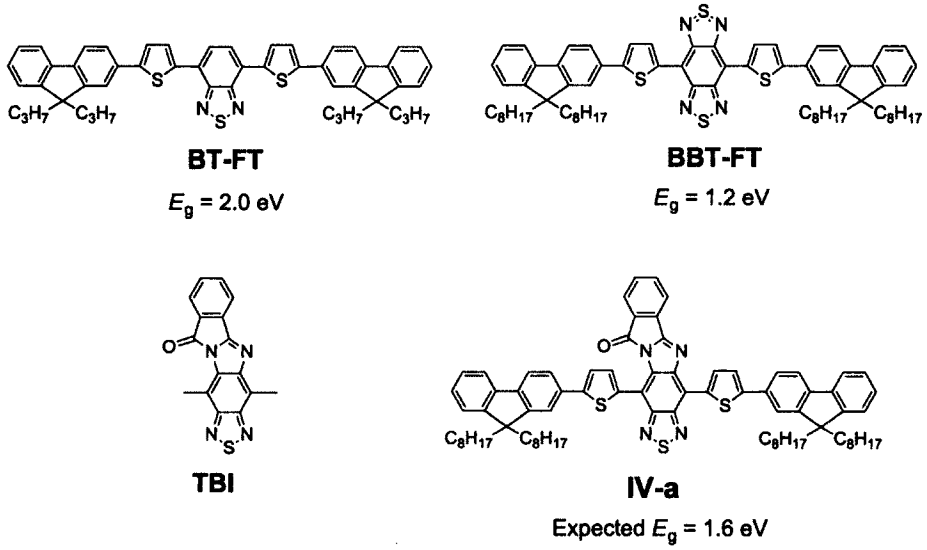

Figure 4.2. Structures of **BT-FT**, **BBT-FT**, **TBI** and **IV-a**.

In this chapter, we proposed and synthesized donor-acceptor compounds with thiadiazolobenzoimidazole (**TBI**) as an acceptor unit (Figure 4.2). The unique feature of the **TBI** is that it has three electron deficient imine groups to contribute to the electron-withdrawing ability of the acceptor with the other nitrogen forming an amide. Therefore, **TBI** is expected to have the electron withdrawing ability in between **BT** and **BBT**. After coupling with the same donor **FT**, the band gap should be in between those of **BT-FT** and **BBT-FT** and will be suitable for OSC application (Figure 4.2).

The **TBI**-containing compounds **IV-a** to **IV-d** can simply be synthesized by reaction between **DABT** and selected anhydrides (Scheme 4.1). The band gap can be tuned by changing the structure of the **TBI** core. Electronegative fluorine atoms which have been reported to be very effective in lowering the HOMO and LUMO levels were introduced in compound **IV-b**. Compound **IV-c** and **IV-d** have larger conjugation length at the acceptor and possess larger band gaps. In order to facilitate the systematic study of relationship between the band gap and the structure, all four compounds have been designed to have the same donor **FT**.

Electrochromism is the property of certain dyes of changing color when placed in an electric field.[21] Since thienyl group of the donor can be oxidized to become a radical cation. Therefore, compounds are electrochromic and can be switched electrochemically to become NIR absorbing at the telecommunication wavelength.

4.2 Results and discussion

4.2.1 Synthesis

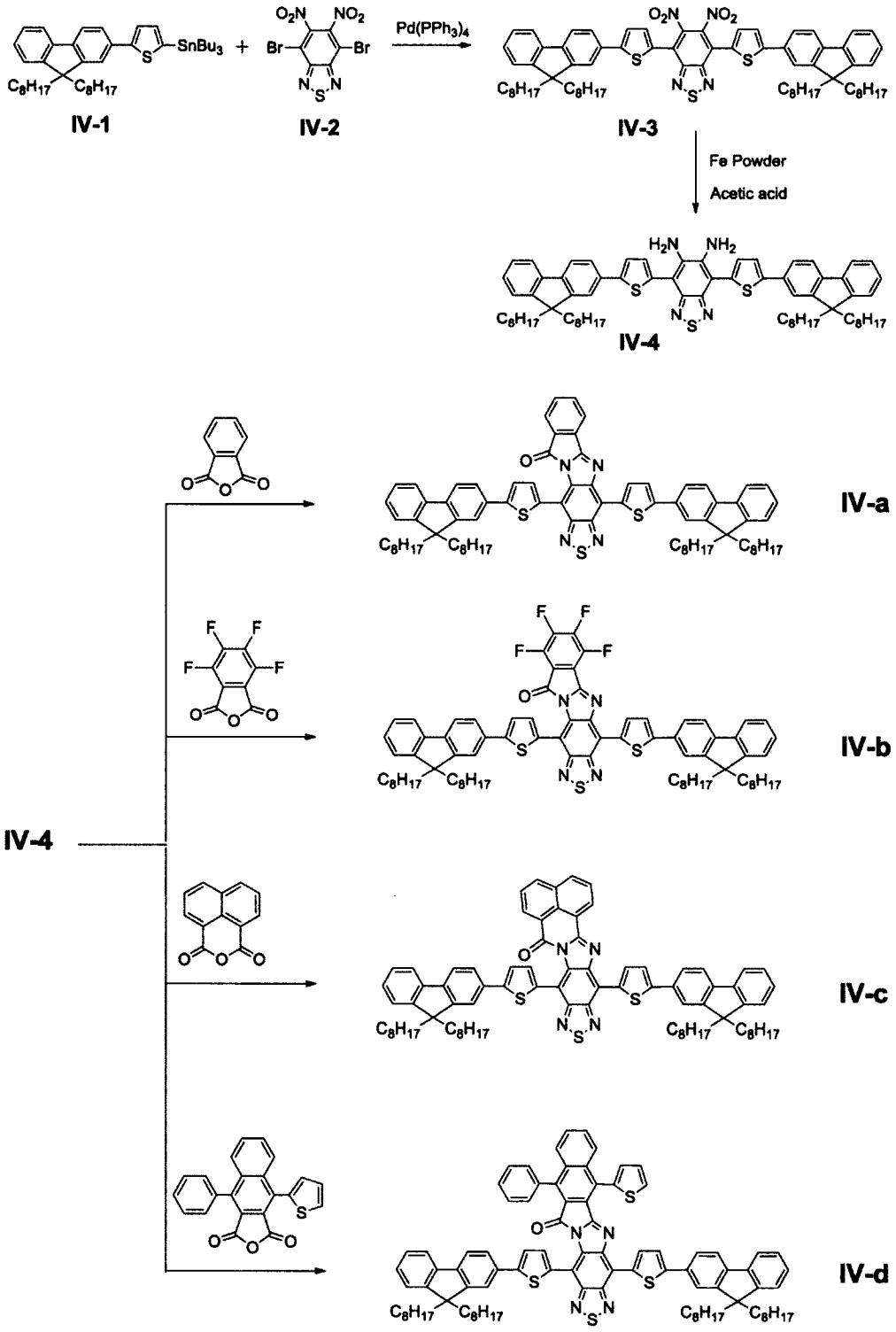

Scheme 4.1. Syntheses of **TBI**-based compounds.

Scheme 4.1 outlines the synthetic routes to the target compounds **IV-a** to **IV-d**. Compound **IV-3** was synthesized by Stille cross-coupling between tributyl(5-(9,9-dioctyl-9H-fluoren-2-yl)thiophen-2-yl)stannane (**IV-1**) and 4,7-dibromo-5,6-dinitrobenzo[c][1,2,5]thiadiazole (**IV-2**) which were prepared according to the literature methods.[19] Reduction of **IV-3** by iron powder in acetic acid afforded compound **IV-4** in reasonable yield (60%).[22] The cyclization of diamines with the corresponding anhydrides in 1,2-dichlorobenzene gave final compounds in 40-80% yields. However, **IV-c** is the only exception which was synthesized in m-cresol. This is due to two reasons: 1) The six-member ring anhydride on 1,8-naphthalic anhydride is less reactive, comparing to the five-member ring anhydride. Therefore, it needs higher temperature to react with the diamine. 2) The six-member ring anhydride creates more steric hindrance with the adjacent groups, in order to overcome the energy barrier higher temperature is needed. Thus, m-cresol was selected because of its high boiling point and proved to be a suitable solvent for making **IV-c**.

These compounds are readily soluble in common organic solvents such as chloroform, dichloromethane, THF, chlorobenzene and toluene, owing to the long alkyl groups. Unlike other small molecules, these compounds have large molecular weights over 1000 g/mol, smooth thin films can be cast or spin coated on glass or ITO.

4.2.2 IR characterization

The IR analysis was done with thin films of compounds cast on the NaCl salt plates. Characteristic peaks of compound **IV-a** to **IV-d** are summarized in Table 4.1. They exhibit C=O band in the range of 1690 – 1757 cm^{-1} and C=C band at around 1600 cm^{-1}. The C=O peaks of **IV-a** and **IV-b** are relatively weak and broad, whereas the ones from **IV-c** and **IV-d** are more intense and sharper.

Table 4.1. Characteristic IR peaks of compound **IV-a** to **IV-d**.

Compound	Characteristic IR peaks (cm^{-1})
IV-a	3060 (C-H sp^2 aromatic), 2926-2853 (and sp^3 aliphatic) 1690 (C=O), 1605 (C=C)
IV-b	3060 (C-H sp^2 aromatic), 2926-2853 (and sp^3 aliphatic) 1715 (C=O), 1623 (C=C)
IV-c	3060 (C-H sp^2 aromatic), 2926-2853 (and sp^3 aliphatic) 1716 (C=O), 1604 (C=C)
IV-d	3060 (C-H sp^2 aromatic), 2926-2853 (and sp^3 aliphatic) 1757 (C=O), 1606 (C=C)

4.2.3 NMR characterization

All compounds were characterized by ^1H NMR and ^{13}C NMR. In $CDCl_3$, the ^1H NMR spectra of **IV-a** and **IV-b** display broad peaks both in aliphatic region and aromatic region. After changing the solvent into d_6-DMSO, some peaks can be recognized, while no split was observed for most of the peaks (Figure 4.3). The reason of these broad peaks is due to the aggregation of the molecules in the solution. Introduction of more polar solvent can break the intermolecular interactions and lower the aggregation. Another reason might be the steric hindrance between the **TBI** core and the **FT** group which limits the free rotation of the donors.

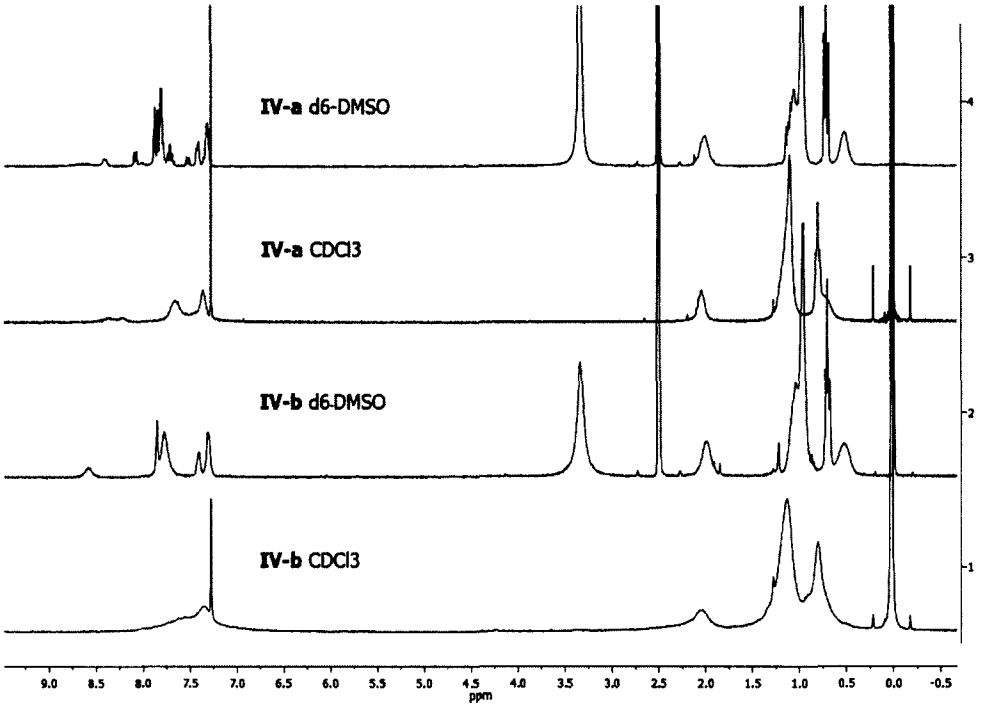

Figure 4.3. ^{1}H NMR spectra of **IV-a** and **IV-b** in $CDCl_3$ and d_6-DMSO.

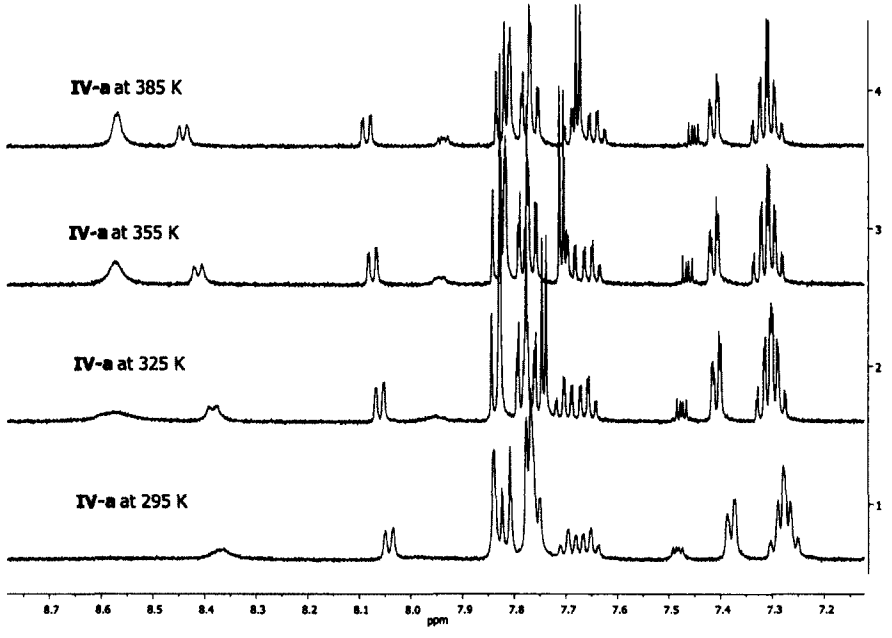

Figure 4.4. ^{1}H NMR spectra of **IV-a** in d_6-DMSO at different temperatures.

In order to obtain better ^{1}H NMR spectra, high temperature ^{1}H NMR characterization were performed on **IV-a** in d_6-DMSO (Figure 4.4). As the temperature increased from 295 K to 385 K, broad peaks became sharper and showed better splits. There is almost no change on the spectra above 385 K. By comparing with the compounds with similar structures,[21] the peak at 8.57 ppm is assigned to the protons on the thiophene and peaks at 8.42 and 8.07 ppm are assigned to the protons on the benzene ring of **TBI** moiety. Because of the presence of the electron-withdrawing **TBI** unit, the chemical shifts of these adjacent protons shifted to a lower field.[21]

The NMR characterization was also done for **IV-b**. Peaks already showed nice splits at 325 K (Figure 4.5). However, from 355 K and above, new peaks showed up and the color of the solution changed from blue to green, suggesting that the compound decomposed at high temperature in d_6-DMSO. Similarly, the peak at 8.57 ppm is assigned to the protons of thienly groups. Because protons on the **TBI** unit were substituted by fluorine, the resonance peaks at 8.42 and 8.07 ppm are absent.

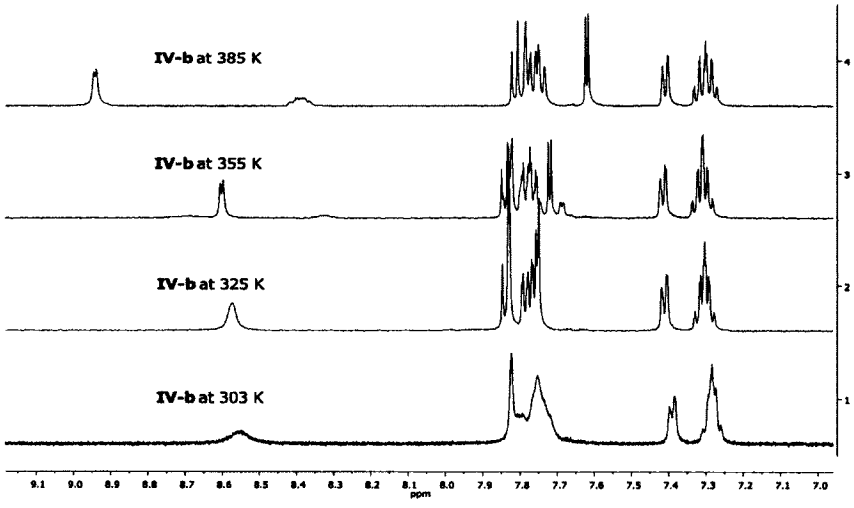

Figure 4.5. ^{1}H NMR spectra of **IV-b** in d_6-DMSO at different temperatures.

4.2.4 Mass spectra data

All compounds were characterized by mass spectrometry (Table 4.2). Mass spectra show molecular ion peaks at *m/z* 1218.61901 and 1427.64735 for compound **IV-a** and **IV-d**, corresponding to the ionized molecule M^+. **IV-b** and **IV-c** show molecular ion peaks at m/z 1308.5 and 1269.65334, respectively, which can be assigned to the ionized molecule $M+NH_4^+$ and $M+H^+$.

Table 4.2. Summary of m/z peaks of compounds.

Compound	Calculated molecular weight	m/z peaks
IV-a	1218.62768	1218.61901 (M^+)
IV-b	1290.5	1308.5 ($M+NH_4^+$)
IV-c	1268.64333	1269.65334 ($M+H^+$)
IV-d	1427.66570	1427.64735 (M^+)

4.2.5 Optical properties

The absorption and emission spectra of compounds **IV-a** to **IV-d** in chloroform and film are shown in Figures 4.6, 4.7 and 4.8, and the data are summarized in Table 4.3. The electronic absorption spectra of these four compounds display two discrete bands (Figure 4.6): the bands in the short wavelength region plus the shoulders ranging from 300 - 450 nm are ascribed to the π-π^* and n-π^* transition of the conjugated aromatic segments, and those in the long wavelength region are attributed to the intramolecular charge transfer (ICT) transitions between the donors and acceptors. The maximum absorption wavelength varies in the order of **IV-b** > **IV-a** > **IV-d** > **IV-c**. The ICT band feature is quite different from reported thiadiaoloquinoxaline containing chomophores, which usually show red shifted ICT

band as conjugation length of the acceptor increases. This could be the result of huge steric hindrance brought by the larger anhydride which negatively affects the planarity of the molecule and hence limits the efficiency of donor-acceptor charge transfer. The colors of the compounds vary according to their absorption characteristics and are blue for **IV-a** and **IV-b**, purple and dark purple for **IV-c** and **IV-d**, respectively.

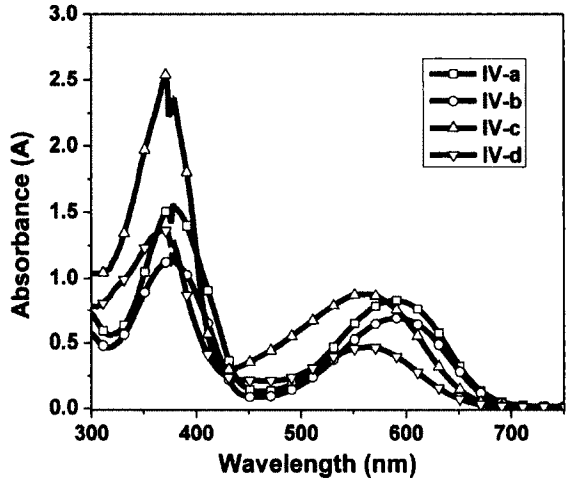

Figure 4.6. UV-vis spectra of **IV-a** to **IV-d** in chloroform.

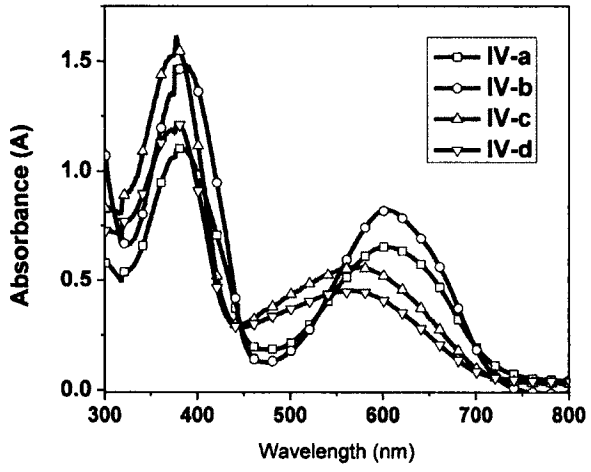

Figure 4.7. UV-vis spectra of **IV-a** to **IV-d** as films.

In comparison with the absorption spectra in solution, the absorption maxima of the films are slightly red-shifted by 3 - 14 nm, indicating slight increase of intermolecular interaction and rigidification in the film state (Figure 4.6).[23] It was reported that the maximum absorptions of **BT-FT** and **BBT-FT** are at 510 and 850 nm, respectively. Comparing to these two, the **TBI** containing compounds have absorption centered at 600 nm, covering more visible light, and are potential useful for molecular organic solar cell application.

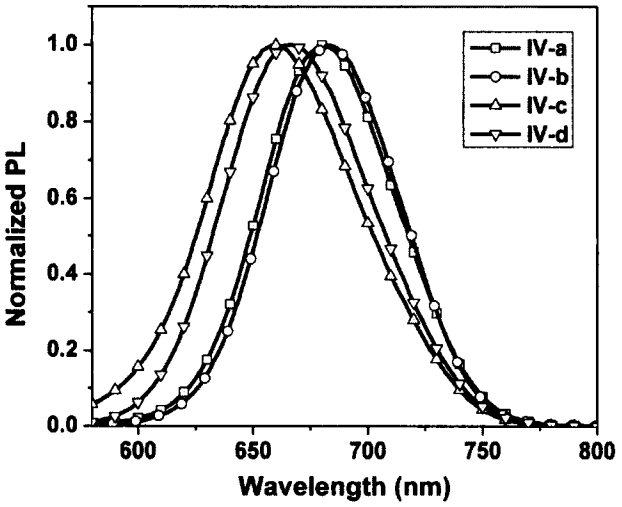

Figure 4.8. PL spectra of **IV-a** to **IV-d** in chloroform.

All compounds show red light emissions with the maximum in the range of 660 - 681 nm (Figure 4.8). The emission wavelengths vary in the same trend as for absorption. The big stokes shift further confirms the presence of ICT in these compound. The quantum yields were calculated and listed in Table 4.3 and are relatively low, which is common for similar red light emitting chromophores.

Table 4.3. Optical properties of **IV-a** to **IV-d**.

Compound	λ_{max}(nm) in chloroform	λ_{max}(nm) film	Excitation (nm)	Emission (nm)	Quantum Yield (%)
IV-a	377/591	382/605	550	681	1.69
IV-b	376/592	387/604	550	683	2.43
IV-c	371/560	376/571	550	660	1.58
IV-d	371/563	376/566	550	666	3.05

4.2.6 Electrochemical properties and band gaps

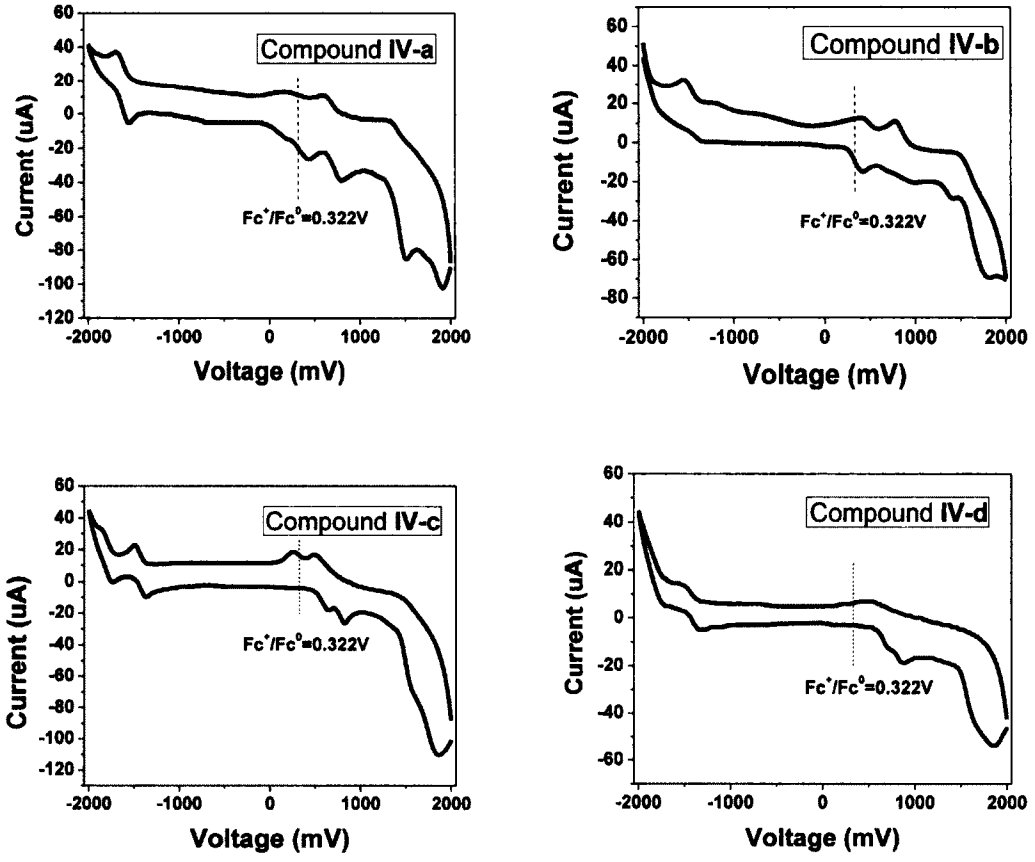

Figure 4.9. CV figures of **IV-a** to **IV-d**.

The electrochemical properties of four compounds were investigated by cyclic voltammetry (Figure 4.9) and the data are summarized in Table 4.4. The cyclic voltammograms were measured in a 0.1 mol/L Bu_4NPF_6/dichloromethane solution using glass carbon as working electrode, platinum wire as counter electrode and silver as pseudoreference electrode. Two quasi-reversible waves were observed for all the compounds during oxidization process, which means two electrons can be removed successively from two thienyl groups to form the radical cation and diradical cation (Figure 4.10). The cathodic scans of compounds showed redox peaks that can be assigned to the reduction of **TBI** core.

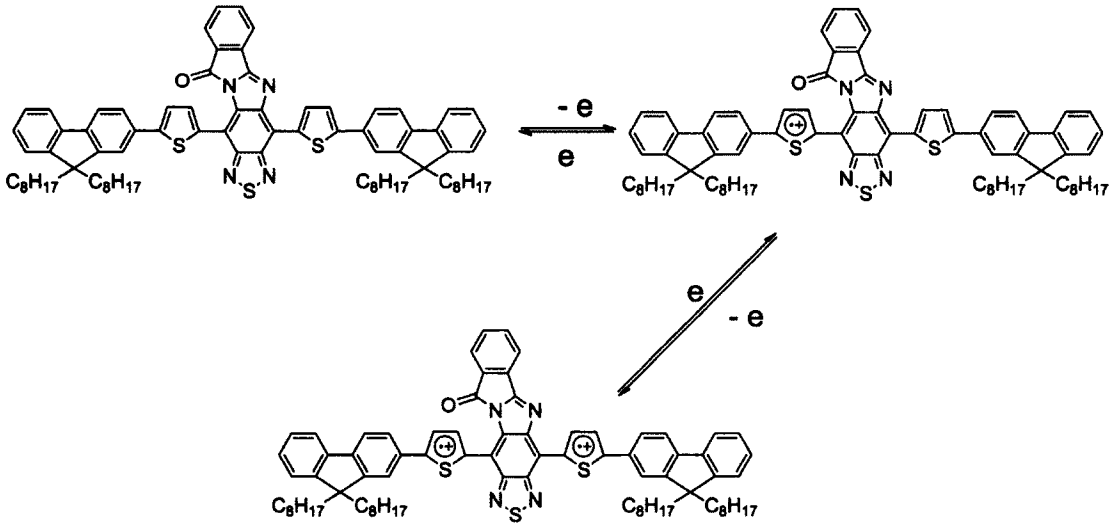

Figure 4.10. Proposed formation of radical cation and diradical cation of **IV-a**.

The onset oxidation potentials and onset reduction potentials vs NHE are within the range of 0.44 to 0.92 V and -0.79 to -1.22 V, respectively. Based on equations below, HOMO and LUMO energy levels as well as band gaps of the compounds were calculated:

$$\text{HOMO} = -\,e(E_{ox}-E_{ferrocene}+4.8)\ \text{eV}$$

$$LUMO = - e(E_{red}-E_{ferrocene}+4.8)\ eV$$

$$Band\ gap = LUMO - HOMO\ eV$$

Where $E_{ferrocene}$ is the potential of ferrocene reference which equals 0.64 V vs NHE. The calculated HOMO, LUMO and band gap values are included in Table 4.4 and energy levels of all compounds are plotted in Figure 4.9.

Table 4.4. Electrochemical properties of **IV-a** to **IV-d**.

Compound	E_{ox}[a] (V)	E_{red}[a](V)	HOMO (eV)	LUMO (eV)	Bandgap (eV)
IV-a	0.44	-1.22	-4.60	-2.94	1.66
IV-b	0.51	-1.09	-4.67	-3.07	1.60
IV-c	0.81	-1.07	-4.97	-3.09	1.88
IV-d	0.92	-1.05	-5.08	-3.11	1.97

[a] The potentials were measured from the onset of the CV curves. The CV of compounds were measured in a 0.1 mol/L Bu_4NPF_6/dichloromethane solution.

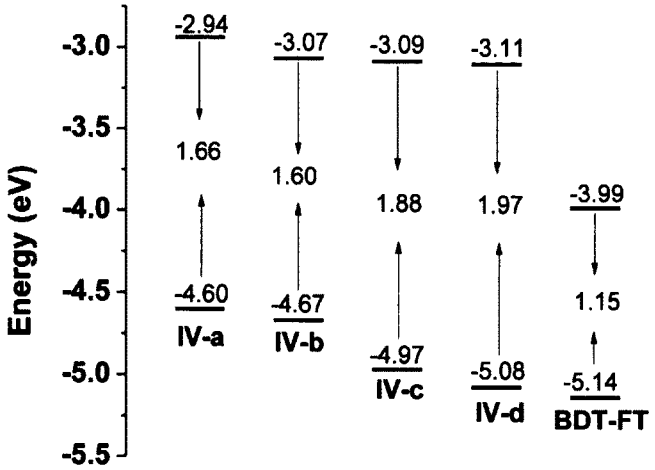

Figure 4.11. Energy levels of **IV-a** to **IV-d**.

As shown in Figure 4.11, compound **IV-a** has a HOMO level of -4.60 eV, a LUMO level of -2.94 eV and a band gap of 1.66 eV. By introducing electron-negative fluorine to **IV-b**, the HOMO and LUMO level decreased at the same time and resulted in a lower band gap of 1.60 eV. This effect is commonly observed for fluorine containing compound and has been utilized to tune the energy levels.[24] Because the larger twist angle between donor and acceptors limits the intermolecular charge transfer over the conjugated backbone of the molecules, compound **IV-c** and **IV-d** have larger band gap of 1.90 eV, along with a low HOMO level located at around -5.0 eV. In comparison to the band gap of **BT-FT**, the band gaps of **TBI** containing compounds are smaller, indicating stronger electron withdrawing ability of **TBI** acceptor. Based on the reported data, compound **BBT-FT** has a very low LUMO level of -3.99 eV (Figure 4.11). Since the LUMO level is determined by electron withdrawing ability of the acceptor in D-A molecule, **TBI** is considered a weaker accepter comparing to **BBT**. Therefore, **TBI** is a moderate acceptor in between **BT** and **BBT** and is able to bring the band gap to 1.6 eV successfully in the case of **IV-a** and **IV-b**.

4.2.7 Electrochromic properties of the chromophores

All compounds were subjected to the investigation for their visible and NIR electrochromism. The film was made from its chloroform solution by spin-coating on ITO glass and the film thickness was about 80 nm. The electrochromism experiments were performed in 0.1 M Et_4NClO_4 acetonitrile solution using platinum wire as counter electrode and silver as pseudoreference electrode. Both positive and negative

voltages were applied, however, spectrum changes were only observed upon oxidation.

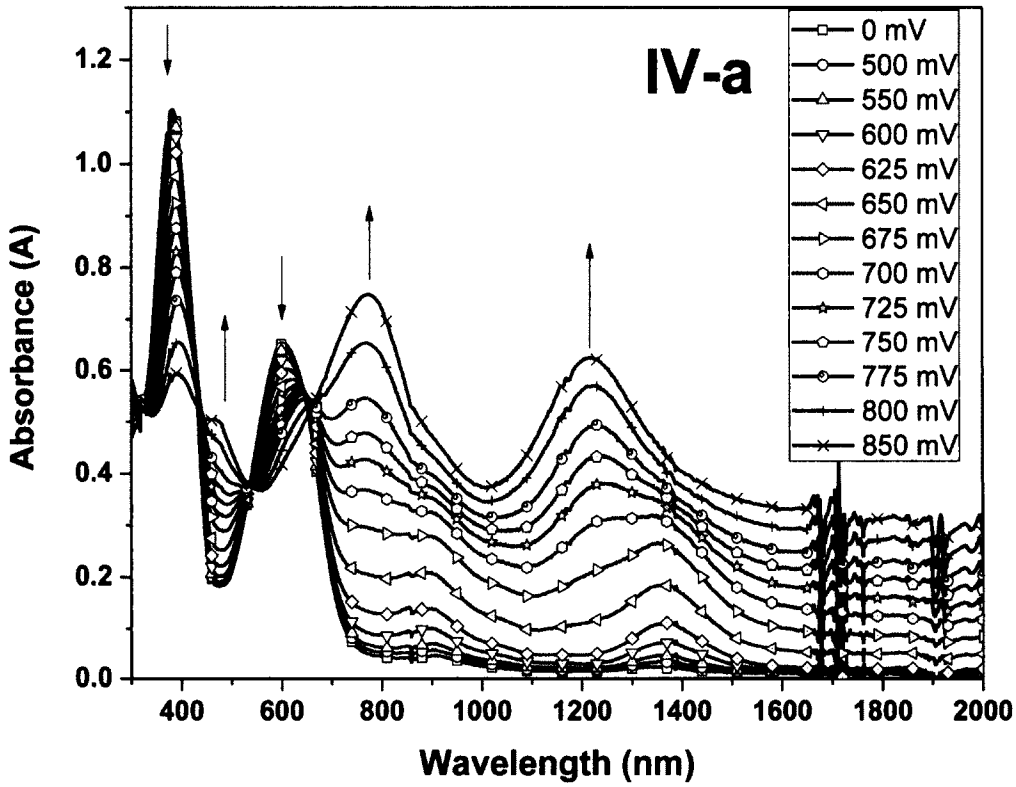

Figure 4.12. Absorption spectra of **IV-a** film on ITO glass in 0.1 M Et_4NClO_4 acetonitrile solution from 500 mV to 850 mV.

For compound **IV-a**, no change on its spectrum was observed below 500 mV. When the applied voltage increased from 500 to 650 mV, the π-π^* absorption band at 382 nm and ICT band at 605 nm decreased gradually and at the same time, new broad bands appeared in the NIR region at 910 and 1380 nm, due to the formation of radical cations (polarons) (Figure 4.12). As the potential was increased to a more positive value of 850 mV, corresponding to the second-step oxidation, the π-π^* transition band and ICT band kept decreasing, while new band appeared at about 800 and 1220 nm, indicating the formation of bipolarons. The spectra kept unchanged upon higher oxidation voltage due to complete conversion.

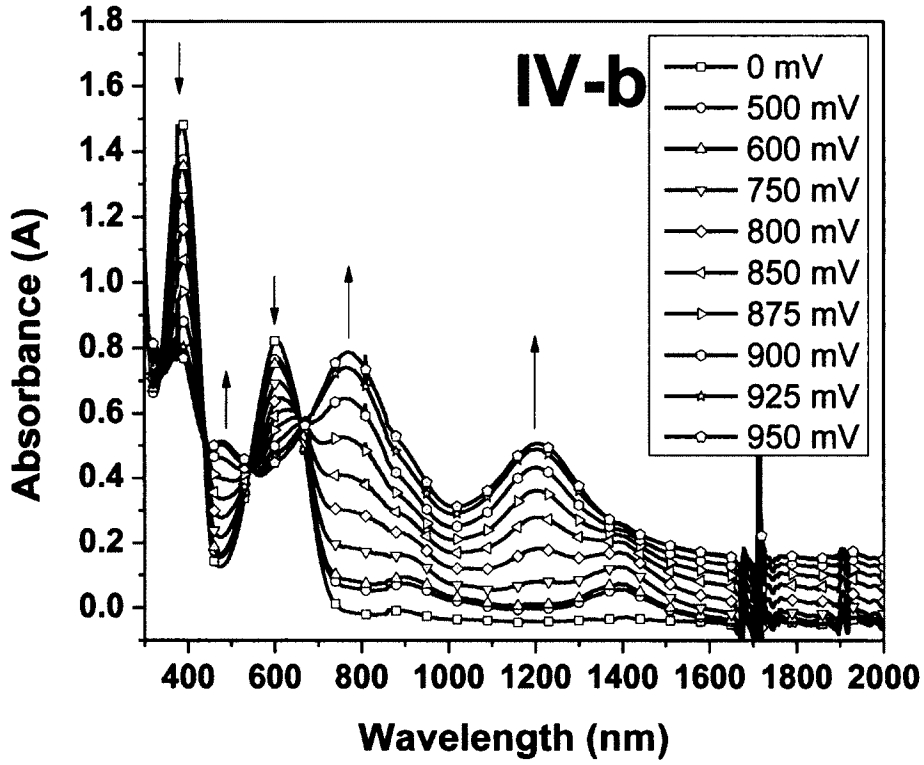

Figure 4.13. Absorption spectra of **IV-b** film on ITO glass in 0.1 M Et_4NClO_4 acetonitrile solution from 500 mV to 950 mV.

Compound **IV-b** showed almost the same electrochromic behavior as compound **IV-a**. No change on the spectra was observed below 500 mV. When the applied voltage increased from 500 to 750 mV, the π-π^* absorption band at 387 nm and ICT band at 604 nm decreased and at the same time, new broad bands appeared at 900 and 1400 nm, due to the formation of radical cations (polarons) (Figure 4.13). As the potential increased to 950 mV, the π-π^* transition band and ICT band kept decreasing as well, while new band appeared at about 790 and 1200 nm, indicating the formation of bipolarons. No change was shown upon further oxidation.

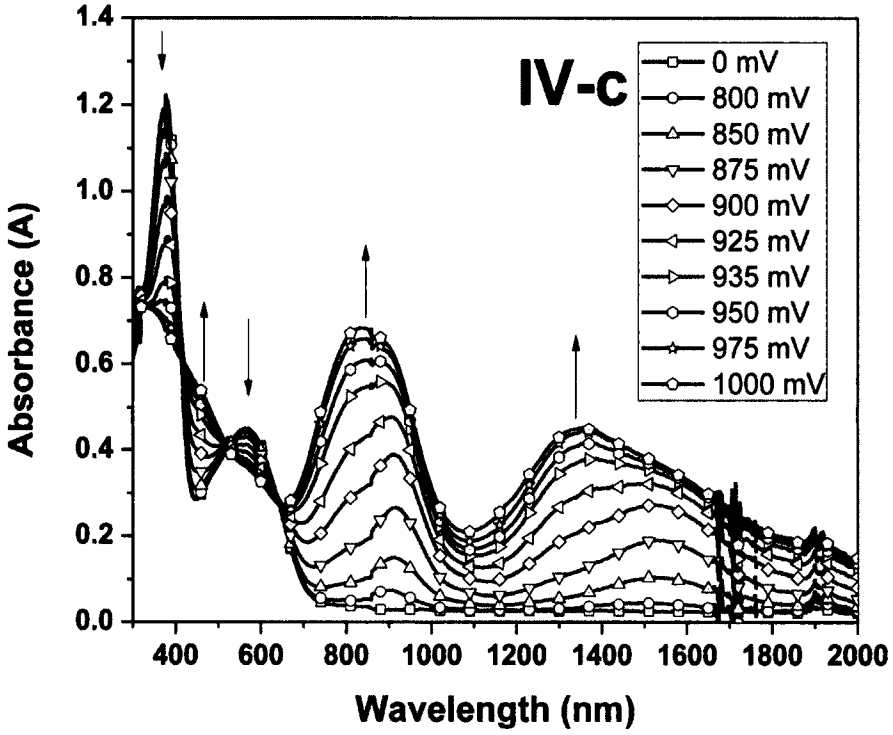

Figure 4.14. Absorption spectra of **IV-c** film on ITO glass in 0.1 M Et_4NClO_4 acetonitrile solution from 800 mV to 1000 mV.

For compound **IV-c**, the spectra exhibited no change until 800 mV, corresponding to E_{ox} of 0.81 V. As the oxidation potential increased from 800 to 875 mV, the π-π^* absorption band at 376 nm and ICT band at 571 nm decreased, meanwhile, new broad bands appeared at 900 and 1520 nm, due to the formation of radical cations (polarons) (Figure 4.14). Further increase of the voltage to 1000 mV resulted in new peaks at 830 and 1350 nm, indicating the formation of bipolarons.

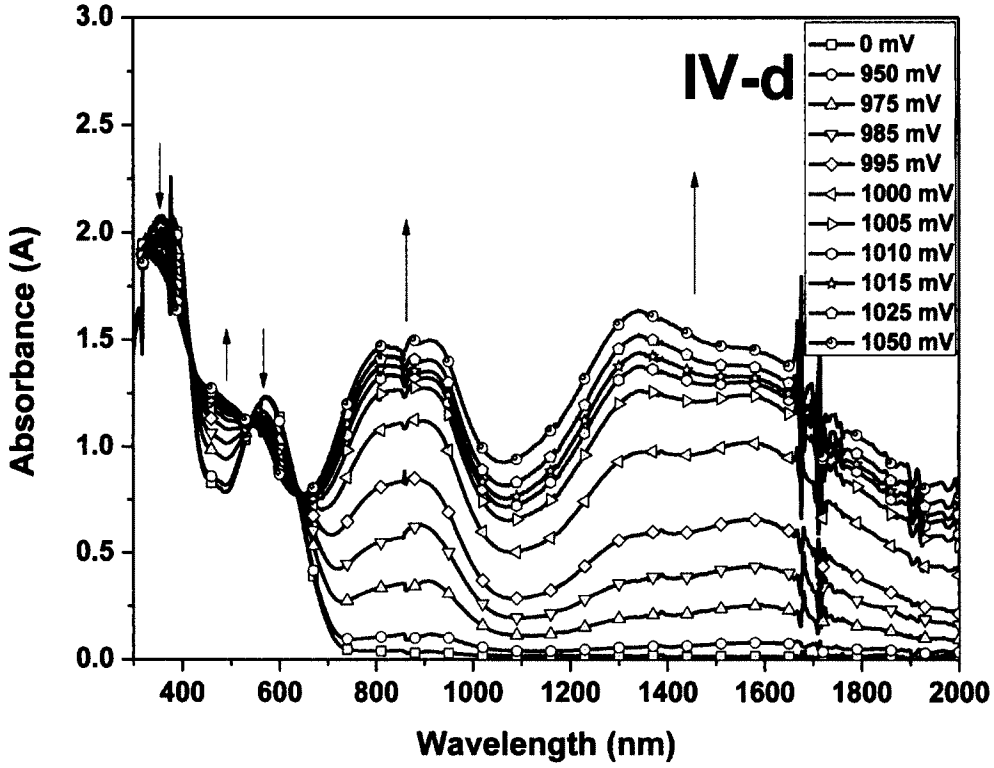

Figure 4.15. Absorption spectra of **IV-d** film on ITO glass in 0.1 M Et_4NClO_4 acetonitrile solution from 950 mV to 1050 mV.

Compound **IV-d** has the higher E_{ox} of 0.92 V, so no oxidation was observed from its spectra below 950 mV. Because the two oxidation potentials of **IV-d** was very close to each other, as the voltage increased, peaks at 1580 and 1350 nm showed up at the same time, which correspond to the radical cation and diradical cation, respectively (Figure 4.15). However, the peak at 1580 nm was more intense below 1005 mV indicating more single radical cation. While above 1005 mV, the band at 1350 nm became more intense indicating more diradical cation formation in the higher voltage. During this oxidation process, new band at around 800 - 900 nm was observed followed by the decrease of the π-π^* transition band and ICT band.

4.3 Conclusion

A series of **TBI** containing compounds have been successfully synthesized by ring closing reaction between **DABT** and corresponding anhydrides. **TBI** unit is carrying three electron deficient imine groups which tune its electron withdrawing ability in between **BT** and **BBT**. Target compounds **IV-a** to **IV-d** showed ICT bands covering from 450 to 700 nm, with band gaps ranging from 1.60 to 1.97 eV. As expected, introduction of fluorine atoms could lower both the HOMO and LUMO levels. However, introducing larger anhydride unit to the acceptor resulted in an increase of band gaps due to larger steric hindrance. Fine films can be easily cast from the solutions of all four compounds, indicating that they are promising materials for molecular organic solar cells. All compounds are electrochromic due to the oxidative behavior of the thienyl groups and can be switched electrochemically to become NIR absorbing at the telecommunication wavelengths.

4.4 Experimental

4.4.1 Materials

Chemicals and reagents purchased from Aldrich and TCI were used directly without further purification. Compound **IV-3** and **IV-4** were prepared according to the literature.[19, 21]

4.4.2 Instruments

^{1}H NMR spectra and ^{13}C NMR spectra were measured on Bruker Advance 300 instrument at 300 MHz and 75 MHz respectively. IR spectra were recorded on Varian 1000 FT-IR Scimitar Series. UV-vis spectra were measured on Perkin ELMER

Lambda 900. PL spectra were measured on ManDEL Scientific RF-1501 spectrofluorophotometer. High Resolution ESI spectra were recorded on the 7.0T Actively Shielded Fourier Transform Ion Cyclotron Resonance Mass Spectrometers. Cyclic voltammograms (CV) and other electrochemical experiments were performed on a BAS 100 electrochemical workstation. Glass carbon working electrode, platinum counter electrode and silver pseudoreference electrode were used together, all the potentials were corrected using ferrocenium/ferrocene (Fc^+/Fc^0) and reported relative to NHE.

4.4.3 Synthesis

Compound IV-a

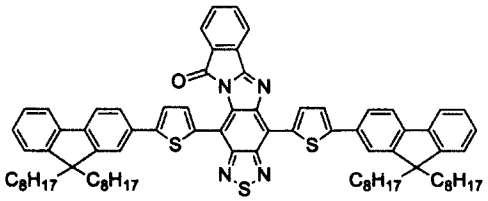

4,7-Bis(5-(9,9-dioctyl-9H-fluoren-2-yl)thiophen-2-yl)benzo[c][1,2,5]thia-diazole-5,6-diamine (1.10 g, 1.00 mmol) and phthalic anhydride (0.22 g, 1.50 mmol) were combined in 1,2-dichlorobenzene (15 ml). The mixture was heated to reflux under argon protection overnight. Then the solvent was removed by reduced pressure evaporation and the residue was purified by column chromatography (silica gel) with CH_2Cl_2 and hexane to afford blue solid (0.97 g, yield 80%). ^1H NMR (300 MHz, DMSO-d_6) δ (ppm): 8.81-8.42 (m, 1H), 8.42-8.39 (d, J = 5.4 Hz, 1H), 8.09-8.07 (d, J = 6.9 Hz, 1H), 7.87-7.50 (m, 13H), 7.43-7.40 (m, 2H), 7.35-7.30 (m, 8H), 2.01 (s, 8H), 1.11-0.96 (m, 40H), 0.73-0.69 (m, 12H), 0.52 (s, 8H). ^{13}C NMR (75 MHz,

$CDCl_3$) δ (ppm): 126.8, 119.8, 55.2, 40.4, 31.8, 30.1, 29.3, 23.8, 22.6, 14.0. ESI-MS (m/z): 1218.61901, calculated: 1218.62768.

Compound IV-b

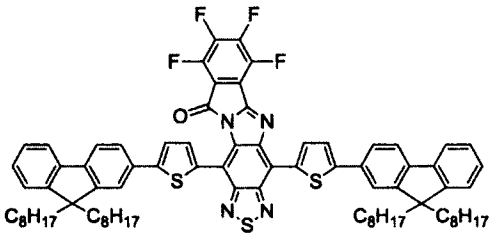

Similar procedures were followed. Tetrafluorophthalic anhydride (0.33 g, 1.50 mmol) was used instead of phthalic anhydride. Blue solid (0.92 g, 71% yield). ^{1}H NMR (300 MHz, DMSO-d_6) δ (ppm): 8.58 (s, 2H), 7.85-7.78 (m, 10H), 7.40-7.30 (m, 6H), 1.99 (s, 8H), 1.04-1.84 (m, 40H), 0.72-0.67 (m, 12H), 0.51 (s, 8H). ^{13}C NMR (75 MHz, $CDCl_3$) δ (ppm): 150.9, 140.5, 126.8, 122.9, 119.7, 55.2, 40.4, 31.8, 30.1, 29.7, 29.3, 23.8, 22.6, 14.0. ESI-MS (m/z): 1308.5 ($M+NH_4^+$), calculated: 1290.6.

Compound IV-c

Similar procedures were followed. 1,8-Naphthalic anhydride (0.30 g, 1.50 mmol) was used instead of phthalic anhydride and the solvent was changed into m-cresol. Purple solid was obtained (0.53 g, yield 42%). ^{1}H NMR (300 MHz, $CDCl_3$) δ (ppm): 9.11-9.02 (m, 2H), 8.62-8.59 (d, J = 7.2 Hz, 1H), 8.29-8.19 (m, 2H), 7.87-7.69

(m, 10H), 7.63-7.53 (m, 2H), 7.42-7.27 (m, 7H), 2.10-2.00 (m, 8H), 1.42-1.27 (m, 40H), 0.78-0.60 (m, 20H). ^{13}C NMR (75 MHz, $CDCl_3$) δ (ppm): 158.3, 154.3, 153.8, 151.5, 151.4, 151.0, 150.9, 150.4, 148.4, 146.3, 143.6, 141.0, 140.8, 140.7, 136.3, 135.3, 134.3, 133.3, 133.1, 132.2, 131.7, 131.4, 130.7, 128.0, 127.6, 127.2, 127.0, 126.9, 126.8, 125.1, 124.8, 123.9, 123.4, 122.9, 122.8, 122.3, 120.2, 120.1, 120.0, 119.8, 119.7, 115.2, 111.3, 55.2, 40.6, 31.8, 30.1, 29.3, 23.9, 22.6, 14.1. ESI-MS (m/z): 1269.65334 ($M+H^+$), calculated: 1268.64333.

Compound IV-d

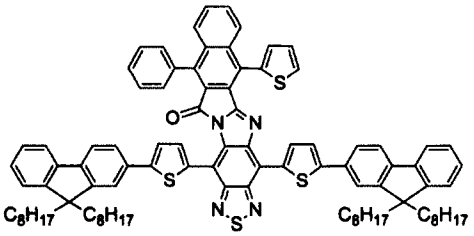

Similar procedures were followed. 4-Phenyl-9-(thiophen-2-yl)naphtho[2,3-c]furan-1,3-dione (0.53 g, 1.50 mmol) was used instead of phthalic anhydride. Purple solid (0.72 g, yield 51%). ^{1}H NMR (300 MHz, $CDCl_3$) δ (ppm): 8.85-7.95 (m, 4H), 7,83-7,24 (m, 28H), 2.10-2.02 (m, 8H), 1.27-1.19 (m, 40H), 0.84-0.67 (m, 20H). ^{13}C NMR (75 MHz, $CDCl_3$) δ (ppm): 151.5, 151.3, 150.9, 141.1, 140.7, 133.6, 133.5, 133.4, 131.7, 130.3, 129.7, 128.8, 128.6, 128.3, 127.7, 127.6, 127.2, 127.0, 126.8, 125.4, 124.9, 122.9, 122.8, 122.6, 120.3, 120.1, 119.9, 119.7, 119.6, 55.3, 55.2, 40.5, 31.8, 30.1, 29.2, 23.8, 22.6, 14.1. ESI-MS (m/z): 1427.64735, calculated: 1427.66570.

References

(1) Wang, C.; Dong, H.; Hu W.; Liu Y.; Zhu, D. *Chem. Rev.* **2012**, *112*, 2208.

(2) Aleshin, A. N.; Lee, J. Y.; Chu, S. W.; Kim, J. S.; Park, Y. W. *Appl. Phys. Lett.* **2004**, *84*, 5383.

(3) Ito, K.; Suzuki, T.; Sakamoto, Y.; Kubota, D.; Inoue, Y.; Sato, F.; Tokito, S. *Angew. Chem., Int. Ed.* **2003**, *42*, 1159.

(4) Chen, Z.; Muller, P.; Swager, T. M. *Org. Lett.* **2006**, *8*, 273.

(5) Chen, J.; Cao Y. *Acc. Chem. Res.* **2009**, *42*, 1709.

(6) Helgesen, M.; Krebs, F. C. *Macromolecules* **2010**, *43*, 1253.

(7) Svensson, M.; Zhang, F.; Veenstra, S. C.; Verhees, W. J. H.; Hummelen, J. C.; Kroon, J. M.; Inganas, O.; Adersson, M. R. *Adv. Mater.* **2003**, *15*, 988.

(8) Grimsdale, A. C.; Chan, K. L.; Martin, R. E.; Jokisz, P. G.; Holmes, A. B. *Chem. Rev.* **2009**, *109*, 897.

(9) Steyrleuthner, R.; Schubert, M.; Howard, I.; Klaumuenzer, B.; Schilling, K.; Chen, Z.; Saalfrank, P.; Laquai, F.; Facchetti, A.; Neher, D. *J. Am. Chem. Soc.* **2012**, *134*, 18303.

(10) Guo, X.; Zhang, M.; Huo, L.; Cui, C.; Wu, Y.; Hou, J.; Li, Y. *Macromolecules* **2012**, *45*, 6930.

(11) Van Duren, J. K. J.; Dhanabalan, A.; van Hal, P. A.; Janssen, R. A. J. *Synth. Met.* **2001**, *121*, 1587.

(12) Zhou, Q.; Hou, Q.; Zheng, L.; Deng, X.; Yu, G.; Cao, Y. *Appl. Phys. Lett.* **2004**, *84*, 1653.

(13) Yang, R.; Tian, R.; Yan, J.; Zhang, Y.; Yang, J.; Hou, Q.; Yang, W.; Zhang,

C.; Cao,Y. *Macromolecules* **2005**, *38*, 244.

(14) Svensson, M.; Zhang, F.; Veenstra, S. C.; Verhees, W. J. H.; Hummelen, J. C.; Kroon, J. M.; Inganas, O.; Andersson, M. R. *Adv. Mater.* **2003**, *15*, 988.

(15) Slooff, L. H.; Veenstra, S. C.; Kroon, J. M.; Moet, D. J. D.; Sweelssen, J.; Koetse, M. M. *Appl. Phys. Lett.* **2007**, *90*, 143506.

(16) Shi, C.; Yao, Y.; Yang, Y.; Pei, Q. *J. Am. Chem. Soc.* **2006**, *128*, 8980.

(17) Qian, G.; Li, X.; Wang, Z. Y. *J. Mater. Chem.* **2009**, *19*, 522.

(18) Qian, G.; Zhong, Z.; Luo, M.; Yu, D.; Zhang, Z.; Wang, Z. Y. *Adv. Mater.* **2009**, *21*, 111.

(19) Qian, G.; Dai, B.; Luo, M.; Yu, D.; Zhan, J.; Zhang, Z.; Ma, D.; Wang, Z. Y. *Chem. Mater.* **2008**, *20*, 6208.

(20) Qian, G.; Zhong, Z.; Luo, M.; Yu, D.; Zhang, Z.; Ma, D.; Wang, Z. Y. *J. Phys. Chem. C* **2009**, *113*, 1589.

(21) Qian, G.; Abu, H.; Wang, Z. Y. *J. Mater. Chem.* **2011**, *21*, 7678.

(22) Luo, M.; Shadnia, H.; Qian, G.; Du, X.; Yu, D.; Ma, D.; Wright, J. S.; Wang, Z. Y. *Chem. Eur. J.* **2009**, *15*, 8902.

(23) Sista, P.; Nguyen, H.; Murphy, J. W.; Hao, J.; Dei, D. K.; Palaniappan, K.; Servello, J.; Kuaratne, R. S.; Gnade, B. E.; Xue, B.; Dastoor, P.; Biewer, M. C.; Stefan, M. C. *Macromolecules* **2010**, *43*, 8063.

(24) Zhou, H.; Yang, L.; Stuart, A. C.; Price, S. C.; Liu, S.; You, W. *Angew. Chem. Int. Ed.* **2011**, *50*, 2995.

Contribution to Knowledge

1. Weak electron acceptors 4-(5-bromothiophen-2-yl)-2-(2-ethylhexyl)-9-phenyl-1H-benzo[f]isoindole-1,3(2H)-dione (**BIDO-1**) and 4,9-bis(5-bromothiophen-2-yl)-2-(2-ethylhexyl)-benzo[f]isoindole-1,3-dione (**BIDO-2**), were designed and synthesized and property-structure relationship of their derivatives were studied.
2. Introducing both weak acceptor (**BIDO-2**) and strong acceptor (**DPP**) in the same polymer can result in broad absorption and improve the photovoltaic performance of the device by increasing the value of the short-circuit current.
3. Electron acceptor thiadiazolobenzoimidazole (**TBI**) can be synthesized by reaction between diaminobenzothiadiazole and anhydride. Three imine groups make it a stronger acceptor comparing to benzothiadiazole (**BT**). Smaller band gaps ranging from 1.60 to 1.97 eV were obtained for compounds **IV-a** to **IV-d**.

APPENDIX A

^{1}H and ^{13}C NMR spectra of compounds and polymers.

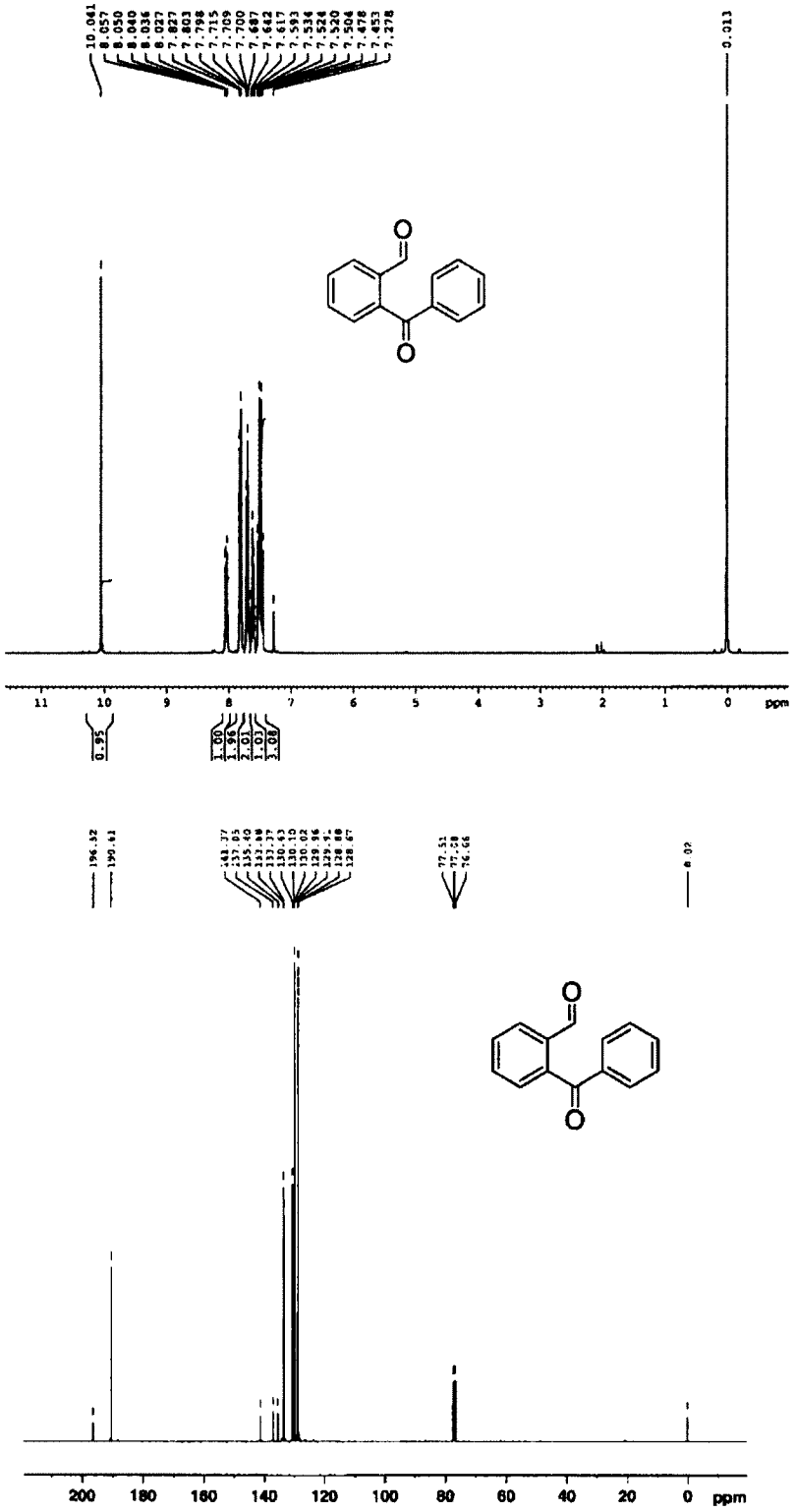

Figure A.1. ^{1}H NMR (300 MHz, $CDCl_3$) and ^{13}C NMR (75 MHz, $CDCl_3$) spectrum of 2-benzoylbenzaldehyde.

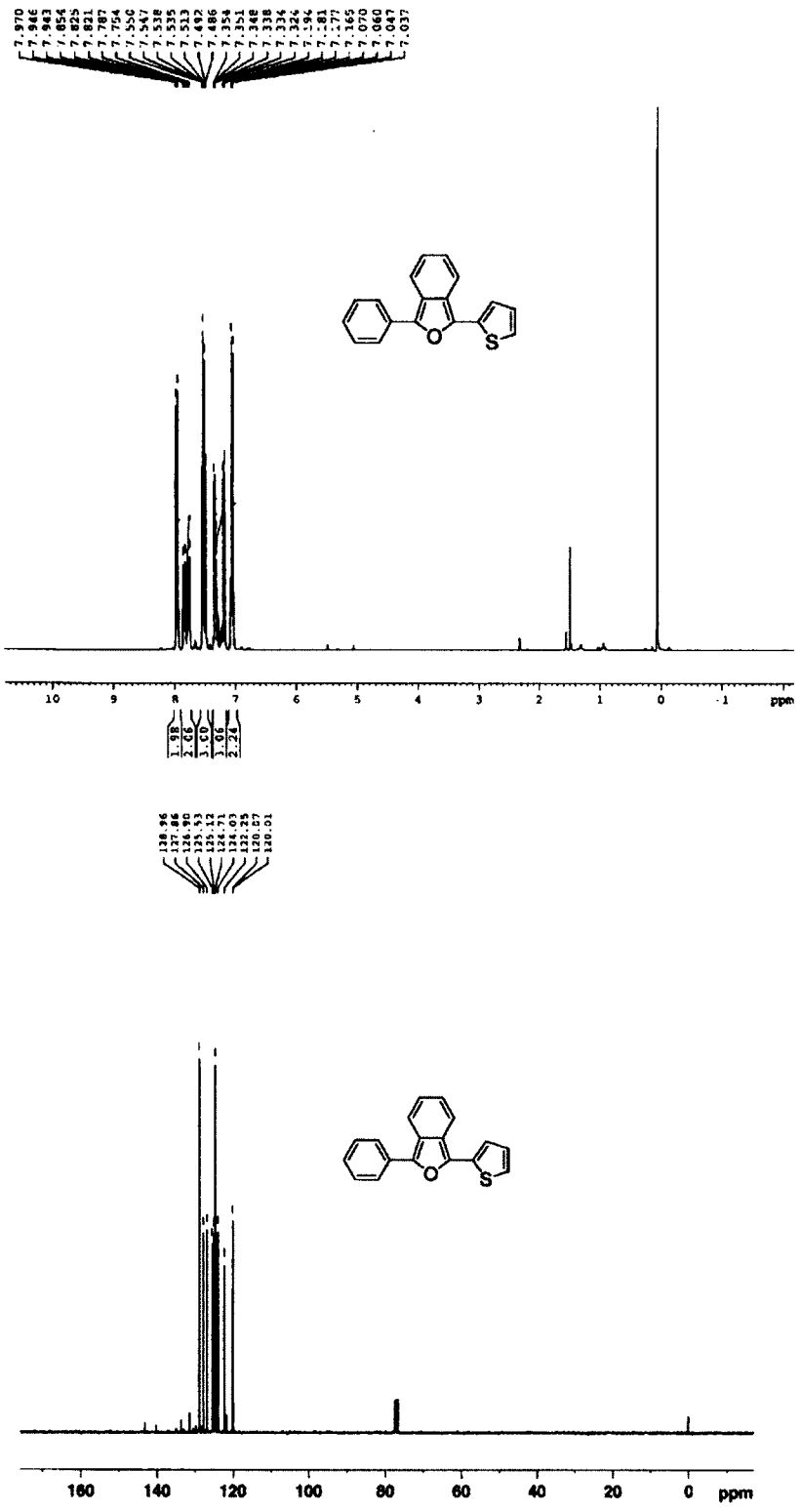

Figure A.2. ^{1}H NMR (300 MHz, $CDCl_3$) and ^{13}C NMR (75 MHz, $CDCl_3$) spectrum of 1-phenyl-3-(thiophen-2-yl)isobenzofuran.

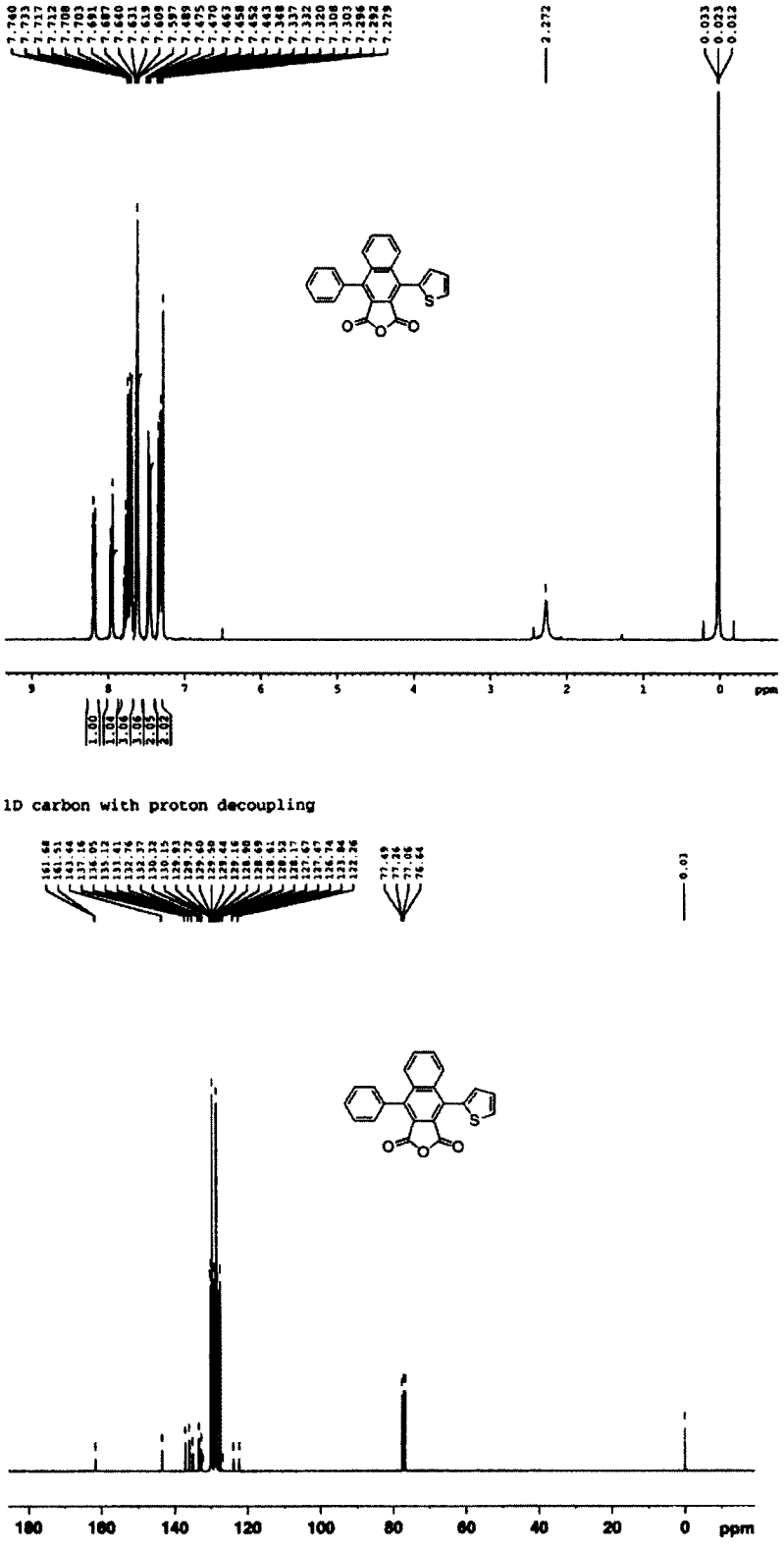

Figure A.3. ^{1}H NMR (300 MHz, $CDCl_3$) and ^{13}C NMR (75 MHz, $CDCl_3$) spectrum of 4-phenyl-9-(thiophen-2-yl)naphtho[2,3-c]furan-1,3-dione.

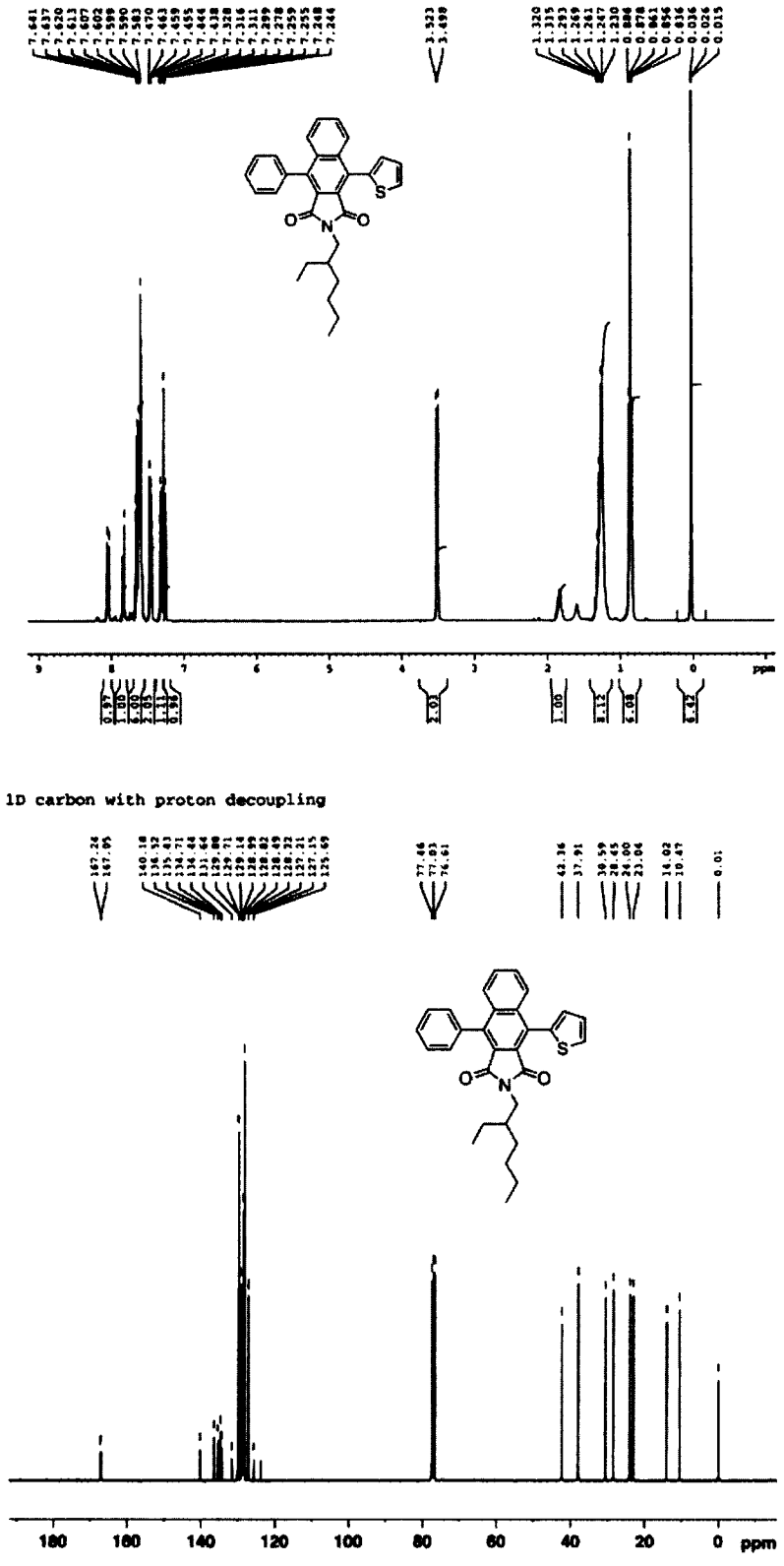

Figure A.4. ^{1}H NMR (300 MHz, $CDCl_3$) and ^{13}C NMR (75 MHz, $CDCl_3$) spectrum of 2-(2-ethylhexyl)-4-phenyl-9-(thiophen-2-yl)-1H-benzo[f]isoindole-1,3(2H)-dione.

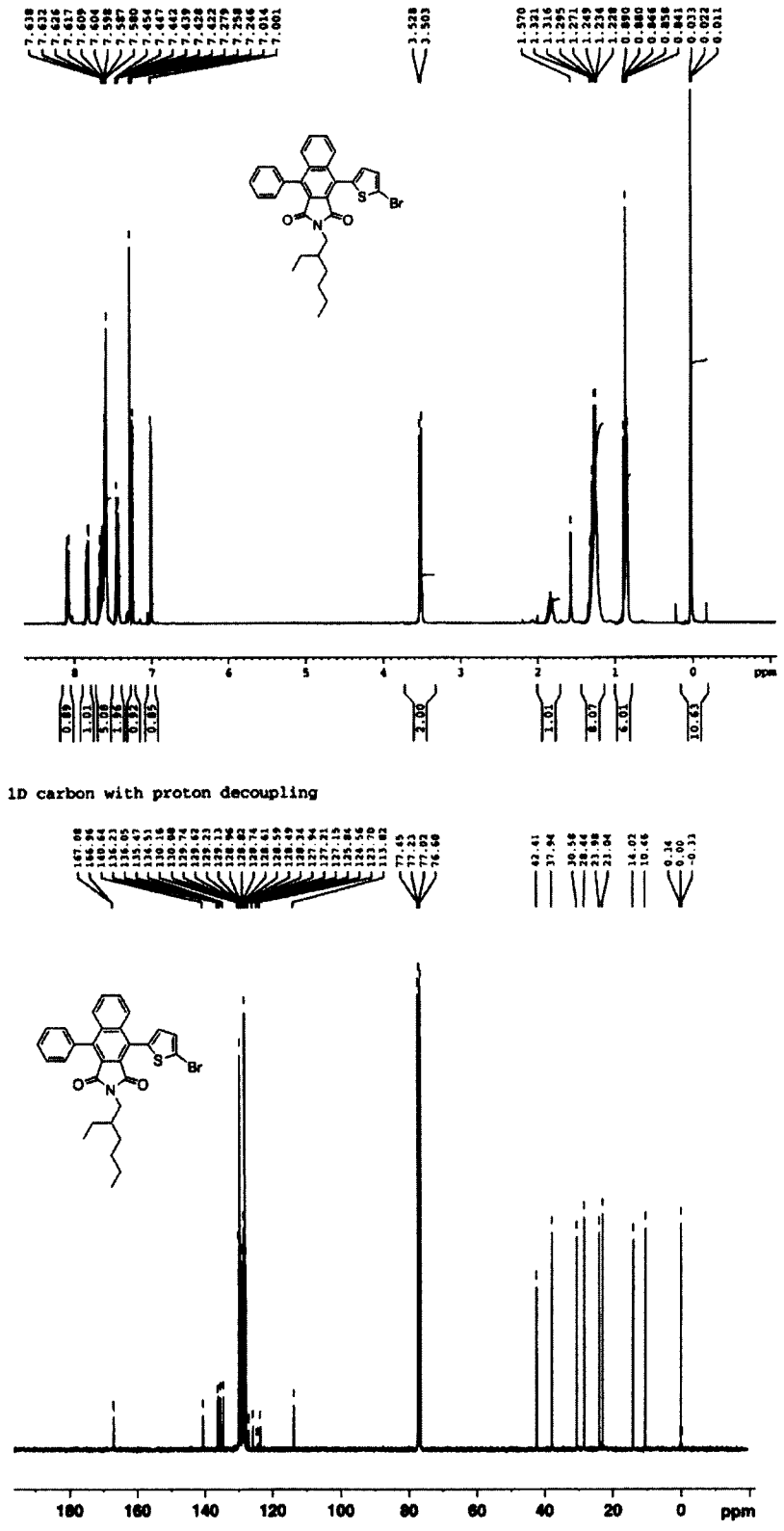

Figure A.5. ^{1}H NMR (300 MHz, $CDCl_3$) and ^{13}C NMR (75 MHz, $CDCl_3$) spectrum of **BIDO-1**.

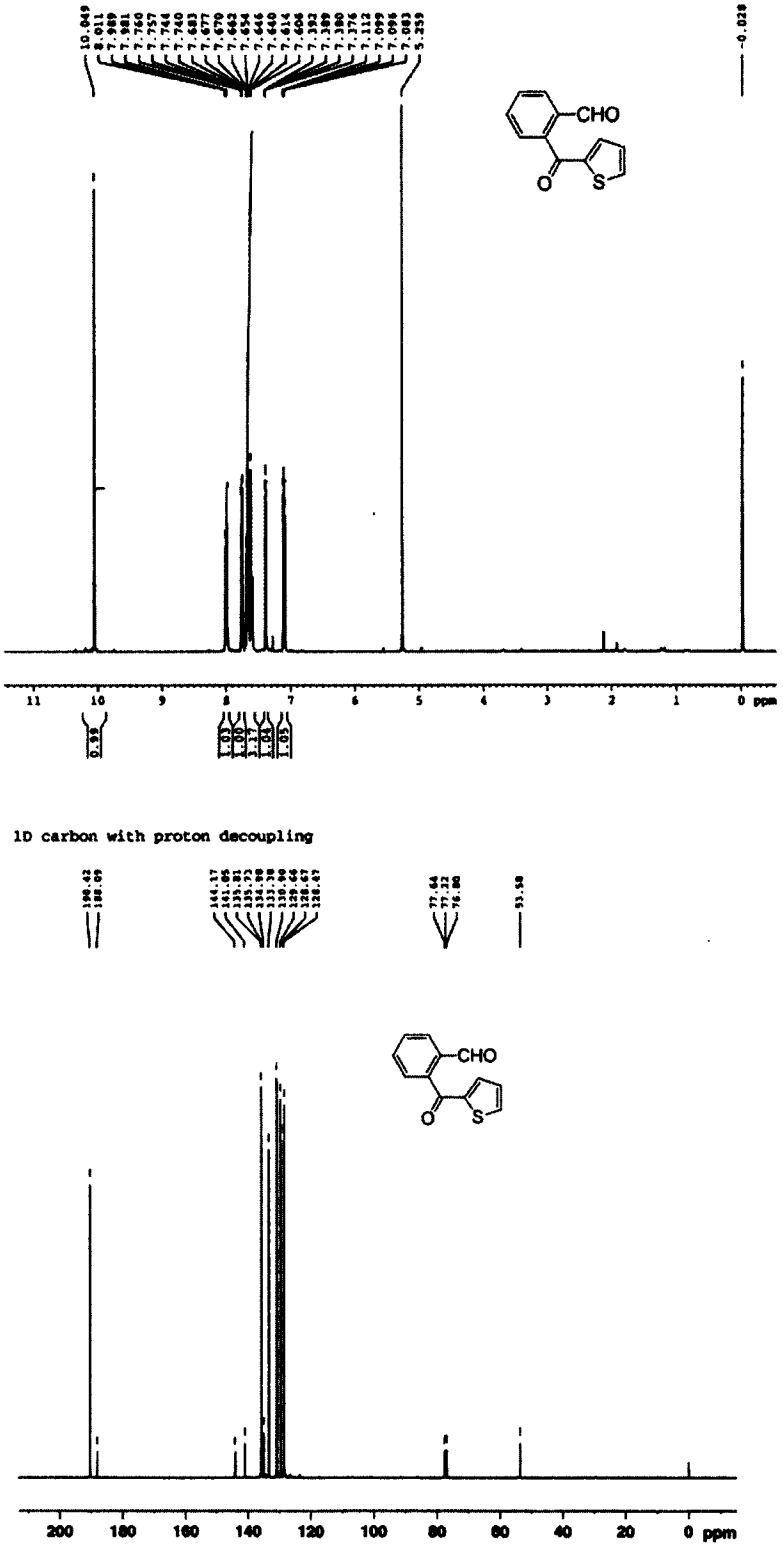

Figure A.6. ^{1}H NMR (300 MHz, $CDCl_3$) and ^{13}C NMR (75 MHz, $CDCl_3$) spectrum of 2-(thiophene-2-carbonyl)benzaldehyde.

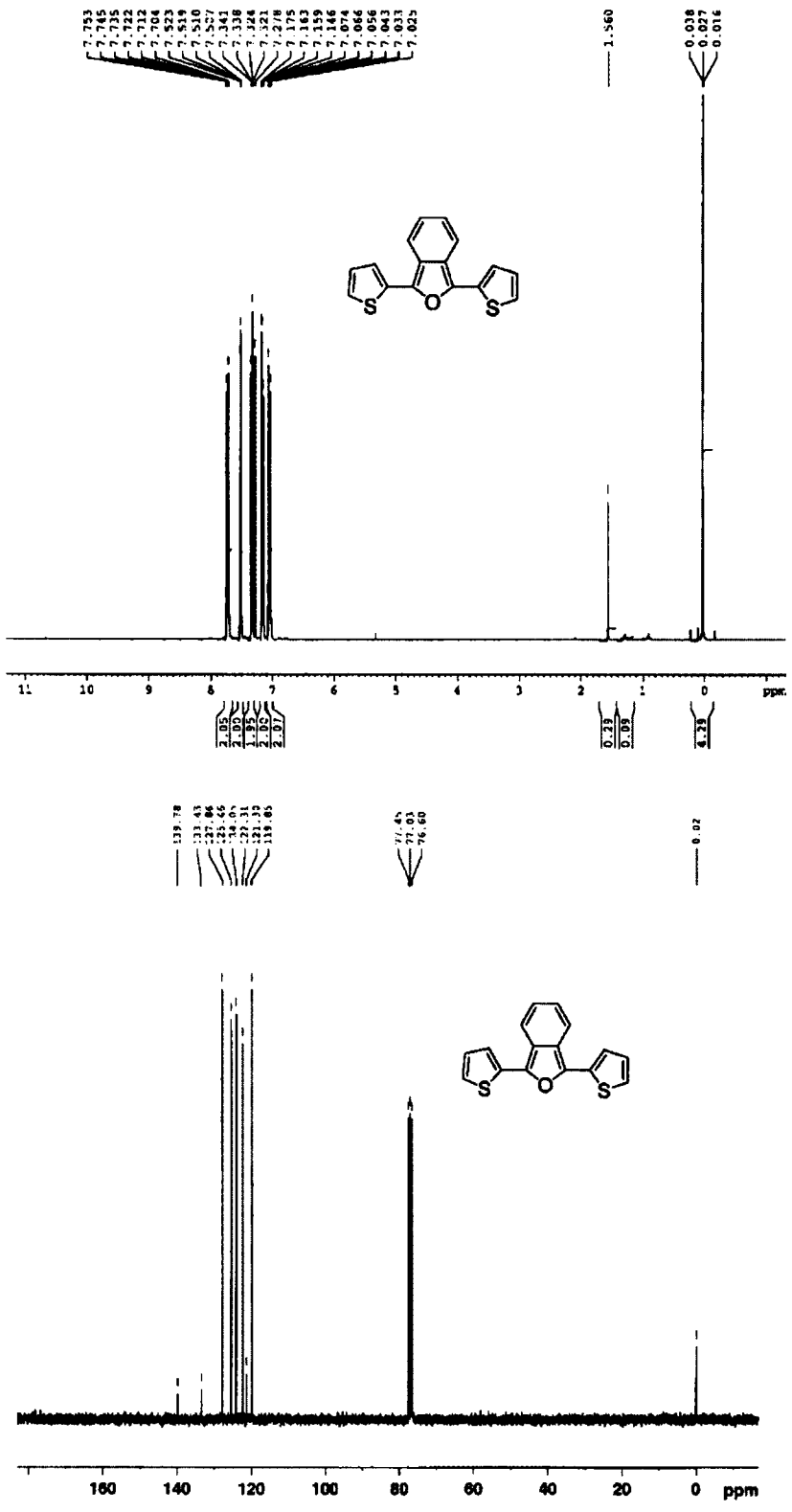

Figure A.7. ^{1}H NMR (300 MHz, $CDCl_3$) and ^{13}C NMR (75 MHz, $CDCl_3$) spectrum of 1,3-di(thiophen-2-yl)isobenzofuran.

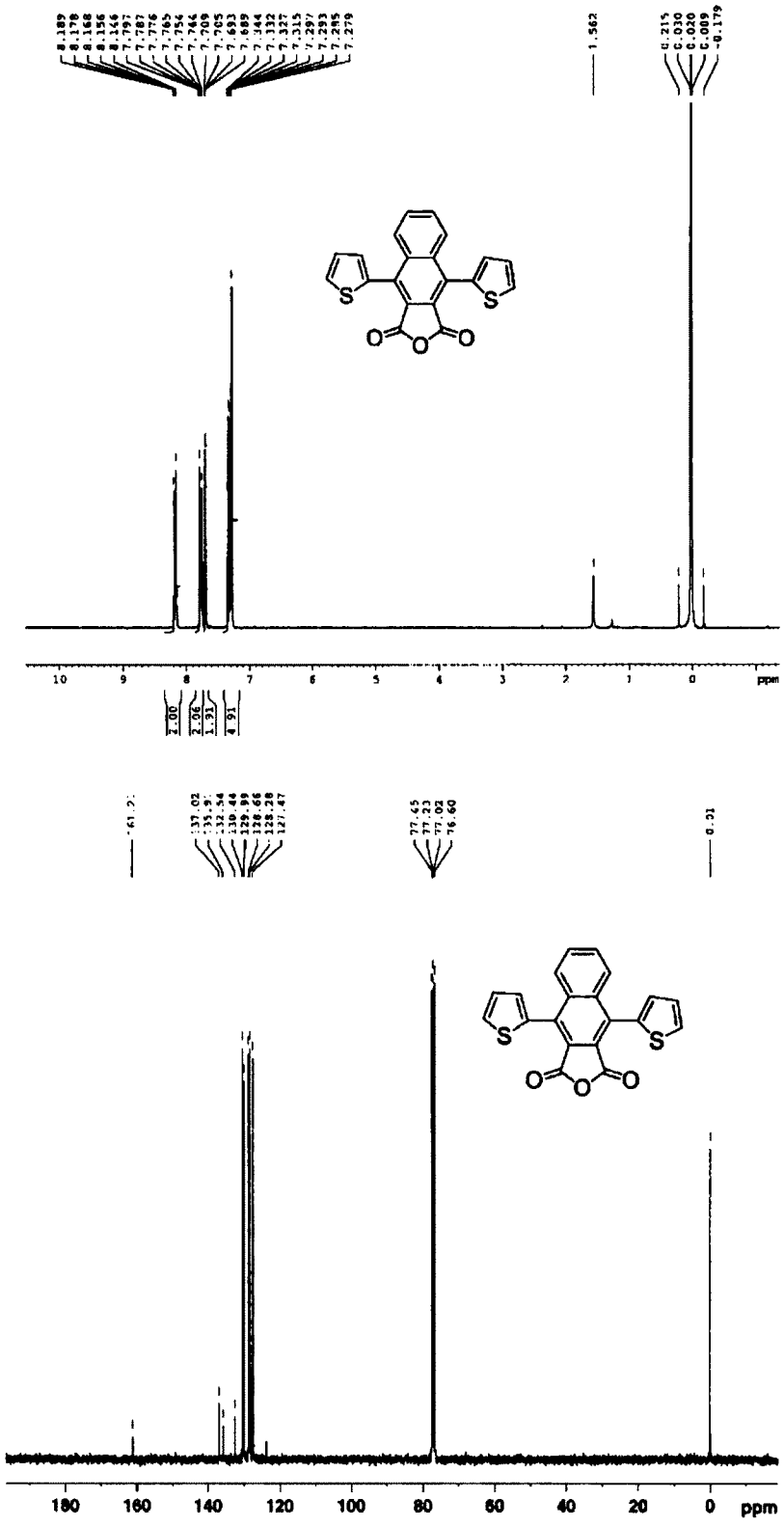

Figure A.8. ^{1}H NMR (300 MHz, $CDCl_3$) and ^{13}C NMR (75 MHz, $CDCl_3$) spectrum of 4,9-di(thiophen-2-yl)naphtho[2,3-c]furan-1,3-dione.

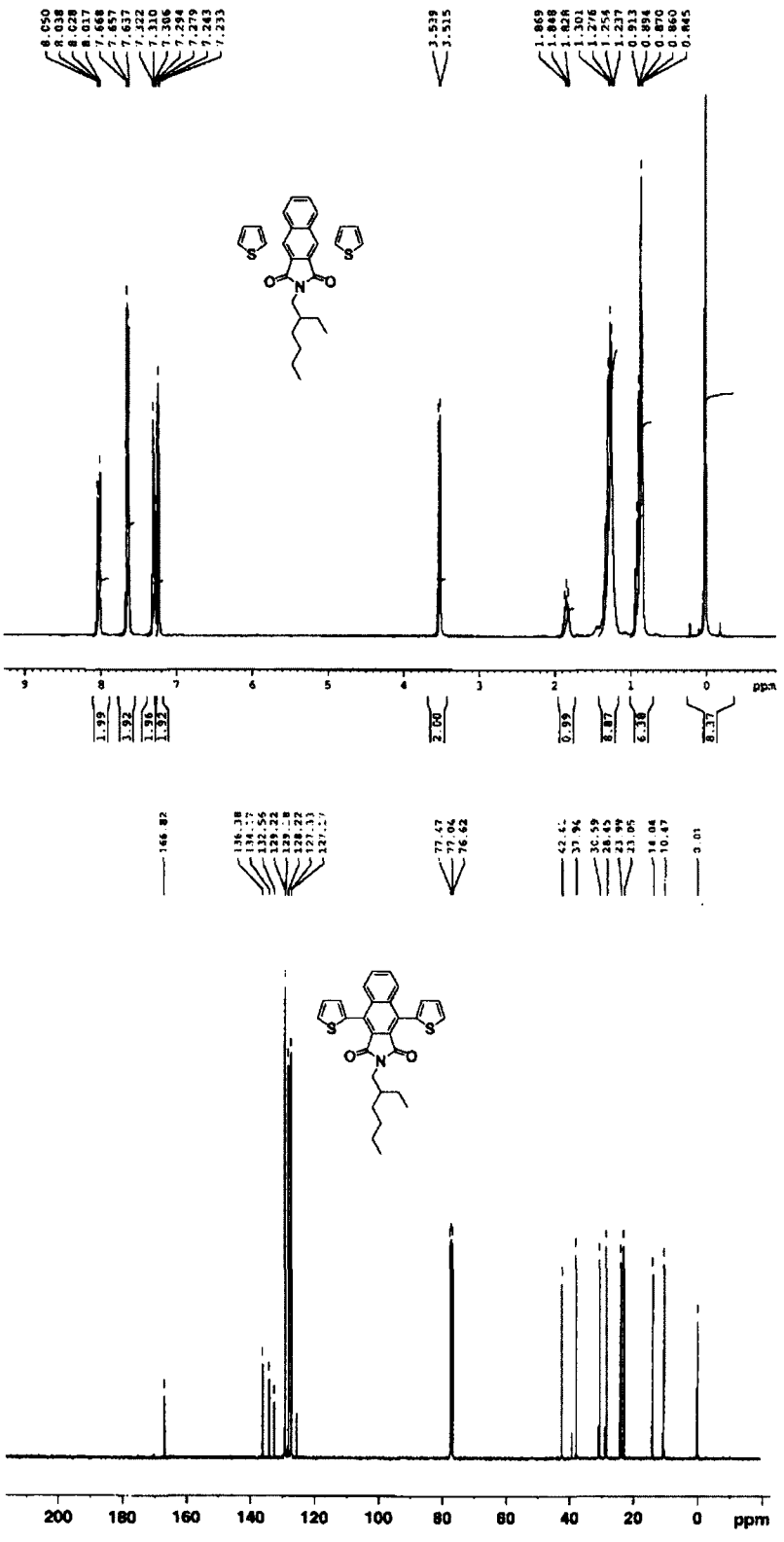

Figure A.9. ^{1}H NMR (300 MHz, $CDCl_3$) and ^{13}C NMR (75 MHz, $CDCl_3$) spectrum of 2-(2-ethylhexyl)-4,9-di(thiophen-2-yl)-1H-benzo[f]isoindole-1,3(2H)-dione.

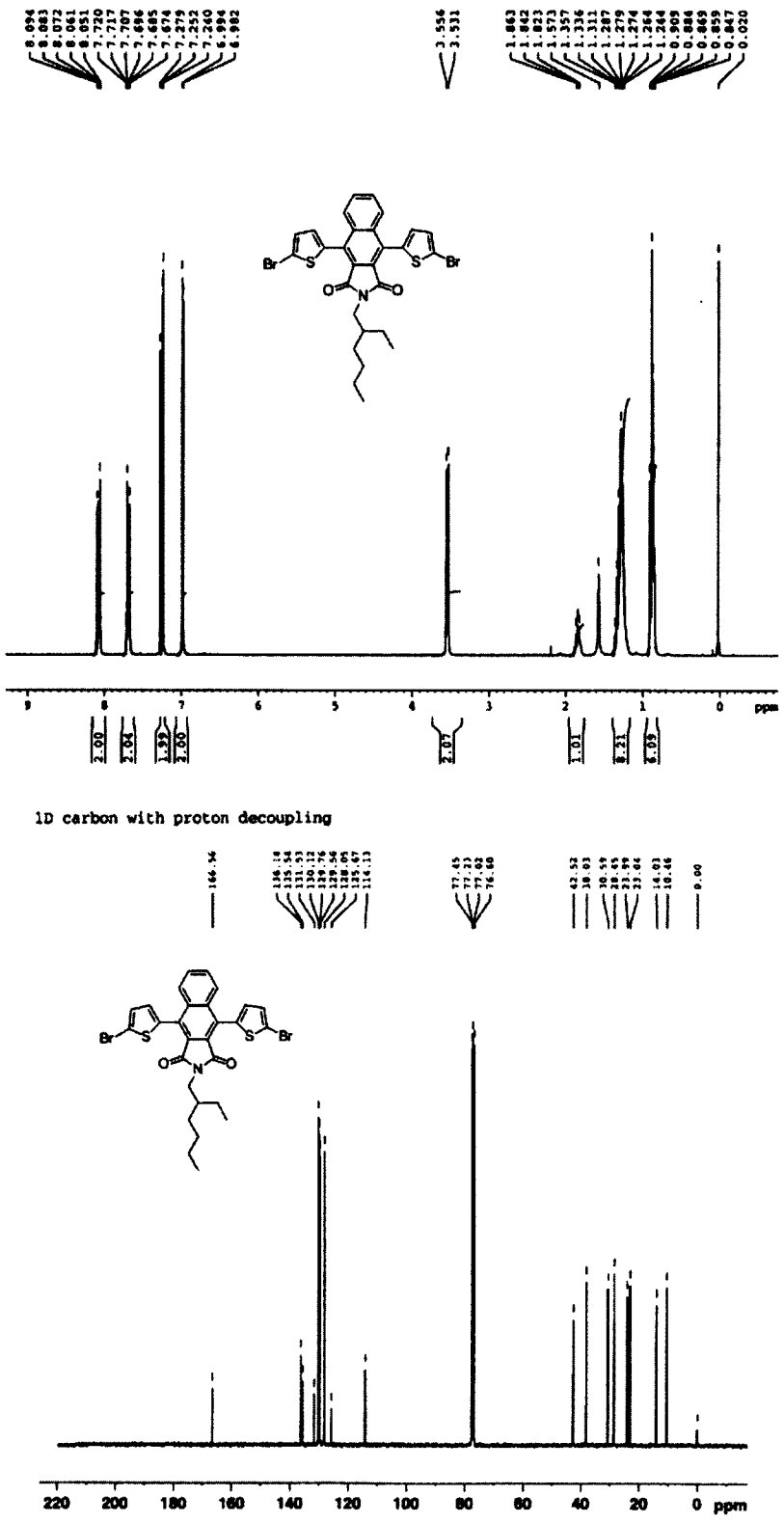

Figure A.10. ^{1}H NMR (300 MHz, $CDCl_3$) and ^{13}C NMR (75 MHz, $CDCl_3$) spectrum of **BIDO-2**.

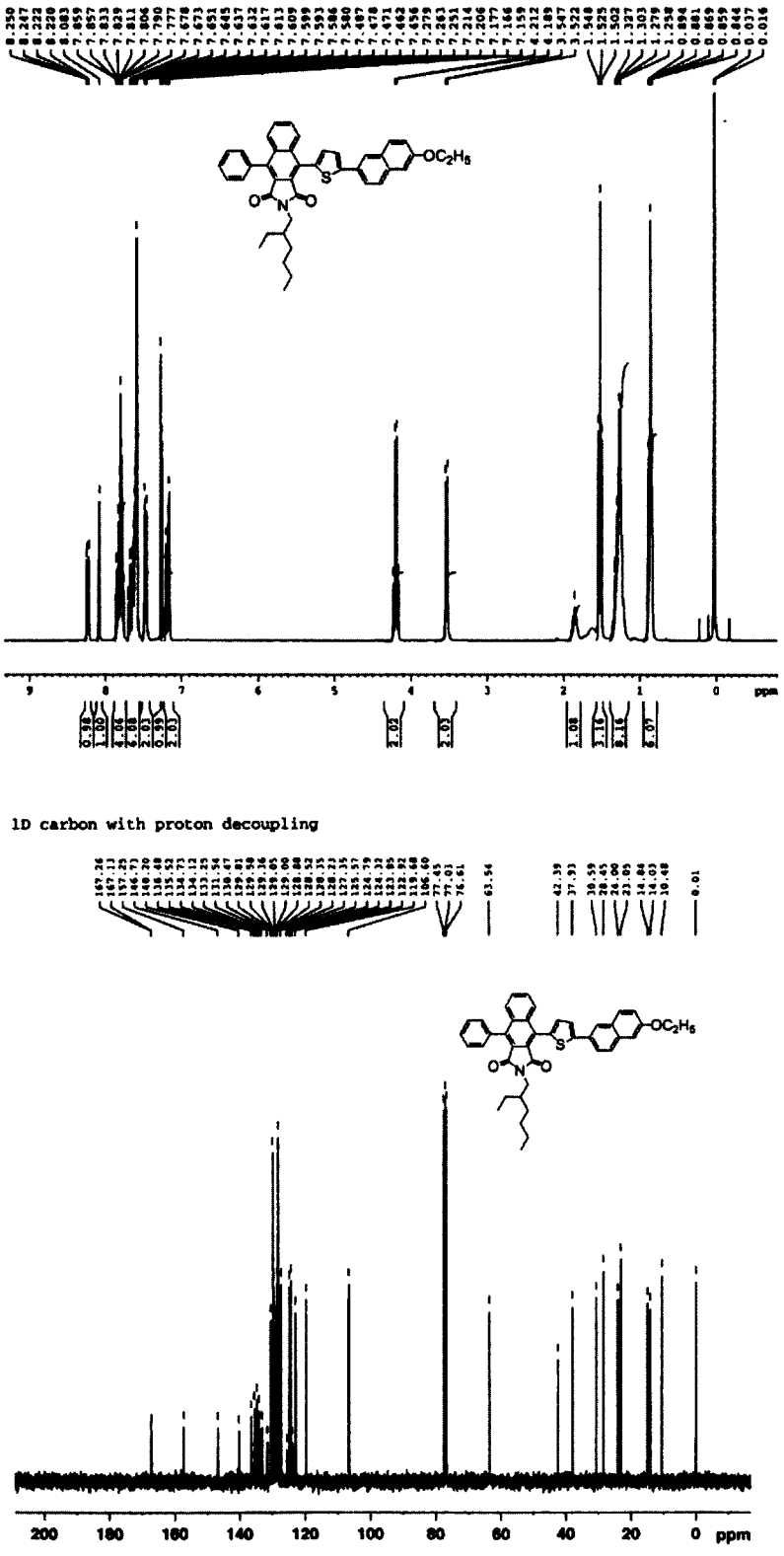

Figure A.11. ^{1}H NMR (300 MHz, $CDCl_3$) and ^{13}C NMR (75 MHz, $CDCl_3$) spectrum of **BIDO-1-EONP**.

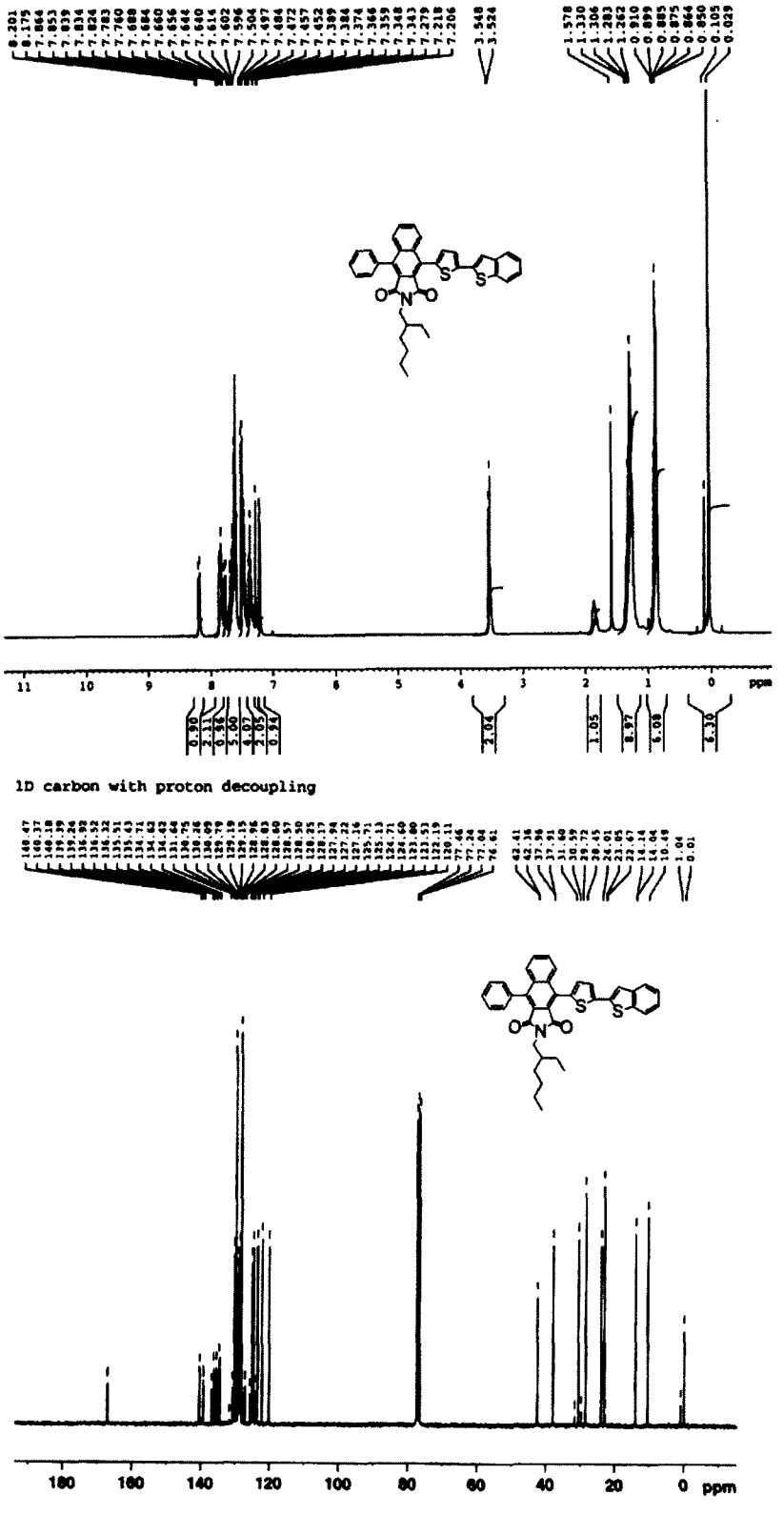

Figure A.12. ^{1}H NMR (300 MHz, $CDCl_3$) and ^{13}C NMR (75 MHz, $CDCl_3$) spectrum of **BIDO-1-BT**.

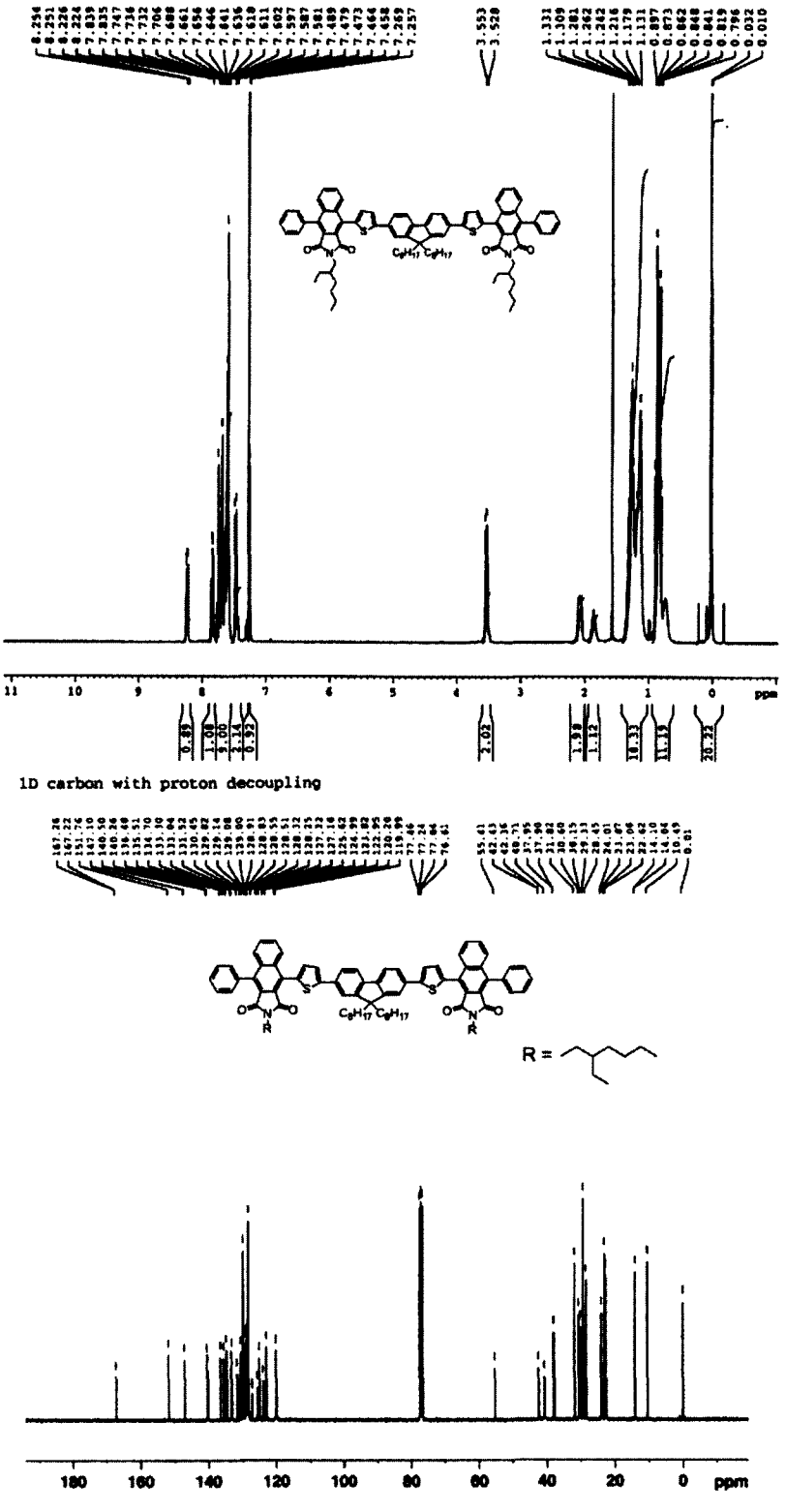

Figure A.13. ^{1}H NMR (300 MHz, $CDCl_3$) and ^{13}C NMR (75 MHz, $CDCl_3$) spectrum of **BIDO-1-FL**.

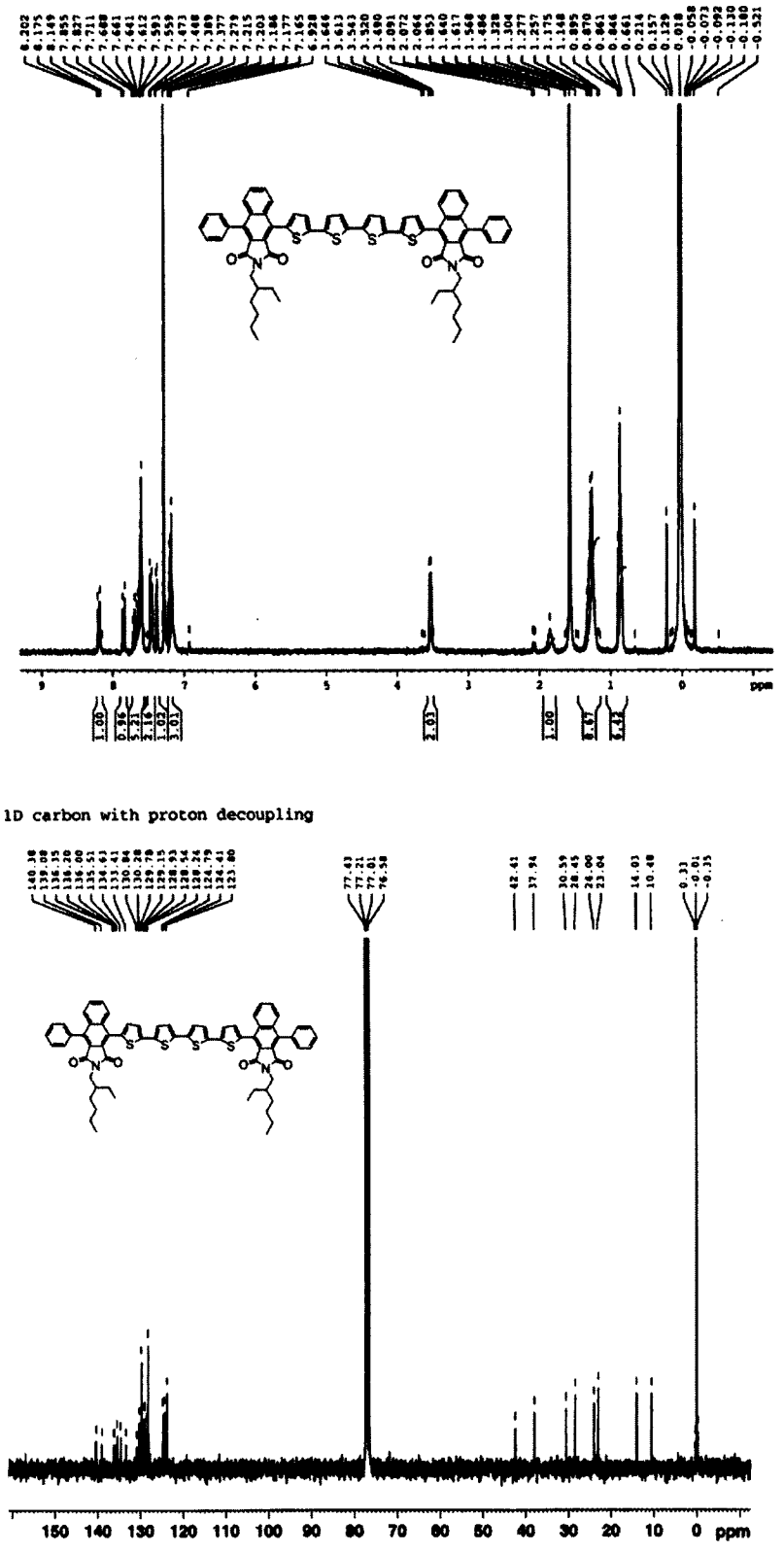

Figure A.14. ^{1}H NMR (300 MHz, $CDCl_3$) and ^{13}C NMR (75 MHz, $CDCl_3$) spectrum of **BIDO-1-DT**.

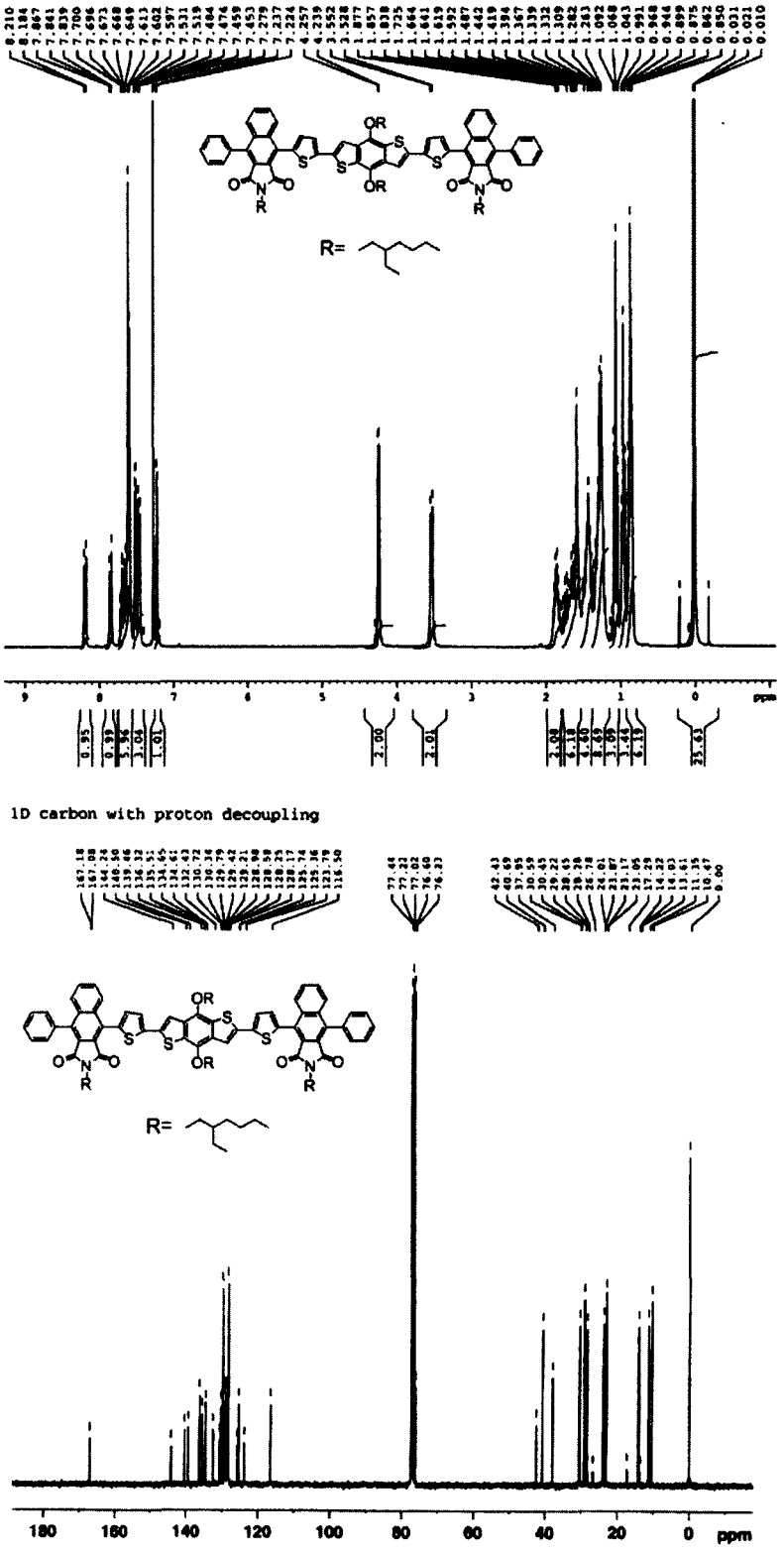

Figure A.15. ^{1}H NMR (300 MHz, $CDCl_3$) and ^{13}C NMR (75 MHz, $CDCl_3$) spectrum of **BIDO-1-BDT**.

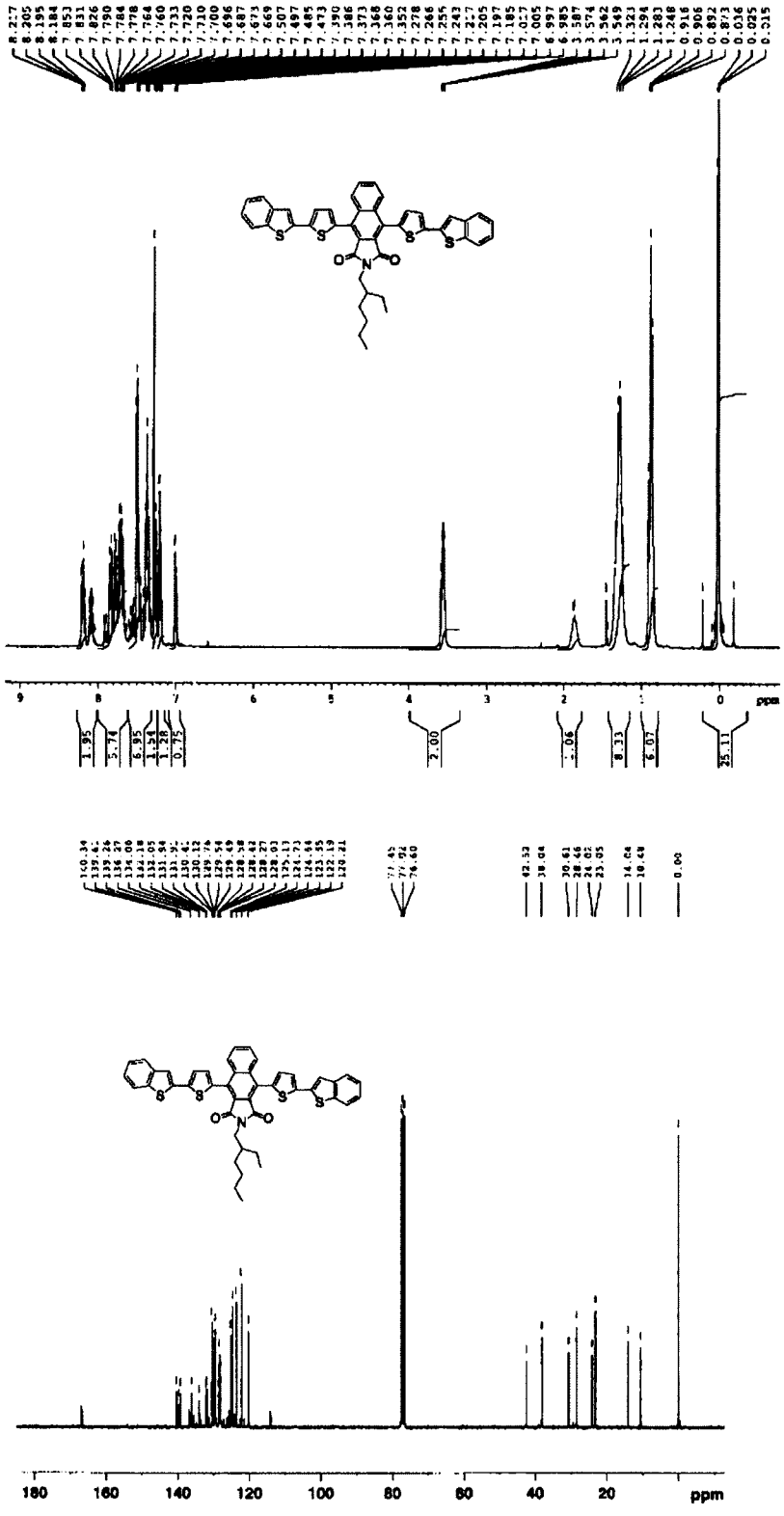

Figure A.16. ^{1}H NMR (300 MHz, $CDCl_3$) and ^{13}C NMR (75 MHz, $CDCl_3$) spectrum of **BIDO-2-BT**.

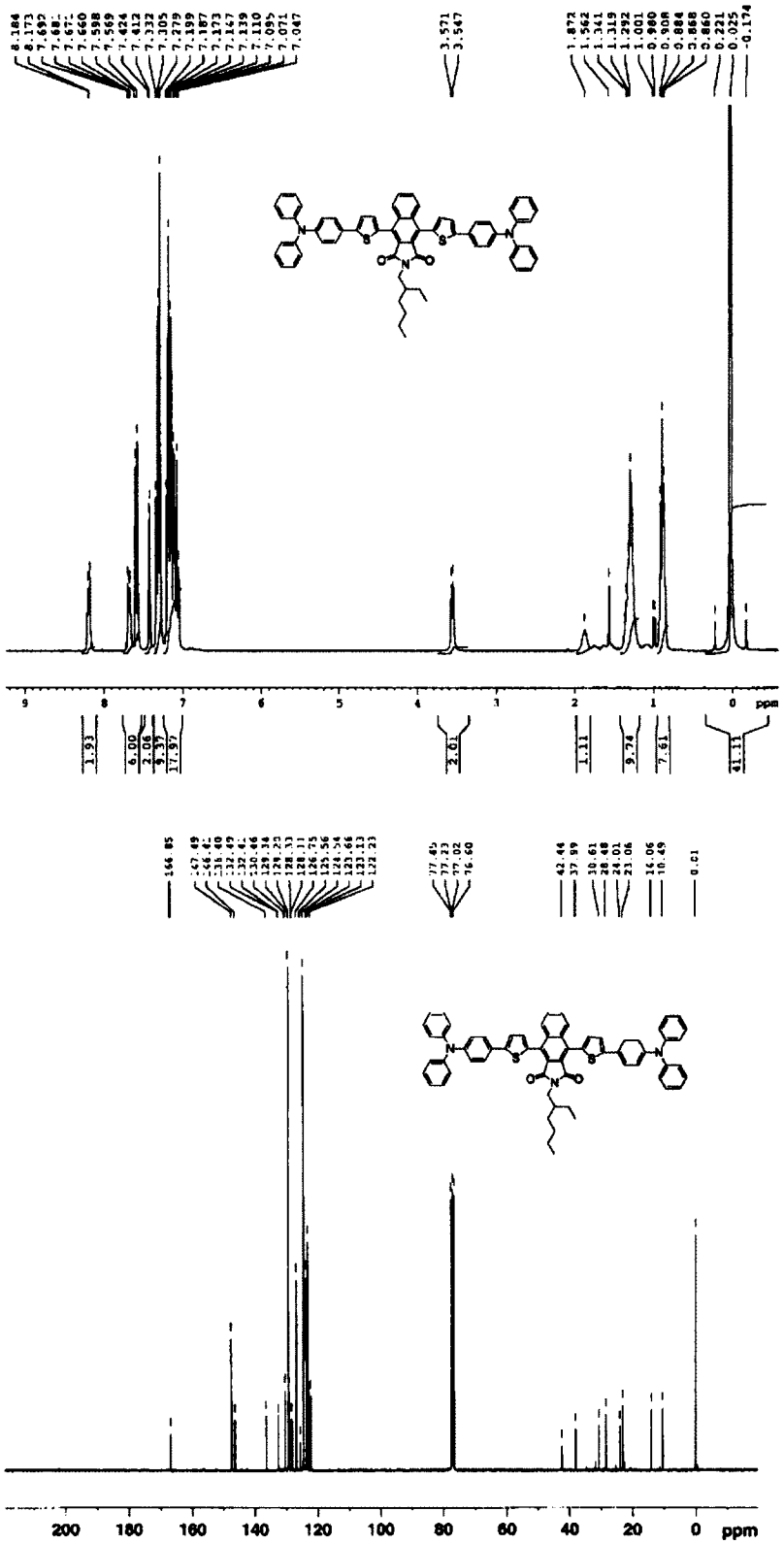

Figure A.17. ^{1}H NMR (300 MHz, $CDCl_3$) and ^{13}C NMR (75 MHz, $CDCl_3$) spectrum of **BIDO-2-TPA**.

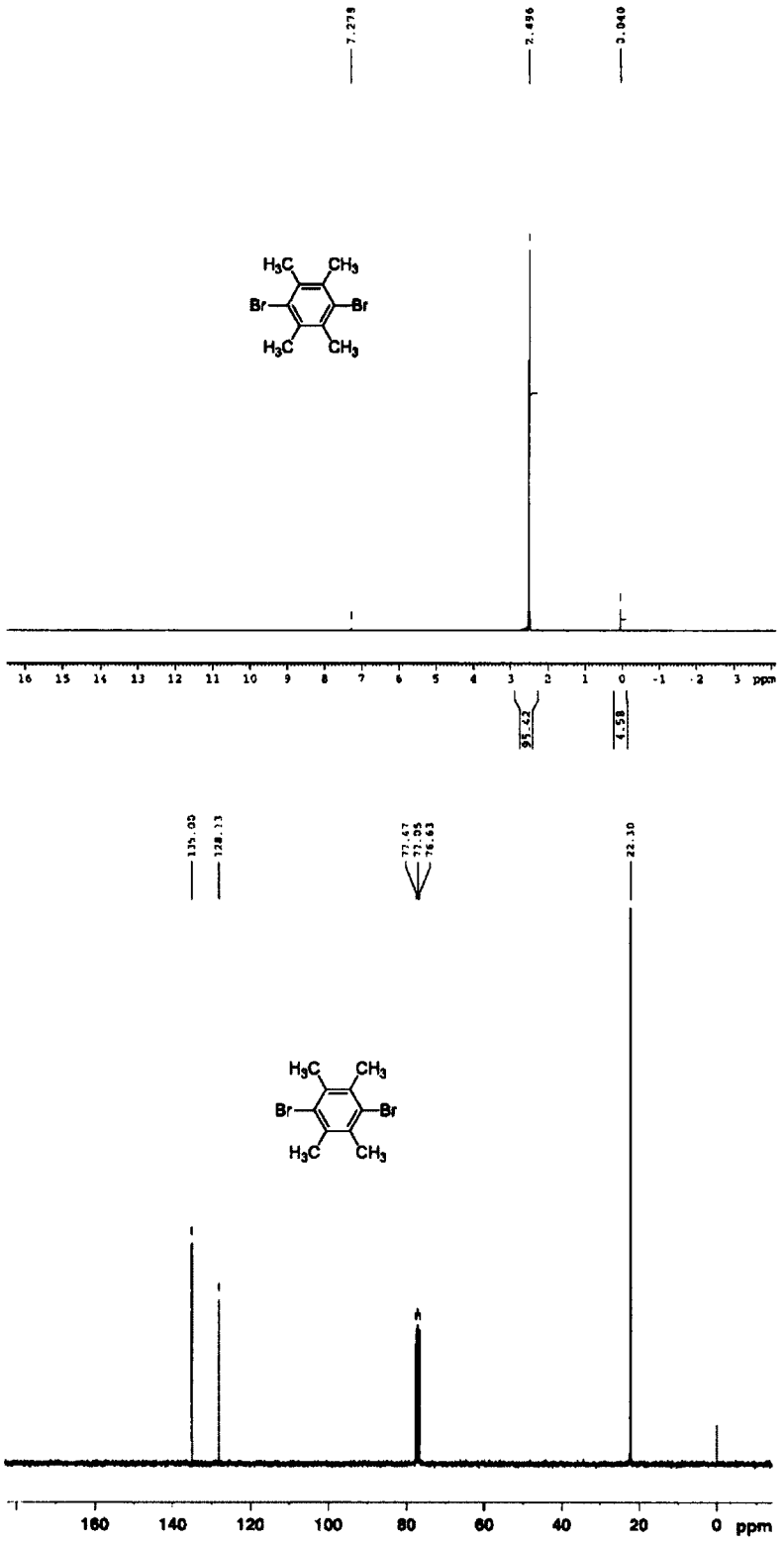

Figure A.18. ^{1}H NMR (300 MHz, $CDCl_3$) and ^{13}C NMR (75 MHz, $CDCl_3$) spectrum of 1,4-dibromo-2,3,5,6-tetramethylbenzene.

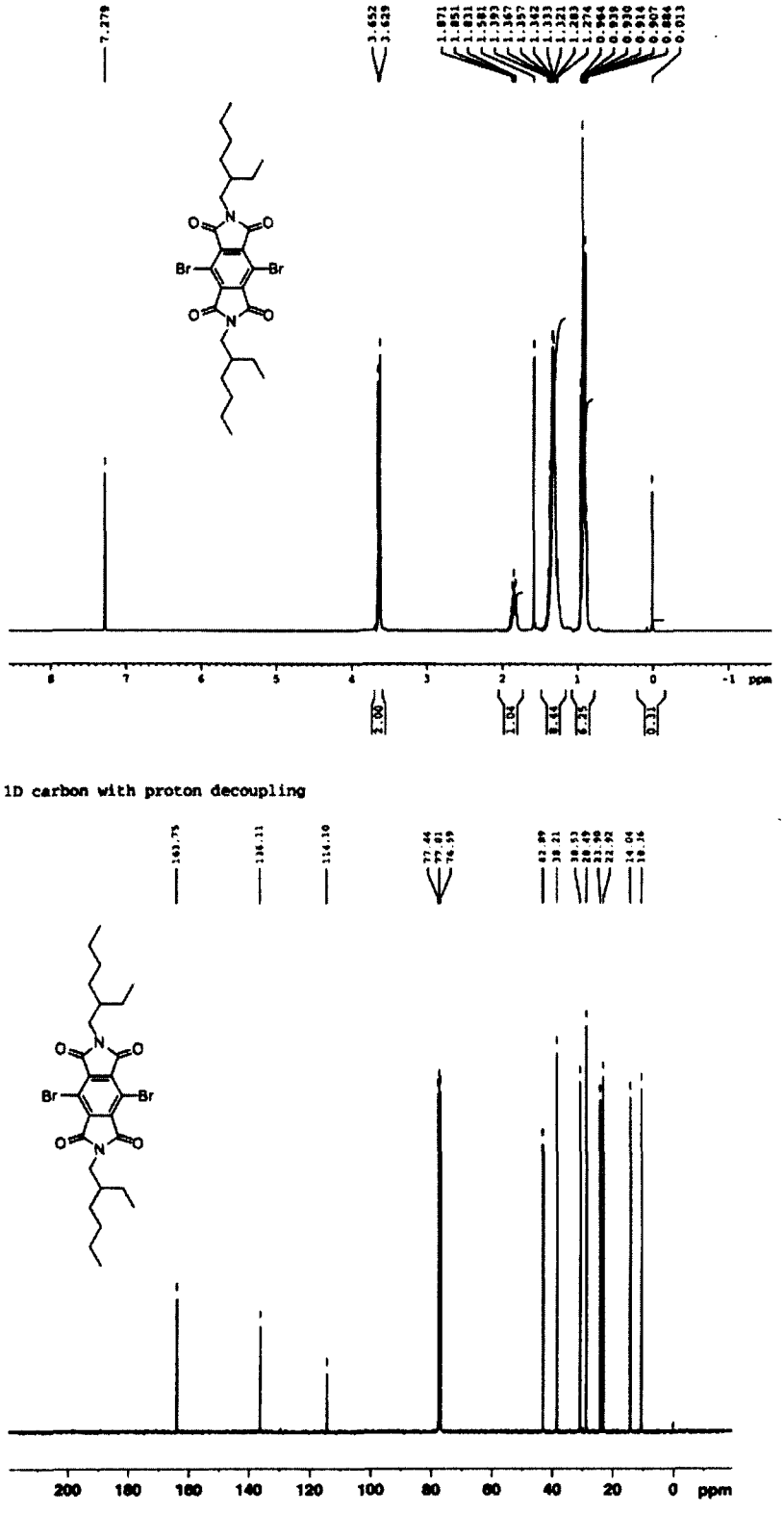

Figure A.19. ^{1}H NMR (300 MHz, $CDCl_3$) and ^{13}C NMR (75 MHz, $CDCl_3$) spectrum of **PMDI**.

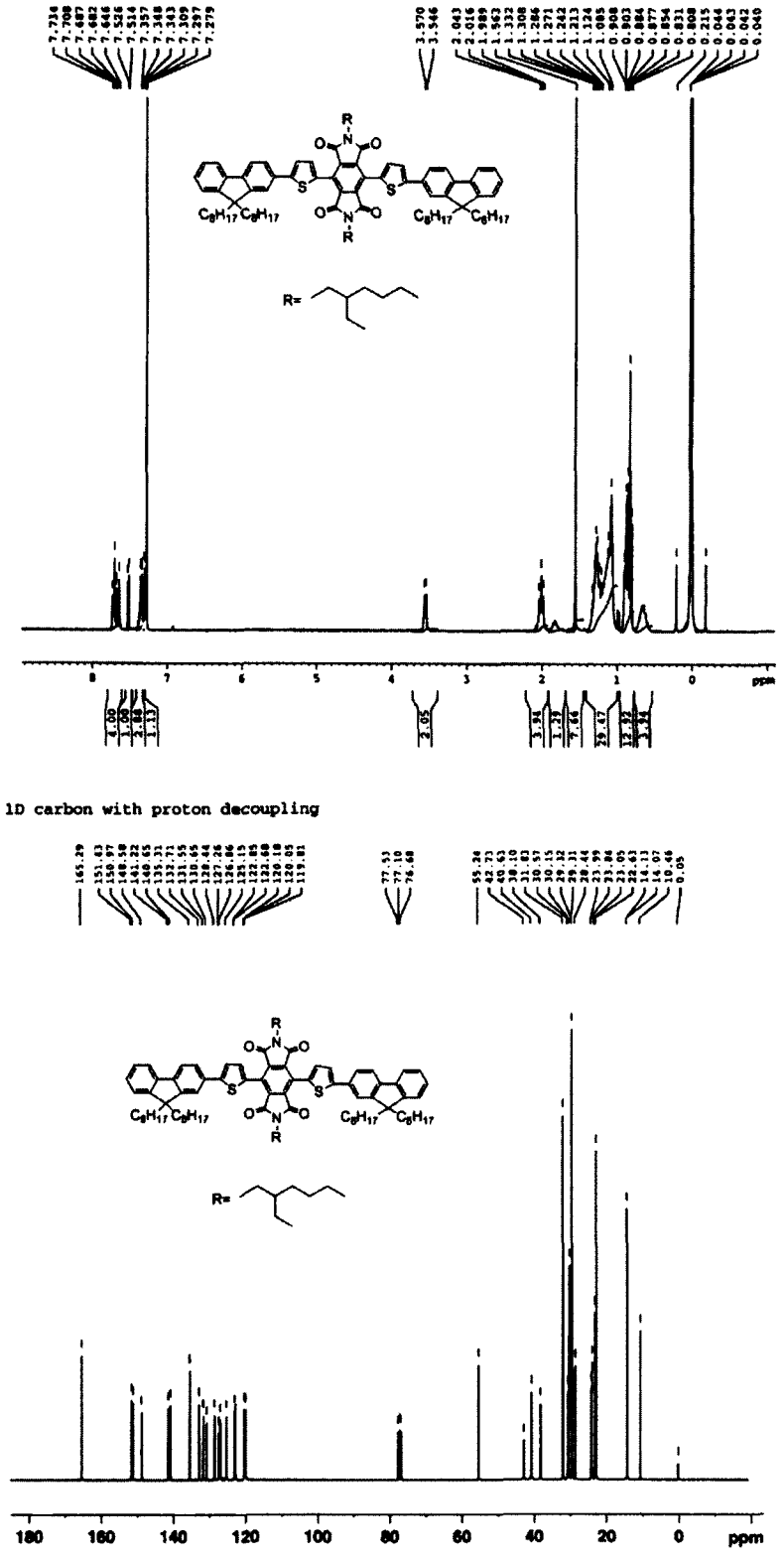

Figure A.20. ^{1}H NMR (300 MHz, $CDCl_3$) and ^{13}C NMR (75 MHz, $CDCl_3$) spectrum of **PMDI-FLT**.

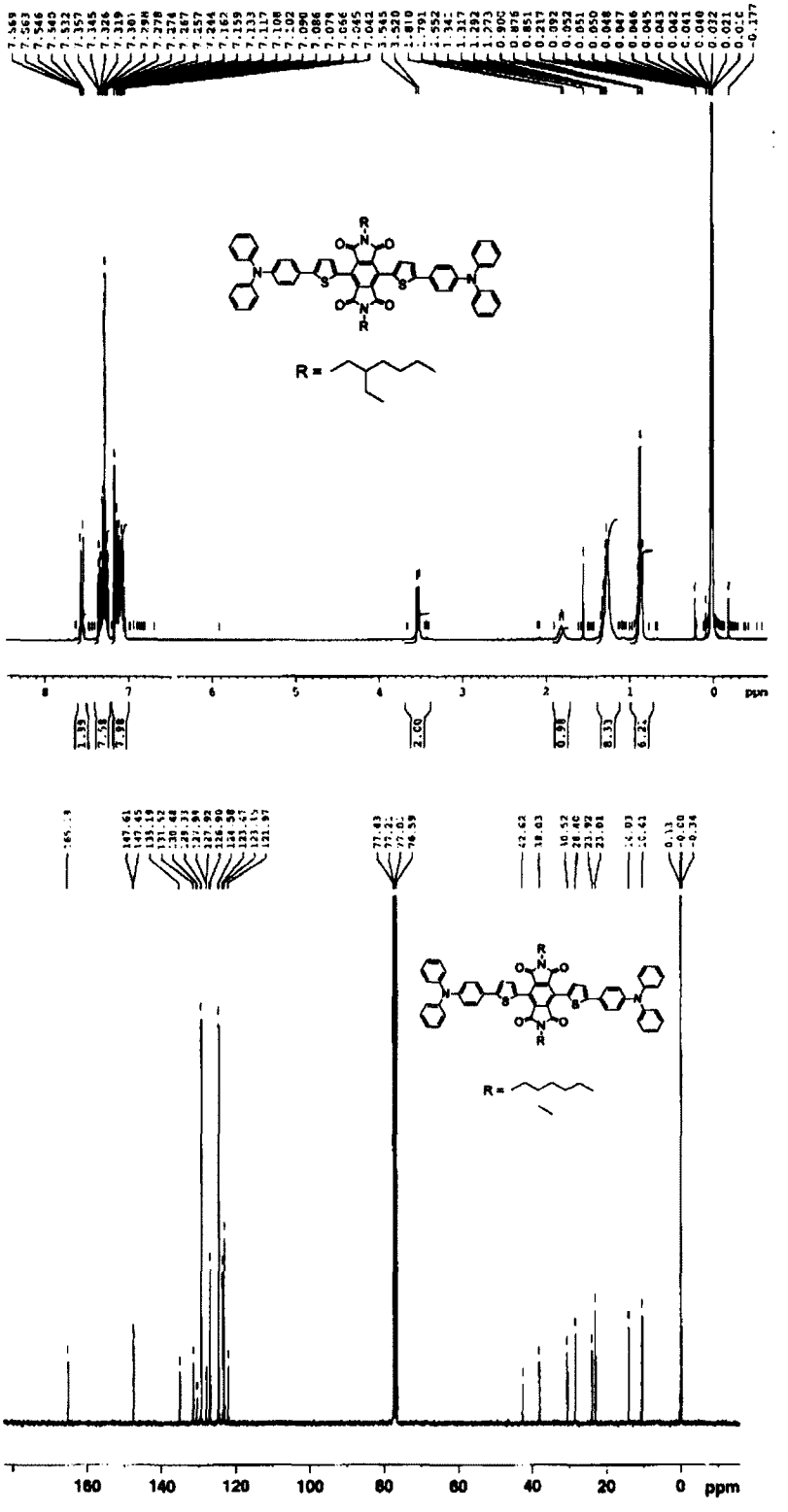

Figure A.21. ^{1}H NMR (300 MHz, $CDCl_3$) and ^{13}C NMR (75 MHz, $CDCl_3$) spectrum of **PMDI-TPAT**.

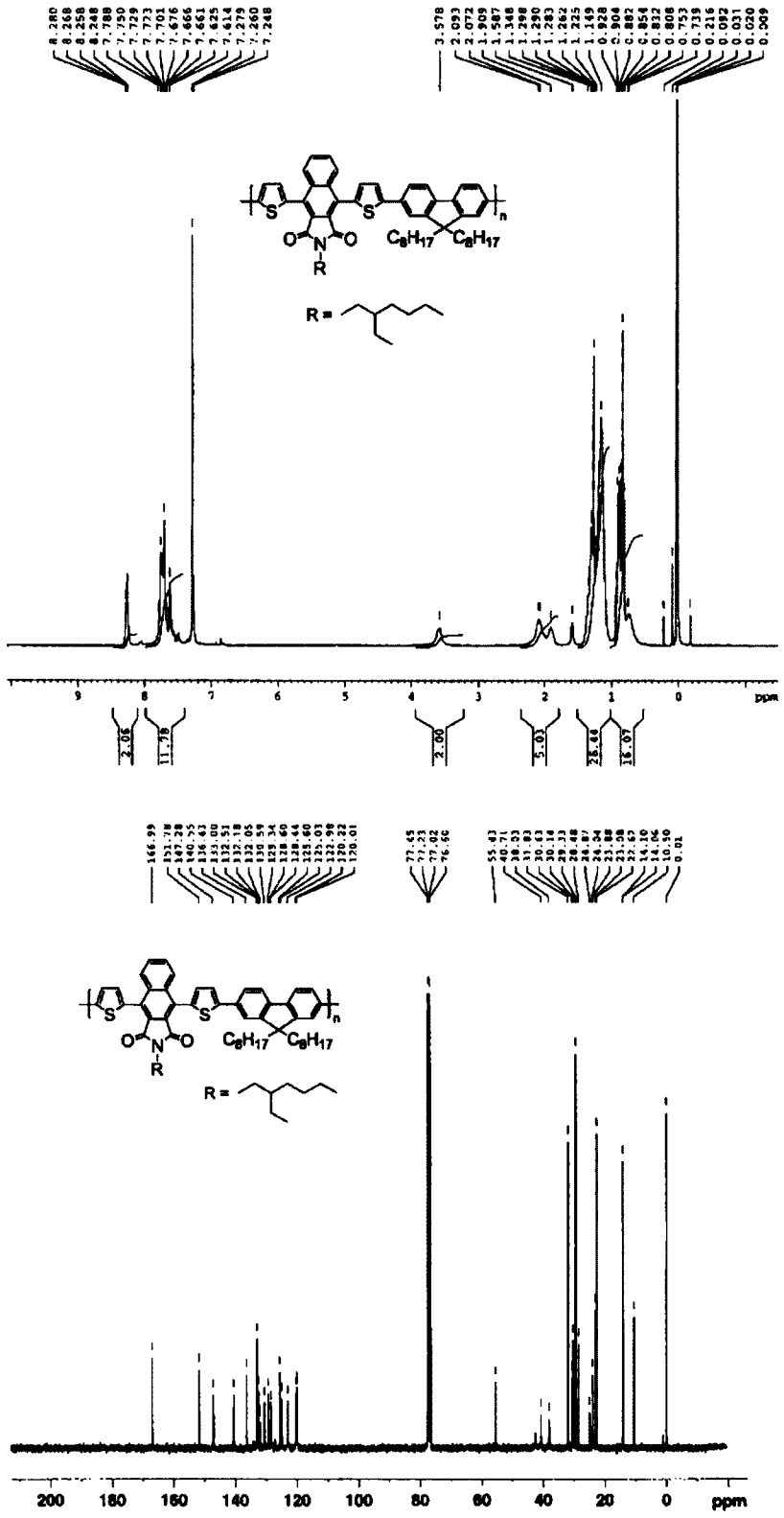

Figure A.22. ^{1}H NMR (300 MHz, $CDCl_3$) and ^{13}C NMR (75 MHz, $CDCl_3$) spectrum of **P1**.

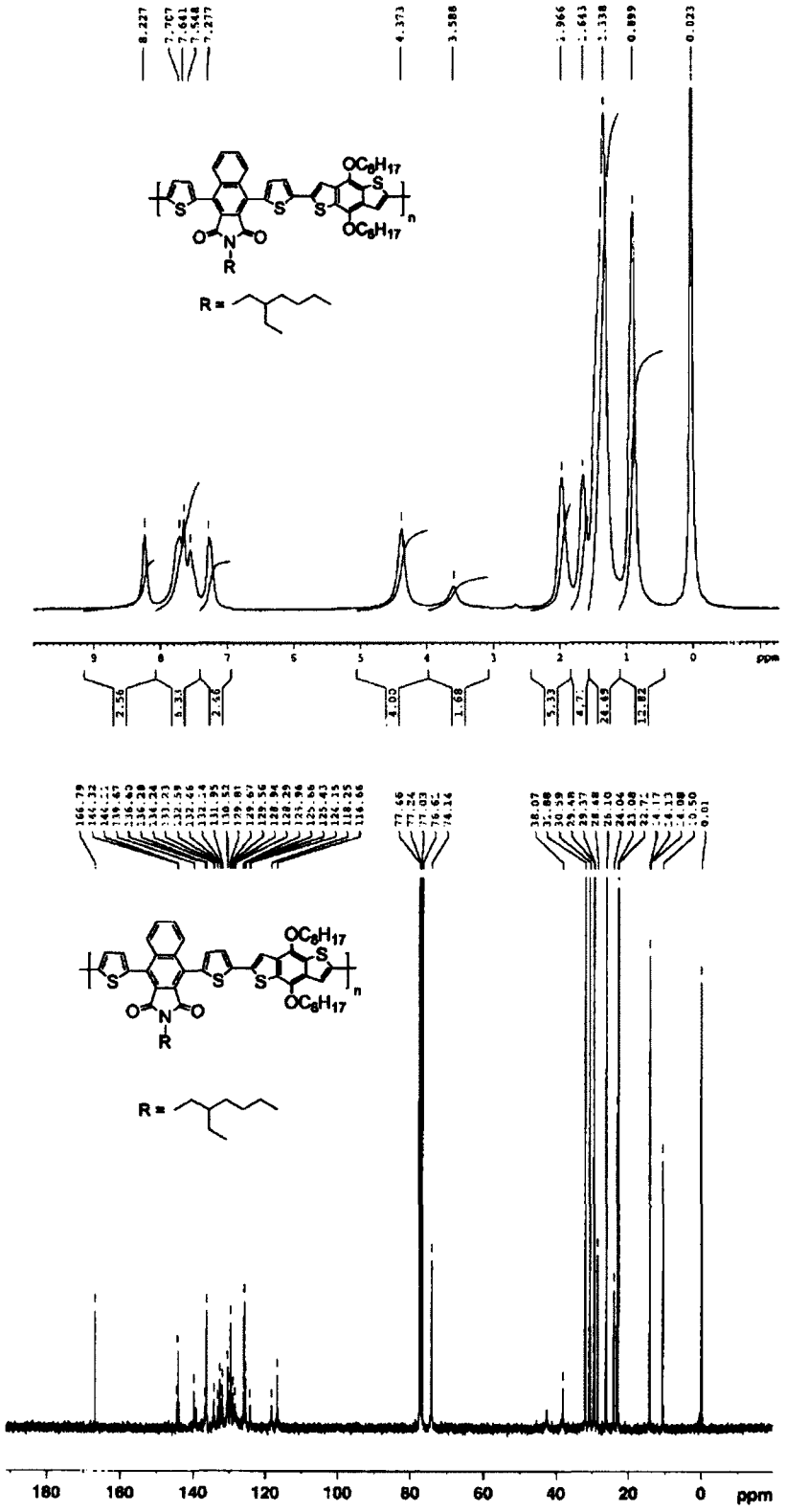

Figure A.23. ^{1}H NMR (300 MHz, $CDCl_3$) and ^{13}C NMR (75 MHz, $CDCl_3$) spectrum of **P2**.

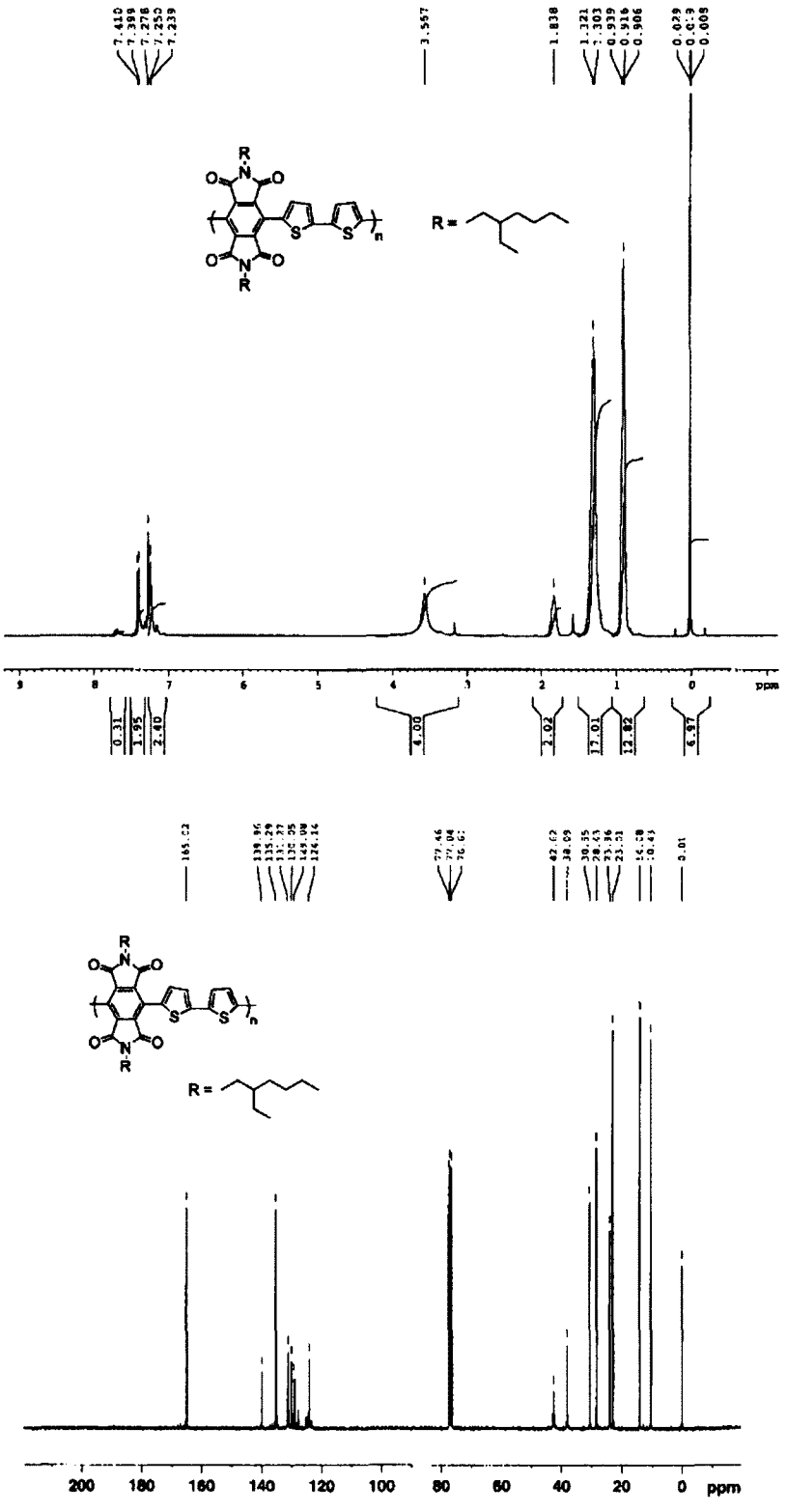

Figure A.24. ^{1}H NMR (300 MHz, $CDCl_3$) and ^{13}C NMR (75 MHz, $CDCl_3$) spectrum of **P3**.

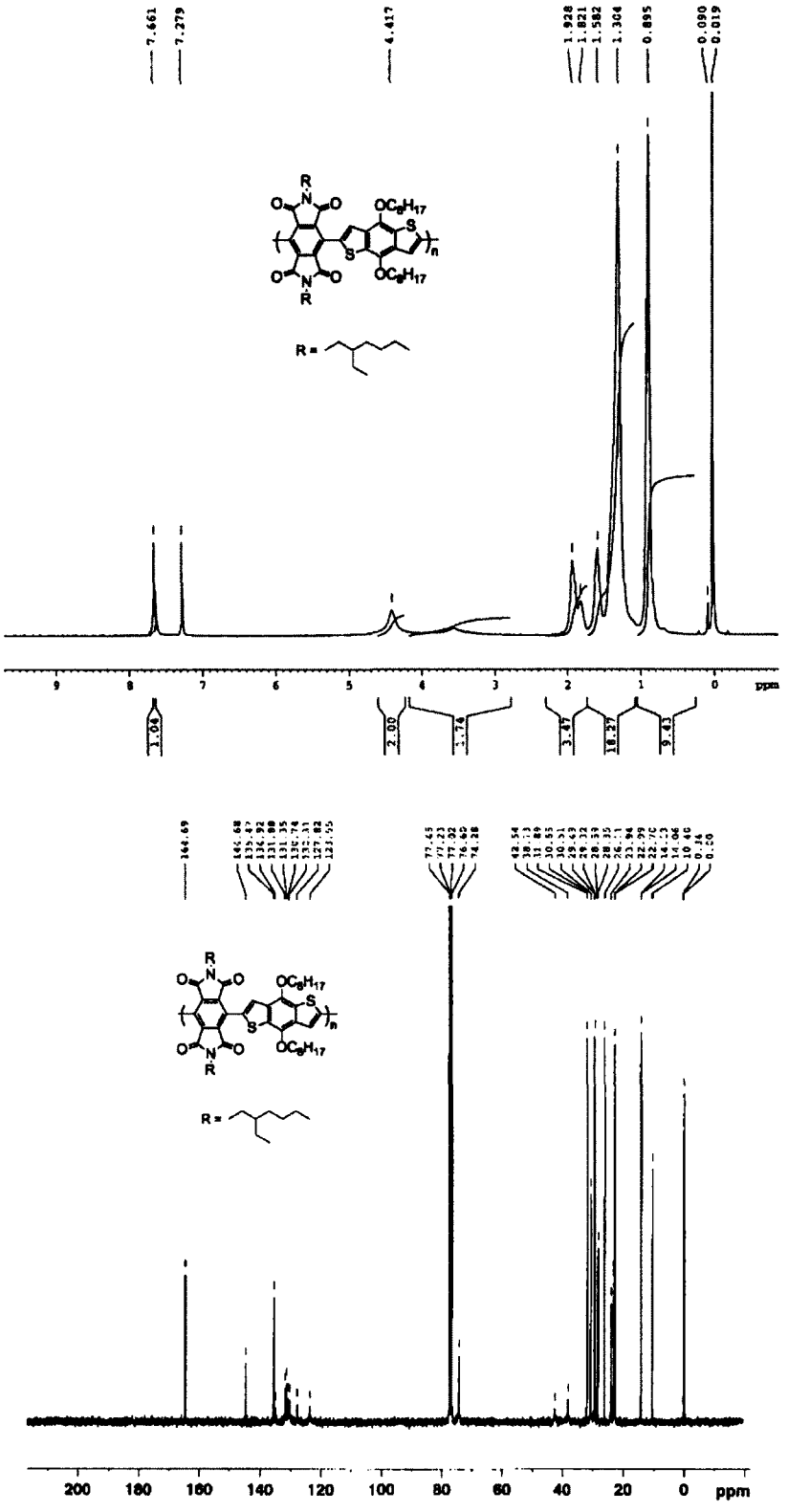

Figure A.25. ^{1}H NMR (300 MHz, $CDCl_3$) and ^{13}C NMR (75 MHz, $CDCl_3$) spectrum of **P4**.

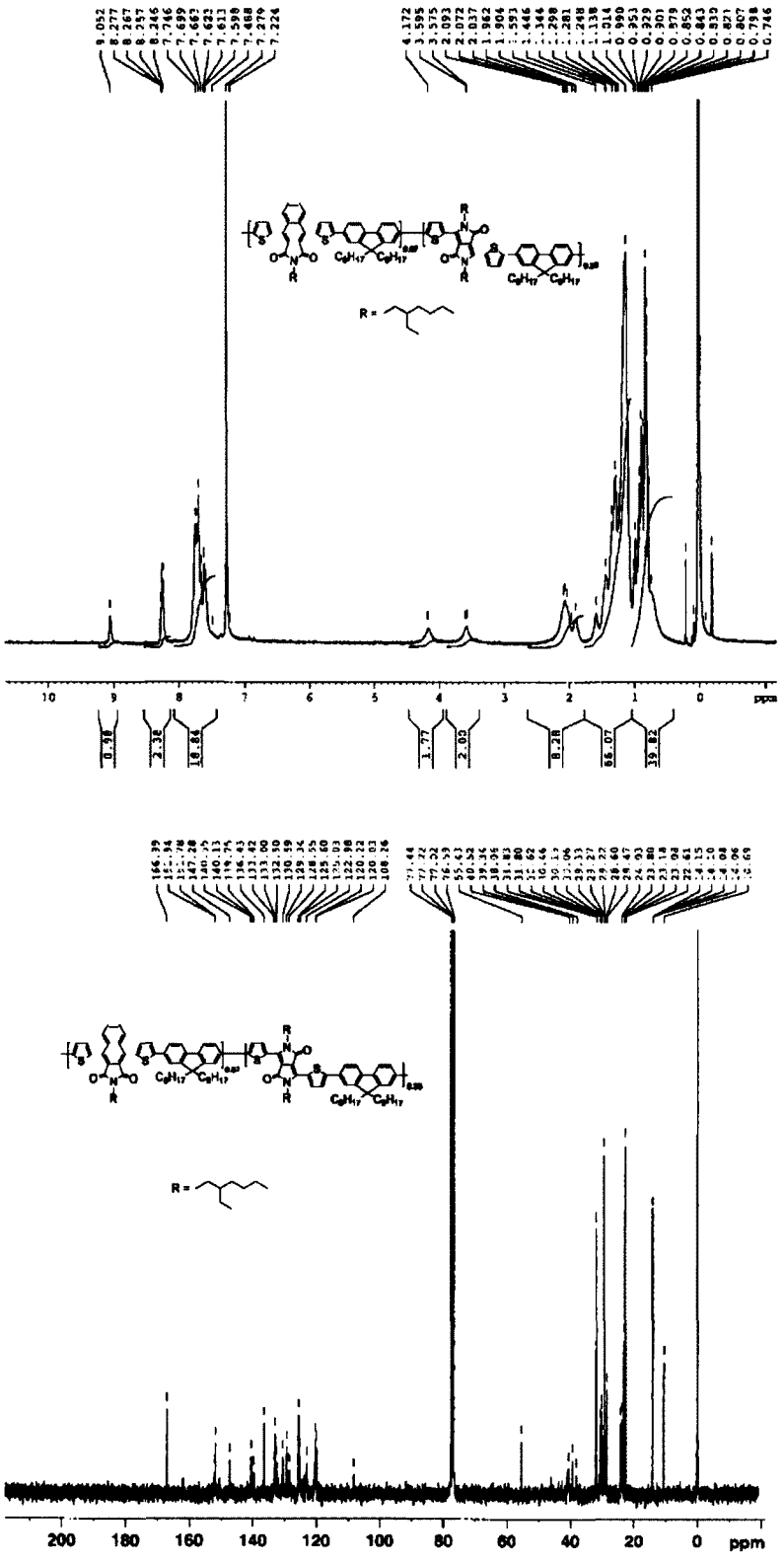

Figure A.26. ^{1}H NMR (300 MHz, $CDCl_3$) and ^{13}C NMR (75 MHz, $CDCl_3$) spectrum of **Pa**.

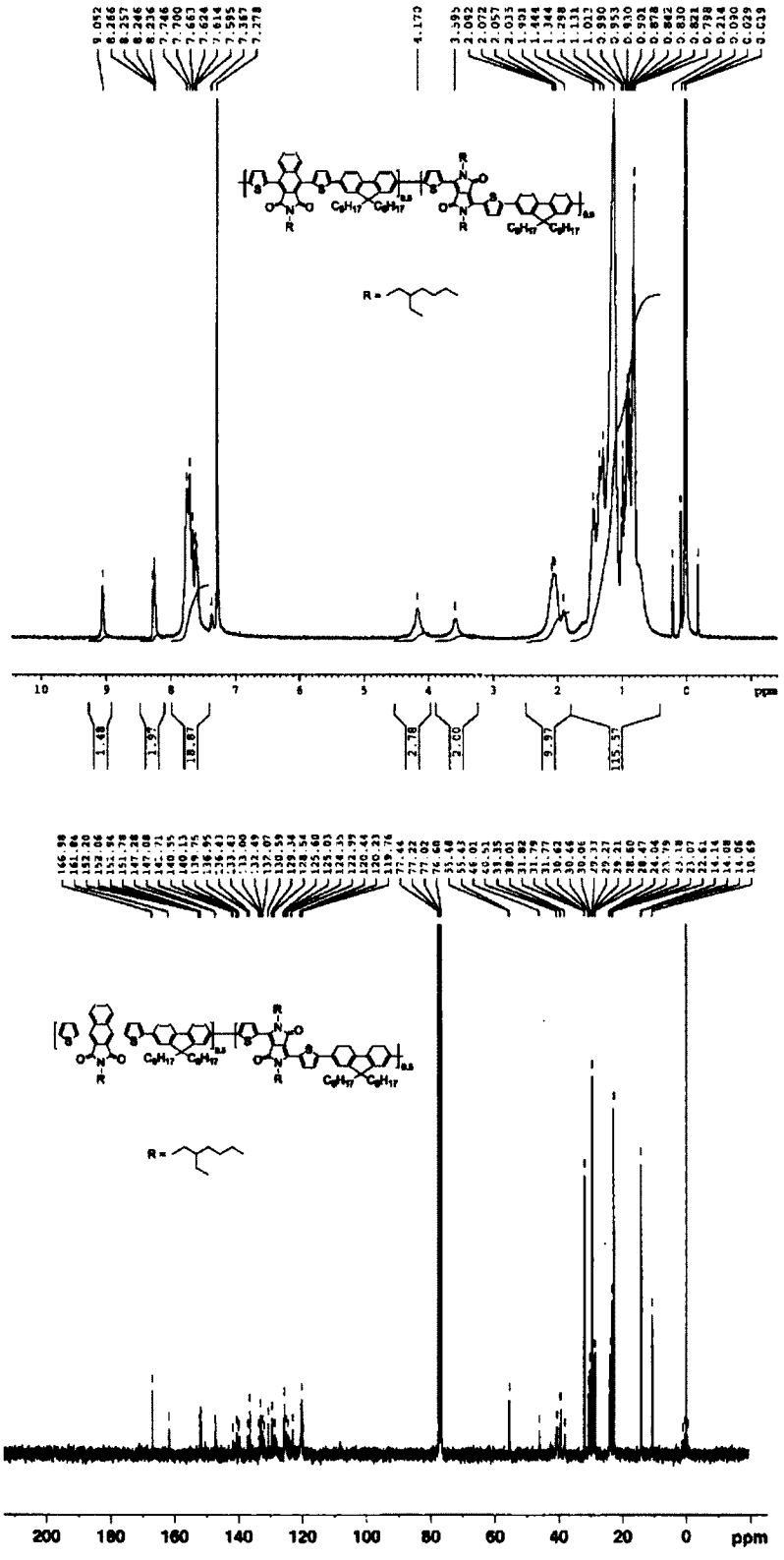

Figure A.27. ^{1}H NMR (300 MHz, $CDCl_3$) and ^{13}C NMR (75 MHz, $CDCl_3$) spectrum of **Pb**.

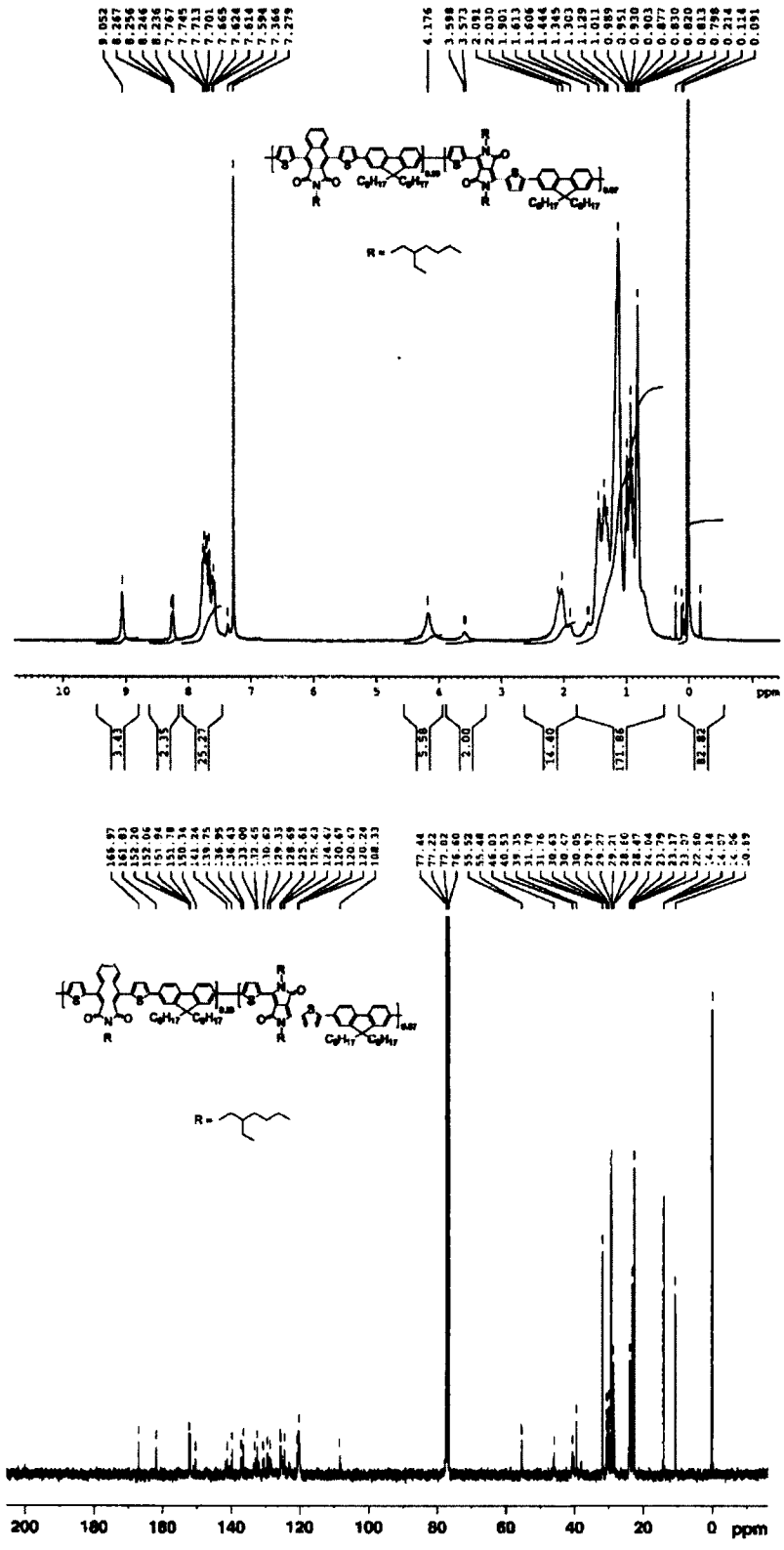

Figure A.28. ^{1}H NMR (300 MHz, $CDCl_3$) and ^{13}C NMR (75 MHz, $CDCl_3$) spectrum of **Pc**.

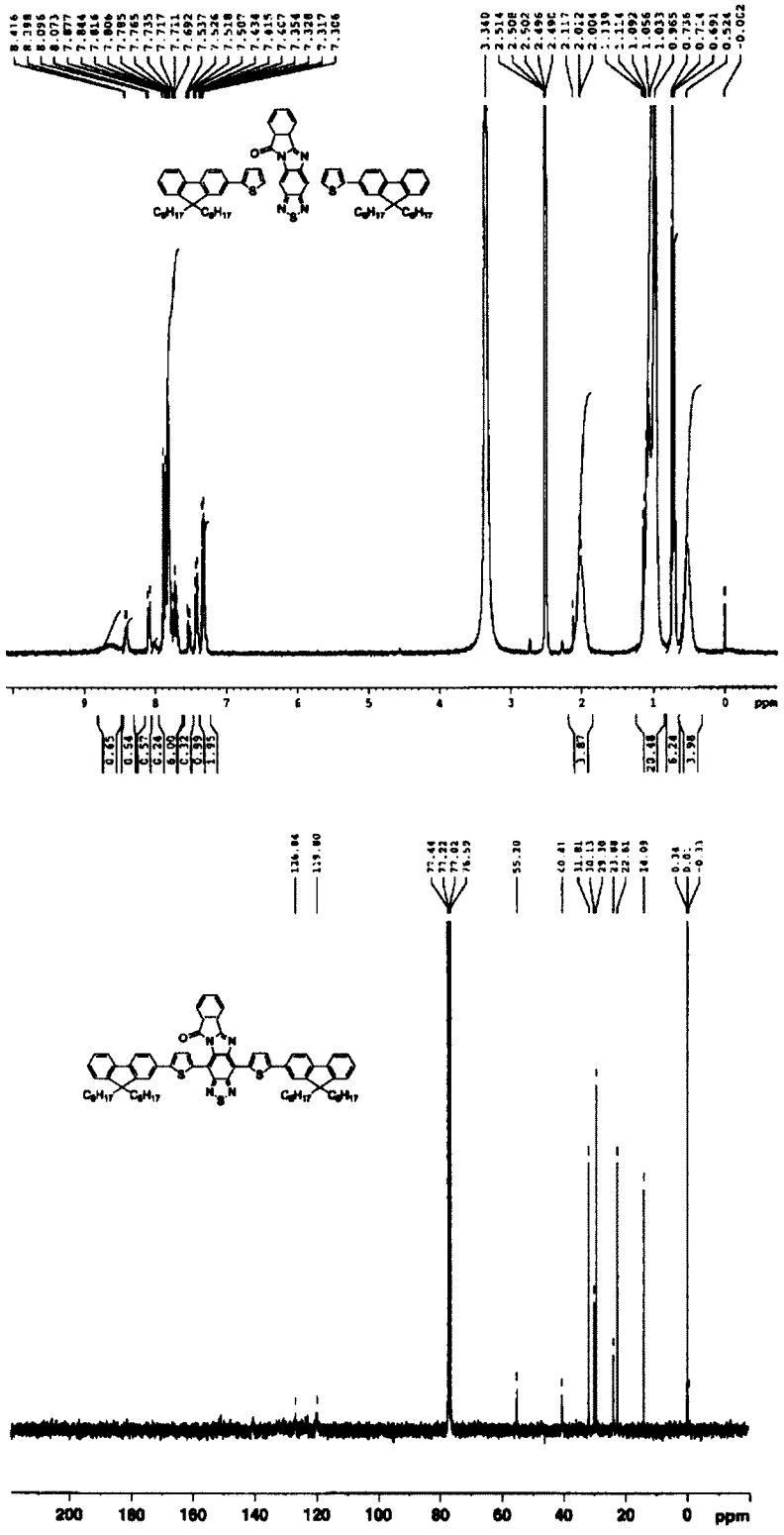

Figure A.29. ^{1}H NMR (300 MHz, DMSO-d_6) and ^{13}C NMR (75 MHz, $CDCl_3$) spectrum of **IV-a**.

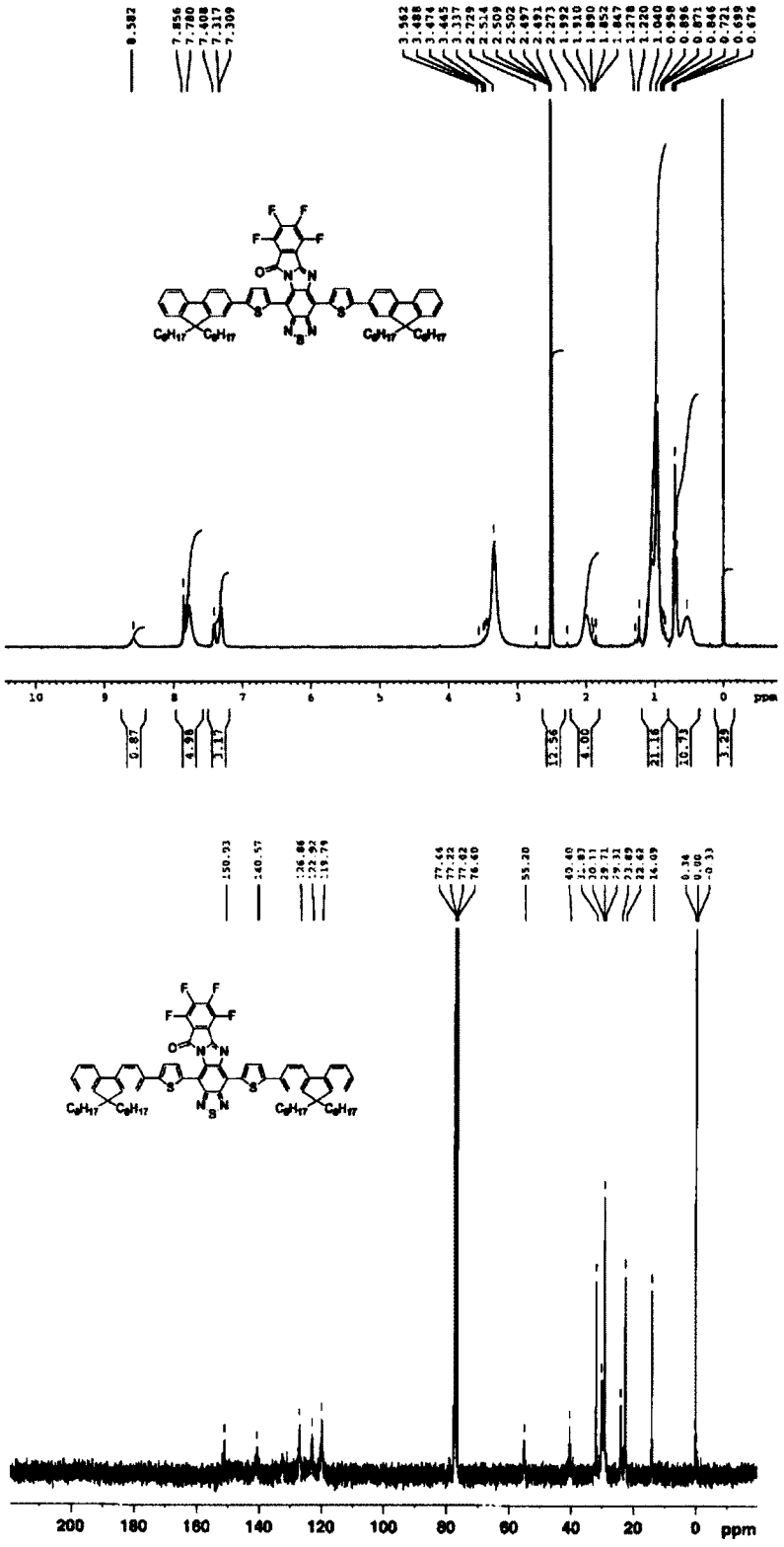

Figure A.30. ^{1}H NMR (300 MHz, DMSO-d_6) and ^{13}C NMR (75 MHz, $CDCl_3$) spectrum of **IV-b**.

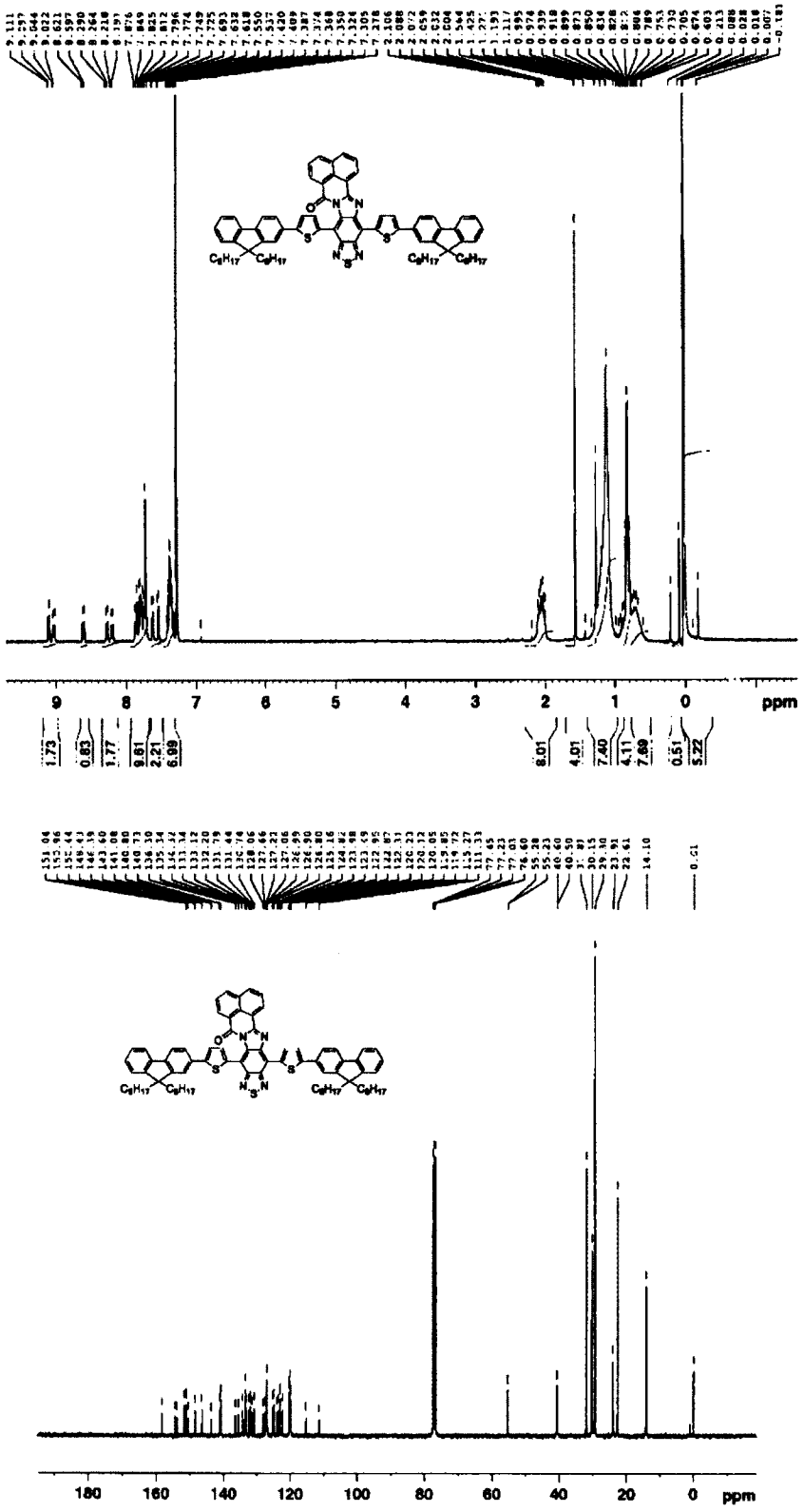

Figure A.31. ^{1}H NMR (300 MHz, $CDCl_3$) and ^{13}C NMR (75 MHz, $CDCl_3$) spectrum of **IV-c**.

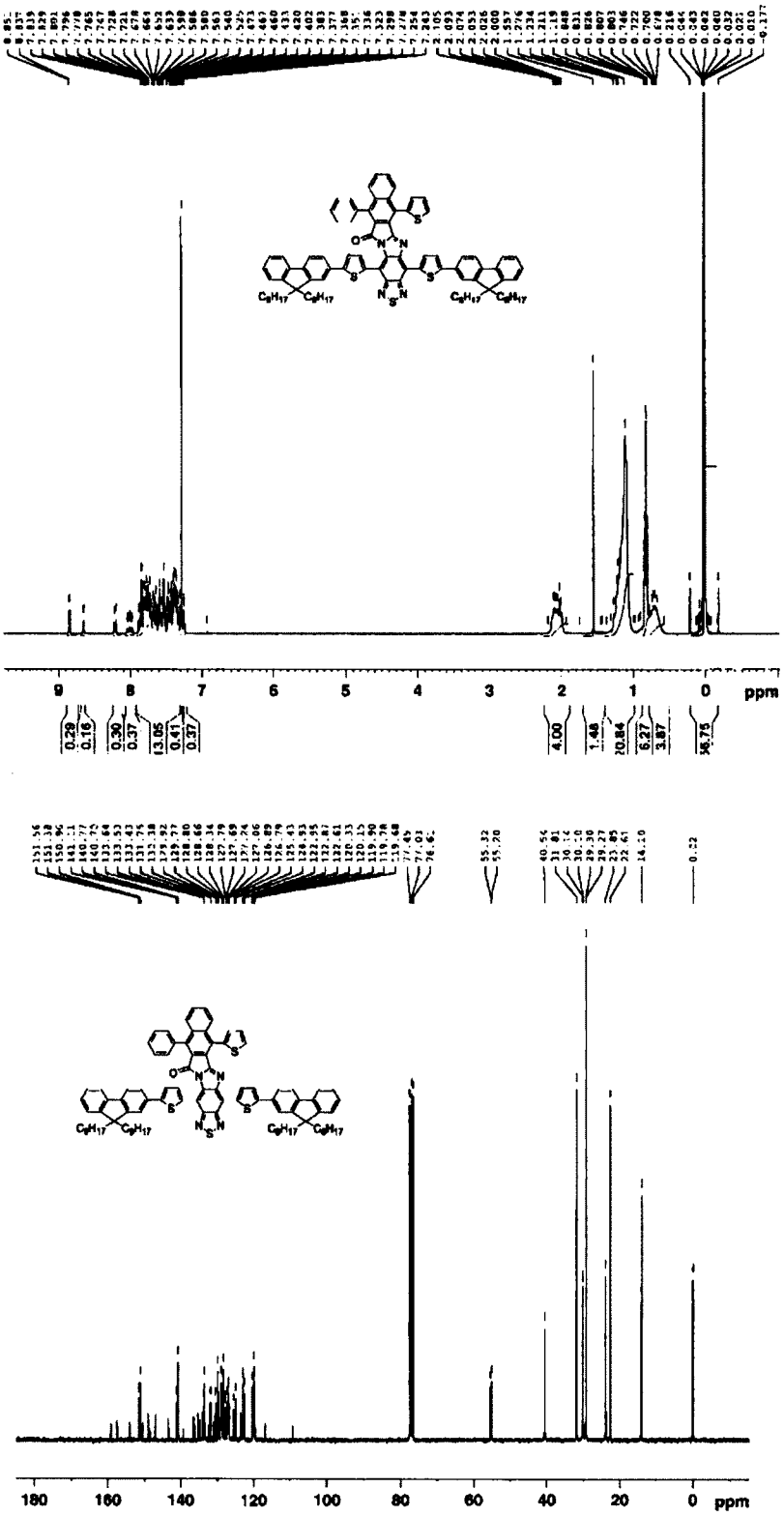

Figure A.32. ^{1}H NMR (300 MHz, $CDCl_3$) and ^{13}C NMR (75 MHz, $CDCl_3$) spectrum of **IV-d**.

APPENDIX B

IR and Mass spectra of compounds and IR spectra of polymers

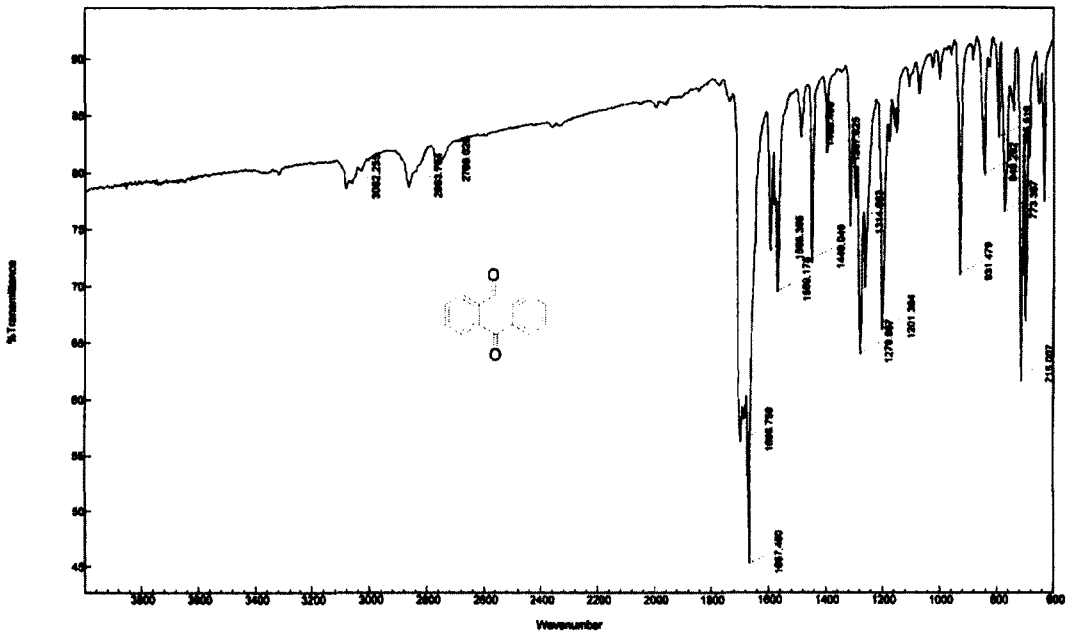

Figure B.1. IR spectrum of 2-benzoylbenzaldehyde.

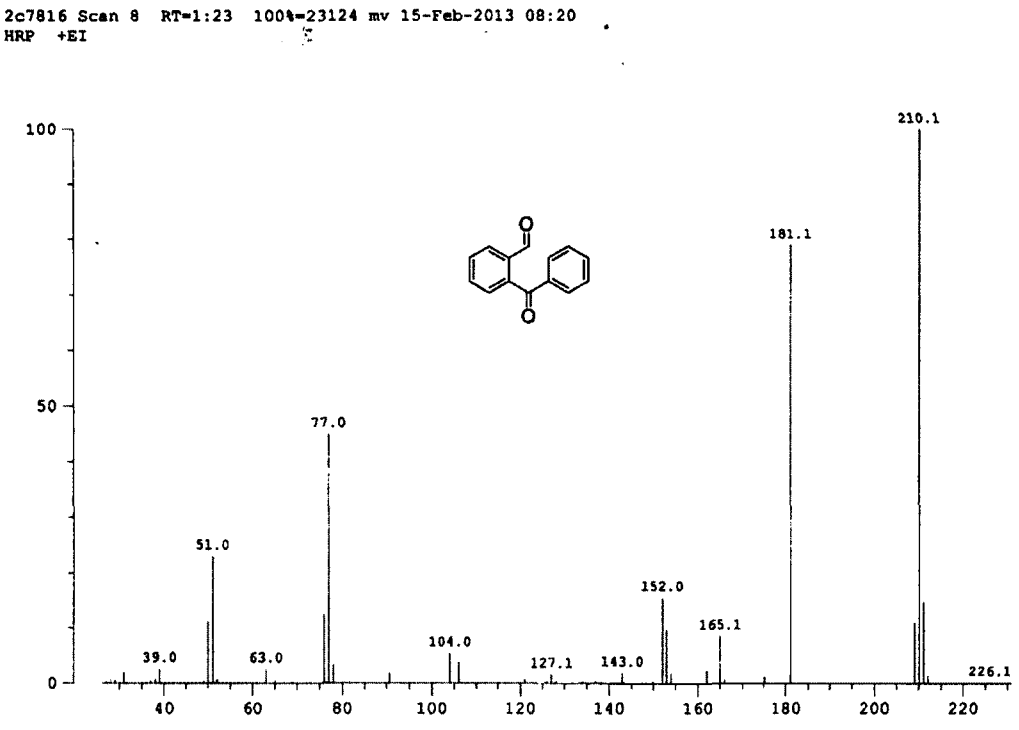

Figure B.2. High resolution mass spectrum of 2-benzoylbenzaldehyde.

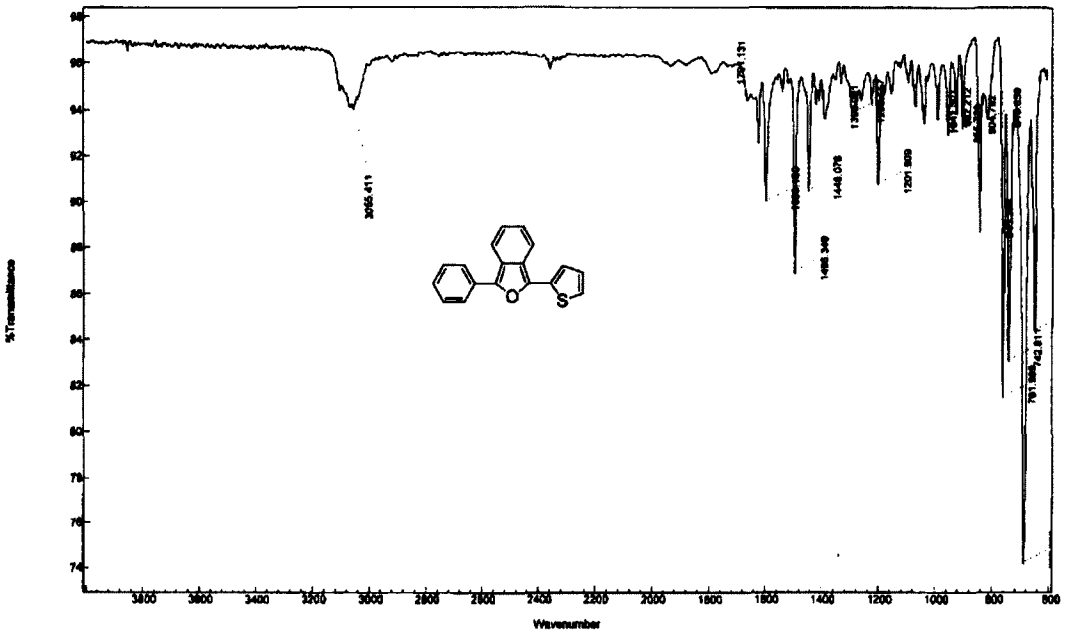

Figure B.3. IR spectrum of 1-phenyl-3-(thiophen-2-yl)isobenzofuran.

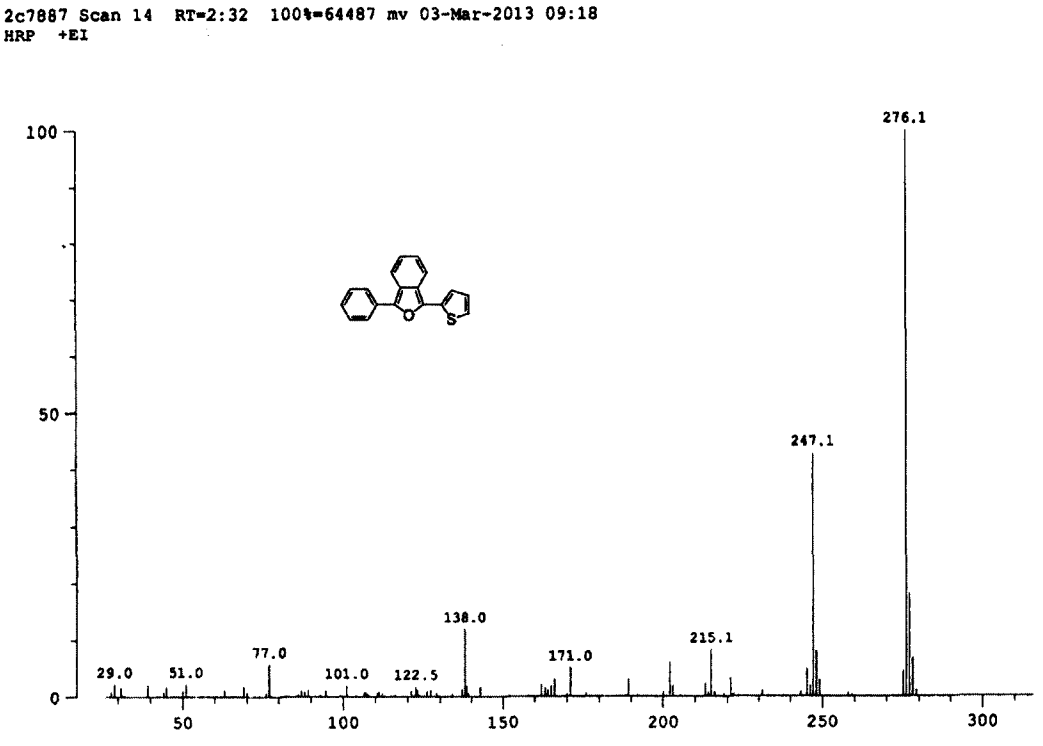

Figure B.4. High resolution mass spectrum of 1-phenyl-3-(thiophen-2-yl)isobenzofuran.

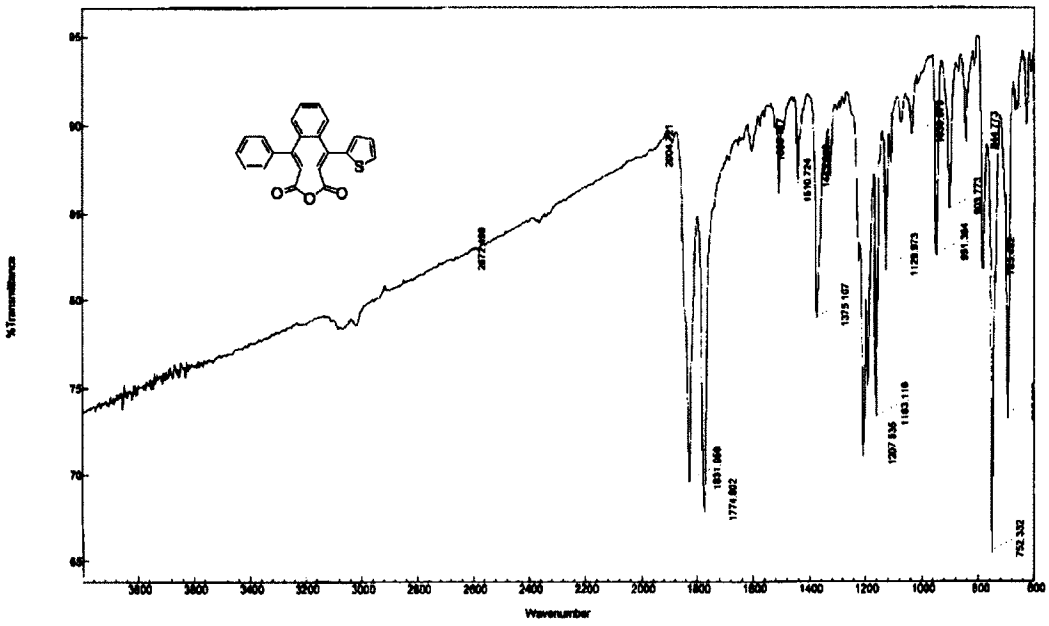

Figure B.5. IR spectrum of 4-phenyl-9-(thiophen-2-yl)naphtho[2,3-c]furan-1,3-dione.

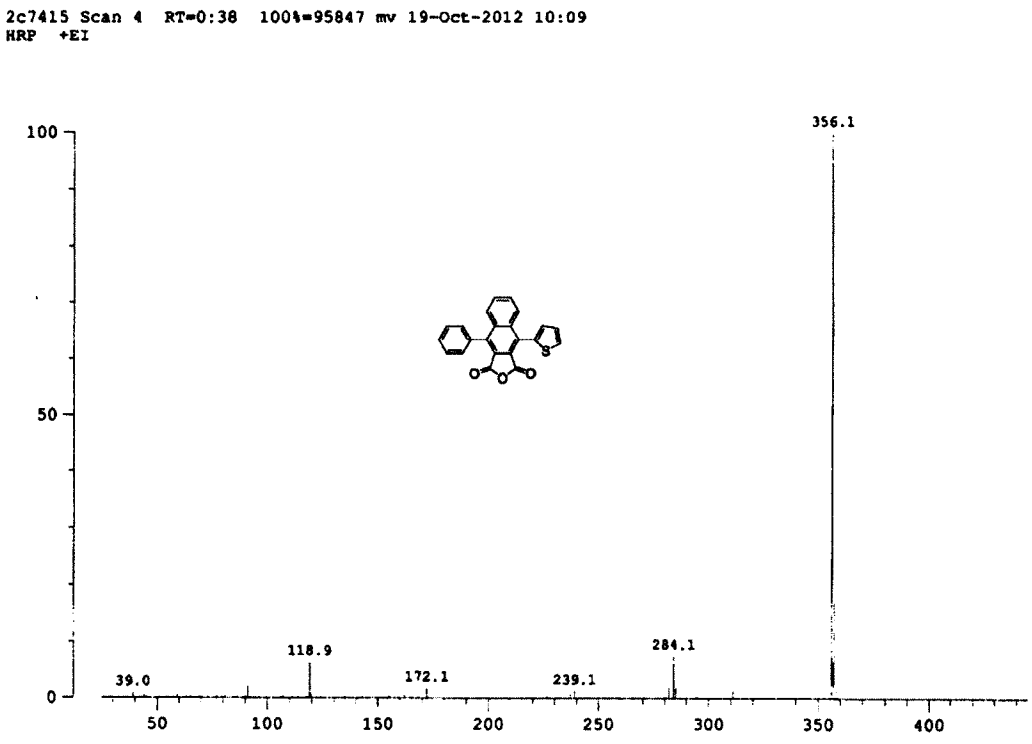

Figure B.6. High resolution mass spectrum of 4-phenyl-9-(thiophen-2-yl)naphtho[2,3-c]furan-1,3-dione.

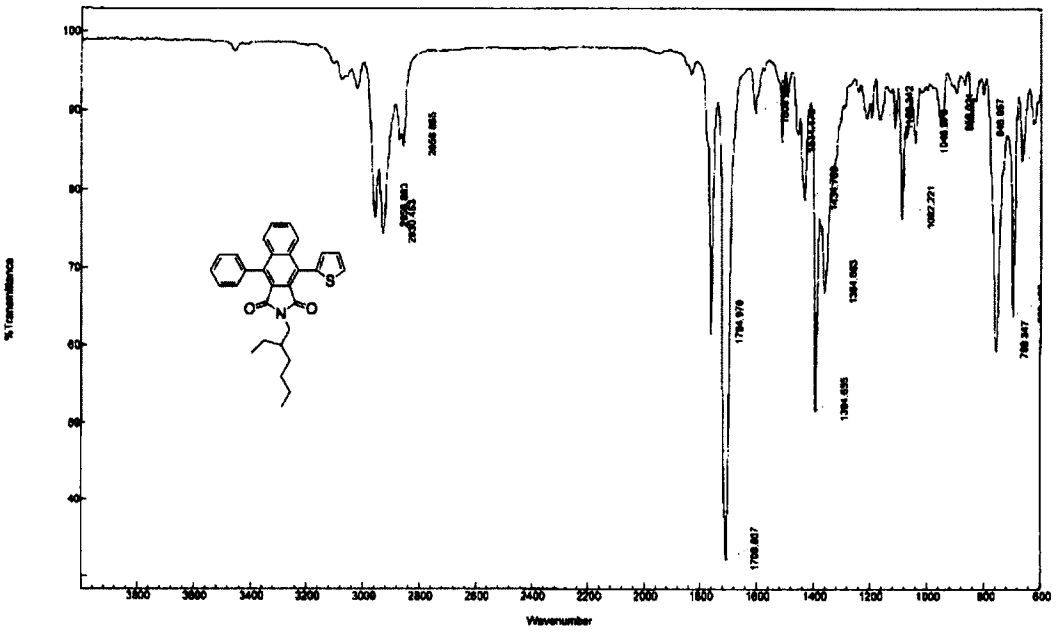

Figure B.7. IR spectrum of 2-(2-ethylhexyl)-4-phenyl-9-(thiophen-2-yl)-1H-benzo[f]isoindole-1,3(2H)-dione.

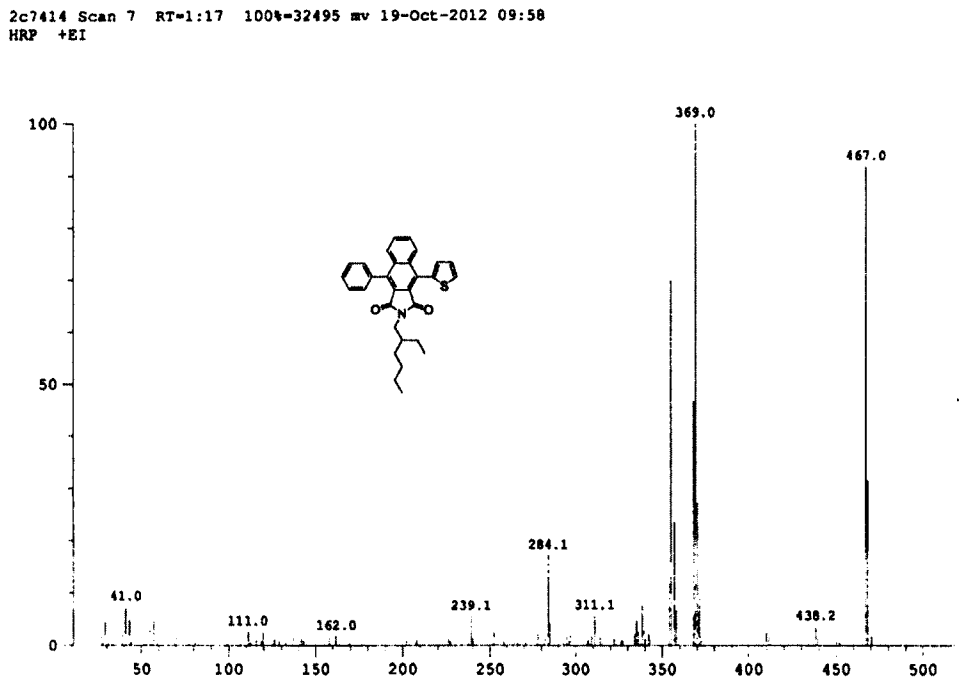

Figure B.8. High resolution mass spectrum of 2-(2-ethylhexyl)-4-phenyl-9-(thiophen-2-yl)-1H-benzo[f]isoindole-1,3(2H)-dione.

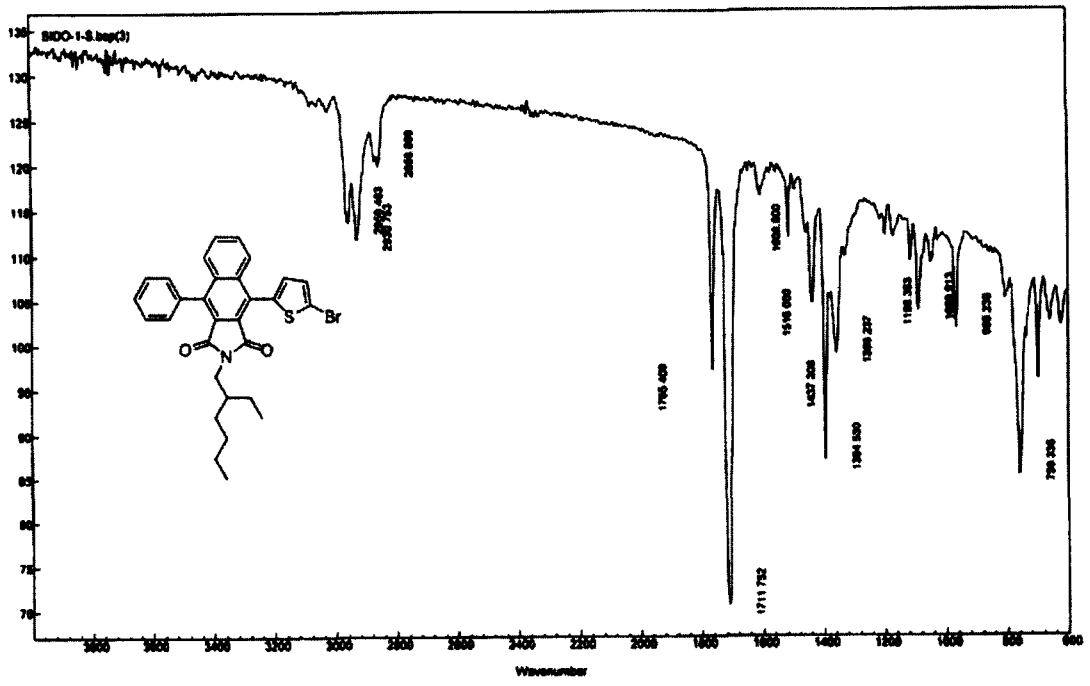

Figure B.9. IR spectrum of **BIDO-1**.

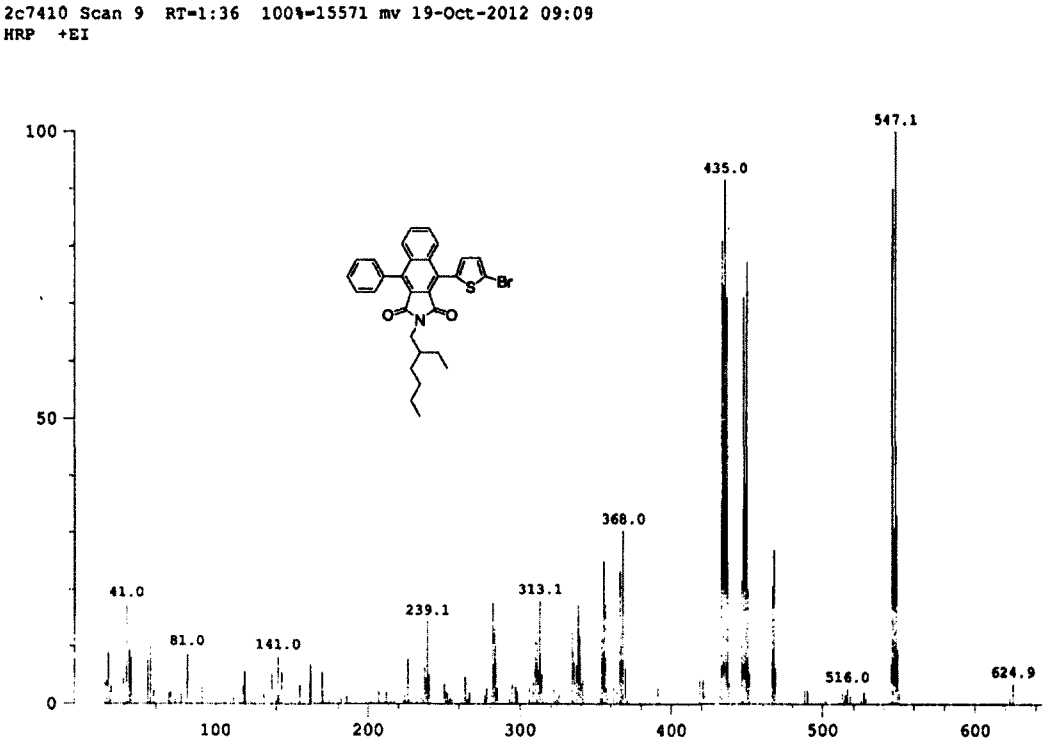

Figure B.10. High resolution mass spectrum of **BIDO-1**.

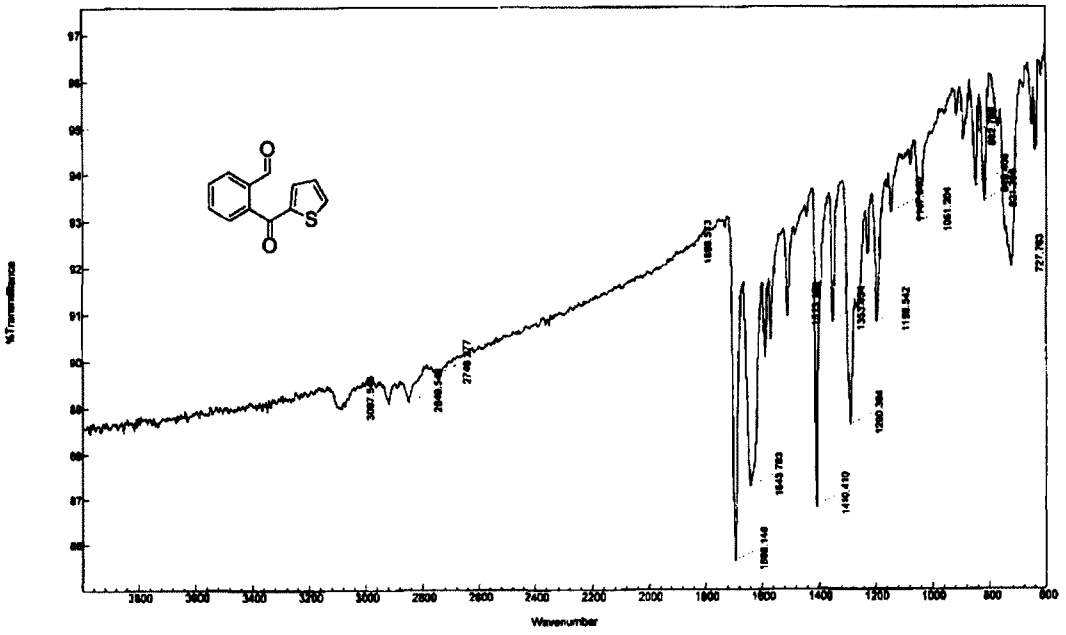

Figure B.11. IR spectrum of 2-(thiophene-2-carbonyl)benzaldehyde.

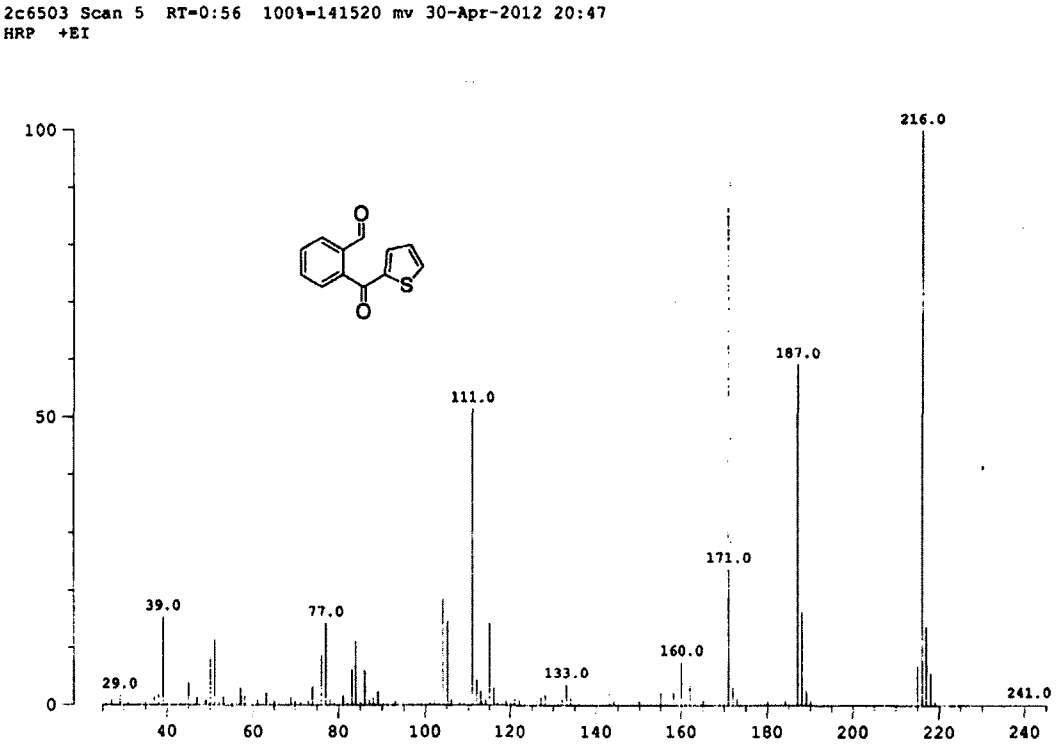

Figure B.12. High resolution mass spectrum of 2-(thiophene-2-carbonyl)benzaldehyde.

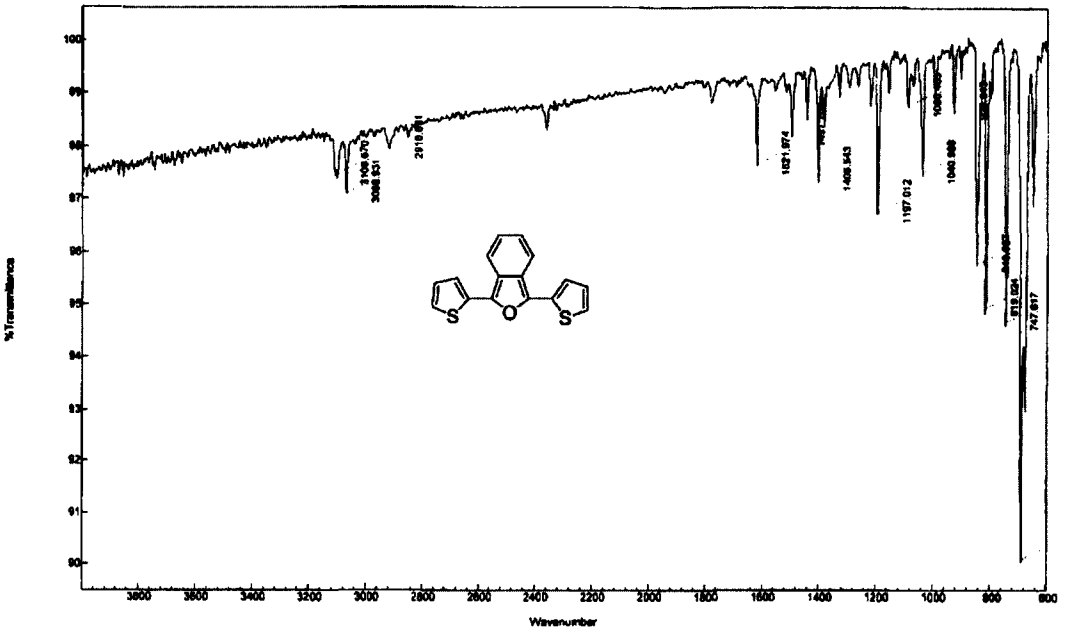

Figure B.13. IR spectrum of 1,3-di(thiophen-2-yl)isobenzofuran.

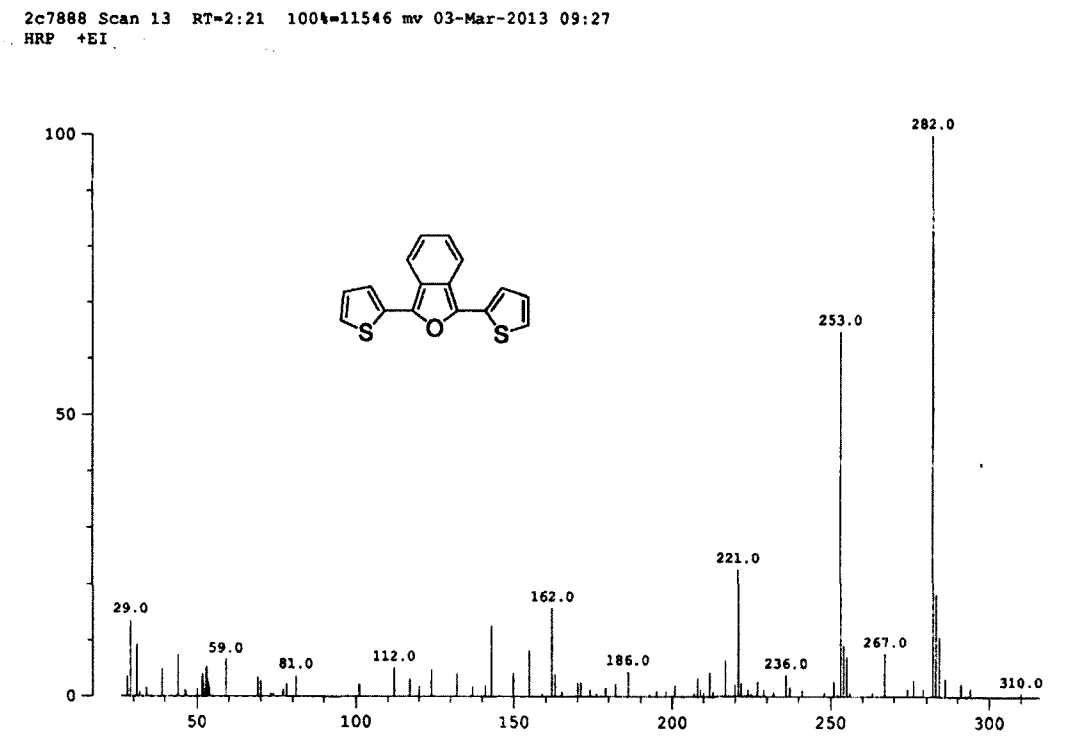

Figure B.14. High resolution mass spectrum of 1,3-di(thiophen-2-yl)isobenzofuran.

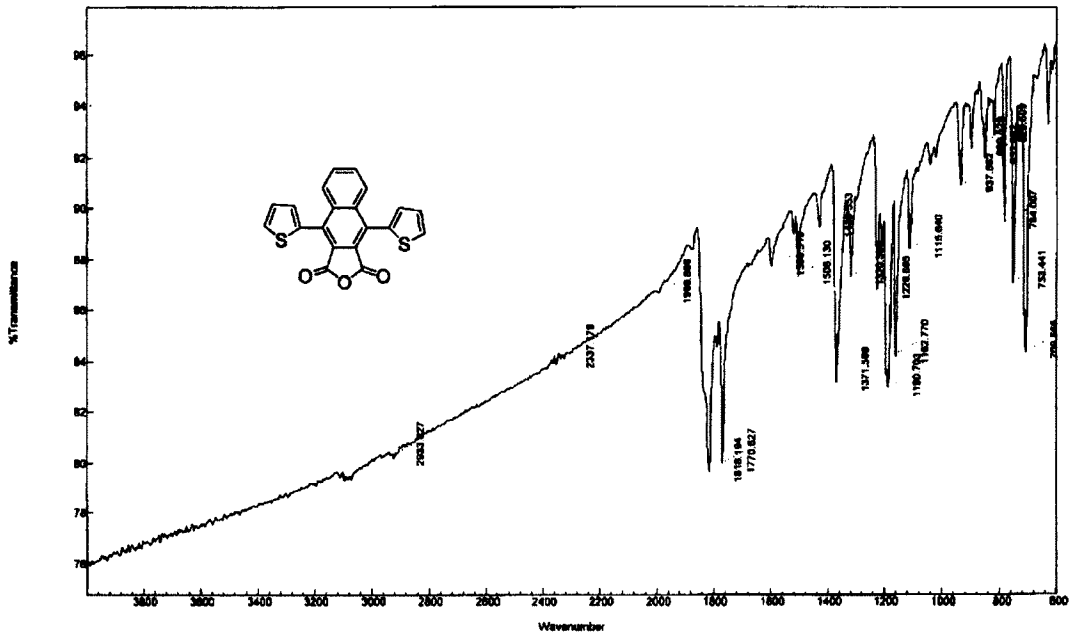

Figure B.15. IR spectrum of 4,9-di(thiophen-2-yl)naphtho[2,3-c]furan-1,3-dione.

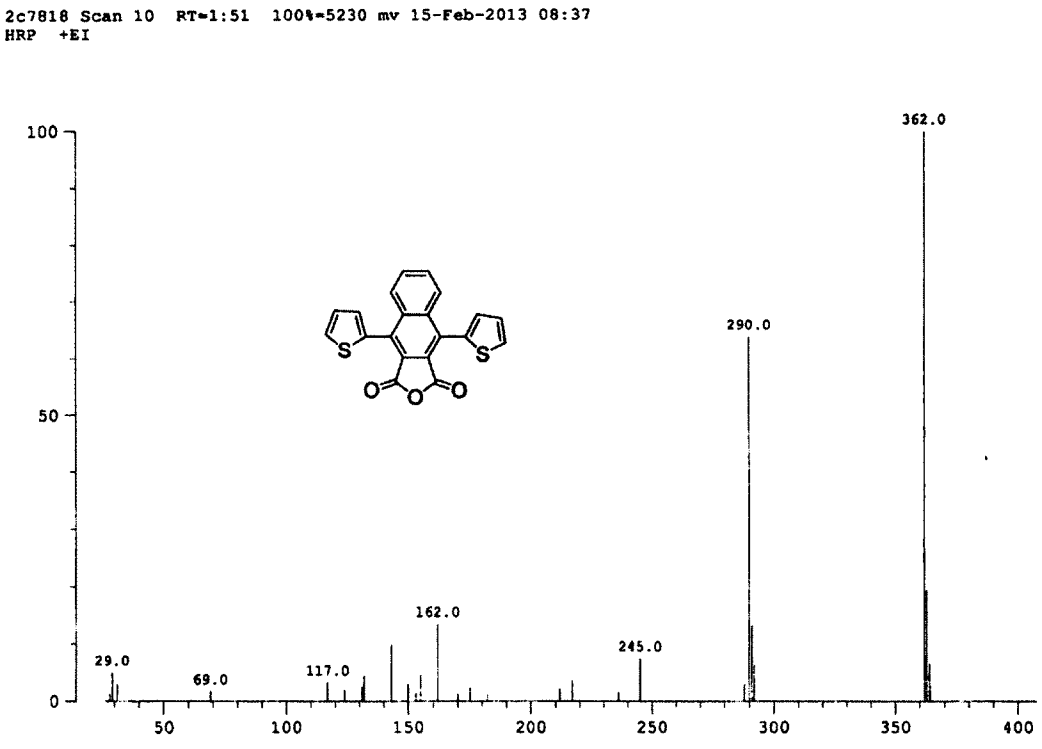

Figure B.16. High resolution mass spectrum of 4,9-di(thiophen-2-yl)naphtho[2,3-c]furan-1,3-dione.

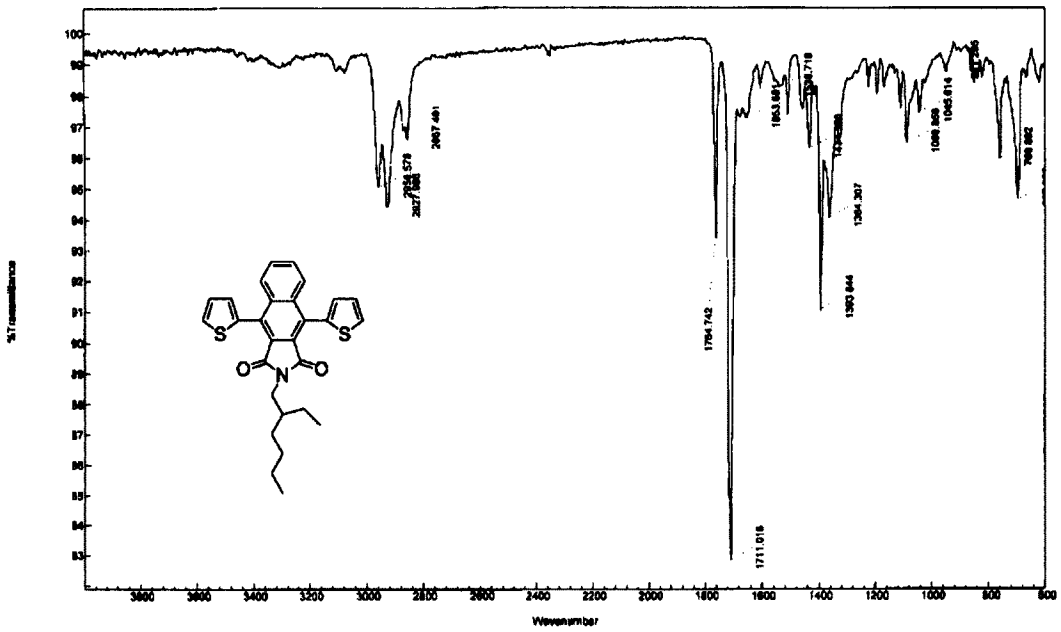

Figure B.17. IR spectrum of 2-(2-ethylhexyl)-4,9-di(thiophen-2-yl)-1H-benzo[f]isoindole-1,3(2H)-dione.

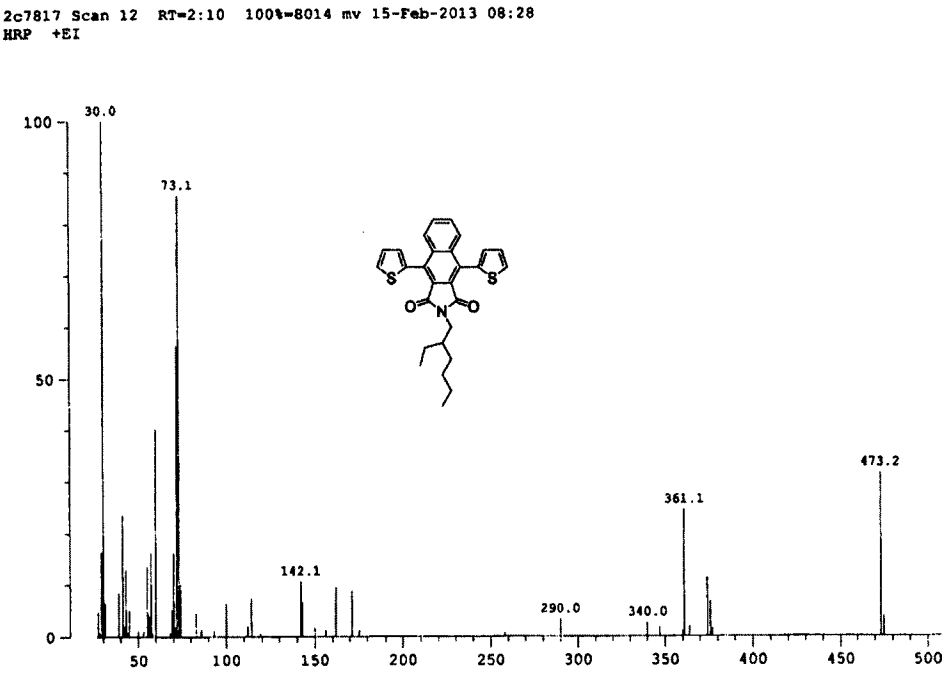

Figure B.18. High resolution mass spectrum of 2-(2-ethylhexyl)-4,9-di(thiophen-2-yl)-1H-benzo[f]isoindole-1,3(2H)-dione.

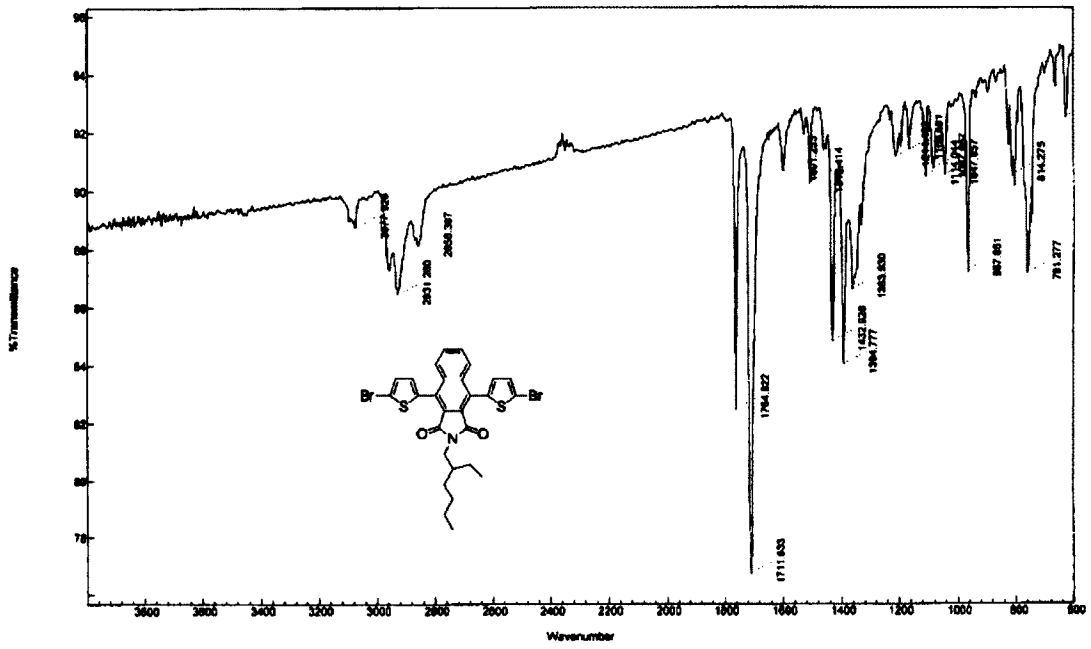

Figure B.19. IR spectrum of **BIDO-2**.

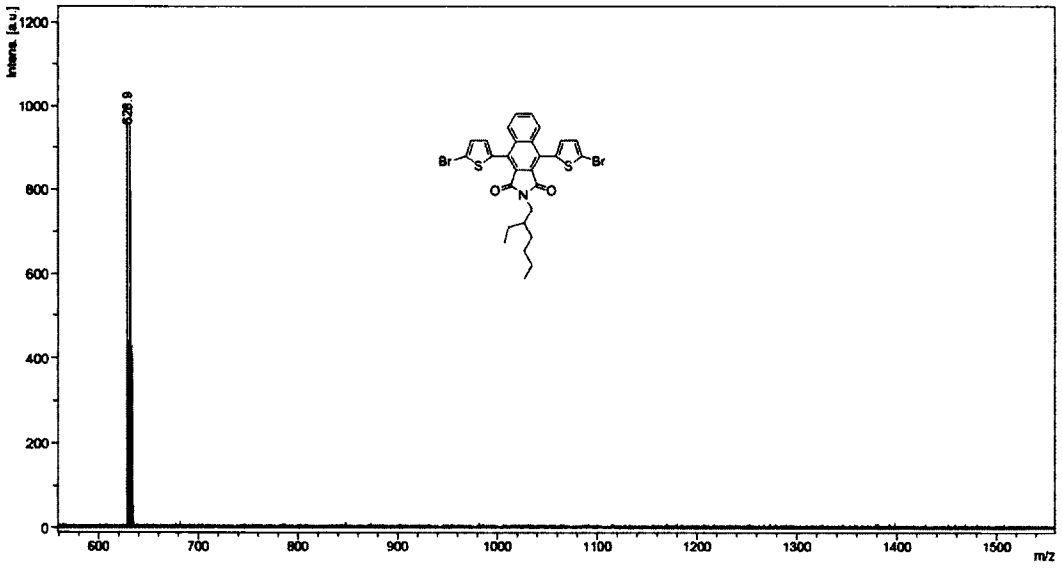

Figure B.20. High resolution mass spectrum of **BIDO-2**.

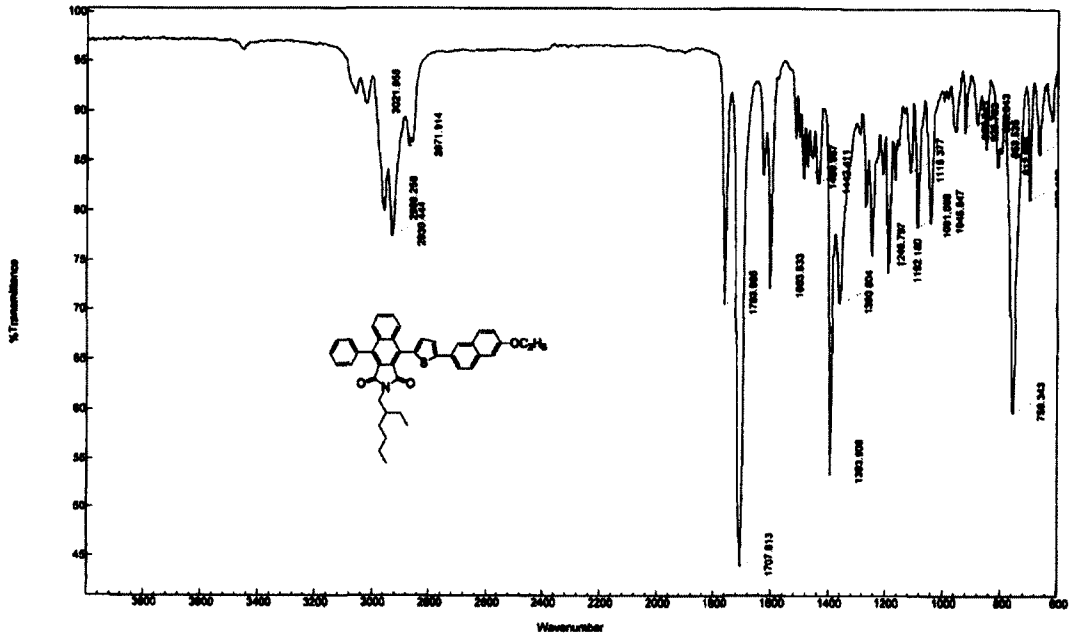

Figure B.21. IR spectrum of **BIDO-1-EONP**.

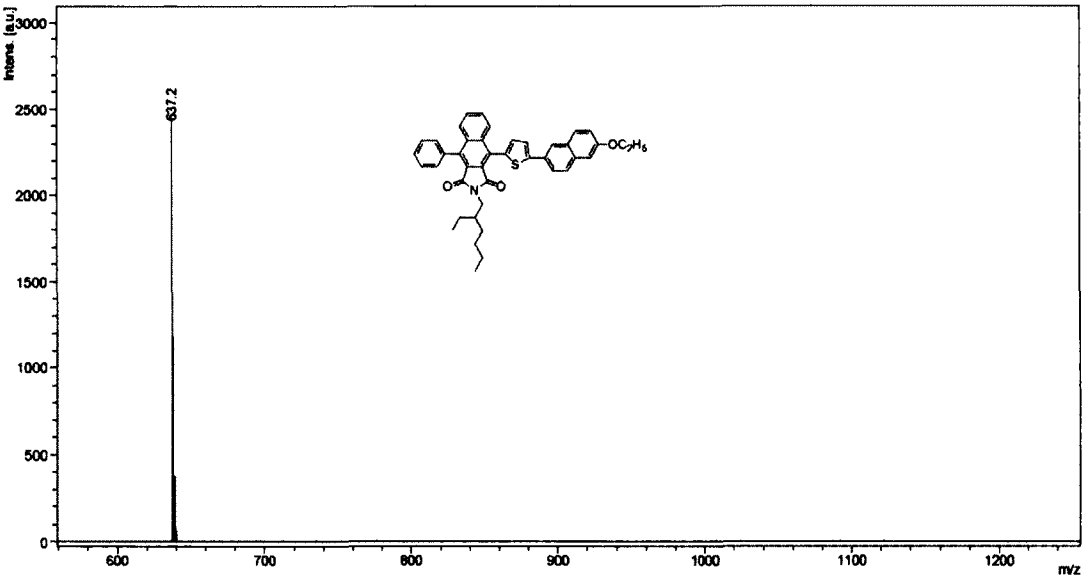

Figure B.22. High resolution mass spectrum of **BIDO-1-EONP**.

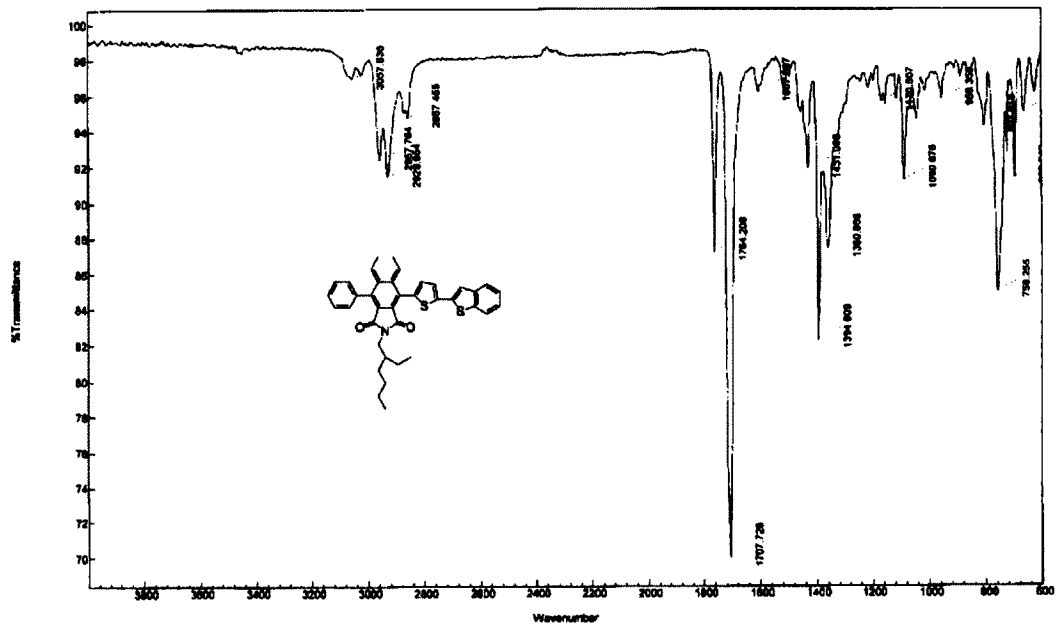

Figure B.23. IR spectrum of **BIDO-1-BT**.

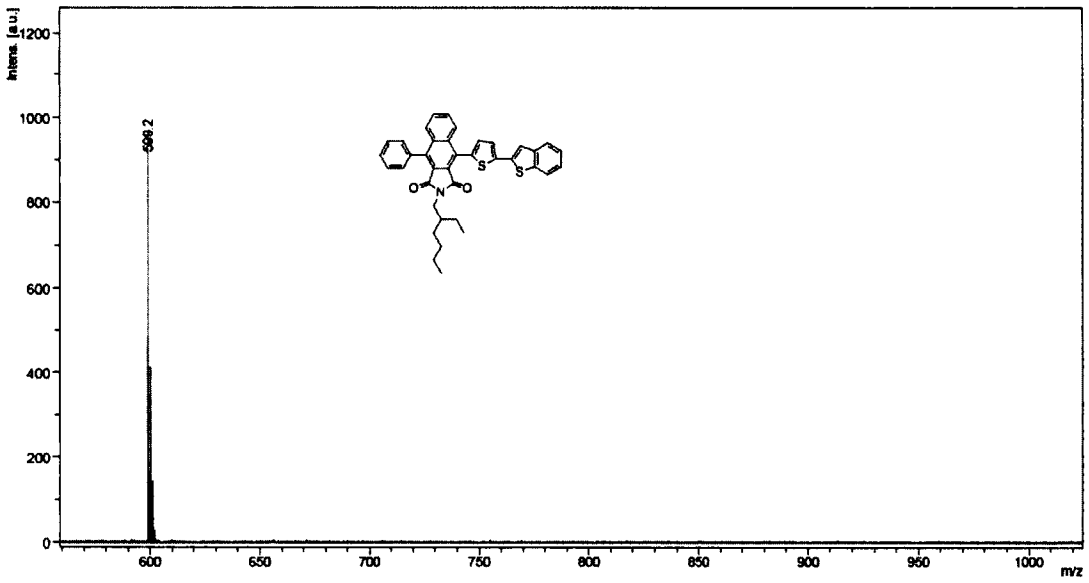

Figure B.24. High resolution mass spectrum of **BIDO-1-BT**.

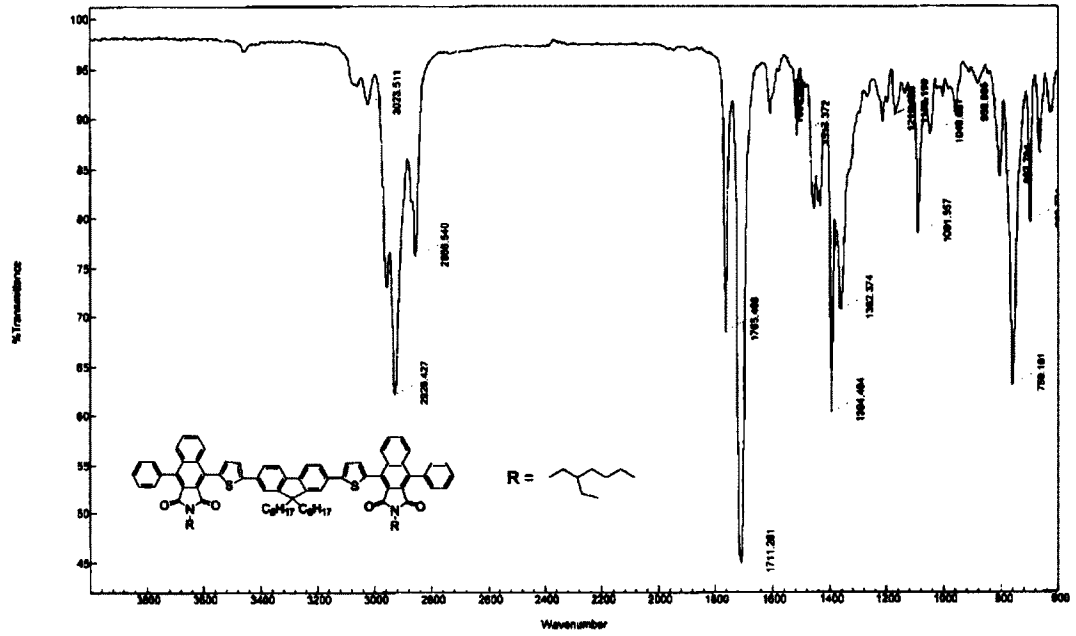

Figure B.25. IR spectrum of **BIDO-1-FL**.

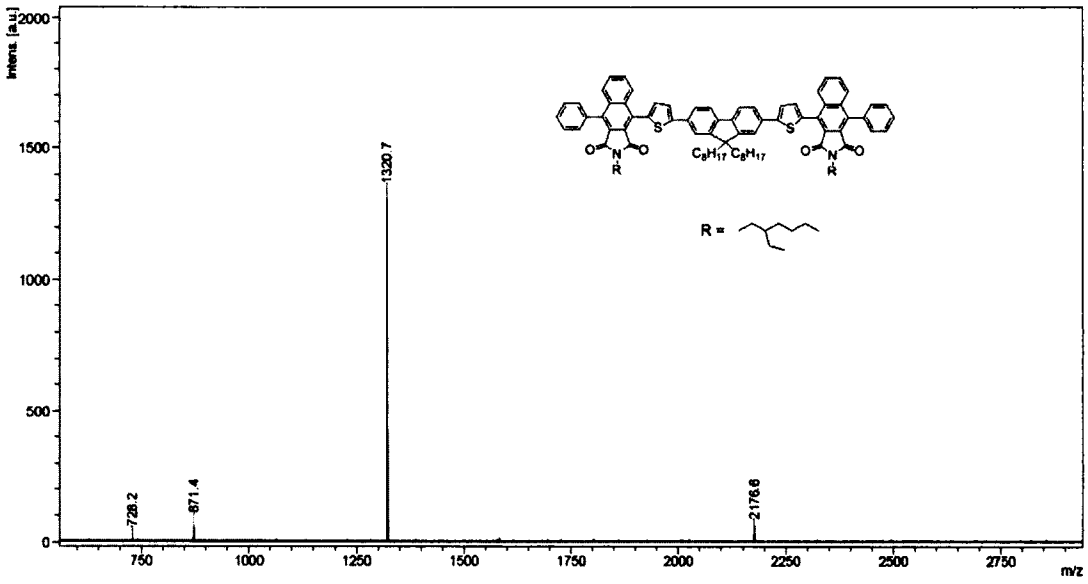

Figure B.26. High resolution mass spectrum of **BIDO-1-FL**.

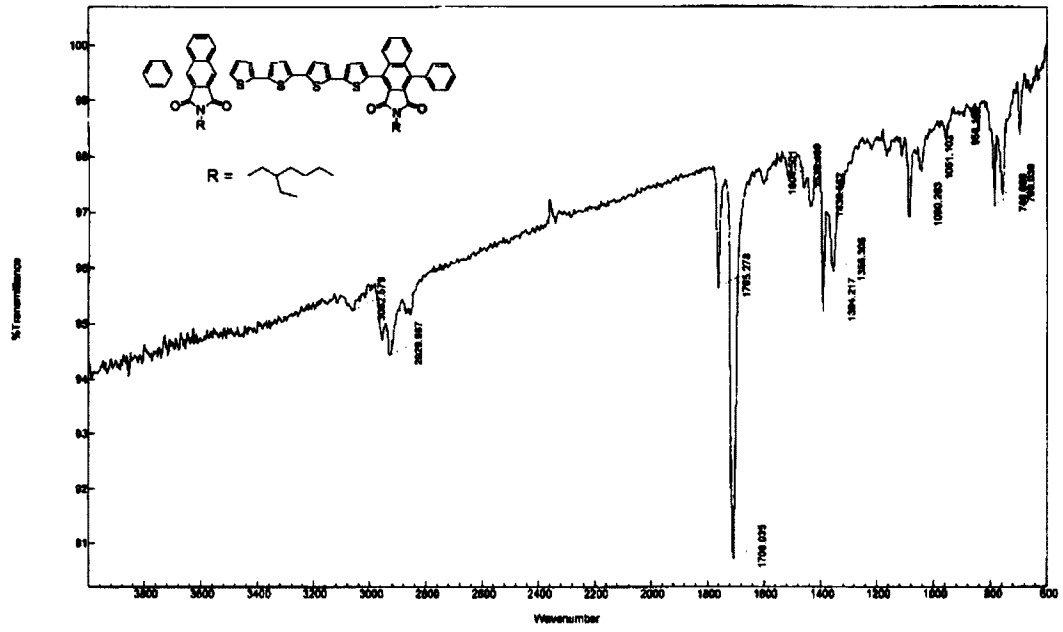

Figure B.27. IR spectrum of **BIDO-1-DT**.

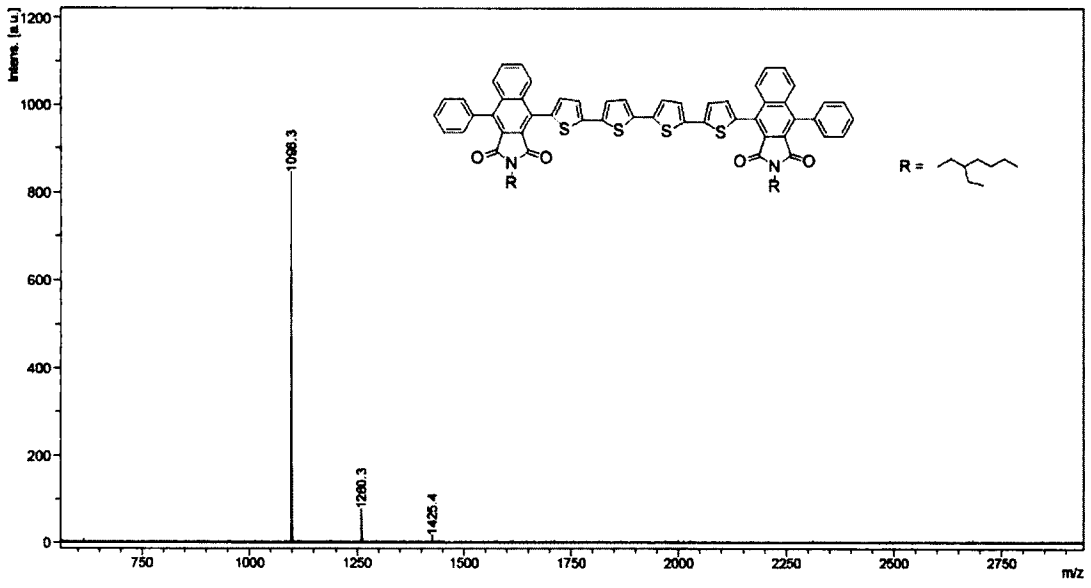

Figure B.28. High resolution mass spectrum of **BIDO-1-DT**.

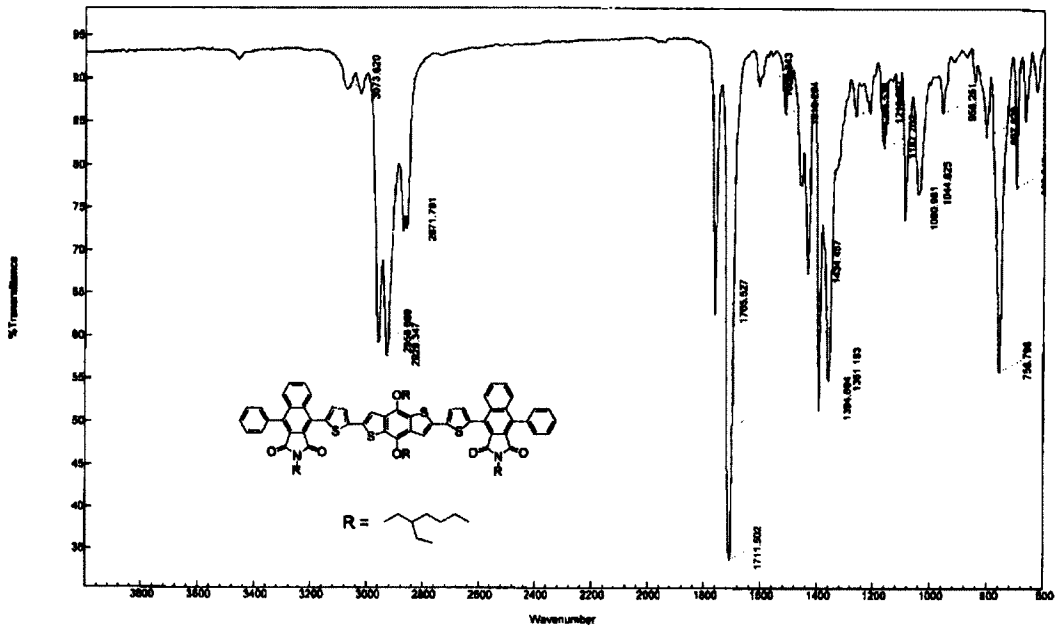

Figure B.29. IR spectrum of **BIDO-1-BDT**.

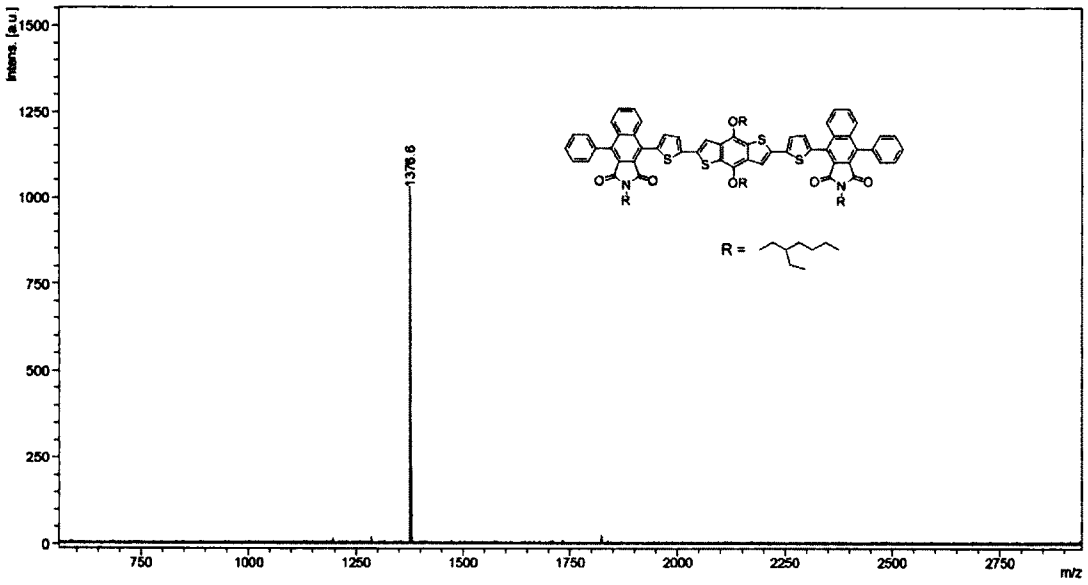

Figure B.30. High resolution mass spectrum of **BIDO-1-BDT**.

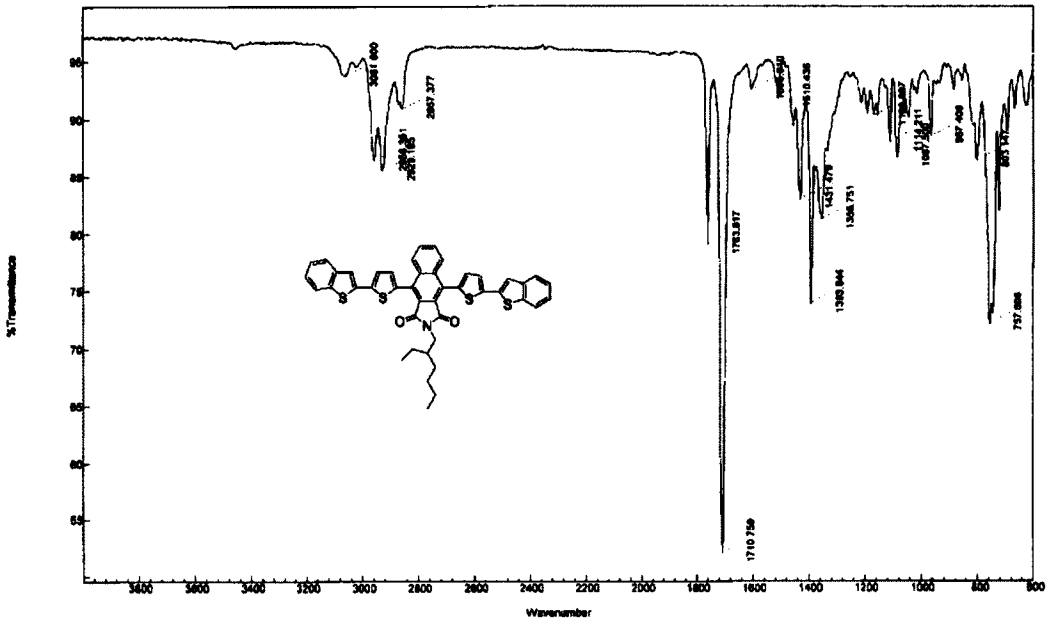

Figure B.31. IR spectrum of **BIDO-2-BT**.

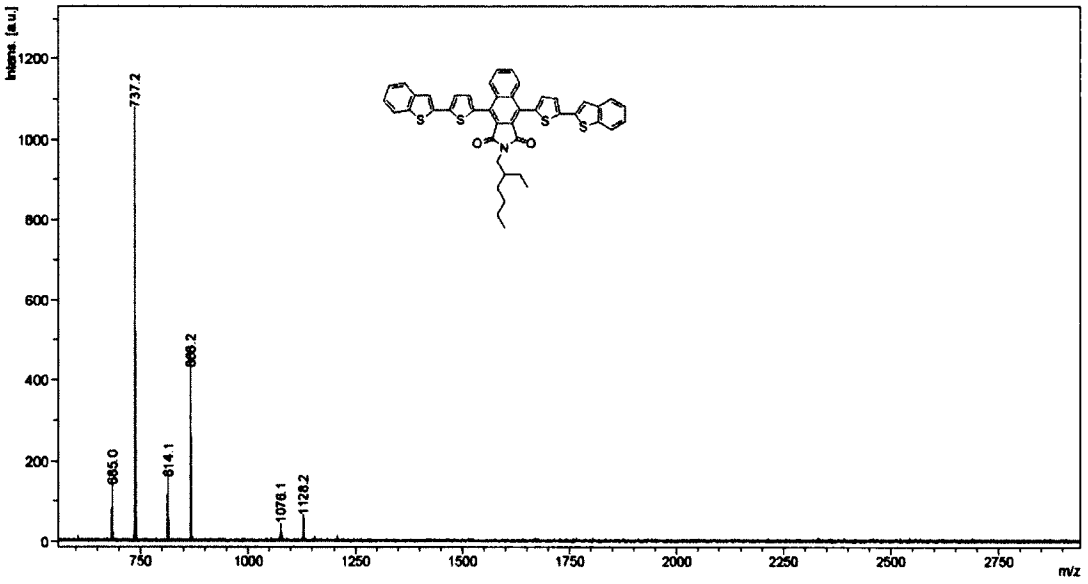

Figure B.32. High resolution mass spectrum of **BIDO-2-BT**.

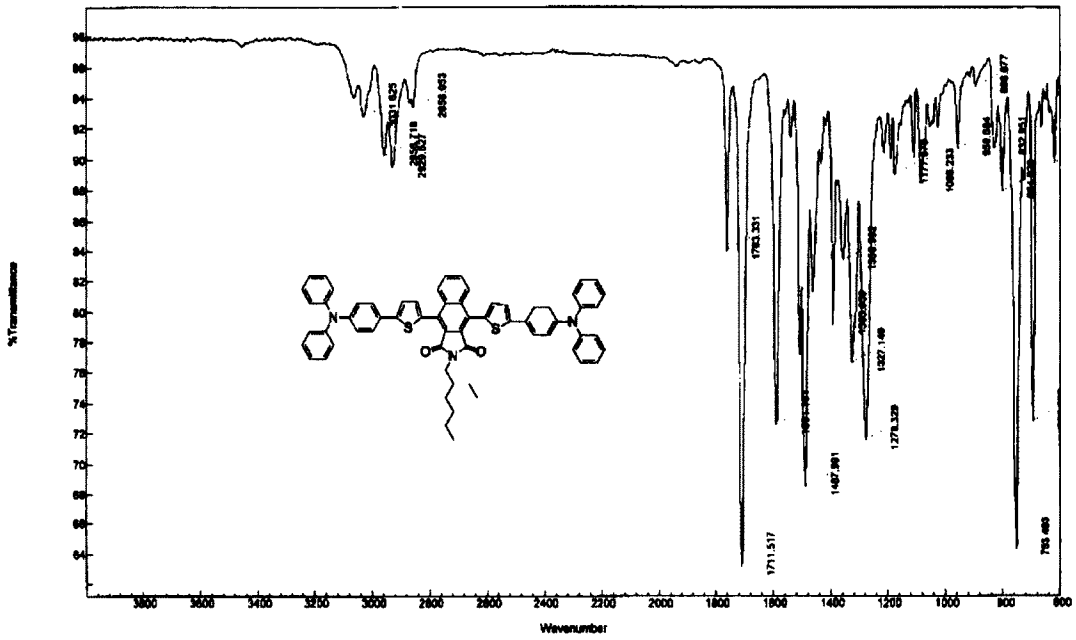

Figure B.33. IR spectrum of **BIDO-2-TPA**.

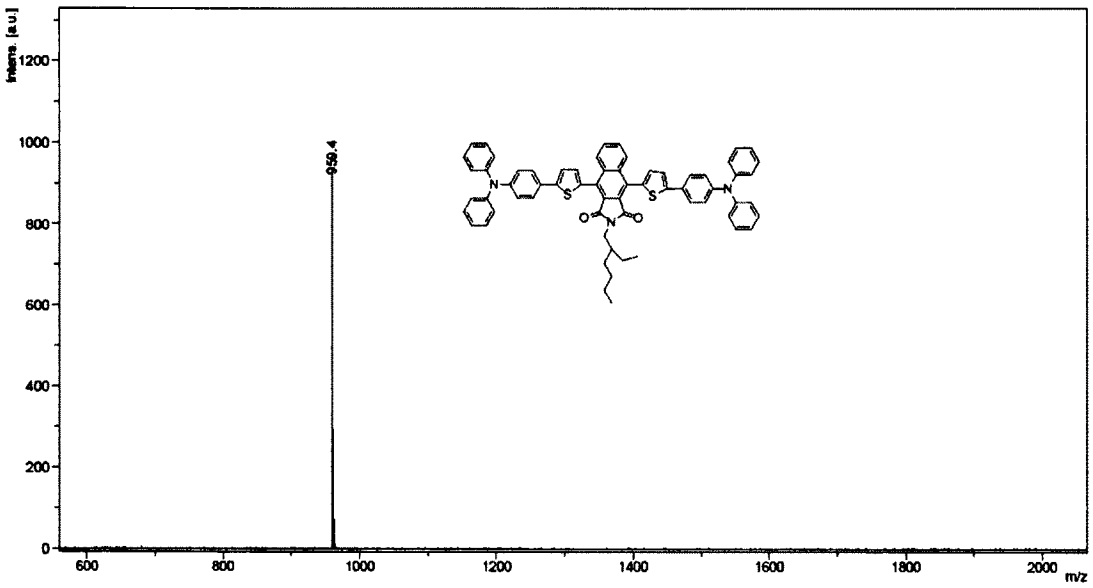

Figure B.34. High resolution mass spectrum of **BIDO-2-TPA**.

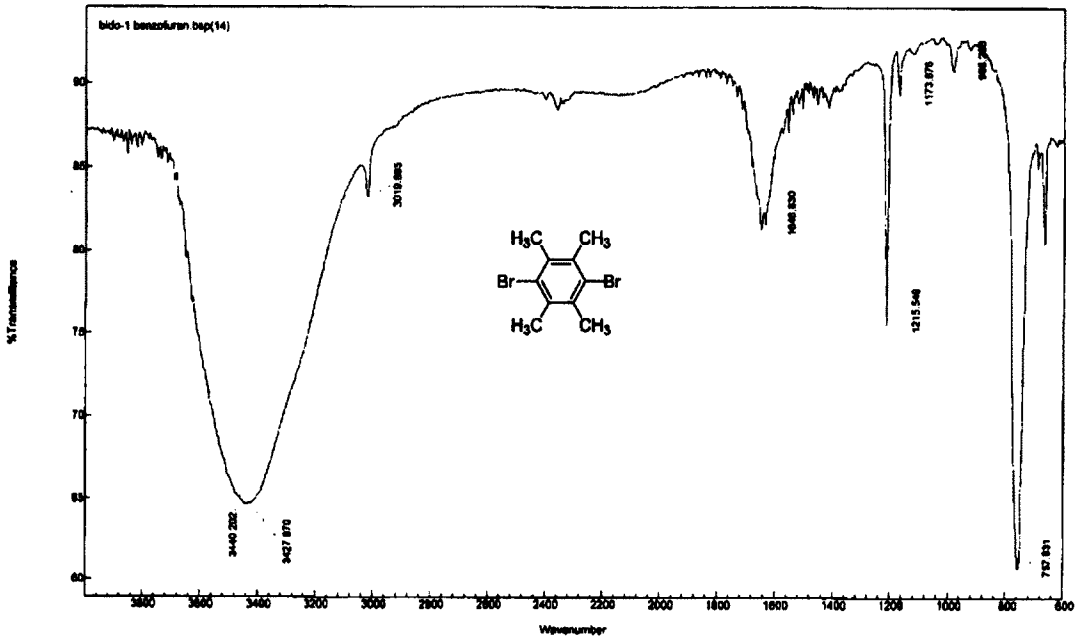

Figure B.35. IR spectrum of 1,4-dibromo-2,3,5,6-tetramethylbenzene.

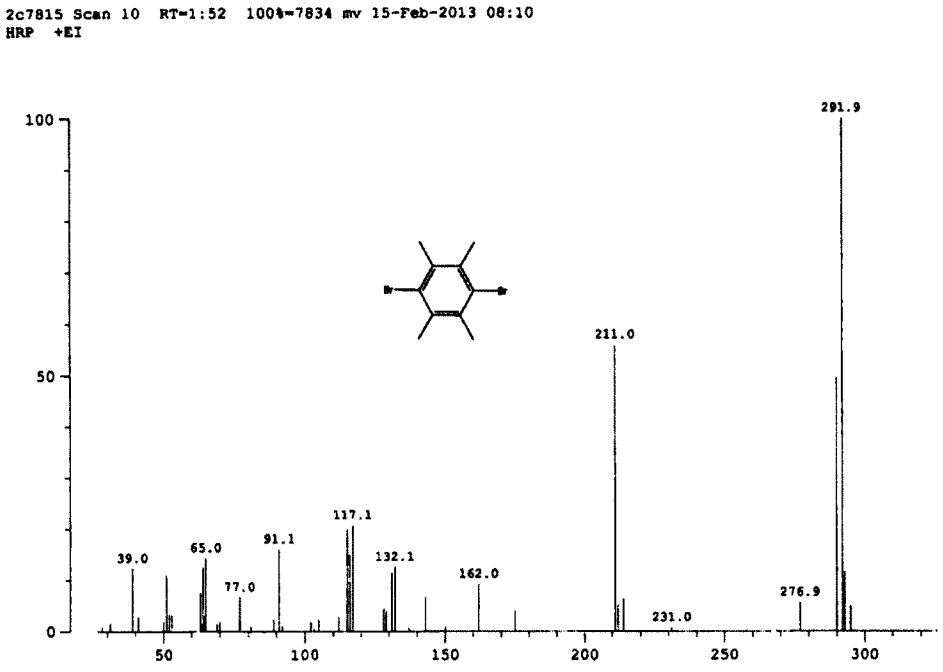

Figure B.36. High resolution mass spectrum of 1,4-dibromo-2,3,5,6-tetramethylbenzene.

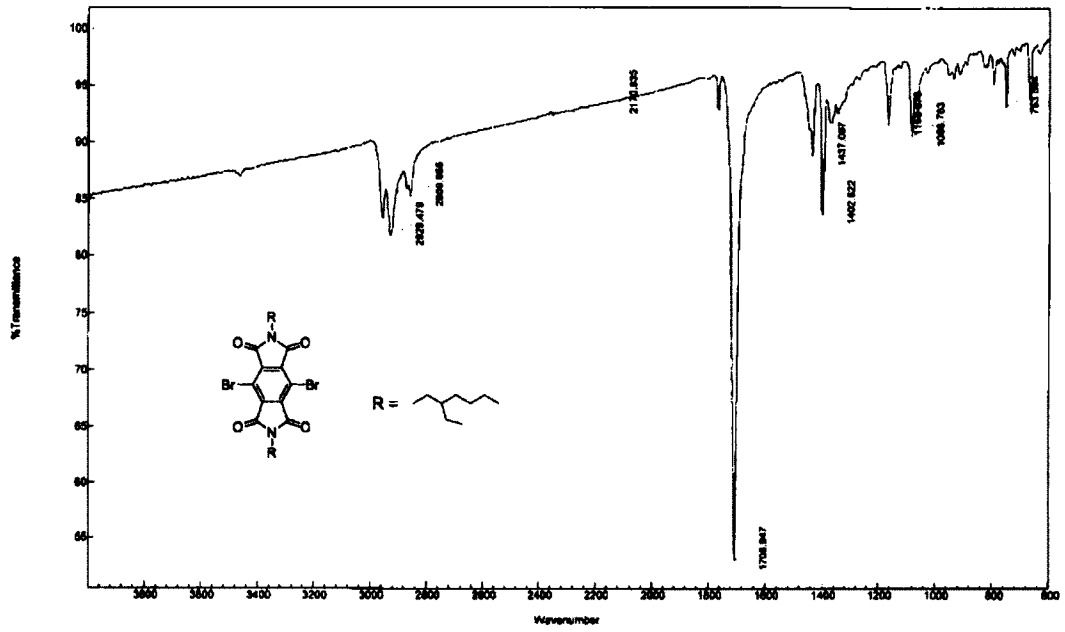

Figure B.37. IR spectrum of **PMDI**.

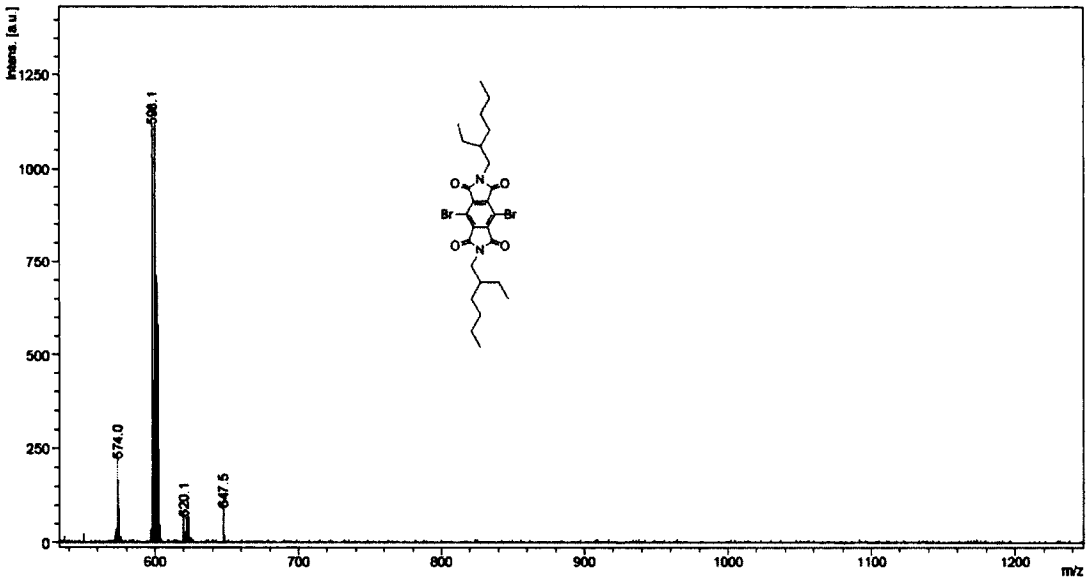

Figure B.38. High resolution mass spectrum of **PMDI**.

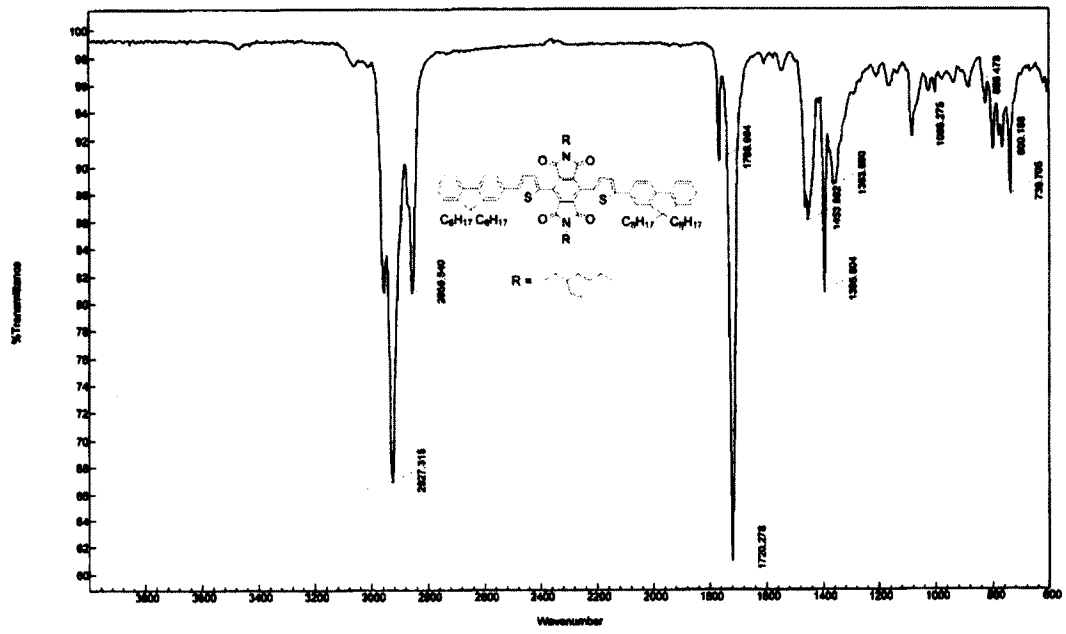

Figure B.39. IR spectrum of **PMDI-FT**.

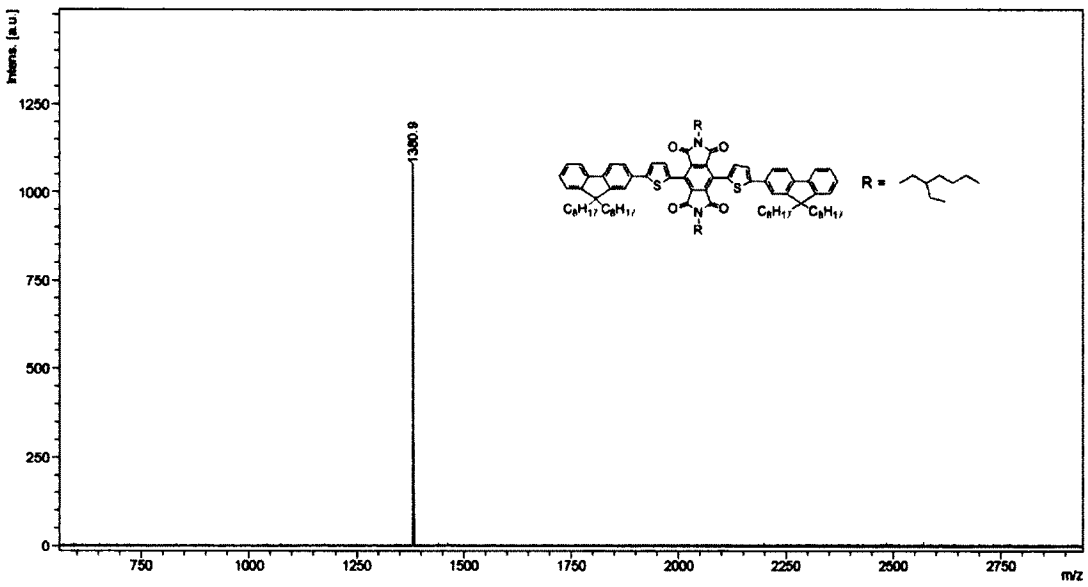

Figure B.40. High resolution mass spectrum of **PMDI-FT**.

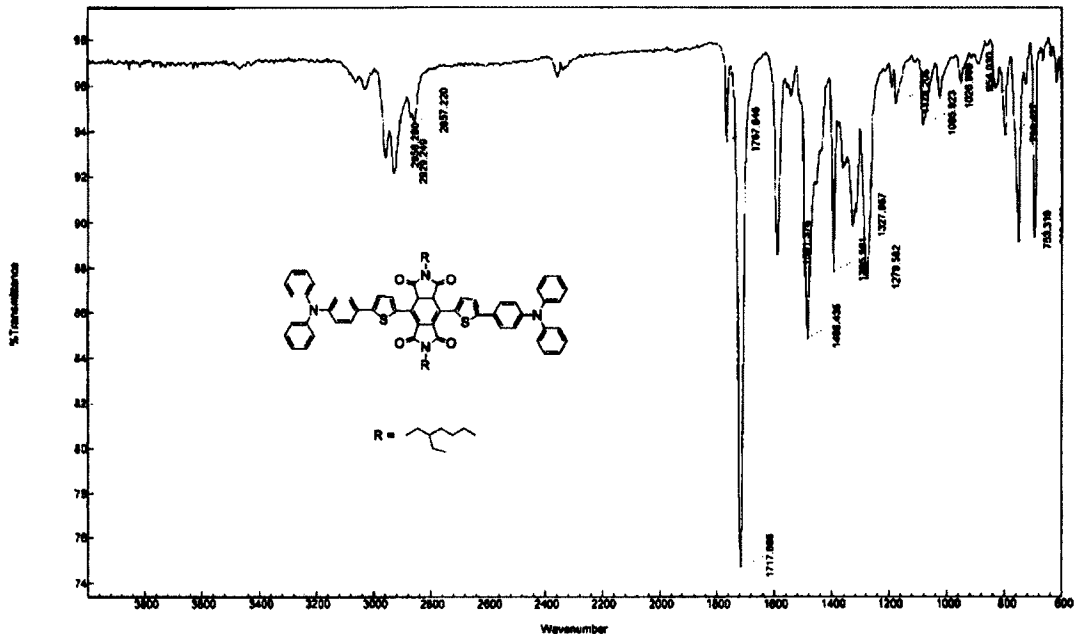

Figure B.41. IR spectrum of **PMDI-TPAT**.

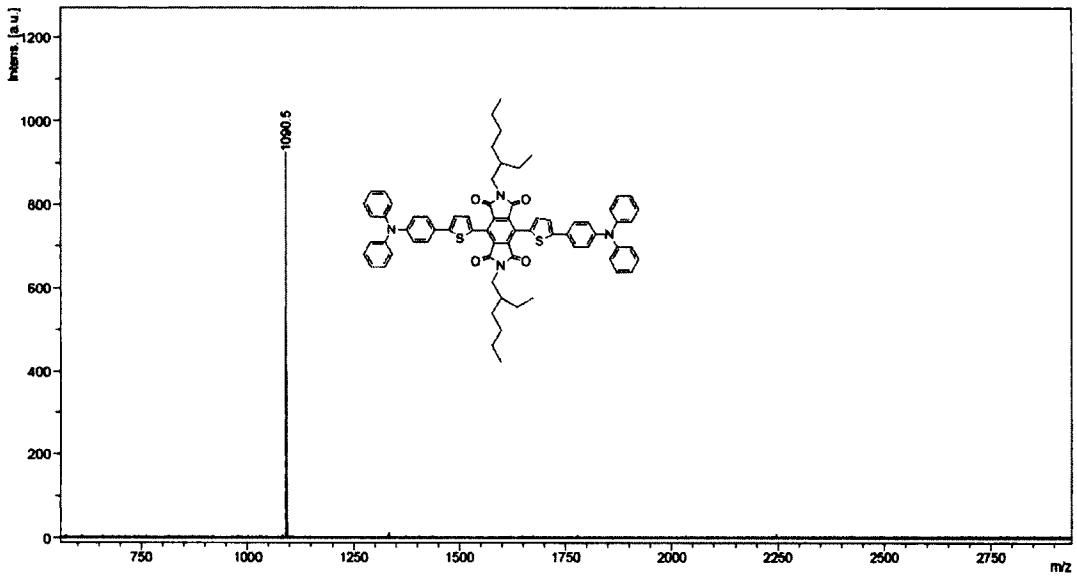

Figure B.42. High resolution mass spectrum of **PMDI-TPAT**.

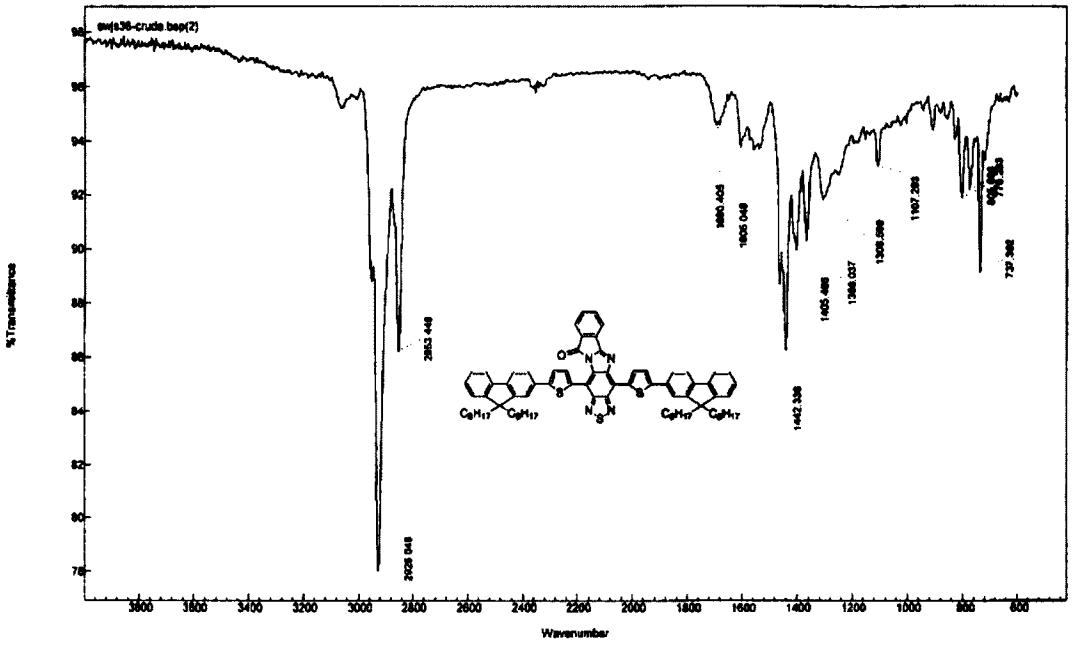

Figure B.43. IR spectrum of **IV-a**.

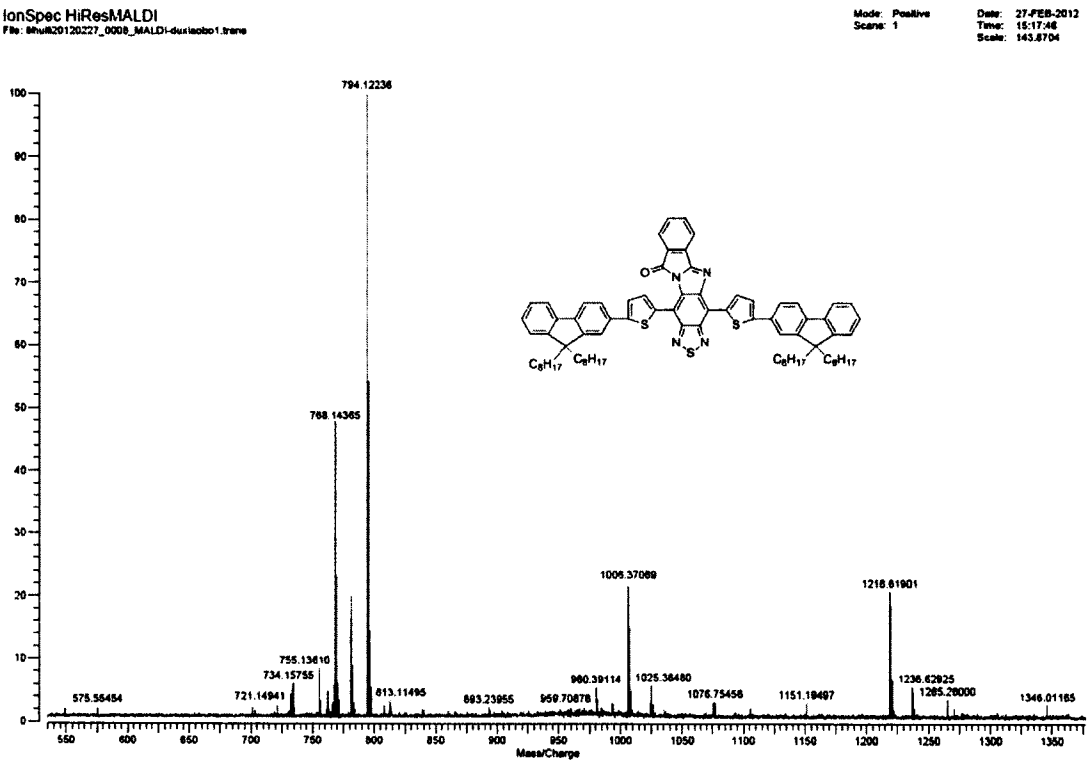

Figure B.44. High resolution mass spectrum of **IV-a**.

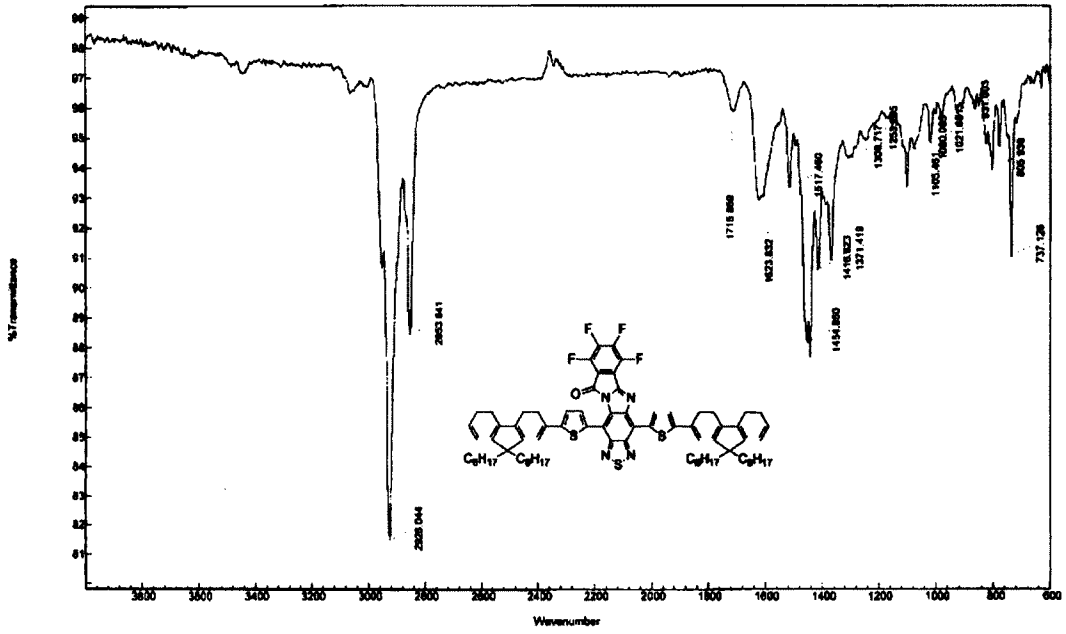

Figure B.45. IR spectrum of **IV-b**.

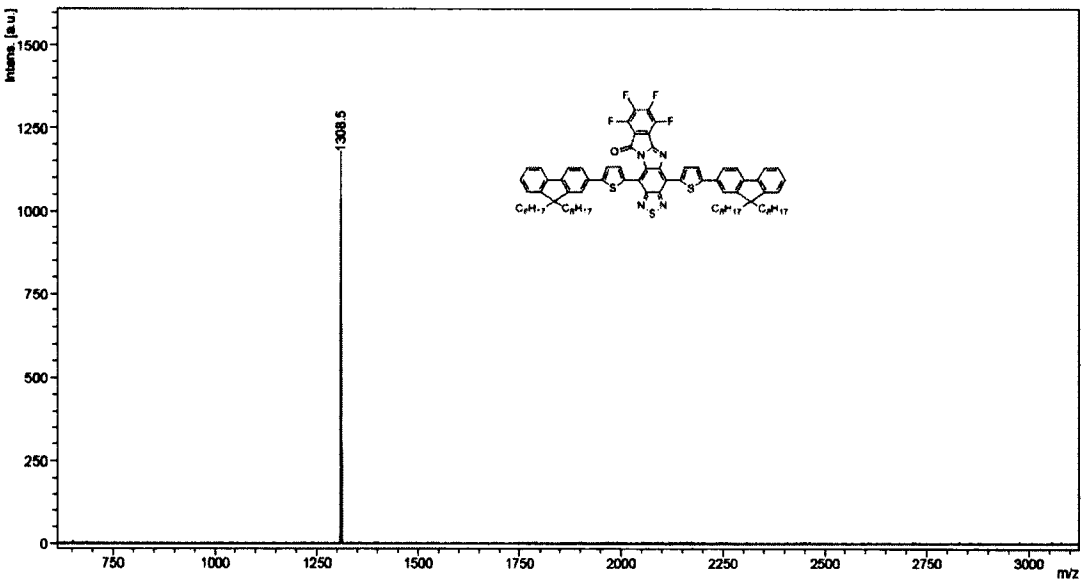

Figure B.46. High resolution mass spectrum of **IV-b**.

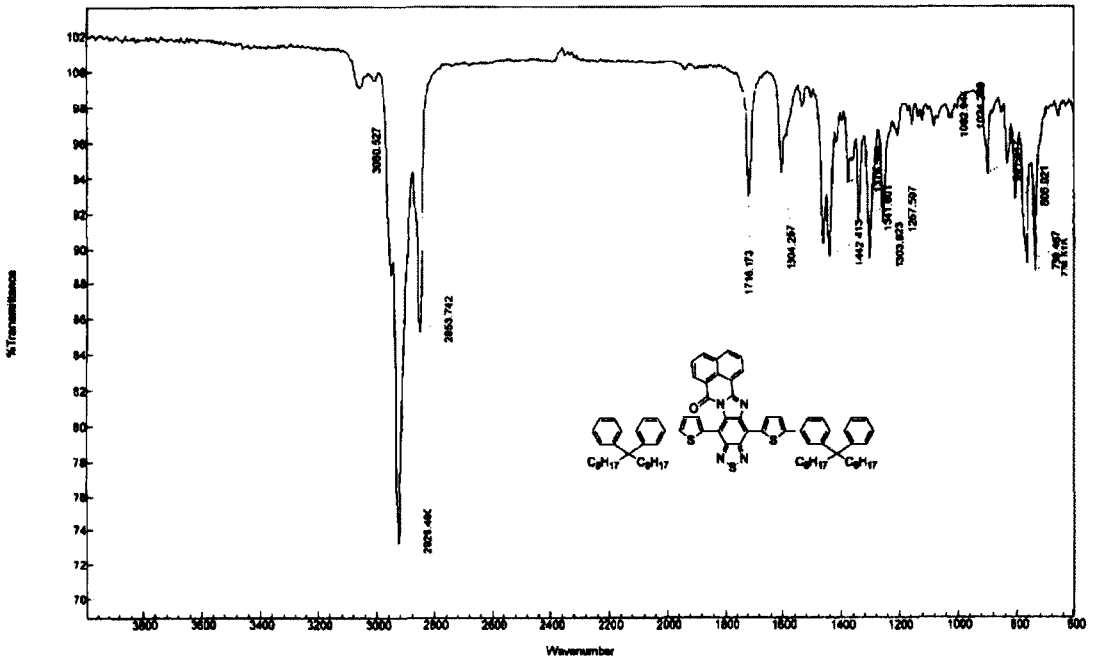

Figure B.47. IR spectrum of **IV-c**.

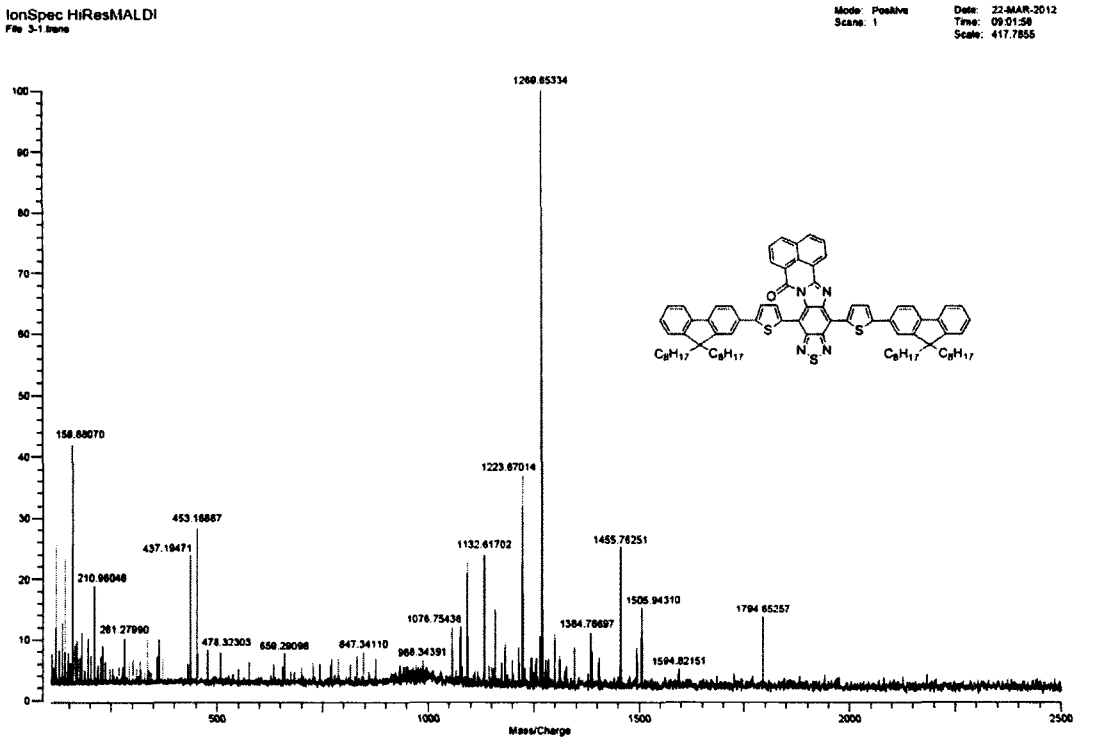

Figure B.48. High resolution mass spectrum of **IV-c**.

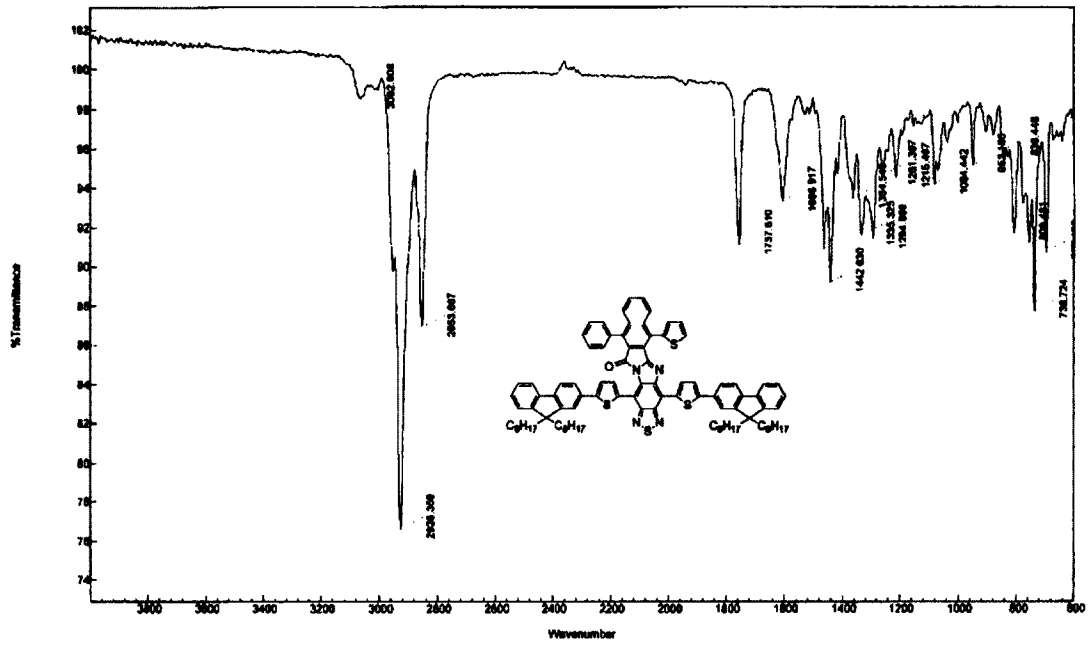

Figure B.49. IR spectrum of **IV-d**.

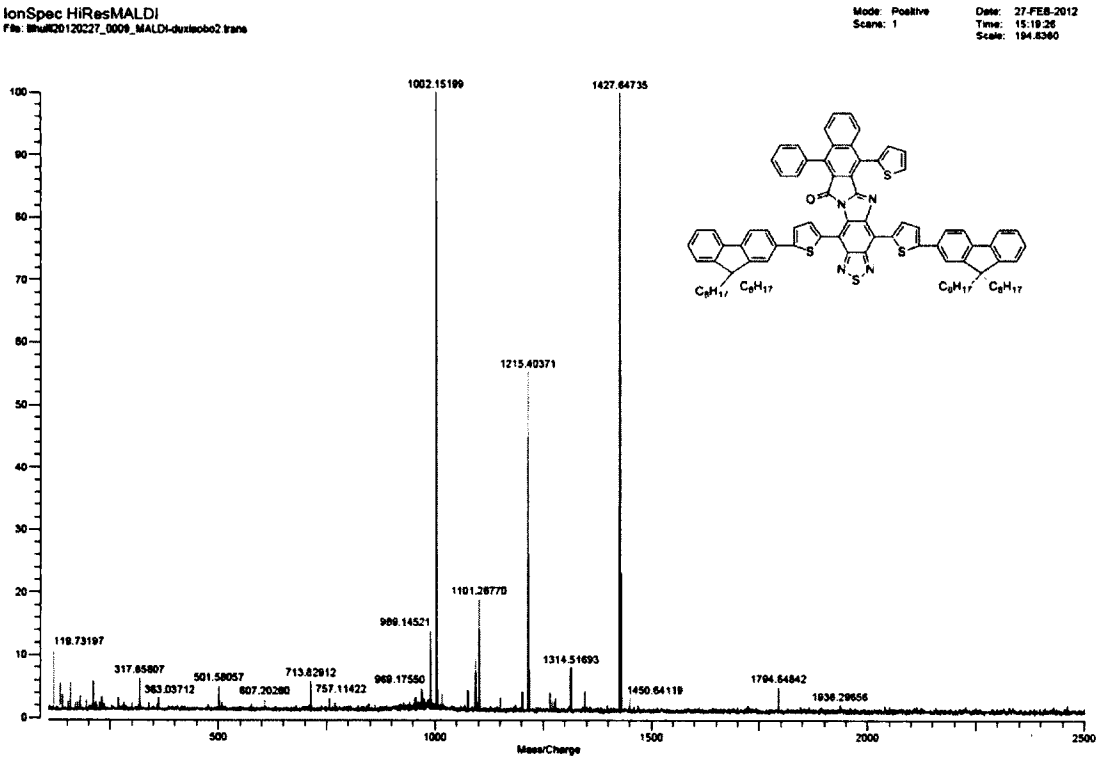

Figure B.50. High resolution mass spectrum of **IV-d**.

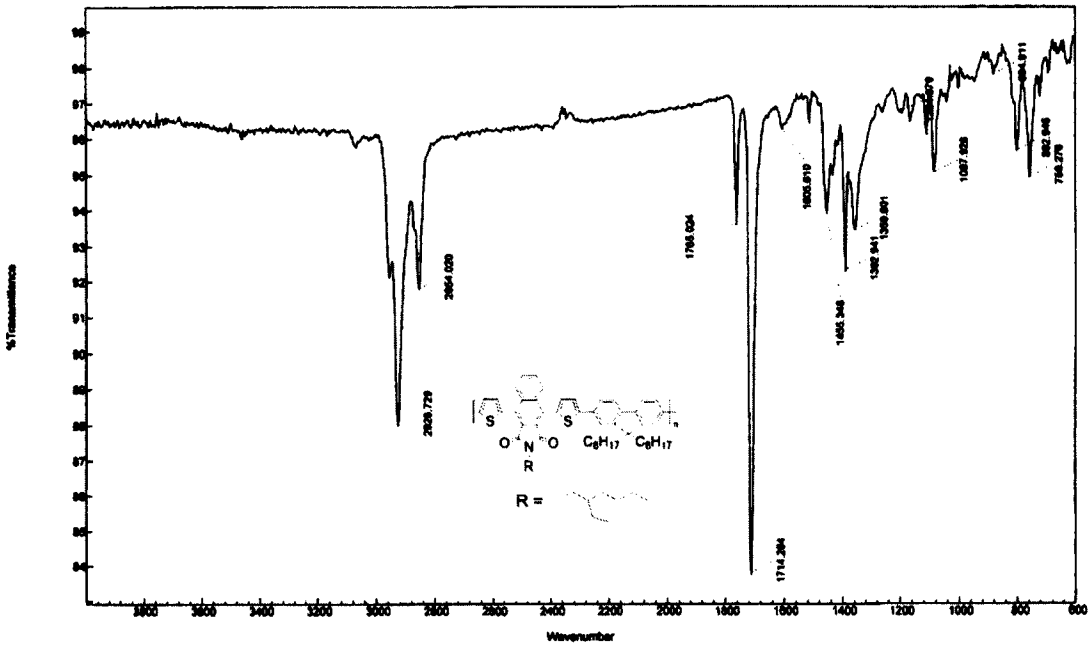

Figure B.51. IR spectrum of **P1**.

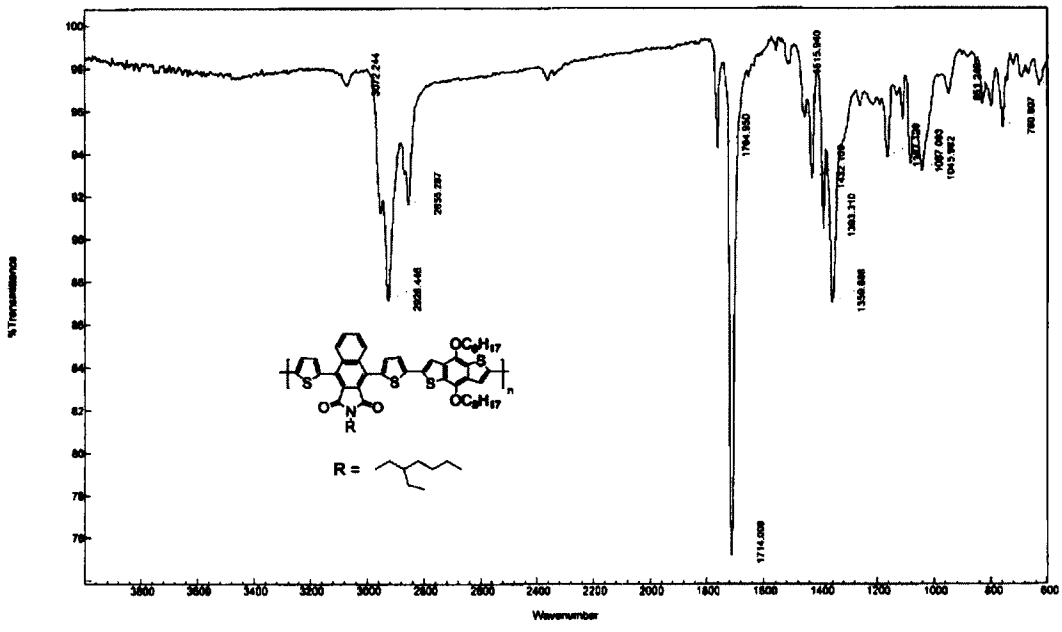

Figure B.52. IR spectrum of **P2**.

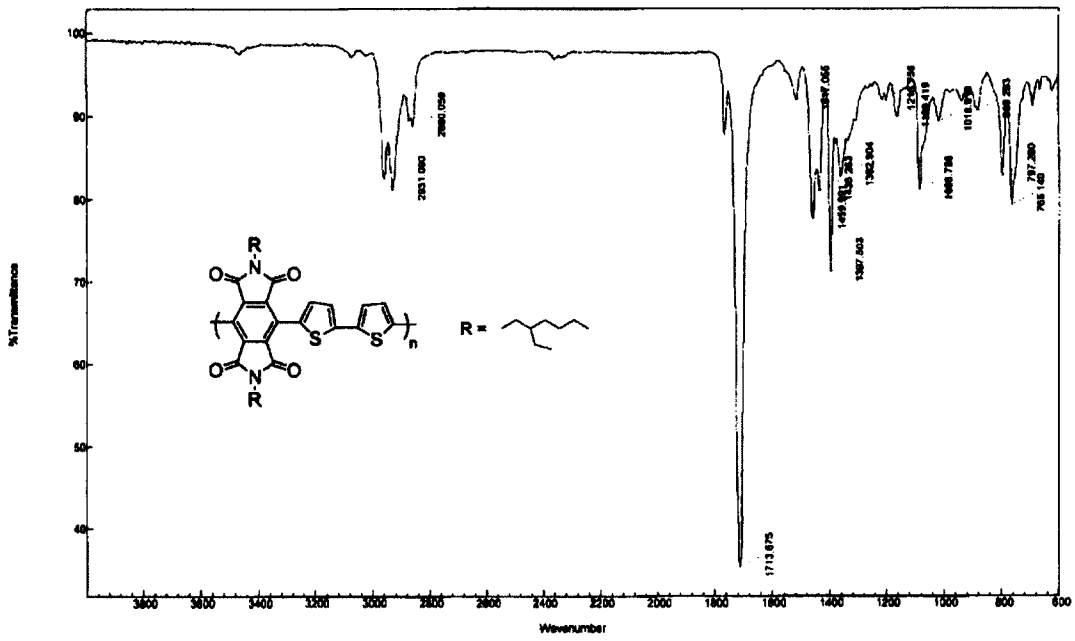

Figure B.53. IR spectrum of **P3**.

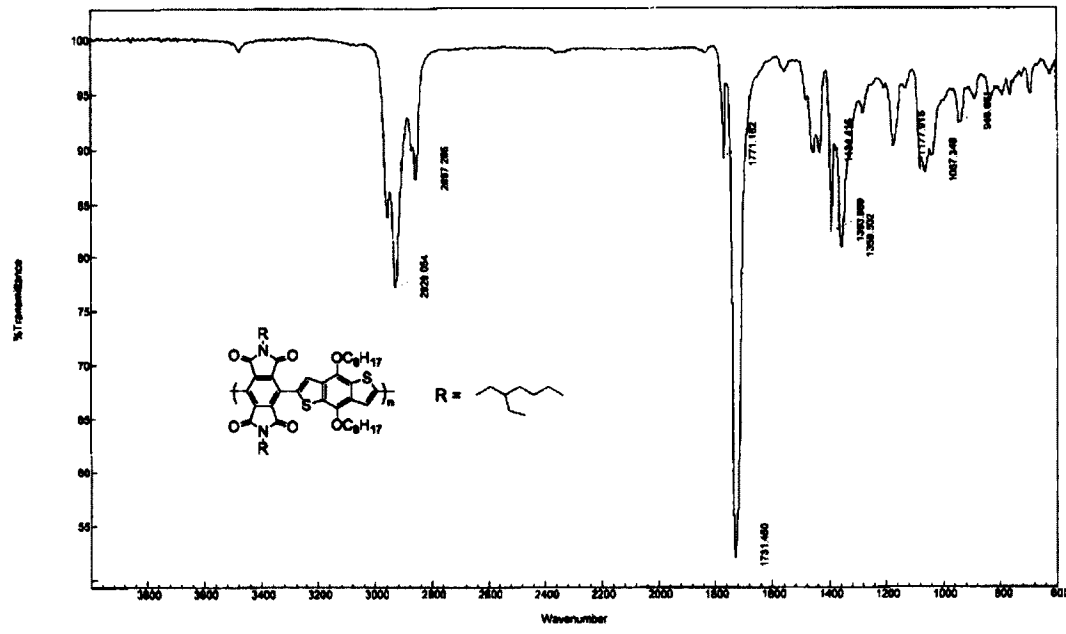

Figure B.54. IR spectrum of **P4**.

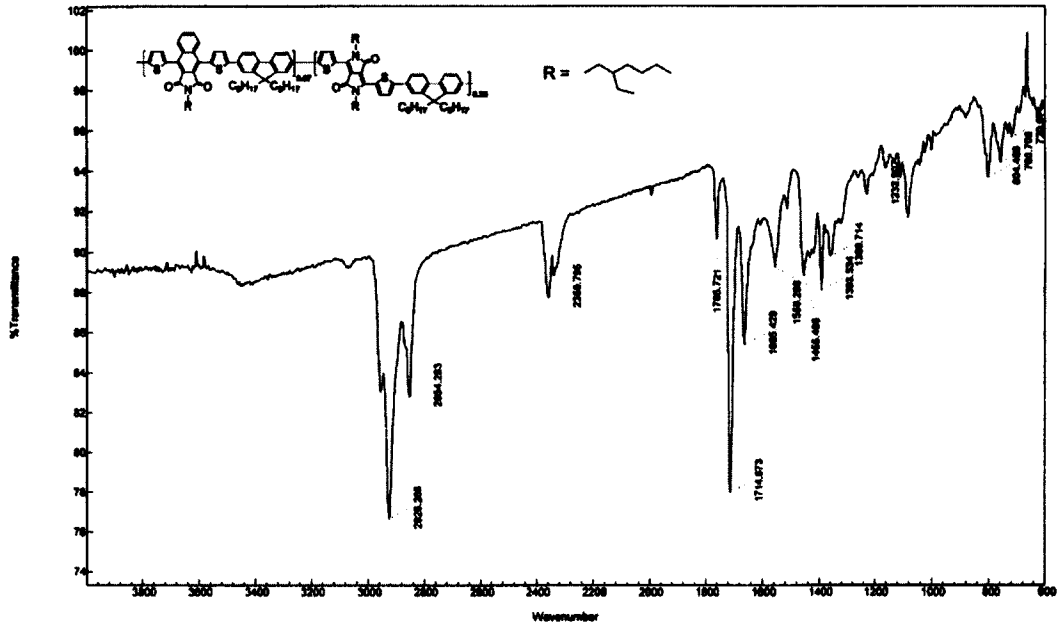

Figure B.55. IR spectrum of **Pa**.

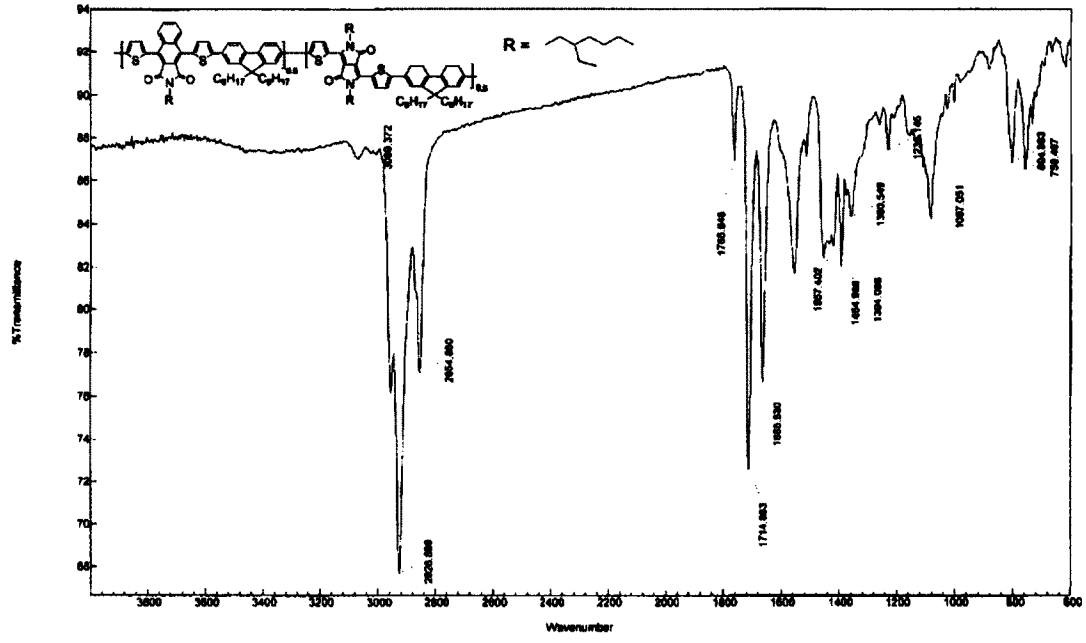

Figure B.56. IR spectrum of **Pb**.

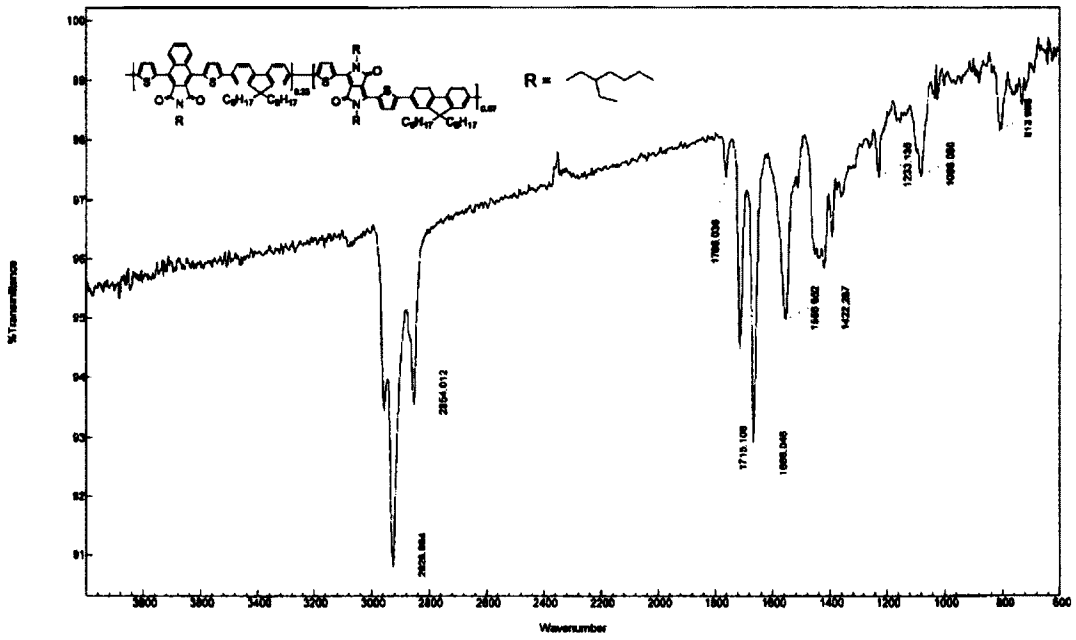

Figure B.57. IR spectrum of **Pc**.

APPENDIX C

CV figures of compounds and polymers.

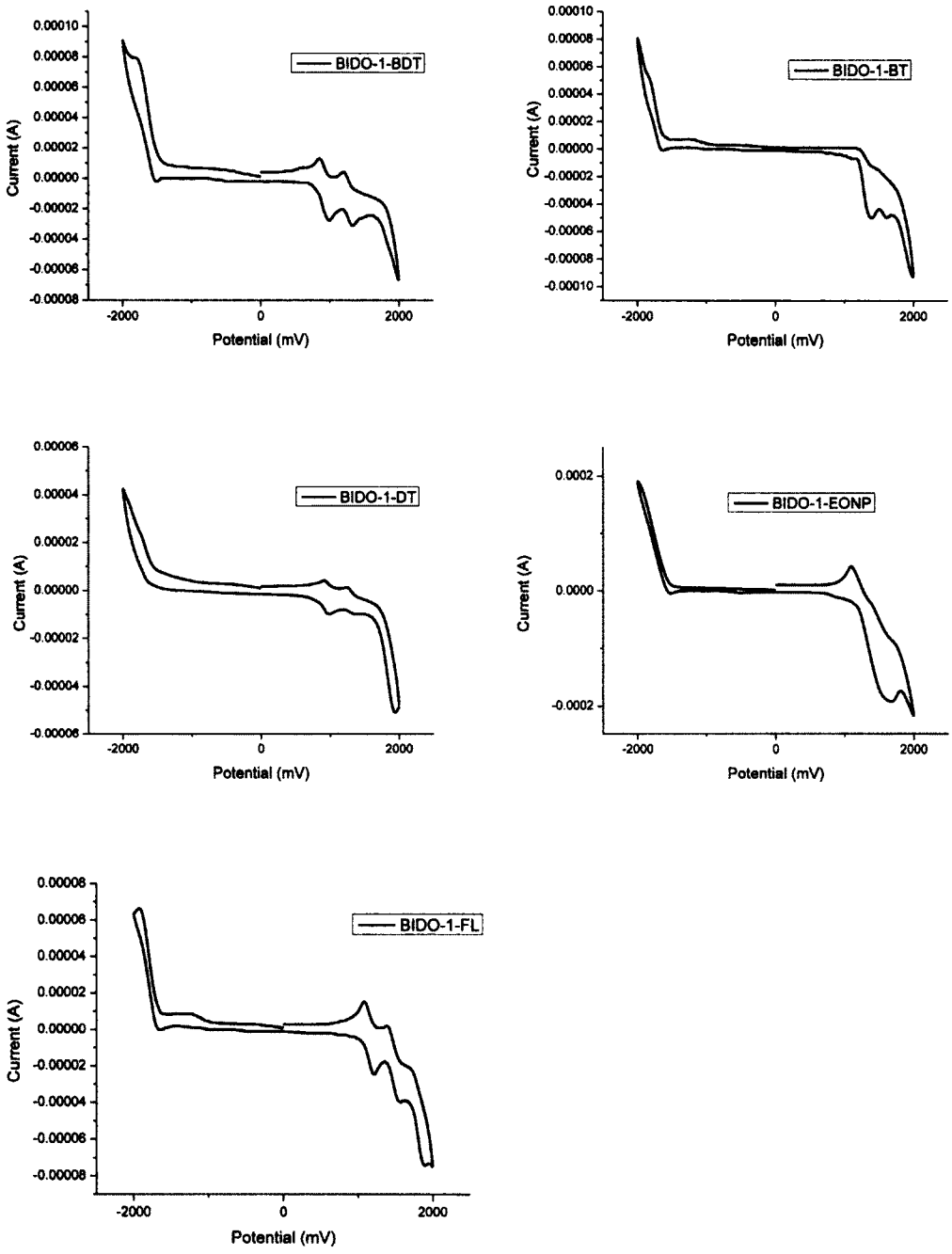

Figure C.1. CV figures of **BIDO-1** derivatives.

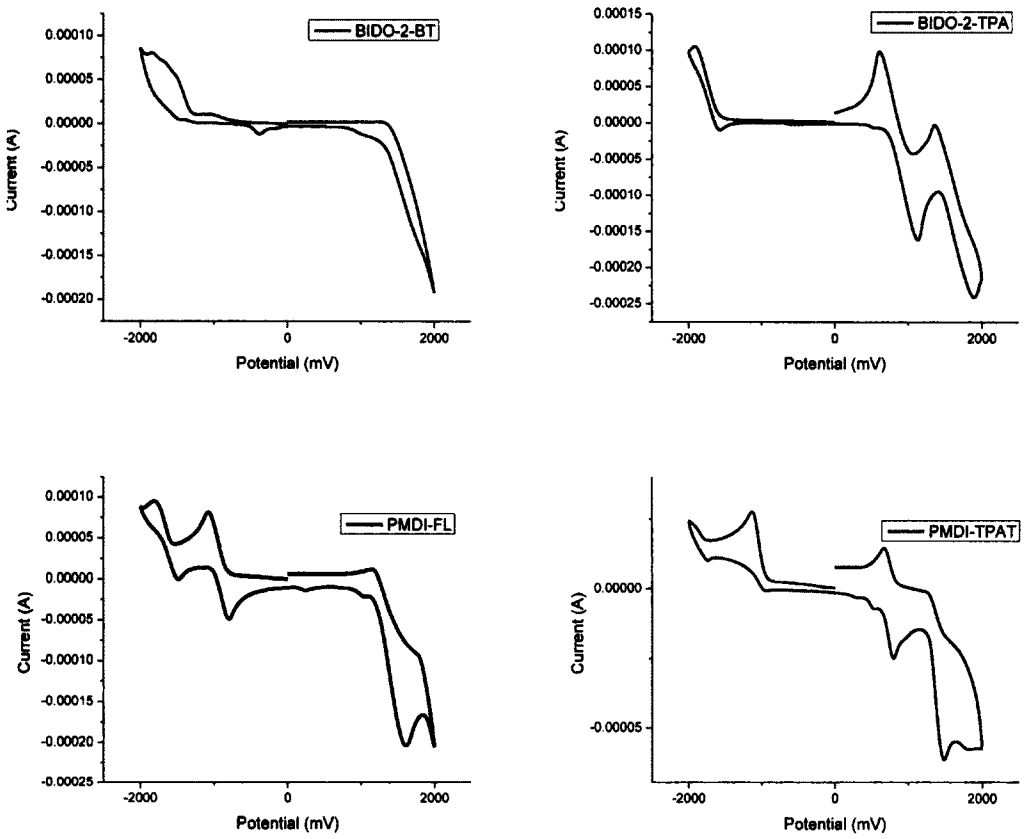

Figure C.2. CV figures of **BIDO-2** and **PMDI** derivatives.

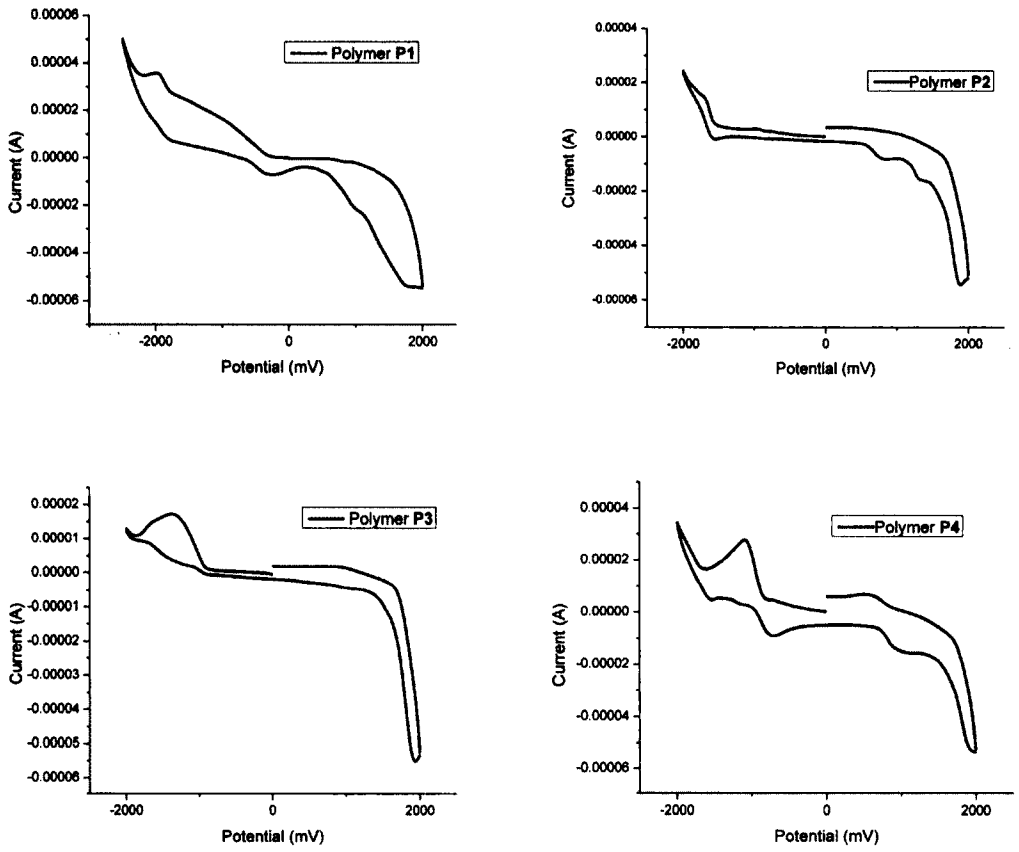

Figure C.3. CV figures of **P1-P4**.

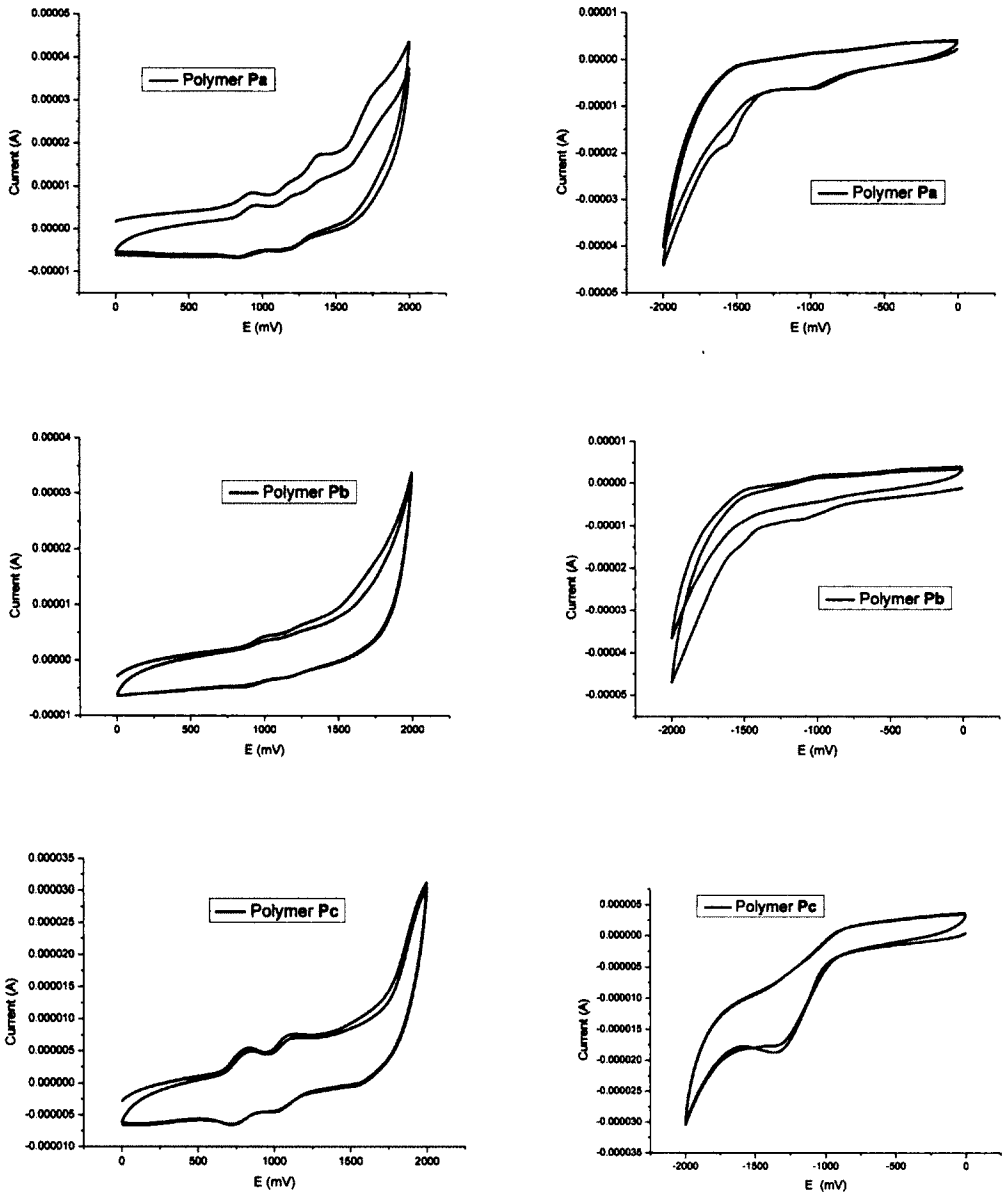

Figure C.4. CV figures of **Pa-Pc**.